I. SUPERSONIC LAMINAR BOUNDARY LAYER ALONG A TWO-DIMENSIONAL ADIABATIC CURVED RAMP

II. NON-LINEAR STABILITY THEORY FOR A LAMINAR, INCOMPRESSIBLE WAKE

Thesis by

Denny Ru-sue Ko

In Partial Fulfillment of the Requirements

For the Degree of

Doctor of Philosophy

California Institute of Technology

Pasadena, California

1969

(Submitted September 4, 1968)

ACKNOWLEDGEMENTS

I would like to express my sincere appreciation to Professor Toshi Kubota for his constant guidance, encouragement, and innumerable "break-through" suggestions throughout the course of my three years of graduate studies at Caltech. I would also like to express my sincere gratitude to Professor Lester Lees for his interest and continued guidance in the investigations, and especially for many valuable discussions in helping me to understand the underlying physics of the problems.

I would also like to thank Professor Wilhelm Behrens for reading Part II of this thesis and making many valuable suggestions.

I would also like to thank the staff of the GALCIT Hypersonic Wind Tunnel: S. Roman, G. Van Halewyn, J. Van Dijk, H. Mazurowski and P. Baloga for their assistance during the wind tunnel tests; the staff of the Aeronautics Shop under G. Carlson for their skill in constructing the models and probes; to Mrs. Truus van Harreveld for her reliable computational assistance; to Mrs. B Wood, Mrs. Jewel Colbert, Miss J. Greene for their assistance in the preparation of the illustrations; and to Mrs. E. Fox and V. Conner for their excellent and speedy typing of this manuscript.

I also wish to acknowledge the sponsorship of the U. S. Army Research Office and the Advanced Research Projects Agency, Contract No. DA-31-124-ARO(D)-33.

I wish to express my sincere appreciation to my wife, Starla, and my daughter, Grace, for providing a joyful, comforting atmosphere at home under all circumstances, which is the key factor

in the completion of this work.

This thesis is dedicated to my parents, whose faith and anticipation in my graduate study in the United States provided me with a constant urge to be one of the best at all times.

ABSTRACT

In Part I, the integral method of Lees and Reeves is applied to study a supersonic laminar boundary layer along a two-dimensional adiabatic curved ramp. The present method of solution requires no prior knowledge of the separation point and can be used to treat relatively weak interaction, including a fully attached flow. It starts with small perturbations of the self-induced interaction on a flat plate; consequently, it can be applied to flows with the hypersonic interaction parameter $\overline{\chi}$, based on the distance of the beginning station of interaction to the leading edge, of the order 1. The effect of the radius of curvature on the separation phenomena is then investigated using this method. The effect of finite ramp length on the interaction is examined by making use sf the characteristics of the singularities associated with the set of moment equations. Satisfactory agreement with the theory is obtained for the corresponding experiments conducted in the Mach 6 wind tunnel at the Graduate Aeronautical Laboratories of the California Institute of Technology.

In Part II, a non-linear theory for the stability of the laminar wake behind a flat plate in an incompressible flow is presented. An integral method is used to investigate the effects of a finite amplitude disturbance on the flow. The flow is decomposed into a mean part, which is independent of time and a fluctuating part, which has a zero time average. The mean flow is assumed to be characterized by two parameters: the centerline velocity defect w_c and the wake half-width b. By using a two-length expansion procedure, the assumption of local, parallel mean flow is justified for the solution of the

fluctuating component to the order considered in the present study. The fluctuation is assumed to be represented by an ascending power series of the amplitude **A.** The coefficients of the power series, as functions of the radial distance y, are then obtained in terms of the two mean flow parameters w_C and b. The three unknowns b, w_c and **A** are then obtained by solving the integral conservation equations of mean momentum, mean energy and fluctuation energy. *In this* integral method, the higher-order effects are introduced systematically by truncating the expansion for the fluctuation at various orders. The coupling between the mean flow and the fluctuation is found to be the most important mechanism in limiting the fluctuation amplitude and determining the mean flow. Satisfactory agreements with the experiment of Sato-Kuriki in the mean flow quantities and the relative development of **the** fluctuations are obtained, including the observed effect of free-stream Reynolds **number.**

TABLE OF CONTENTS

TABLE OF CONTENTS (Cont'd)

TABLE OF CONTENTS (Cont'd)

PART I. SUPERSONIC LAMINAR BOUNDARY LAYER ALONG A TWO-DIMENSIONAL ADIABATIC CURVED RAMP*

*A portion of this work has been presented at the ALAA 6th Aerospace Science Meeting, in conjunction with Professor T. Kubota (AIAA Preprint #68-109).

LIST OF FIGURES - PART I

LIST OF FIGURES - PART I (Cont'd)

LIST OF SYMBOLS - PART I

a = speed of sound

B = $\mathcal{H} + (1+m_e)/m_e$

C = $(\mu/\mu_\infty)/(T/T_\infty)$; Chapman-Rubesin parameter

$D(M_e, \mathcal{H})$ = $(J-\mathcal{H}J')f+(\mathcal{H}-1)J+[(2\mathcal{H}+1)J'-3J]B$

f = $2\mathcal{H}+(3\gamma-1)/(\gamma-1)+[(\gamma+1)/(\gamma-1)]m_e\mathcal{H}/(1+m_e)$
$+(M_e^2-1)/[m_e(1+m_e)]$

$\mathcal{H}$ = θ_i/δ_i^*

$h(\delta_i^*, M_e)$ = $(\tilde{R}e/C)\delta_i^*(1+m_e)\tan\Theta/[me(1+m_\infty)]$

J = θ_i^*/δ_i^*

k = iterating parameter defined in **Eqn.** (4)

M = Mach number

m = $0.5(\gamma-1)M^2$

N_1 = $(J-\mathcal{H}J')h + (\mathcal{H}R-PJ) + (PJ'-R)B$

N_2 = $J(\mathcal{H}-1)h + (PJ-\mathcal{H}R)f + [(2\mathcal{H}+1)R-3JP]B$

N_3 = $[(2\mathcal{H}+1)J'-3J]h + (R-PJ')f + [3JP-(2\mathcal{H}+1)R]$

P = $(\delta_i^*/U_e)(\partial U/\partial Y)_{Y=0}$, wall shear stress function

p = static pressure

Pr = Prandtl number

R = $\dfrac{2\delta_i^*}{U_e^2}\displaystyle\int_0^{\delta_i}\left(\frac{\partial U}{\partial Y}\right)^2 dY$, dissipation function

R_c = radius of curvature

Re_x = $u_\infty x/\nu_\infty$, Reynolds number

Re = $a_\infty M_e/\nu_\infty$

u, v = velocity components parallel and normal to surface

U = Stewartson transformed velocity = $(a_\infty/a_e)u$

x, y = coordinates parallel and normal to surface

Y = Stewartson transformed coordinate;

$$dY = (a_e/a_\infty)(\rho/\rho_\infty)dy$$

Z = $\int_0^{\delta_i} (U/U_e)dY/\delta_i^*$

= inclination of the local tangent to surface

α_m = total compression angle

α_T = expansion angle at end of ramp

β = $a_e p_e/(a_\infty p_\infty) = [(1+m_\infty)/(1+m_e)]^{0.5(3\gamma-1)/(\gamma-1)} p_{t_e}/p_{t_\infty}$

γ = specific heat ratio

δ = boundary-layer thickness

δ^* = $\int_0^\delta \left[1 - \frac{\rho u}{\rho_e u_e}\right] dy$, boundary-layer displacement thickness

δ_i^* = $\int_0^{b_i} \left[1 - \frac{U}{U_e}\right] dY$, transformed displacement thickners

θ_i = $\int_0^{\delta_i} \frac{U}{U_e}\left[1 - \frac{U}{U_e}\right] dY$, transformed momentum thickness

θ_i^* = $\int_0^{\delta_i} \frac{U}{U_e}\left[1 - \frac{U^2}{U_e^2}\right] dY$, transformed mechanical energy thickness

Θ = local flow angle at y = 6, $\tan^{-1}(v_e/u_e)$

μ = viscosity

ν = Prandtl-Meyer angle; also kinematic viscosity, μ/ρ

ρ = gas density

χ = $0.25(\gamma-1)^2 \overline{\chi}$

$\overline{\chi}$ = $M_\infty^3 (C/Re_x)^{\frac{1}{2}}$, hypersonic interaction parameter

Subscripts

B – Blasius

c – sharp expansion corner at the model trailing edge

e – edge of boundary layer

i – transformed

w. i. – weak-interaction

∞ – freestream, upstream

0 – zeroth order

1 – first order

2 – second order

Superscript

" ' " = derivative with respect to H

1 Introduction

Considerable progress has been made on the problems involving the interaction of a boundary layer and the external supersonic flow through the efforts of many investigators[1-5] in the past several years. Recently the analytical method of integral moments has been applied by Lees and Reeves[6] and by Klineberg[7] for laminar flow. Satisfactory agreement with the experiments for shock-impingement problems and for sharp corners has been obtained. Therefore, this method with a slight modification is employed to investigate the separation phenomena of a two-dimensional flow in a gradually turning concave surface.

In the previous experimental and analytical works, an infinite reattaching length has been assumed. For many cases of practical importance, however, the length available is finite, and it is desirable to predict its effects on the interaction. This problem is also examined by making use of the singularities of the moment equations. The analytical results are supplemented by the corresponding experiments conducted in the GALCIT Mach 6 wind tunnel with only adiabatic flow considered.

2 Analytical Approach

2A. Differential Equations

The coordinate system used is shown in Fig. 1, x being the distance from the leading edge along the surface and y the distance away from the surface along its normal. It is well known that the boundary-layer equations are the same as those for a flat plate,

provided the radius of curvature is large in comparison with the boundary-layer thickness.*

For an adiabatic laminar flow with Pr = 1, the governing integral moment equations reduce to the following forms:[6, 7]

Continuity

$$B\frac{d\delta_i^*}{dx} + \delta_i^*\frac{dH}{dx} + f\frac{\delta_i^*}{M_e}\frac{dM_e}{dx} = \beta\frac{1+m_e}{m_e(1+m_\infty)}\tan\Theta$$

Momentum

$$H\frac{d\delta_i^*}{dx} + \delta_i^*\frac{dH}{dx} + (2H+1)\frac{\delta_i^*}{M_e}\frac{dM_e}{dx} = \frac{\beta CP}{\tilde{R}e\,\delta_i^*} \qquad (1)$$

Moment of Momentum

$$J\frac{d\delta_i^*}{dx} + \delta_i^* J'\frac{dH}{dx} + 3J\frac{\delta_i^*}{M_e}\frac{dM_e}{dx} = \frac{\beta CR}{\tilde{R}e\,\delta_i^*}$$

The boundary-layer velocity profile is assumed to be of the form $u/u_e = f(y_i/\delta_i^*; H)$, and all integral properties are assumed to be functions of H only in the present formulation. Their relations are given by Klineberg[7] through solutions of the similar-flow equations. Equations (1), together with a relation between the flow angle Θ at the edge of the boundary layer and the local external Mach number M_e, form a set of first-order, non-linear, ordinary differential equations for the three unknowns $M_e(x)$, $H(x)$, and $\delta_i^*(x)$. For simplicity, the Prandtl-Meyer relation is used for the external supersonic flow, i.e.,

*As the radius of curvature becomes comparable to the boundary-layer thickness, the coordinate system chosen may cause crossing of the normals inside the boundary layer. This possibility, in fact, places a limitation on the total ramp angle allowed in the present analysis.

$$\Theta(x) = \nu(M_\infty) - \nu(M_e) - \alpha(x) \tag{2}$$

where ν is the Prandtl-Meyer angle and $\alpha(x)$ is the inclination of the local tangent to the surface, measured positive counterclockwise from the direction parallel to the velocity at upstream infinity. In order to facilitate a parametric study of the present problem, the curved surface connecting two flat plates is simply formed by an arc of constant radius. Therefore, $\alpha(x)$ is given as (Fig. 1)

$$\alpha(x) = \begin{cases} 0, & x \leq x_1 \\ (x-x_1)/R_c, & x_1 < x < x_2 \\ (x_2-x_1)/R_c \equiv \alpha_m, & x > x_2 \end{cases}$$

Solving Eqn. (1) for the derivative yields

$$\begin{aligned} \frac{\delta_i^*}{M_e}\frac{dM_e}{dx} &= \frac{\beta C}{\tilde{R}e\,\delta_i^*}\frac{N_1(M_e, H, \delta_i^*)}{D(M_e, H)} \\ \delta_i^*\frac{dH}{dx} &= \frac{\beta C}{\tilde{R}e\,\delta_i^*}\frac{N_2(M_e, H, \delta_i^*)}{D(M_e, H)} \\ \frac{d\delta_i^*}{dx} &= \frac{\beta C}{\tilde{R}e\,\delta_i^*}\frac{N_3(M_e, H, \delta_i^*)}{D(M_e, H)} \end{aligned} \tag{3}$$

(D, N_1, N_2, and N_3 are given in the List of Symbols.) In the following analysis, the Chapman-Rubesin parameter will be taken as a constant equal to 1, without losing generality.

2B. Starting Solutions

In the previous application of the integral method to similar interaction problems,[6] the boundary layer entering the interaction zone was assumed to be a Blasius flow, and the values of M_e and δ_i^* at the beginning of the interaction were determined by requiring the derivatives dM_e/dx and dH/dx to vanish for $H = H_B$. However, when $\bar{\chi}$ based on the distance of the beginning of interaction from the leading edge is not small, the starting scheme prescribed previously is inadequate to obtain a solution.† A more precise method has to be devised to provide the starting solutions for the present problem in which the disturbance on the flat-plate boundary layer becomes smaller as the radius of curvature is increased. The same technique to be discussed here is equally applicable for the other types of interaction problems.

When a laminar boundary layer in a supersonic flow approaches a disturbance, small but relatively rapid changes occur in the boundary-layer characteristics. In such cases, perturbation in the external flow has to be considered simultaneously with the boundary-layer perturbation, even in a region where the interaction is weak otherwise. The extent of this region is of the order of $M_e\delta$, and the deviation from the ordinary flat-plate weak interaction grows exponentially downstream. In this region of local strong interaction, the perturbations of M_e, H, and δ_i^* are not independent. The relation

† In the previous flat-plate problems,[6] the starting point of the integration was taken well into the interaction zone. In this case, a solution was possible even with relatively large errors in the initial conditions.

between them, derived in Appendix A of ref. 9 for the limiting case of hypersonic flow, is given by

$$\delta_i^* - \delta_{i0}^* = -k\left[(1+2H)J' - 3J\right]\delta_{i0}^* ,$$

$$H - H_0 = k(1-H)J , \qquad (4)$$

$$M_e - M_{e0} = k(HJ' - J)M_{e0} ,$$

where the subscript 0 denotes the undisturbed quantities, and k is an undetermined constant.

The weak-interaction solution for a flat-plate flow consistent with the present formulation is obtained by expanding each of the three dependent variables M_e, H, and δ_i^* in terms of an asymptotic series in $\bar{\chi}$, the hypersonic interaction parameter. For the range of $\bar{\chi}$ involved in the present study (order 1), it was found necessary to include terms of second order in $\bar{\chi}$ or higher. The details are described in Appendix A. The result is

$$M_e/M_\infty = 1 + m_1\chi + m_2\chi^2 + m_3\chi^3 \ln\chi$$

$$H = H_B + H_1\chi + H_2\chi^2 \qquad (5)$$

$$\delta_i^* = \delta_{i_B}^*\left[1 + \delta_1\chi + (\delta_2 - 2\epsilon_2 \ln\chi)\chi^2\right]$$

where H_B and $\delta_{i_B}^*$ are the Blasius values given by

$$H_B = 0.3842, \qquad \delta_{i_B}^* = 1.724\, x/(Re_x)^{\frac{1}{2}}$$

Expressions for the coefficients can be found in Appendix A.

With these preliminary considerations of the nature of the solution near the beginning of the interaction zone, the method of

solution for flow past a curved ramp with given geometry is described as follows.

For a given freestream condition, an initial point x_0 on the flat approaching section is chosen. The flow conditions are determined from the second-order weak-interaction expansion plus a perturbation from the local strong-interaction solution. The value of k is chosen to be only a fraction of the maximum value discussed in Appendix A of ref. 9 in order to assure the validity of linearization used in obtaining them. Using these initial conditions, the integration of the set of equations is performed on an IBM 7090 computer. Since there is no way of knowing a priori the correct x_0 for a given ramp geometry and freestream conditions, this point is obtained by fixing the value of k and varying x_0 until a qualitatively correct solution is obtained; i. e., the integral curve goes smoothly through the separation and reattachment points, if it separates, but does not necessarily satisfy the downstream boundary condition. Then, fixing $x_{0'}$ the magnitude of k is used as the iteration parameter to find the correct integral curve that satisfies the downstream conditions. Checks have been made on the sensitivity of the solution curve to the choice of x_0. The fact that two different values of x_0 (not too far apart) result in identical solution curves with different values of k supports the validity of the approach used in the present study.

2. C. Downstream Condition for an Infinite Ramp

When unlimited ramp length is available, the appropriate downstream condition is $H \to H_B$ and $M_e \to M_{\infty+}$, the inviscid downstream Mach number. In terms of **Eqns.** (3), this condition requires

that N_1 and N_2 vanish simultaneously but D, $N_3 \neq 0$ as shown in detail in Appendix B of ref. 9. As pointed out by Lees and Reeves,[6] there must be a Mach number undershoot and, therefore, a static pressure overshoot, before the final equilibrium flow is achieved. *

Because of the singular nature of this downstream condition, it is not possible to achieve this condition numerically. In the computations, the integration is considered to be completed when $N_2 = 0$ at some x sufficiently far away from the reattachment that it has no effect on the location of the separation and reattachment points.

2D. Downstream Condition for a Finite Length Ramp

In any practical case the ramp length is finite, and the effect of the sharp expansion corner at the trailing edge of the ramp on the interaction has to be examined. From Eqns. (3), the curve defined by $D(M_e, H) = 0$ is a locus of singularities in the $M_e - H$ plane. When the boundary-layer flow approaches an expansion corner, it feels the downstream disturbance through the subsonic part of the layer. The flow accelerates and the velocity profile becomes fuller (H increases). When the angle of turning is large enough, the integral curve intersects the D = 0 curve. The point of intersection is called the critical point. When the corner is rounded, N's must vanish at the critical point. When the expansion corner is sharp, we expect some singular behavior. (This is analogous to the location of the sonic point in the inviscid supersonic blunt-body flow.) It is therefore assumed that the slopes will approach infinity with the dependent

*From the nature of solutions near the Blasius point, there must also be an overshoot in H, which was not pointed out by them.

variables, M_e, δ_i^* and H, being physical quantities, remaining finite at the corner. To show that the assumption is consistent with the solution of Eqns. (3) near the corner, we linearize the equation by letting

$$dM_e/dx \sim (x_c-x)^{-\beta_1}, \quad dH/dx \sim (x_c-x)^{-\beta_2}, \quad d\delta_i^*/dx \sim (x_c-x)^{-\beta_3} \qquad (6)$$

for $x \leq x_c$, with x_c defining the corner location. Because of the requirement mentioned, $0 < \beta_1$, β_2 and $\beta_3 < 1$. Furthermore, by linearizing around the critical point in the phase space, it can be shown that dM_e/dH and $d\delta_i^*/dH$ are finite as $x \to x_c$, which requires that $\beta_1 = \beta_2 = \beta_3$. Note that the assumption requires $D \to 0$ in Eqns. (3) but $N_i \neq 0$ $(i = 1, 2, 3)$ as $x \to x_c$. Using Eqn. (6), the expansions in (x_c-x) for the quantities M_e, H and δ_i^* can be obtained near x_c. Substituting them into Eqns. (3), and collecting terms of the same order in (x_c-x), it can be easily shown that $\beta_1 = \frac{1}{2}$. Therefore, we have, up to the first term in (x_c-x)

$$M_e = M_c - k_1(x_c-x)^{\frac{1}{2}}, \quad H = H_c - k_2(x_c-x)^{\frac{1}{2}}, \quad \delta_i^* = \delta_{i_c}^* + k_3(x_c-x)^{\frac{1}{2}} \qquad (7)$$

where the subscript c refers to the conditions at x_c, and k_1, k_2 and k_3 are positive constants that can be obtained in terms of the conditions at x_c. Because of the singular behavior when x is used as the independent variable for integration near the corner, the independent variable is changed from x to H when some arbitrary given reference slope dH/dx is exceeded. (The reference value is chosen to guarantee that the integral curve belongs to the family described by Eqn. (7).) No difficulties are encountered in this plane because the

N's do not vanish at the corner. A complete solution curve is obtained when the initial itexatian parameter places the branch paint at the physical trailing edge of the ramp. The adequacy of the preceding approximation has to be examined by comparisons with the experimental results, which will be discussed in the next section.

Studies on the supersonic flow near a smooth expansion corner have indicated that, at a given fxeestream condition, the flow will remain subcritical for a small enough turning angle. In such cases, the integral curve will not intersect the D = 0 curve; hence, it may proceed smoothly past the corner, approaching its downstream conditions. This angle for the present freestream conditions has been estimated to be only a few degrees, even with a quite large radius of curvature, and it decreases with decreasing radius of curvature, Therefore, an estimate on the minimum expansion angle required to apply the present approximation may be obtained. *

3 Experimental Study

The experimental study was conducted in the GALCIT hypersonic wind tunnel with a nominal Mach number of 6. The reservoir temperature was always kept at 275°F to prevent flow condensation for the present experiments. The variation in the freestream Reynolds number was achieved by changing the stagnation pressure, which ranged from 0 psig to 100 psig corresponding to a range of freestream Reynolds number between 30,000 per inch and 230,000

*A detailed study on the supersonic flow around an expansion corner is being carried out by K. Victoria at the California Institute of Technology.

per inch.

A total number of six models have been designed for the present test program. They are made of nondeforming tool steel (Ketos) with a width of 5 inches spanning the tunnel. All models start with a flat plate section having a sharp ($\leq$ .003") leading edge followed by the curved ramp. The total ramp angle, being limited by the tunnel blockage problem, was chosen to be 10 degrees. The dimensions of each model are tabulated in the table of Fig. 1. Models A-1 and A-2 are designed to study the effect of curvature. Together with the limiting sharp corner case of Lewis, [1] these provide a fairly wide range of the curvature parameter x_1/R_c. Models B-1 and B-2, supplemented by model A-1, are used to study the effect of a finite reattaching length on the flow. Model B-2-1 has been designed to provide a test on the effect of the expansion angle at the model trailing edge. Model A-3 is a scale-up version of model A-2, to be used for Reynolds number correlation.

All models are instrumented with static pressure orifices, 0.012 inches in diameter distributed along the model centerline. The static pressures were recorded on a multiple-tube silicone manometer-board. The system was checked for leaks both before and after each test.

Pitot probes with a flattened (0.002" x 0.005") tip were used for the flow field surveys. Two probes with different angle of attack were used for surveying the boundary layer in order to minimize the effect of angle of attack on the probe readings. The pitot pressures were measured with a Statharn 5-psia pressure

transducer. The pressure transducer was calibrated before and after the test with its reference side kept below 0.5 μ Hg. and showed no noticeable changes. The measurements were recorded on the Y-scale of a Moseley autograph. The X-scale indicating the probe position was transmitted by a helipot. The axial position of the probe relative to the model leading edge was determined before each run. The distance away from the model surface was obtained by having the probe tip in contact with the surface.

In order to compare with the analytical predictions, extreme care has been taken in achieving a two-dimensional, laminar flow. Side plates properly designed were mounted on the models to assure two-dimensionality. As shown by Lewis,[1] a limiting flow, closely simulating a two-dimensional flow, may be approached for a mocler-ately large aspect ratio (defined as the ratio of the spacing between the side plates to the model length). Therefore, the side plates were first installed at various spacings to find out the proper spacing for each model. After setting the correct spacing, the velocity profiles at various stations along the model were obtained from the Pitot surveys, with the assumption of constant stagnation temperature across the boundary layer. These profiles were then compared with the asymptotic laminar profile corresponding to the downstream Mach number. Laminar flow over the complete model was confirmed when none of the profiles measured became fuller than the asymptotic one. The details of the assurance of two-dimensionality and the confirmation of a laminar flow are well described by Lewis. Only those results corresponding to a laminar flow are presented here to

compare with the theory. The rest of the experimental results, which are transitional in the sense of the previous criterion, are summarized in Appendix B.

In practice, the model cannot be aligned perfectly with the freestream flow direction. In order to estimate the uncertainty in the measurements, a preliminary test on the effect of a small angle of attack on the overall interaction phenomena was performed. Model A-1 was rotated about 0.5° with respect to the tunnel axis and the static pressures along the model surface were recorded to compare with those taken with model aligned to the axis. The comparison is shown in Fig. 2. Within the accuracy in the pressure readings, the ratio remains practically constant at all stations. Therefore, we may conclude that the effect of the angle of attack is to change the static pressure measurements by a constant factor over the whole interaction region, at least for the small angle range investigated. In other words, the measured pressure distributions are scaled by the static pressure encountered around the leading edge section. This result may also explain the high pressure ratios reported by Lewis over the whole model when the average test section freestream static pressure was used to normalize the measurements. Because of this finding, the static pressure ahead of the model has been used as $p_{-\infty}$ for normalizing all the data presented. However, it must be kept in mind that a constant proportional shift of the static pressure data is possible due to the uncertainty in the flow alignment.

4 Results and Discussion

4A. Comparison between Theory and Experiment

Only the test results of model A-1 are compared with the theory. The same degree of agreement exists for all other cases. Fig. 3 shows the comparison of $p/p_{-\infty}$ distribution. The general agreement including the pressure in the weak-interaction region of the flat plate and the falling pressure in the region near the sharp trailing edge is fairly good. The difference in the pressure level from the prediction near the trailing edge is caused partly by the transverse pressure gradient existing near a sharp expansion corner. The theoretically determined separation point shown in Fig. 3 agrees satisfactorily with an oil film observation. The velocity profiles, δ^*, and θ at each station are calculated from the pitot pressure survey using Crocco's temperature-velocity relation for zero pressure gradient and the Prandtl number 0.725.[10] The transformed form parameter is then obtained from

$$H = \frac{(1+m_e)\,\theta/\delta^*}{1-m_e\,\theta/\delta^*} \quad .$$

The results are compared with the theoretical predictions in Fig. 4. The agreement is quite good. The comparison of the displacement thickness δ^* is shown in Fig. 5. The general trend is again in accordance with the theory, but a difference of 30% exists. This is partially a consequence of the inaccuracy in the measurements very close to the wall. Moreover, the ratio $p_{te}/p_{t\infty}$, which has been taken to be unity in the theoretical calculation, is actually a

function of x due to the different degrees of entropy jump at the bow shock experienced by the streamlines entering the boundary-layer edge. Near the beginning of the interaction, $p_{te}/p_{t\infty}$ has been found to be only 0.5 for the present experiment. This discrepancy suggests the inclusion of the non-isentropic relation for a more accurate calculation using the moment method.

4B. Curvature Effect

Fig. 6 shows the effect of the radius of curvature from the theoretical calculation. Because the extent of the separated region decreases with increasing radius, the effect is not very apparent. The largest radius of curvature has kept the flow from separation anywhere in the region of adverse pressure gradient in this 10^{o} compression turn. However, calculation assuming local similarity and inviscid pressure distribution will show that this is not possible. The interaction of the boundary layer with the external flow has appreciably reduced the adverse pressure gradient and therefore prevents boundary-layer separation in this case.

The experimental results of the curvature effect are shown in Fig. 7. In order to include the limiting case of zero radius of curvature investigated by Lewis,[1] the results for a high Reynolds number are presented. The flow, for the two models tested, became transitional around station x = 4.0 in. (judged from the velocity profiles measured). However, from the upstream influence predicted by the method of Section 2D, this effect is expected to be small on the separated region. The comparison between

models A-1 and A-2 shows that the effect of the radius is well-predicted by the theory. Shown on the same figure is the limiting case of the sharp corner of Lewis, which is nearly identical to the result of model A-1. It is also of interest to note that the pressures measured near the end of models do not show the falling trend predicted by the laminar theory proposed because of the greatly decreased upstream propagation in a turbulent boundary layer.

4C. Ramp Length Effect

The effect of finite ramp length is shown in Fig. 8. The agreement of experiment with theory is very good. As expected, model A-1, having a length of 3.825 in. after the effective corner, corresponds essentially to the case of an infinite reattaching length at this Reynolds number. Theoretical calculation for a longer reattaching length did not alter the points of separation and reattachment, which showed the effectively infinite reattaching length for models A-P and A-2. The ramp on model B-1 ended about 7 boundary-layer thicknesses after the theoretically predicted reattachment point. Accordingly, it caused a very little change in the points of separation and reattachment from the ones corresponding to an infinite length. Therefore, the pressure distributions are nearly identical with model A-1 except that the peak pressure obtained is lower because of the insufficient length for pressure rise after the reattachment. Model B-2 was purposely designed to have the model end slightly before the reattachment point predicted for model A-1. With the short ramp, the length of the separated region is reduced, and the pressure distribution shows no recognizable inflection as

compared with the other cases. Also the maximum pressure on the ramp is only about a half of the inviscid pressure rise. Notice that the total turning angle for all cases is still 10.15^{o}. Finally, an experiment was conducted to test the effect of the expansion angle at the trailing-edge corner. Model B-2-1 is identical to model B-2 except for a 10^{o} expansion turn instead of 100^{o} at the trailing edge of the model. The pressures measured on model B-2-1 are compared with the results of model B-2 in Fig. 9, together with the theoretical predictions. The two measurements agree almost exactly except for the last two data points, so that we may consider the assumption used in Section 2D to be a valid one.

4D. Reynolds Number Effect

Because of the limitations of the test facilities, pure laminar flow over the models can only be achieved for a very limited Reynolds number range. Thus, the effects of Reynolds number on model A-1 based on the numerical calculations are shown in Fig. 10, where the nondimensionalized pressures $P_N = (p-p_{-w.i.})/(p_{+w.i.}-p_{-w.i.})$ are plotted against x for four different Reynolds numbers. $p_{-w.i.}$ and $p_{+w.i.}$ are the weak-interaction pressure distributions corresponding to the upstream and downstream conditions, respectively, for the same distance x measured from the leading edge. As the Reynolds number increases, the separated region becomes larger, and consequently the pressure "plateau" becomes more evident, as shown by Lewis[1] and by Needham[5] for a sharp corner.

5 Conclusions

1) An analysis for the perturbations at the beginning of the interaction is incorporated in the integral method for solving the boundary-value problem of the boundary-layer interaction as an iterative initial-value problem. This approach requires no a priori knowledge of the separation point and is applicable for flows without separation.

2) Increasing the radius of curvature decreases the length of the separated region and may result in a completely attached flow (for the 10^{o} turn investigated) when the radius of curvature is large enough. For a small radius of curvature, the result differs only slightly from that of a sharp corner.

3) The measured static pressures agree satisfactorily with the values predicted by the moment method. The form parameter $H = \theta_i/\delta_i^*$ calculated from the data is in good agreement with the theoretical prediction, and the experimentally determined displacement thickness δ^* is also in fairly good agreement with the theory.

4) The effect of ramp length can be predicted by the present method by making use of the singular solution of the moment equations. When the ramp ends around the reattachment point estimated for an infinite length, the separated region becomes smaller, and not only the final pressure level but also the pressure over the entire interaction region decreases. Experimental results show good agreement with the predictions of the effect of finite ramp length.

Appendix A

A Second-Order Weak Interaction Expansion for Moderately Hypersonic Flow Past a Flat Plate*

In the case of $M_\infty >> 1$, the self-induced weak pressure interaction expansions were well-developed (e.g., Ref. 11) and found to agree satisfactorily with experimental results.(12,13) However, in some applications, the solutions for large but finite Mach numbers are desirable. Furthermore, the terms of higher order in $\overline{\chi}$ are sometimes required in the expansions. An alternate method is therefore proposed here to obtain a set of expansions up to order $\overline{\chi}^2$. It is applied to flow past an adiabatic flat plate in the present analysis. Extension to a wall with heat transfer is self-evident.

The integrated moment equations for a two-dimensional, laminar, compressible flow with adiabatic wall are (Pr = 1.0).(6)

Continuity

$$B\frac{d\delta_i^*}{dx} + \delta_i^*\frac{dH}{dx} + f\frac{\delta_i^*}{M_e}\frac{dM_e}{dx} = \beta\frac{1+m_e}{m_e(1+m_\infty)}\tan\Theta \qquad (A1)$$

Momentum

$$H\frac{d\delta_i^*}{dx} + \delta_i^*\frac{dH}{dx} + (2H+1)\frac{\delta_i^*}{M_e}\frac{dMe}{dx} = \frac{PCP}{\tilde{R}e\delta_i^*} \qquad (A2)$$

Moment of momentum

$$J\frac{d\delta_i^*}{dx} + \delta_i^*\frac{dJ}{dH}\frac{dH}{dx} + 3J\frac{\delta_i^*}{M_e}\frac{dM_e}{dx} = \frac{\beta CR}{\tilde{R}e\delta_i^*} \qquad (A3)$$

---

*Published in AIAA Journal, vol. 5, No. 10, Oct. 1967, together with Prof. T. Kubota.

where

$$\tan\Theta = v_e/u_e = (d\delta^*/dx) - (\delta - \delta^*)(d/dx)\left[\ell n(\rho_e u_e)\right] \qquad (A4)$$

All integral properties are assumed to be functions of a single parameter $H = \theta_1/6_i^4$ in the present formulation. The flow angle at the edge is assumed to be connected with M_e through the Prandtl-Meyer relation, i.e., $\Theta = \nu_\infty - \nu_e(M_e)$. To put the equations in a suitable form for the analysis, introduce the following non-dimensional length:

$$\hat{x} = \frac{16u_\infty x}{(\gamma-1)^4 M_\infty^6 \nu_\infty C} \qquad \hat{\delta} = \frac{4u_\infty \delta_i^*}{(\gamma-1)^2 M_\infty^3 \nu_\infty C} \qquad (A5)$$

such that

$$(\hat{x})^{-\frac{1}{2}} = \left[(\gamma-1)^2/4\right]\overline{\chi} \qquad (A6)$$

Then, the following forms of series expansion in $\overline{\chi}$ [i.e., in $(\hat{x})^{-\frac{i}{2}}$] are assumed:

$$\hat{M} = M_e/M_\infty = 1 + (m_1/\hat{x}^{\frac{1}{2}}) + (m_2/\hat{x}) + (m_3/\hat{x}^{3/2})\,\ell n\hat{x} + \ldots \qquad (A7)$$

$$H = H_B + (h_1/\hat{x}^{\frac{1}{2}}) + (h_2/\hat{x}) + \ldots \qquad (A8)$$

$$\hat{\delta} = \delta_0\hat{x}^{\frac{1}{2}}\left[1 + (\delta_1/\hat{x}^{\frac{1}{2}}) + (\epsilon_2/\hat{x})\ell n\hat{x} + (\delta_2/\hat{x}) + \ldots\right] \qquad (A9)$$

The term of $([1/\hat{x}]\ell n\hat{x})$ in the $\hat{\delta}$ expansion was found necessary to obtain second-order correction terms, as will be shown later. Substituting these expressions into the three equations and equating terms of the same power in $(\hat{x}^{-\frac{1}{2}})$, the following relations for the coefficients in the series are obtained:

$$\delta_0 = (2P_B/\mathcal{H}_B)^{\frac{1}{2}} = (2R_B/J_B)^{\frac{1}{2}} \tag{A10}$$

$$m_1 = -\delta_0 \frac{(1+m_\infty)[1+\mathcal{H}_B+(1/m_\infty)]}{(\gamma-1)M_\infty(M_\infty^2-1)^{\frac{1}{2}}} \tag{A11}$$

$$\delta_1 - \frac{P_B'}{P_B}h_1 = \left[\frac{1+\mathcal{H}_B}{\mathcal{H}_B} - \frac{3\gamma-1}{\gamma-1}\frac{m_\infty}{1+m_\infty}\right] m_1 \tag{A12}$$

$$\delta_1 - 2m_1 = \frac{R_B'}{R_B}h_1 - \frac{3\gamma-1}{\gamma-1}\frac{m_\infty}{1+m_\infty}m_1 \tag{A13}$$

$$m_2 = m_1^2\left\{\frac{m_\infty}{1+m_\infty} - \frac{12}{2(M_\infty^2-1)} - \frac{(M_\infty^2-1)Z_B}{(1+m_\infty)[1+m_\infty(1+\mathcal{H}_B)]}\right\} \tag{A14}$$

$$2\epsilon_2 - \left(\frac{P_B'}{P_B}+\frac{1}{\mathcal{H}_B}\right)h_2 + \left(\frac{3\gamma-1}{\gamma-1}\frac{m_\infty}{1+m_\infty} - 3 - \frac{2}{\mathcal{H}_B}\right)m_2 = \frac{1}{\mathcal{H}_B}(h_1\delta_1+2m_1\delta_1)+3m_1\delta_1 + \left(\frac{2}{\mathcal{H}_B} - \frac{3\gamma-1}{\gamma-1}\frac{P_B'}{P_B}\frac{m_\infty}{1+m_\infty}\right)m_1h_1 - \frac{3\gamma-1}{2(\gamma-1)} \times \frac{\{m_\infty-[(4\gamma-2)/(\gamma-1)]m_\infty^2\}}{(1+m_\infty)^2}m_1^2 + \frac{1}{2}\frac{P_B''}{P_B}h_1^2 \tag{A15}$$

$$2\epsilon_2 - \left(\frac{J_B'}{J_B} + \frac{R_B'}{R_B}\right) h_2 + \left(\frac{3\gamma-1}{\gamma-1}\,\frac{m_\infty}{1+m_\infty} - 5\right) m_2 =$$

$$\frac{1}{2}\left(\frac{J_B''}{J_B} + \frac{R_B''}{R_B}\right) h_1^2 + \frac{J_B'}{J_B}\, h_1 \delta_1 - \frac{3\gamma-1}{2(\gamma-1)} \times$$

$$\frac{\left\{m_\infty - [(4\gamma-2)/(\gamma-1)]\, m_\infty^2\right\}}{(1+m_\infty)^2}\; m_1^2 + 5 m_1 \delta_1 +$$

$$\left(3\,\frac{J_B'}{J_B} - \frac{3\gamma-1}{\gamma-1}\,\frac{m_\infty}{1+m_\infty}\,\frac{R_B'}{R_B}\right) m_1 h_1 \qquad \text{(A16)}$$

In these expressions, primes indicate differentiation with respect to H. Eqn. (A10) determines the Blasius value H_B and δ_0. If only first-order (up to order $\overline{\chi}$) approximation is needed, Eqns. (A11-13) yield enough relations to determine δ_1, m_1, and h_1. In Eqns. (A10-16), δ_2 does not enter, and Eqns. (A15) and (A1b) would over-specify h_2 if ϵ_2 were absent.

Examination of equations in the M_e-H-$\hat{\delta}$ space shows that the weak interaction solution must have the form

$$M_e = M_\infty + (\hat{m}_1/\hat{\delta}) + (\hat{m}_2/\hat{\delta}^2) + \ldots$$

$$H = H_B + (\hat{h}_1/\hat{\delta}) + (\hat{h}_2/\hat{\delta}^2) + \ldots \qquad \text{(A17)}$$

Hence

$$\hat{\chi} = (C_0/2)\hat{\delta}^2 \left[1 + (2C_1/C_0)(1/\hat{\delta}) + (2C_2/C_0)(1/\hat{\delta}) \ln\hat{\delta} + \ldots\right] \qquad \text{(A18)}$$

From Eqns. (A9) and (A18), we obtain

$$\delta_2 = \tfrac{1}{2}(\delta_1^2 + 4\epsilon_2 \ln\delta_0) \tag{A19}$$

Using (A17), m_3 can be easily determined as

$$m_3 = -\epsilon_2 m_1 \tag{A20}$$

To summarize, the second-order weak interaction expansions are given as follows with $\chi = [(\gamma-1)^2/4]\overline{\chi}$:

$$\begin{aligned} M_e/M_\infty &= 1 + m_1\chi + m_2\chi^2 + m_3\chi^3 \ln\chi \\ H &= H_B + h_1\chi + h_2\chi^2 \\ \delta_i^* &= \delta_0(\nu_\infty x C/u_\infty)^{\frac{1}{2}} [1 + \delta_1\chi + \{\delta_2 - 2\epsilon_2 \ln\chi\}\chi^2] \end{aligned} \tag{A21}$$

For $\gamma = 1.40$, substituting in the values corresponding to Blasius flow, we obtain the expressions for the coefficients

$$\begin{aligned} \delta_0 &= 1.7239 \\ m_1 &= -4.3097 \frac{[1.3842 + (1/m_\infty)](1+m_\infty)}{M_\infty[(M_\infty^2-1)^{\frac{1}{2}}]} \\ m_2 &= m_1^2\left[\frac{m_\infty}{1+m_\infty} - \frac{1}{2(M_\infty^2-1)} - \frac{1.8727(M_\infty^2-1)}{(1.3842m_\infty+1)(1+m_\infty)}\right] \\ h_1 &= -0.2268m_1 \\ \delta_1 &= -0.5002h_1 + \left(\frac{2-6m_\infty}{1+m_\infty}\right)m_1 \end{aligned} \tag{A22}$$

$$h_2 = 0.1517(-3.2053m_2 + 23.828h_1^2 - 0.4746h_1\delta_1 -$$

$$3.2053m_1\delta_1 + \{4.0264 + 56.531\,[m_\infty/(1+m_\infty]\}m_1h_1)$$

$$\epsilon_2 = 4.5844h_2 + \left(4.1026 - \frac{4m_\infty}{1+m_\infty}\right)m_2 +$$

$$1.013h_1\delta_1 + 4.1026m_1\delta_1 +$$

$$\left(2.6026 - 26.264\,\frac{m_\infty}{1+m_\infty}\right)m_1h_1 -$$

$$3.4217h_1^2 - \frac{(2m_\infty - 18m_\infty^2)}{(1+m_\infty)^2}\,m_1^2$$

The expressions for static pressure, displacement thickness, and skin friction are easily derived from Eq. (A22) as follows:

$$\begin{cases} p/p_\infty = 1 + p_1\chi + p_2\chi^2 + p_3\chi^3\,\ell n\chi \\ \delta^*/x = \delta_0^*\,(1+\delta_1^*\chi - 2\epsilon_2\chi^2\,\ell n\chi^2 + \delta_2^*\chi^2) \\ \dfrac{C_f(Re_x/C)^{1/2}}{0.664} = 1 + C_{f_1}\chi + 2\epsilon_2\chi^2\ell n\chi + C_{f_2}\chi^2 \end{cases} \tag{A23}$$

where

$$p_1 = -7K_3m_1$$

$$p_2 = 3.5K_3\{\,[(8m_\infty - 1)/K_2]m_1^2 - 2m_2\}$$

$$p_3 = [14m_\infty/(1+m_\infty)]m_3$$

$$\delta_0^* = K_1\,\frac{\delta_0}{(Re_x/C)^{\frac{1}{2}}}$$

$$\delta_1^* = \left[6K_3 + 2 - (2/K_1)\right]m_1 + \delta_1 + (m_\infty/K_1)h_1$$

$$\delta_2^* = \left[6K_3 + \frac{2m_\infty}{K_1}\right]m_2 + \delta_2 + \frac{m_\infty}{K_1}\,h_2 +$$

$$K_3\left[\frac{3+15m_\infty}{K_2} + \frac{1+17.611m_\infty}{K_1}\right]m_1^2 + \qquad \text{(A24)}$$

$$2\,\frac{K_3}{K_1}\,(1 + 4m_\infty)m_1h_1 + \frac{m_\infty}{K_1}\,h_1\delta_1 + \left[6K_3+2 - \frac{2}{K_1}\right]m_1\delta_1$$

$$C_{f_1} = 6.5661h_1 - \delta_1 + \left[(1-8m_\infty)/K_2\right]m_1$$

$$C_{f_2} = 6.5661h_2 - 6.8435h_1^2 + \delta_1^2 - \delta_2 + \frac{1-8m_\infty}{K_2}\,m_2 +$$

$$\frac{45K_3(8m_\infty-3)}{K_2}\,m_1^2 + \frac{8m_\infty-1}{K_2}\,m_1\delta_1 -$$

$$6.5661h_1\left[\delta_1 + \frac{(8m_\infty-1)}{K_2}\,m_1\right]$$

where

$$K_1 = 1 + 1.3842m_\infty \qquad K_2 = 1+m_\infty$$

$$K_3 = m_\infty/K_2$$

For large values of m_∞, Eqn. (A23) becomes

$$\begin{cases} p/p_\infty = 1 + 0.334\overline{\chi} + 0.0478\overline{\chi}^2 \\ \dfrac{\delta^*}{x} = 0.4772\,\dfrac{M_\infty^2}{(Re_x/C)^{\frac{1}{2}}}\,\left[1 - 0.093\overline{\chi} \ldots\right] \\ C_f(Re_x/C)^{\frac{1}{2}} = 0.664 + 0.114\overline{\chi} + \ldots \end{cases} \qquad \text{(A25)}$$

Compare with the results quoted in ref. 11 for Pr = 1

$$p/p_\infty = 1 + 0.335\bar{\chi} + 0.0481\bar{\chi}^2$$

$$\delta^* = 0.4788 \frac{M_\infty^2}{[(Re_x/C)^{\frac{1}{2}}]} \qquad \text{(A26)}$$

$$C_f(Re_x/C)^{\frac{1}{2}} = 0.664 + 0.115\bar{\chi}$$

The perfect agreement between two approaches is expected because of the identity of the Prandtl-Meyer flow and tangent wedge approximations to the second order in small angles. However, the finite Mach number effect can be seen from the previous expansions to be quite large. For example, at $M_\infty = 5.8$ the expansion for static pressure is

$$p/p_\infty = 1 + 0.3756\bar{\chi} + 0.0771\bar{\chi}^2 + 0.0061\bar{\chi}^3 \ln(0.04\bar{\chi}) \qquad \text{(A27)}$$

This explains, at least partially, why the pressure measured by J. Kendall[12] at $M_\infty = 5.8$ is higher than the values given by (A26); but much better agreement was obtained for Bertram's experiments, which were carried out at a nominal Mach number of 9.6.[13] The static pressure curve given by Eqn. (A27) is shown in Fig. 11 together with Kendall's data.[12] Also shown on the same plot is the limiting case of infinite Mach number indicating the finite Mach number effect.

Appendix B: Transitional Data

Because of the difficulty in obtaining a laminar flow over the complete model in the present testing facility, a large portion of the experimental results have to be categorized as transitional or turbulent. It has been shown by various workers (e.g., Lewis, Needham, Chapman, et al.) that a transitional or turbulent separated flow is markedly different from a laminar one. The comparison of the transitional data with the results of a laminar theory is therefore excluded from the main text. This appendix serves the purpose of collecting the transitional data and hoping to provide some clue to a possible reformed transitional or turbulent theory.

The measured static pressure distributions at three different freestream Reynolds numbers for models A-1 and A-2 are plotted in Figs. B-1 to B-3. The flows on the model for these cases have been classified as transitional judging from the measured Mach number profiles. Nevertheless, the calculated distributions of the present laminar theory are also shown in the corresponding plots for comparison.

At a freestream Reynolds number per inch of 91,000, the agreement is fairly good. The difference appears in the relatively abrupt change in the slope of the static pressure distribution about 1'' after the theoretically predicted reattachment point. This change in slope may be explained by the additional cushioning effect to the flow provided by the relatively thicker boundary layer when it becomes transitional. The region where such deviation in slope occurs coincides with the station having a fuller Mach number profile than

the asymptotic laminar one. As the freestream Reynolds number increases, transition occurs further upstream. Based on the previous theoretical considerations, we have learned that the extent of upstream influence of a sharp corner is limited to a few boundary-layer thicknesses. Therefore, we may assume that as long as transition occurs several boundary-layer thicknesses downstream of the theoretically predicted reattachrnent point, the separation phenomena is practically laminar. The flow at $Re_\infty/in. = 91,000$ is likely to be this case as indicated in Fig. B-1. However, as the transition region moves closer to the reattachment point, or even ahead of it, the overall flow becomes what Chapman[2] classified as a transitional separation. The two larger Reynolds number cases shown in Figs. B-2 and B-3 correspond to this situation. The effects of transition, as indicated by these results, are delaying the separation and lowering the pressure level at the corresponding station from the laminar case.

It is also interesting to note that the trend of falling pressure near the end of the model, which is predicted theoretically and observed experimentally when laminar flow prevails over the complete model, is no longer observed in these transitional cases. This is expected for a transitional flow and incidentally provides a means to detect the existence of a laminar flow over the complete model.

The measured pressure distribution for models B-1 and B-2 at higher Reynolds numbers are shown in Figs. B-4 to B-9 together with the corresponding predictions of the laminar theory. The insufficient reattaching length bas also resulted in a laminar

flow over the complete model at higher Reynolds numbers. For model B-1, the measured Mach number profiles and the good agreement with the laminar theory (including the falling pressure at the end of the model) suggest the existence of a laminar separated flow up to Re_{∞} = 136, 000. For the shortest model tested **(B-2),** it is believed that a laminar flow existed over the complete model even for Re_{∞} = 210,000.

Figs. B-10 to B-12 show the effect of model length on the pressure distributions at higher Reynolds numbers. The effect of transition on the slope of the pressure distribution discussed previously is further confirmed by comparing the results of models B-1 and A-1. Fig. B-10 shows that the effect of transition on model A-1 does not affect the separated region as suggested for that Reynolds number. Some effect appears in Fig. B-11 for the case of Re_{∞} = 136, 000. For Re_{∞} = 210, 000, even model B-1 possesses a transitional flow. It may be noted that the pressure at corresponding station after the plateau becomes consistently higher for the shorter model, which is again a consequence of the decreasing level of fluctuation for the shorter model.

A Reynolds number correlation is intended by using model **A-3.** By varying the freestream conditions, the results of model A-3 may be compared with that of model A-2. Fig. B-13 shows the correlation of the surface pressure distributions. Because of the noise level existing in the present wind tunnel, both cases correspond to a transitional flow. The correlation is very good indeed. Fig. B-14 shows the correlation at a different Re_{x_C}. In order to **achieve**

the same Re_{x_c} for the two models, it turns out that model **A-3** has been tested at a freestream condition corresponding to a laminar boundary layer on the present wind-tunnel wall, which has kept the flow laminar over the complete model. On the other hand, the higher turbulence level at the freestream condition for model **A-2** has definitely caused a transitional flow on that model. Therefore, the correlation fails in Fig. B-14. However, it provides a further evidence on the effect of transition as indicated by the lower pressure at corresponding stations and the non-falling pressure at the end of the model.

References

1. Lewis, J. E., "Experimental Investigation of Supersonic Laminar, Two-dimensional Boundary Layer Separation in a Compression Corner with and without Cooling," Ph. D. thesis, 1967, California Institute of Technology; AIAA Journal, Vol. 6, No. 1, Jan. 1968, pp. 7-14.

2. Chapman, D. R., Kuehn, D. M. and Larson, H. K., "Investigation of Separated Flows in Supersonic and Subsonic Streams with Emphasis on the Effect of Transition," Rept. 1356, 1958, NACA.

3. Hakkinen, R. J. et al., "The Interaction of an Oblique Shock Wave with a Laminar Boundary Layer," Memo 2-18-59W, 1959, NASA.

4. Sterrett, J. R. and Emery, J. C., "Extension of Boundary Layer Separation Criteria to a Mach Number of 6. 5 by Utilizing Flat Plates with Forward Facing Steps," TN D-618, 1960, NASA.

5. Needham, D. A., "Laminar Separation in Hypersonic Flow," Ph. D. thesis, 1965, University of London.

6. Lees, L. and Reeves, B. L., "Supersonic Separated and Reattaching Laminar Flows: I. General Theory and Application to Adiabatic Boundary Layer-Shock Wave Interactions," AIAA Journal, Vol. 2, No. 11, Nov. 1964, pp. 1907-1920.

7. Klineberg, J. M., "Theory of Laminar Viscous-Inviscid Interactions in Supersonic Flow," Ph. D. thesis, 1968, California Institute of Technology.

8. Grange, J., Klineberg, J. M. and Lees, L., "Laminar Boundary-Layer Separation and Near-Wake Flow for a Smooth Blunt Body at Supersonic and Hypersonic Speeds," AIAA Journal, Vol. 5, No. 6, June 1967, pp. 1089-1096.

9. Ko, D. R. S. and Kubota, T., "Supersonic Laminar Boundary Layer along a Two-Dimensional Adiabatic Curved Ramp", AIAA 6th Aerospace Meeting, New York, N. Y., Jan. 22-24, 1968, #68-109.

10. Howarth, L., ed., Modern Developments in Fluid Dynamics, High Speed Flow. Vol. 1, Chap. 10, Boundary Layers. Oxford University Press, London, 1953.

11. Hayes, W. D. and Probstein, R. F., Hypersonic Flow Theory Academic Press Inc., New York, 1959.

12. Kendall, J. M., Jr., "An Experimental Investigation of Leading Edge Shock-Wave Boundary-layer Interaction at Mach 5.8," J. Aeronaut. Sci. 24, 47-56, 1957.

13. Bertram, M. H., "Boundary Layer Displacement Effects in Air at Mach Number of 6.8 and 9.6," **NACA TN** 4133, 1957.

Model Dimensions

Model	Rc	X_1/R_c	X_c	X_L	α_m	α_L
A-1	2.0"	1.0	2.175"	6.0"	10.15°	100°
A-2	11.6"	0.1	2.175"	6.0"	10.12°	100°
B-1	2.0"	1.0	2.175"	4.0"	10.15°	100°
B-2	2.0"	1.0	2.175"	3.0"	10.15°	100°
B-2-1	2.0"	1.0	2.175"	3.0"	10.15°	10°
A-3	20.0"	0.1	3.75"	9.4"	10.15°	100°

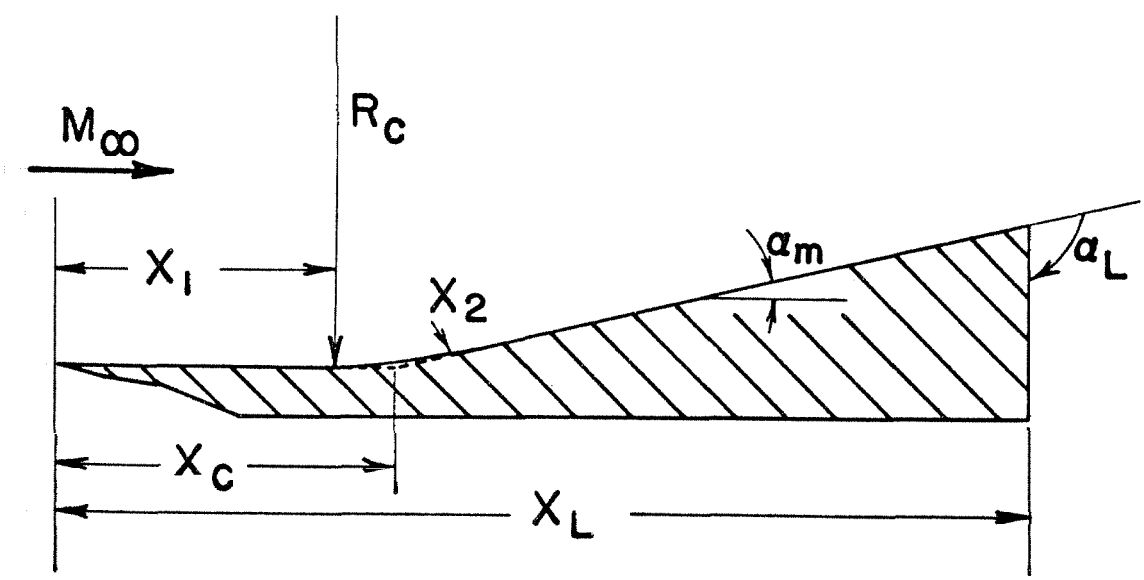

FIG. 1 MODEL CONFIGURATION **AND DIMENSIONS**

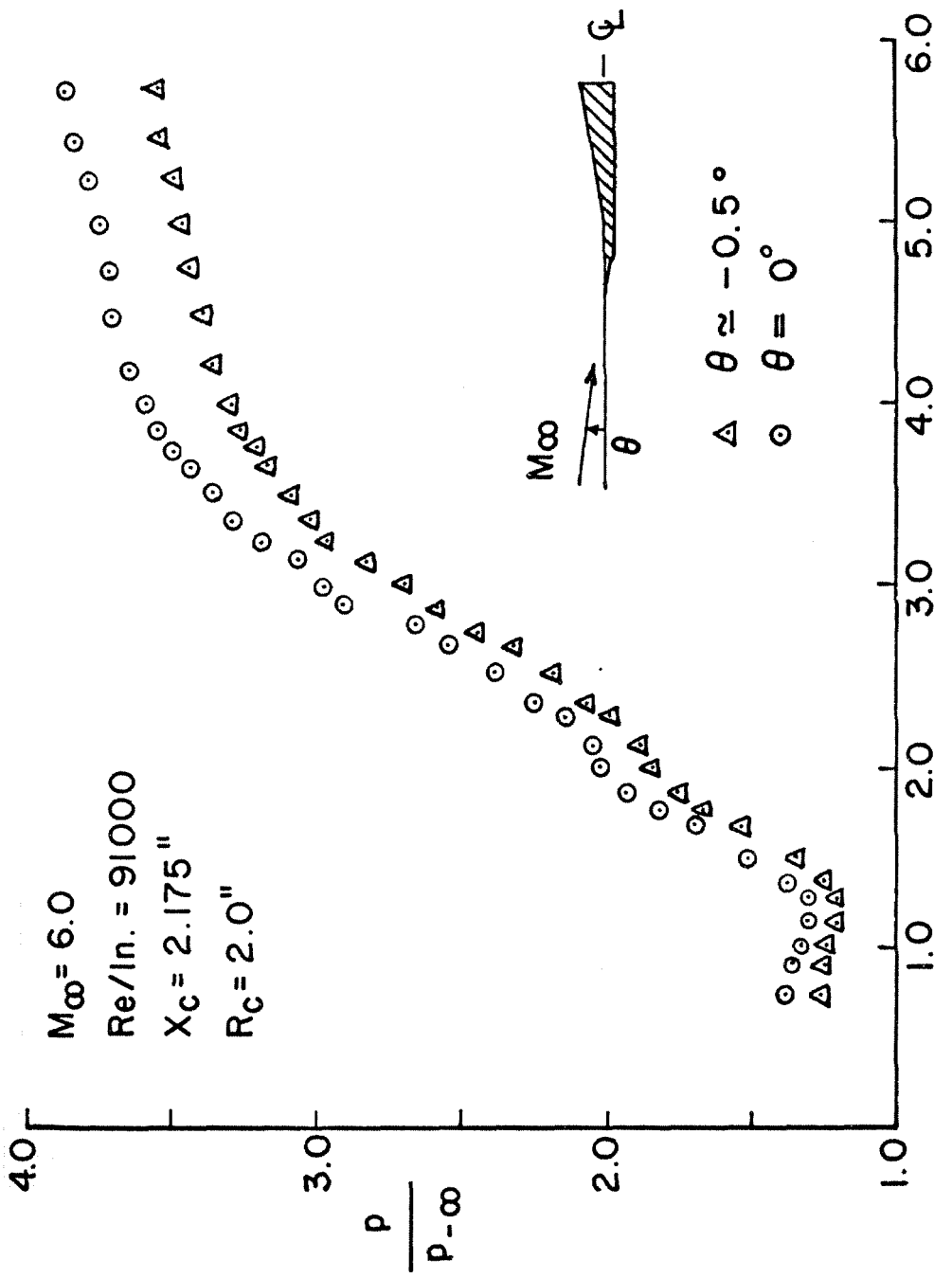

FIG. 2 EFFECT OF ANGLE OF ATTACK

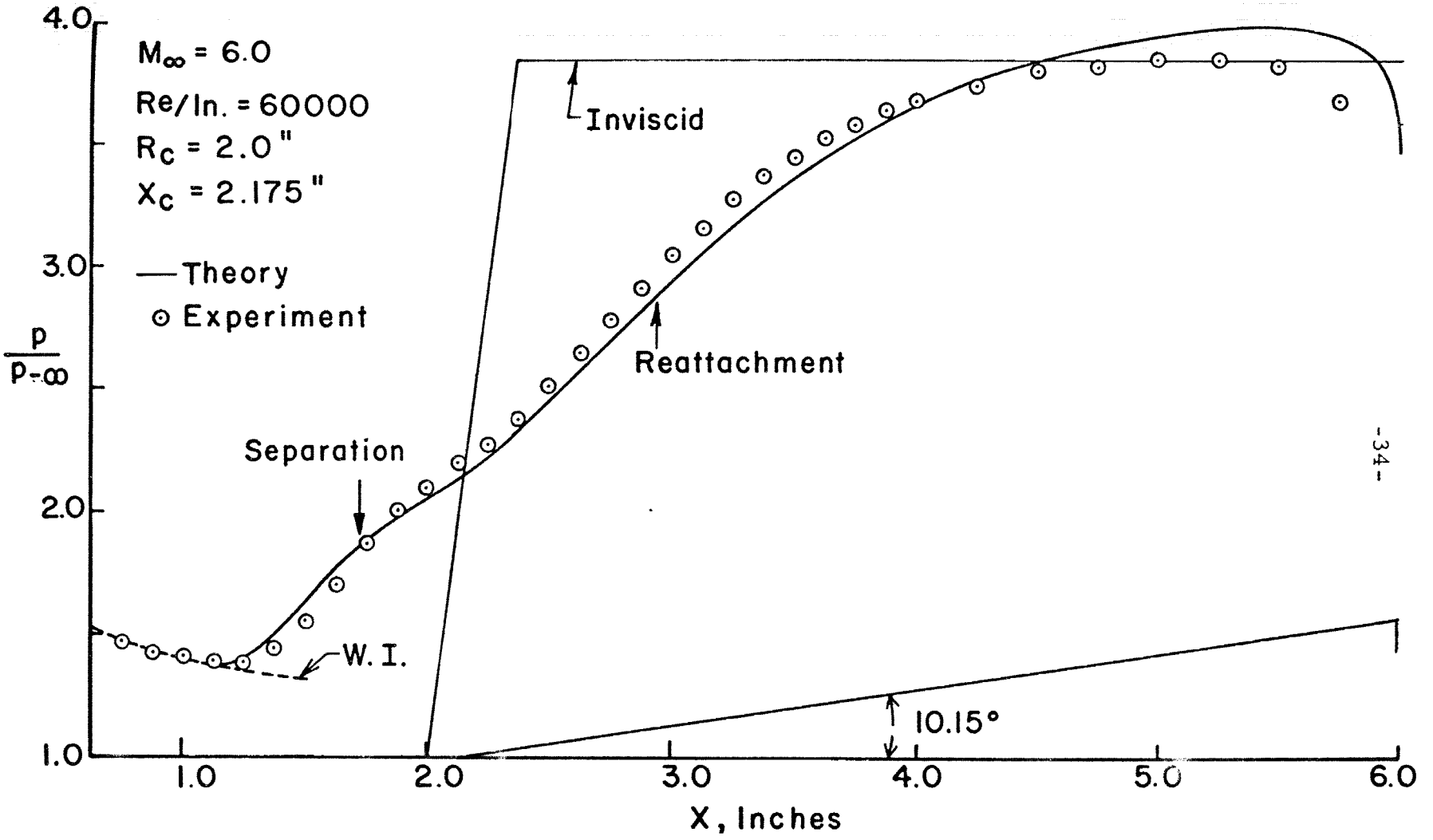

FIG. 3 COMPARISON OF STATIC PRESSURE RESULT

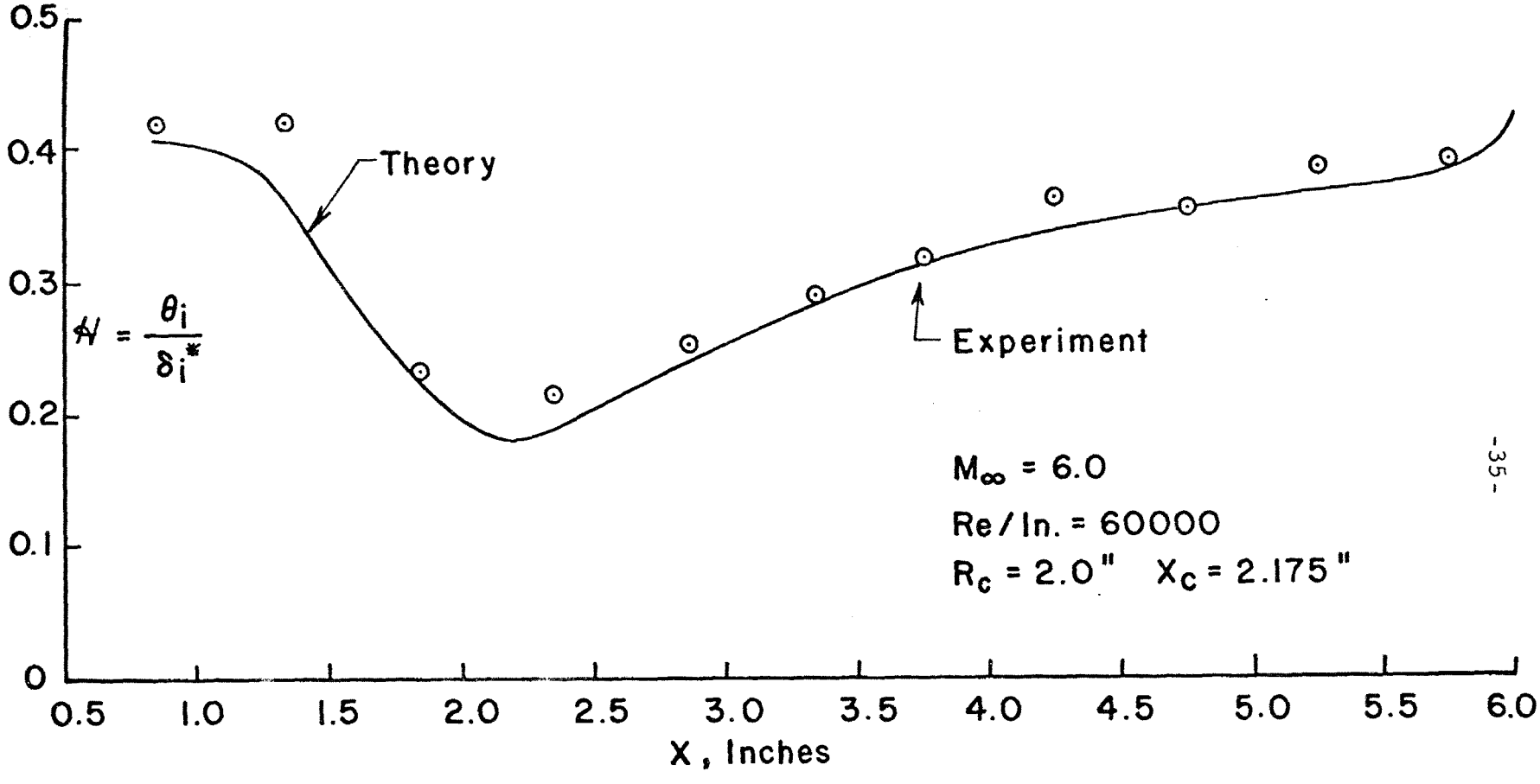

FIG. 4 COMPARISON OF Λ

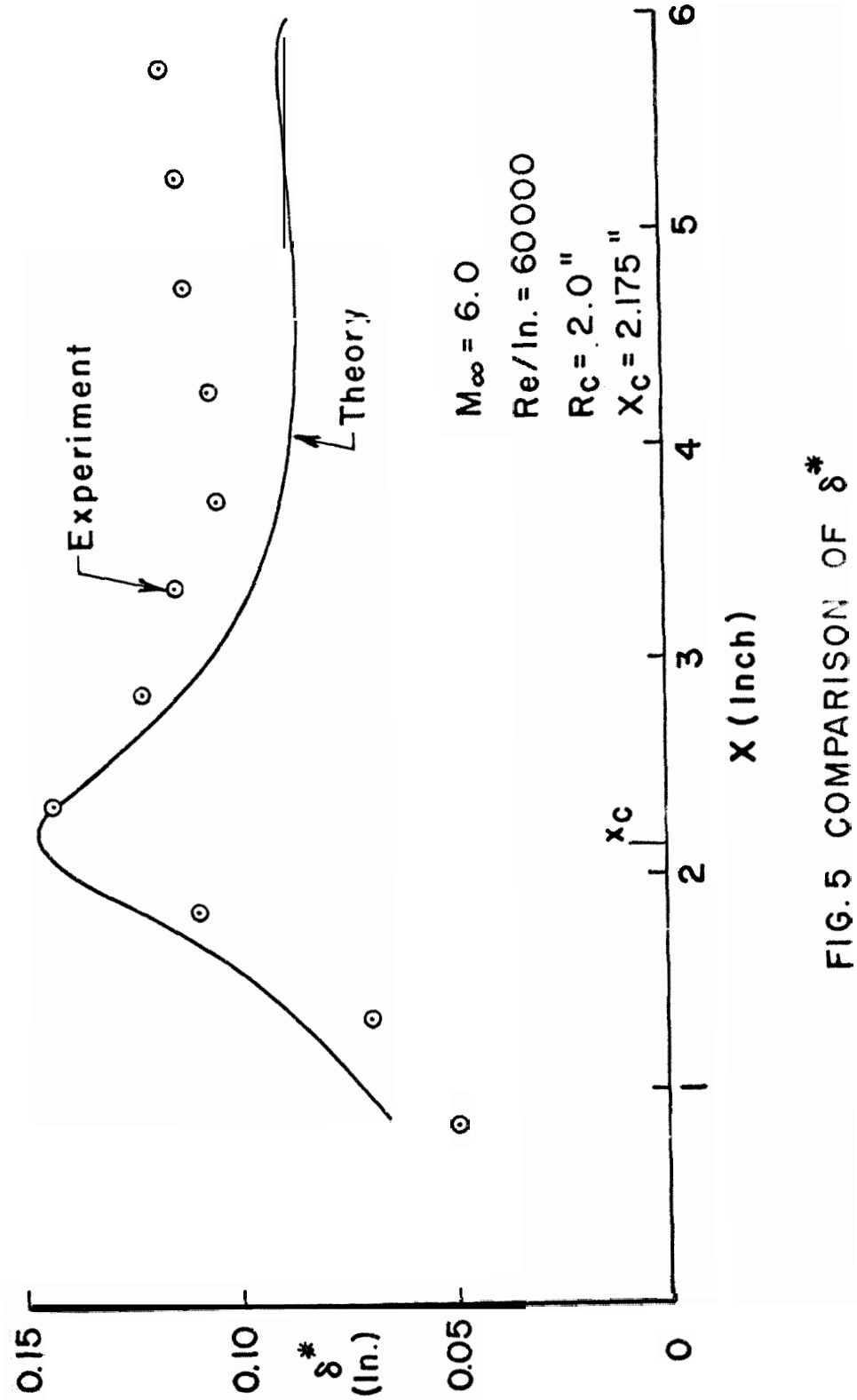

FIG. 5 COMPARISON OF δ^*

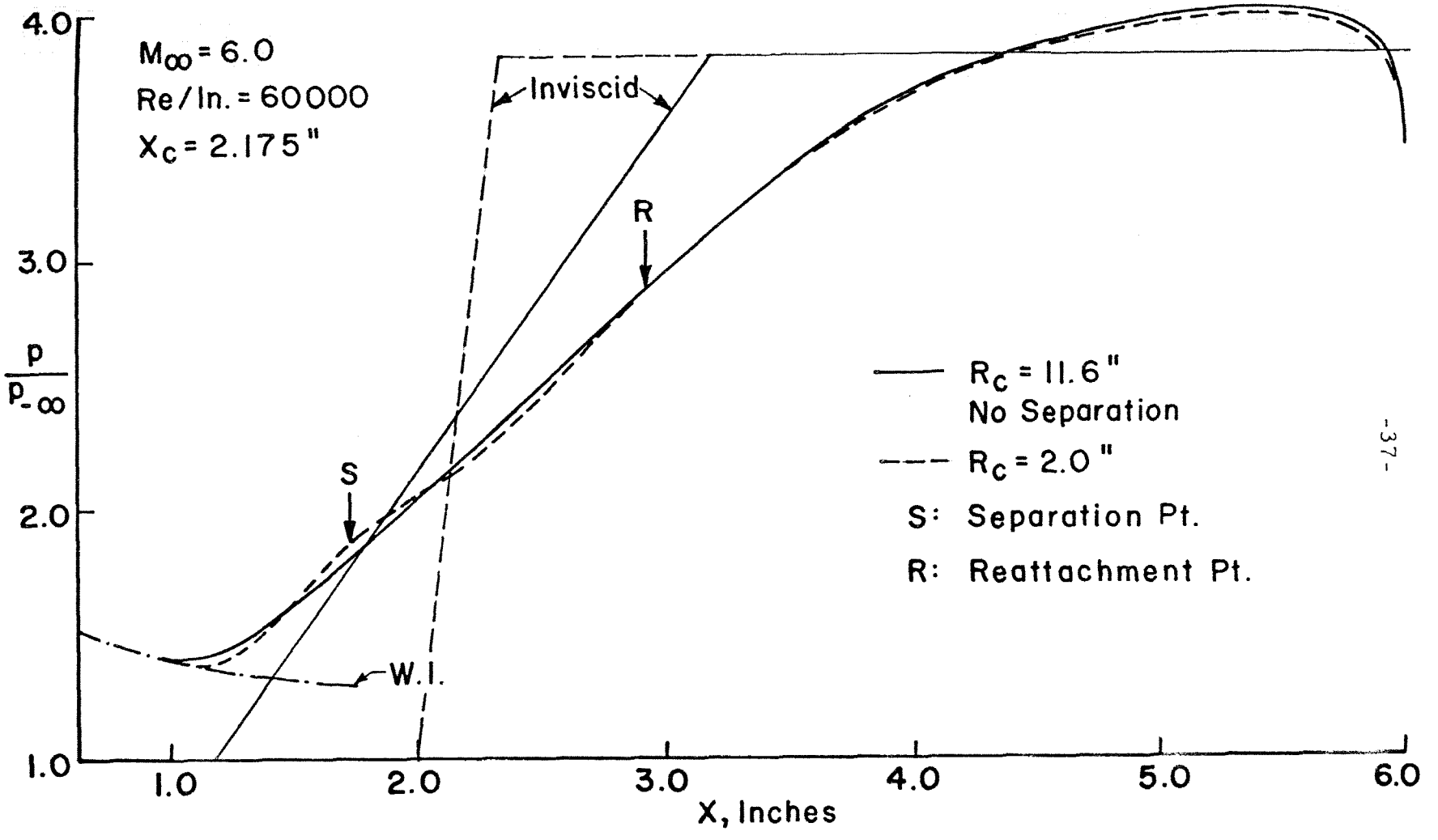

FIG. 6 CURVATURE EFFECT (THEORETICAL)

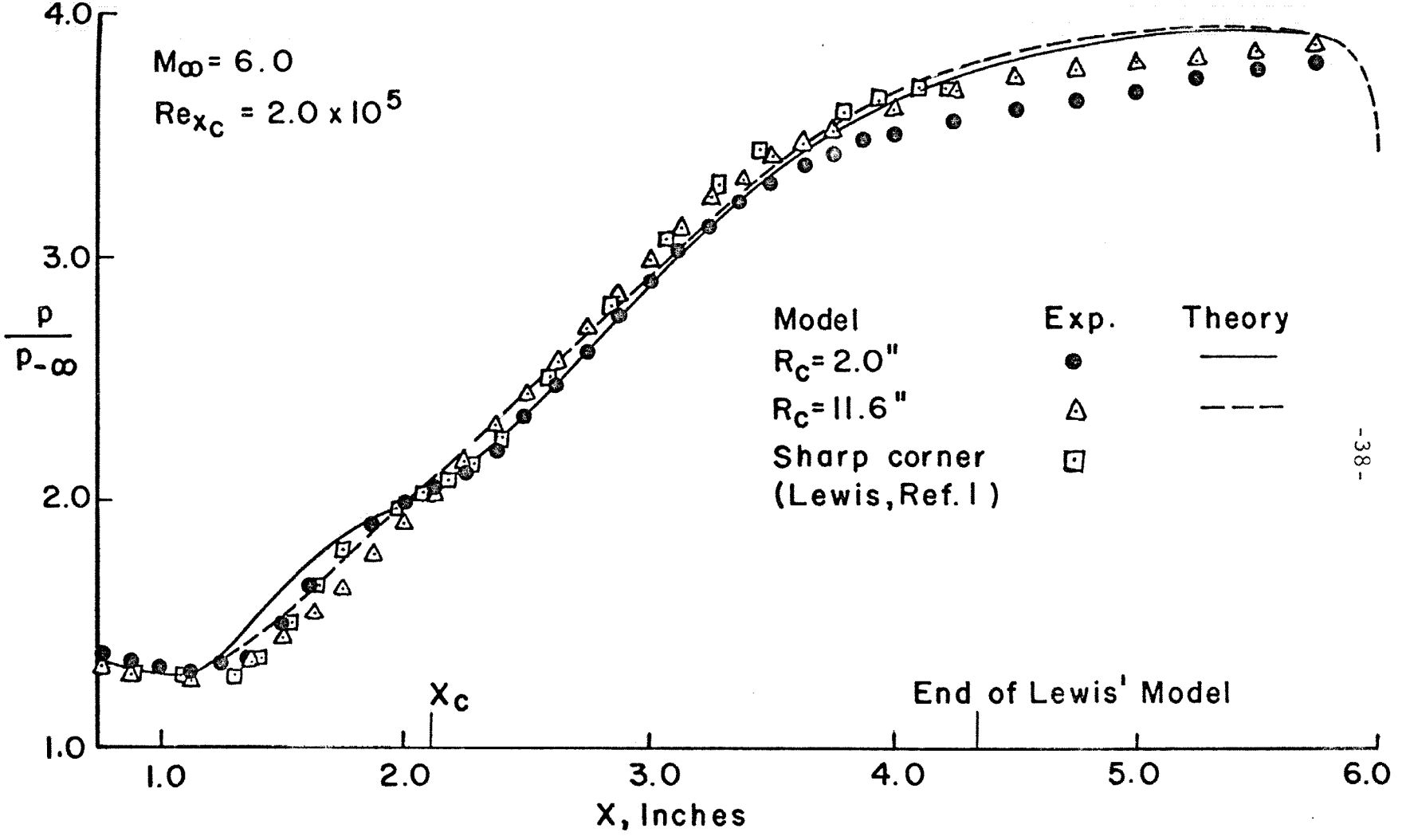

FIG. 7 CURVATURE EFFECT (EXPERIMENTAL)

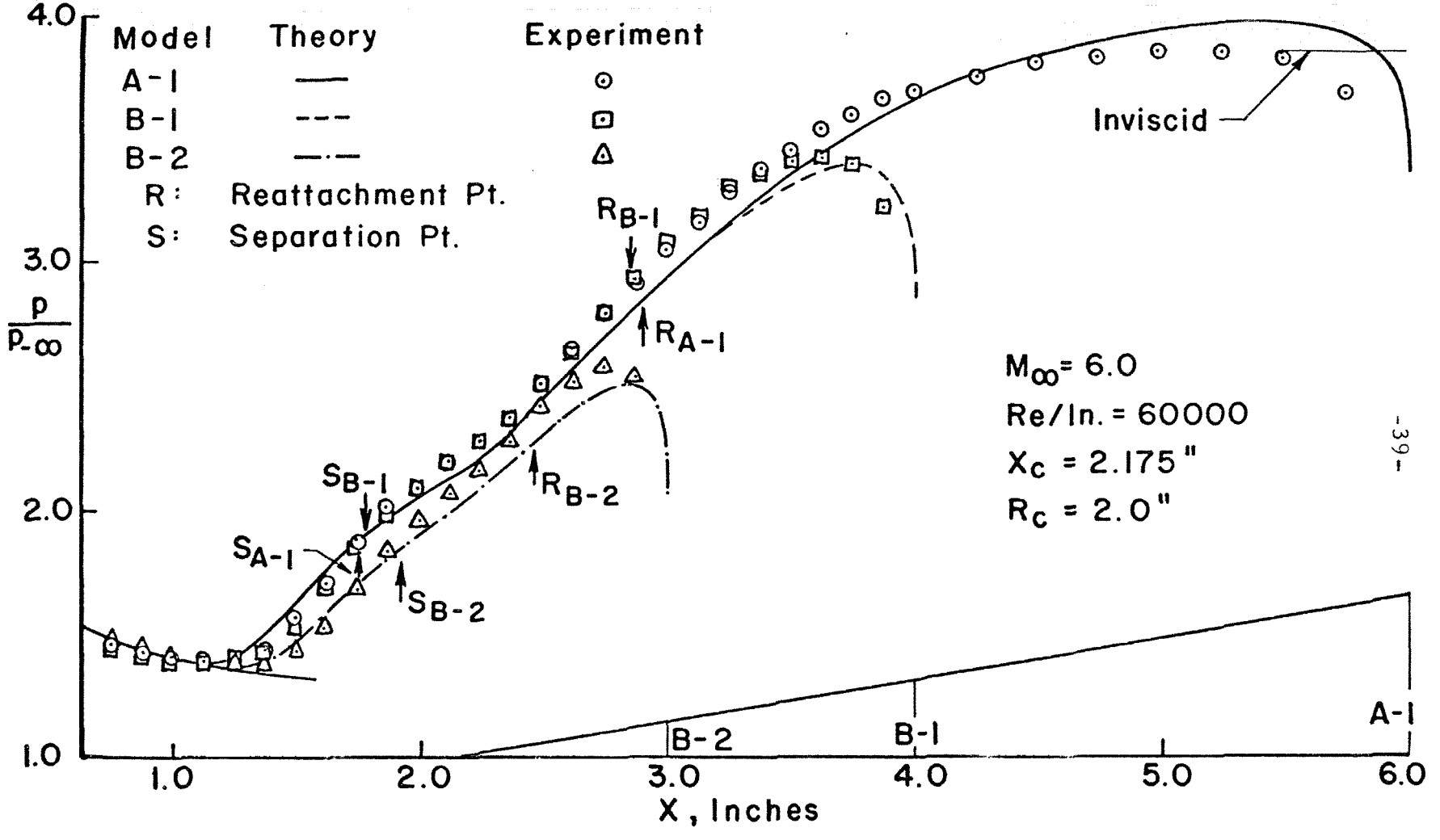

FIG. 8 EFFECT OF RAMP LENGTH (EXPERIMENTAL AND THEORETICAL)

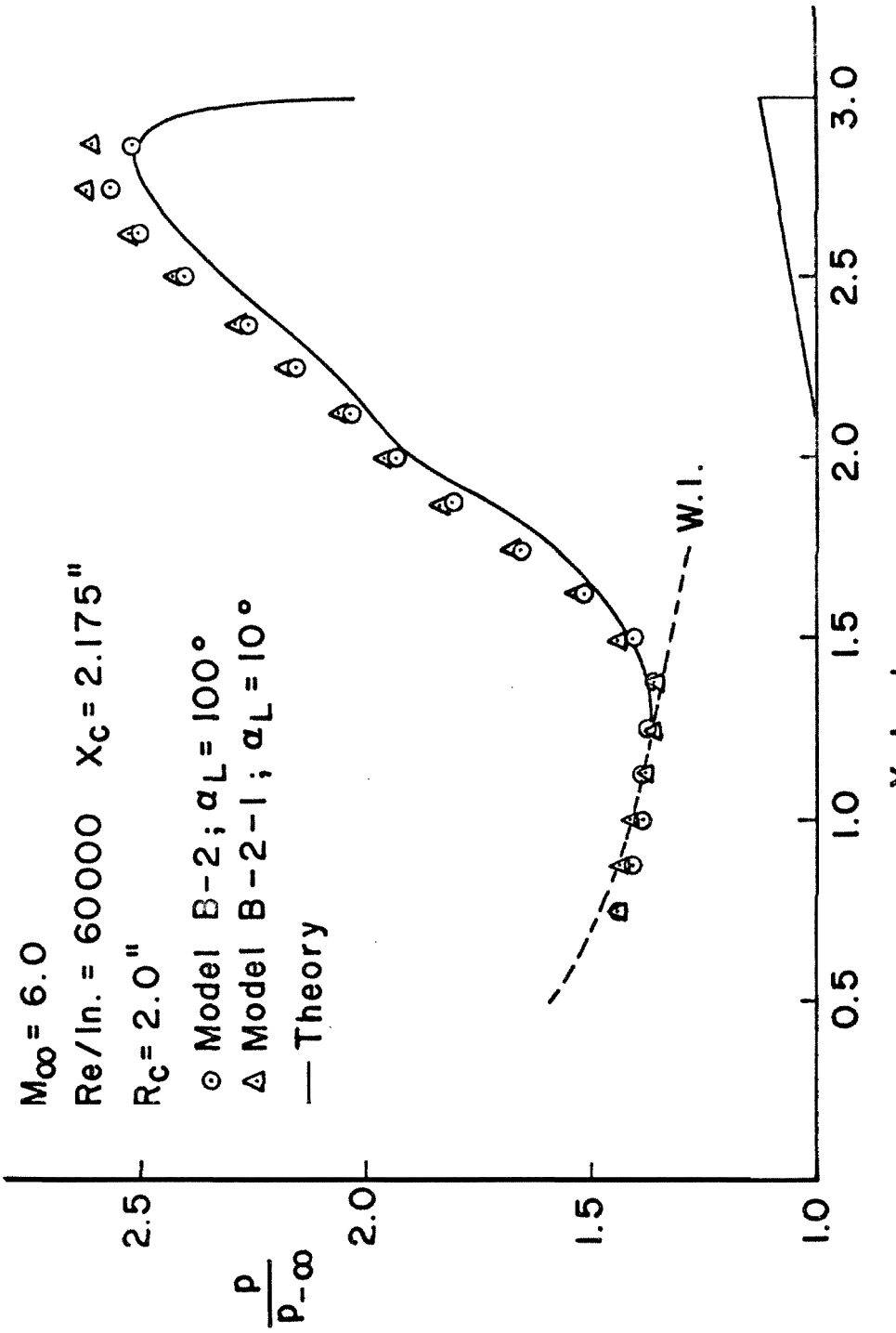

FIG. 9 EFFECT OF EXPANSION ANGLE AT TRAILING EDGE

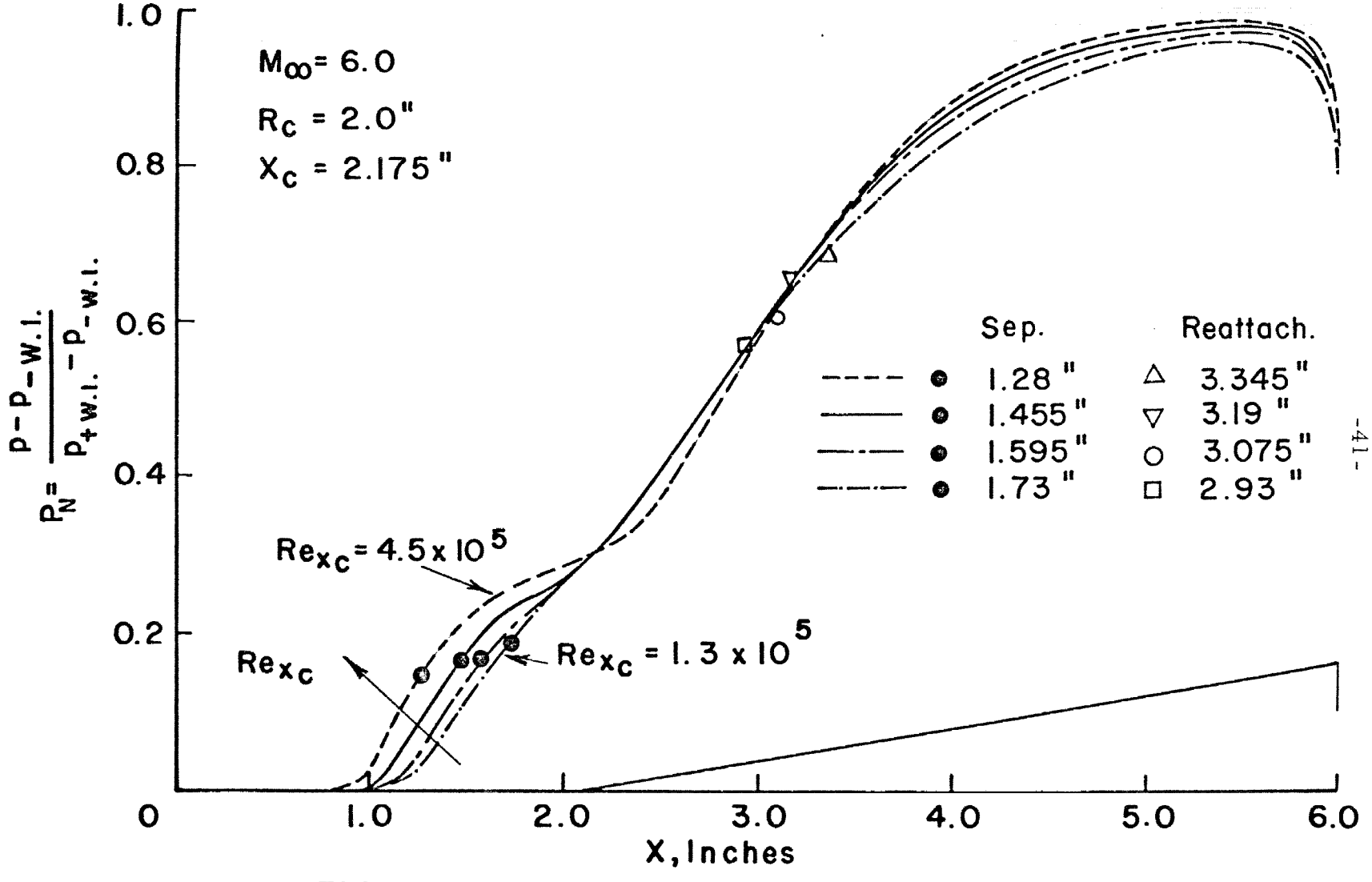

FIG. 10 REYNOLDS NUMBER EFFECT (THEORETICAL)

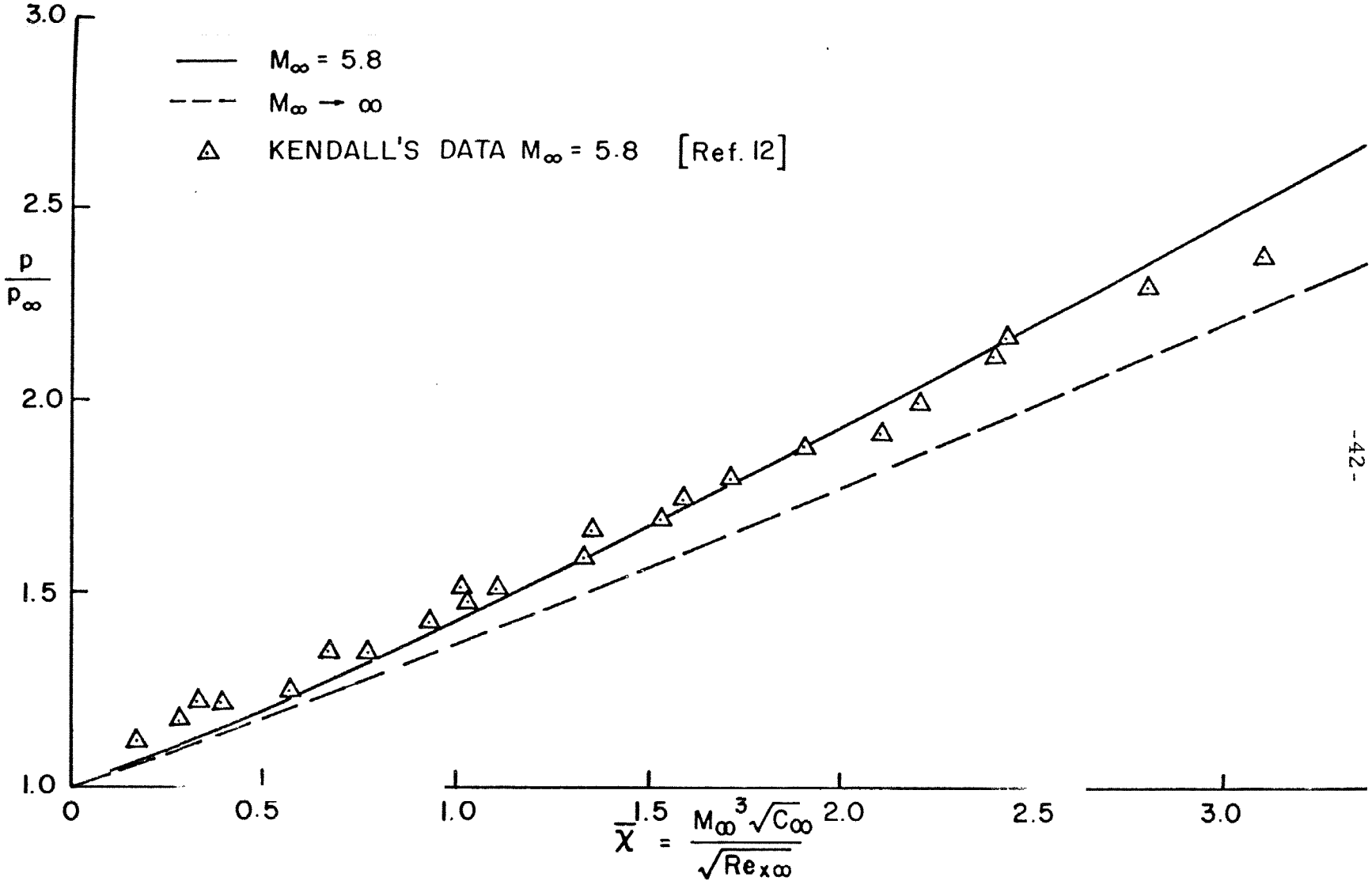

FIG. II EFFECT OF FINITE MACH NUMBER ON WEAK INTERACTION INDUCED PRESSURE

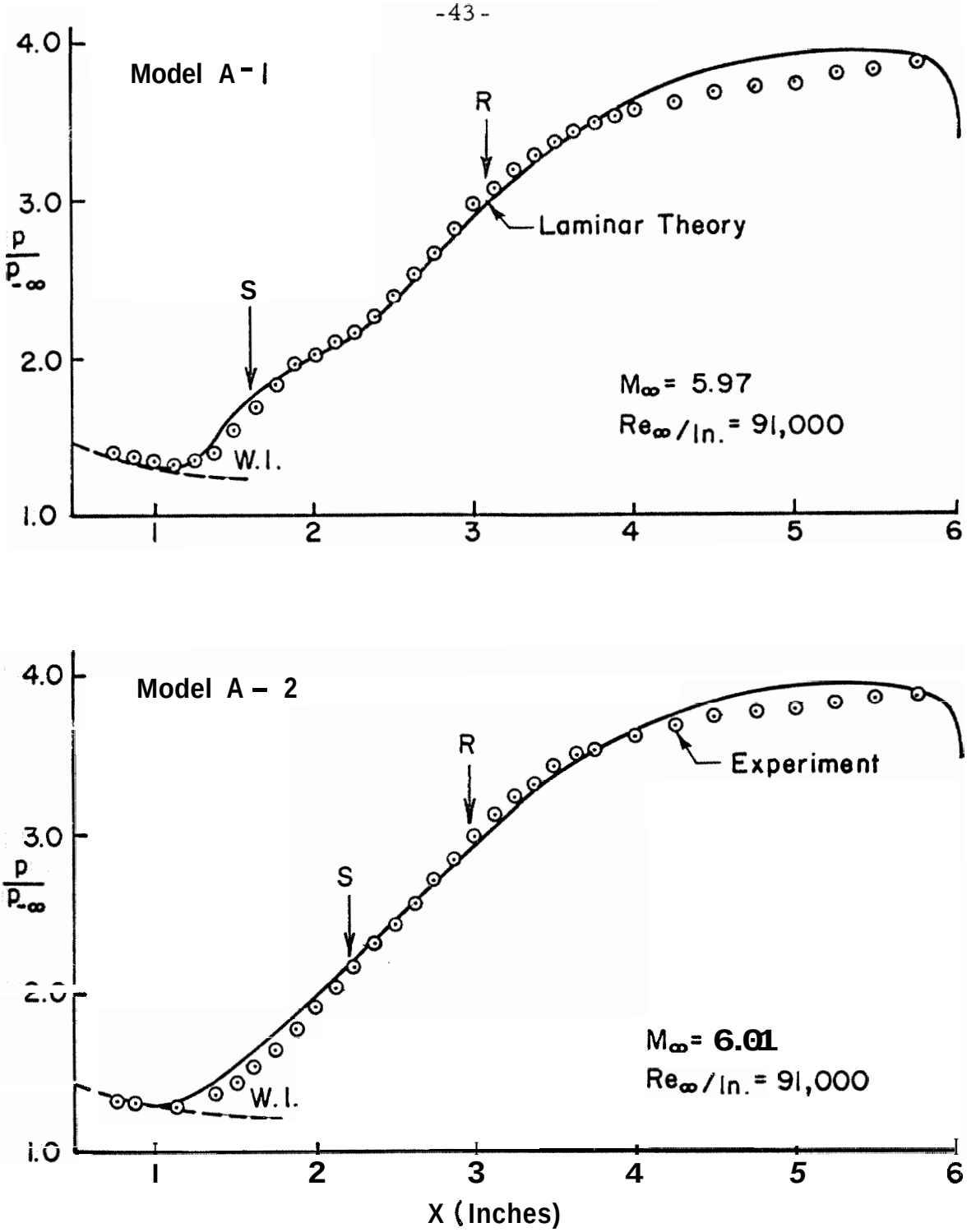

Fig. B1. Static Pressure Distributions for Models A-1 and A-2 at Re_∞/in. = 91,000

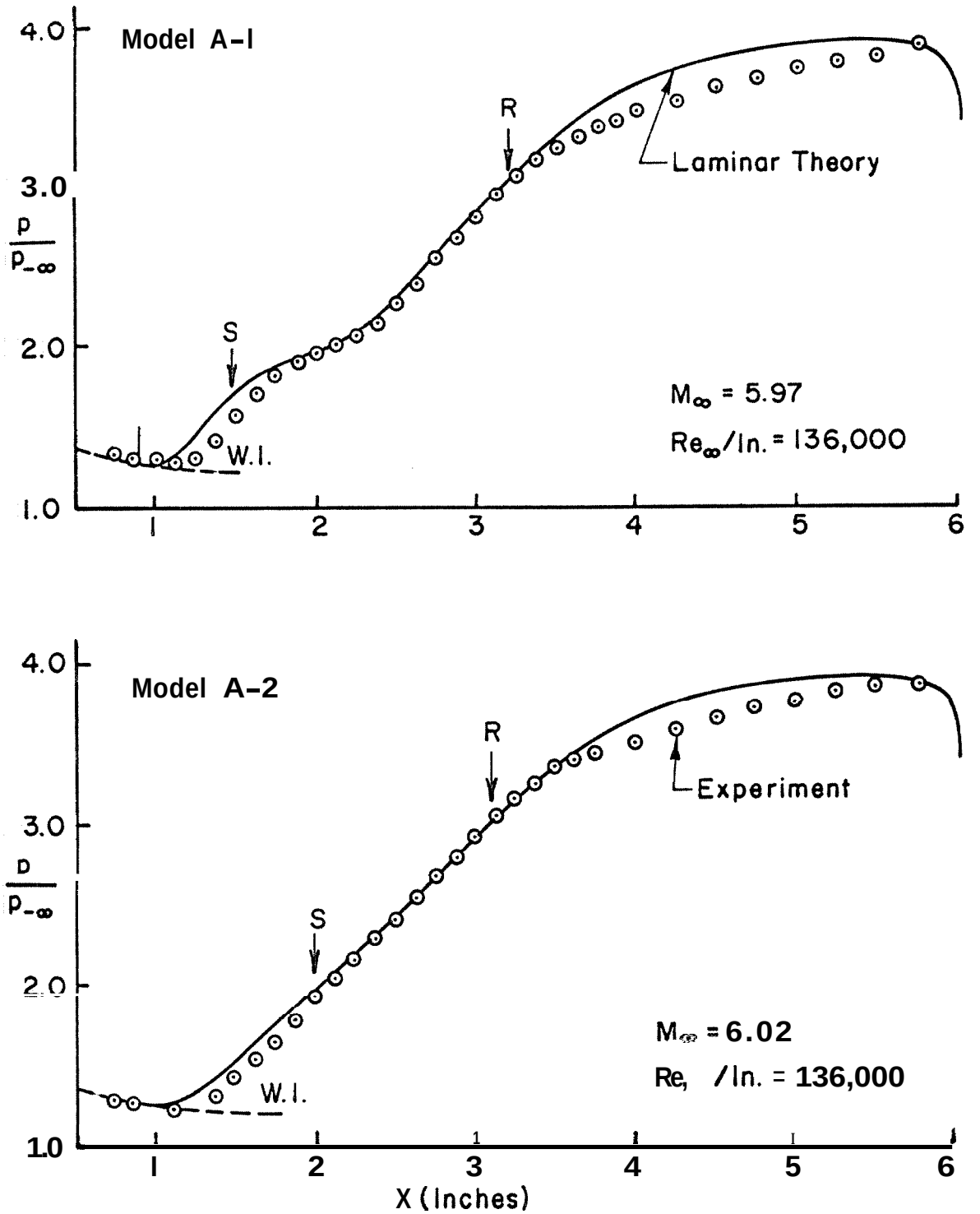

Fig. B2. Static Pressure Distributions for Models A-1 and A-2 at $Re_\infty/in. = 136,000$

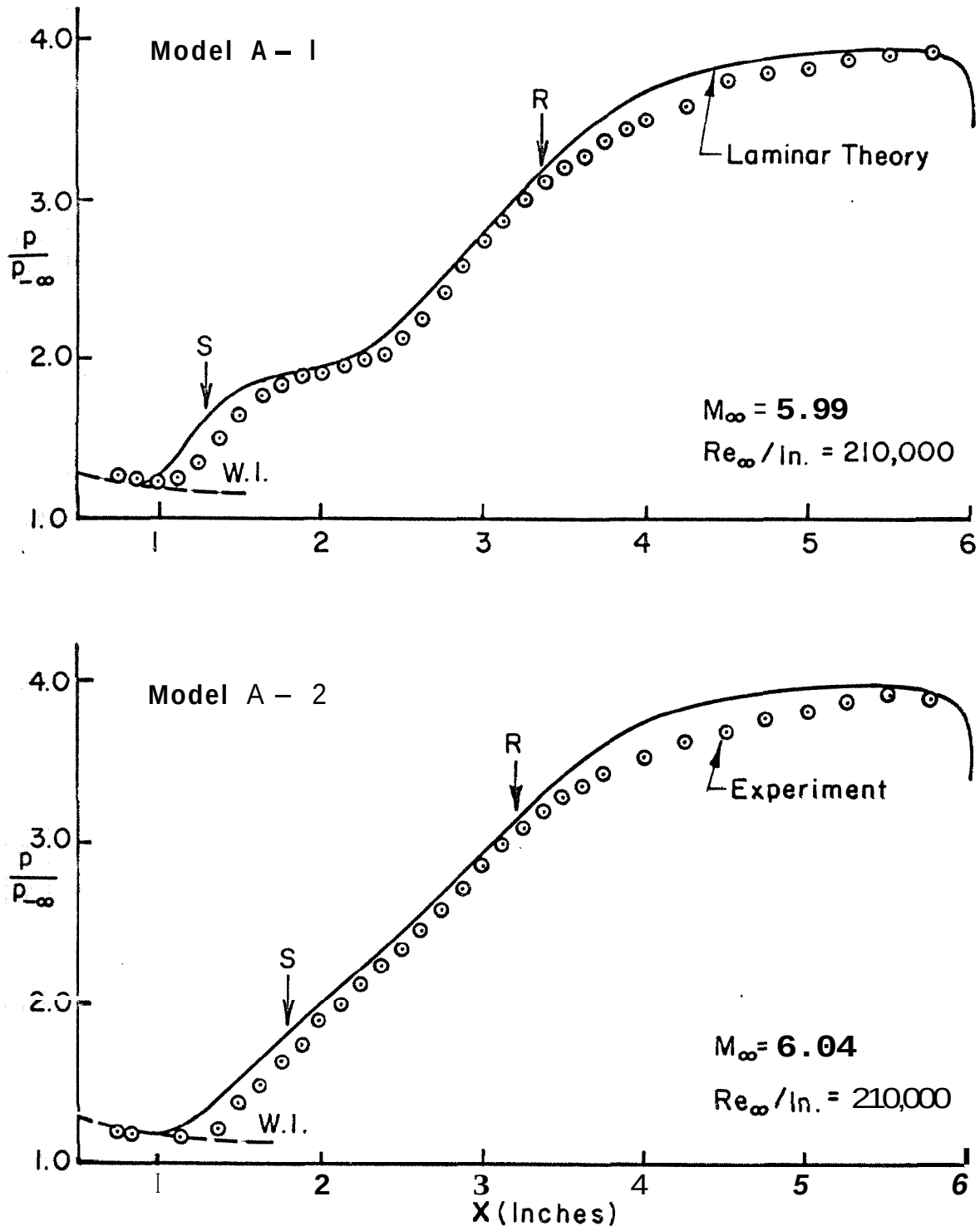

Fig. B3. Static Pressure Distributions for Models A-1 and A-2 at Re_∞/in. = 210,000

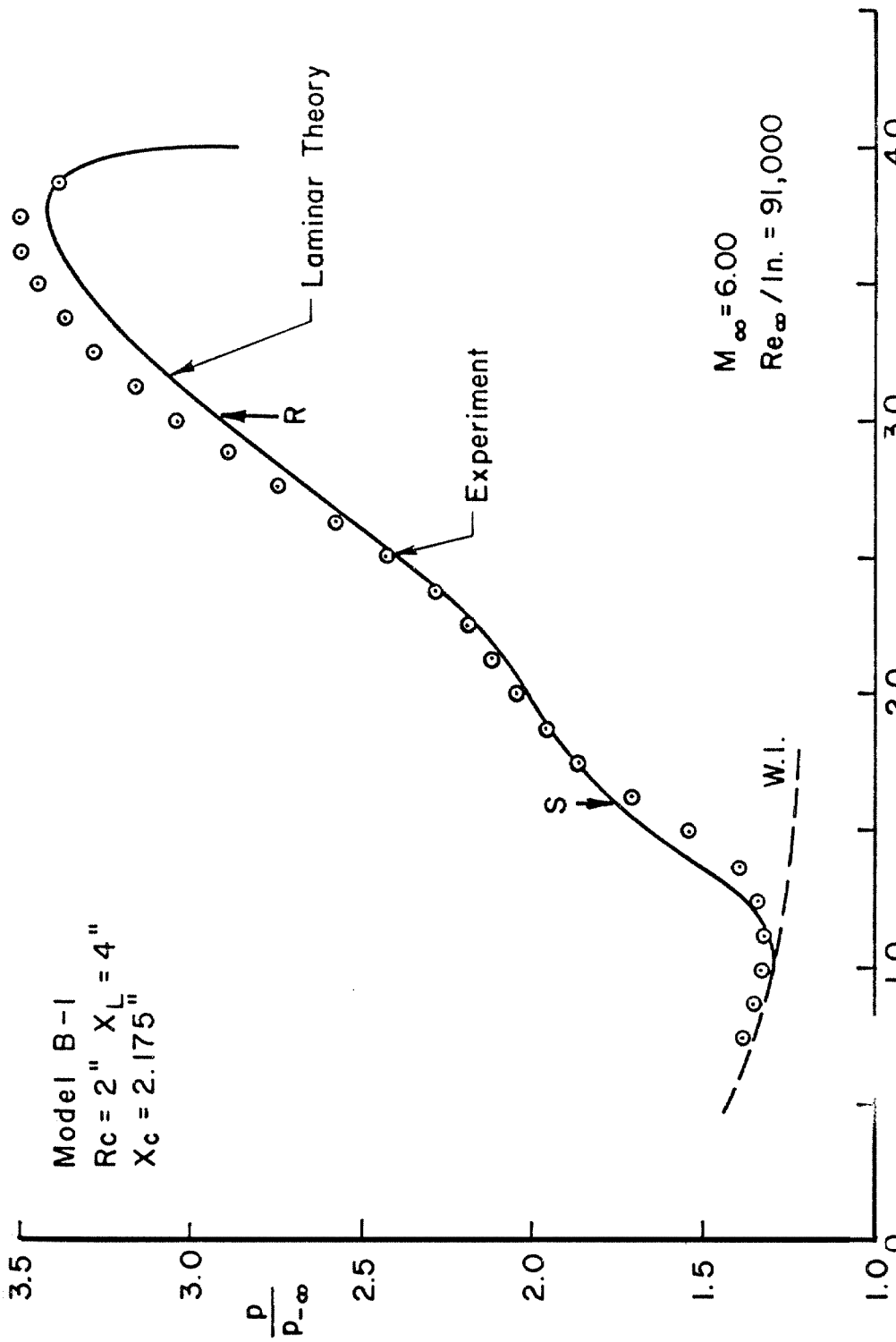

Fig. B4. Static Pressure Distribution for Model B-1 at Re_∞/in. = 91,000

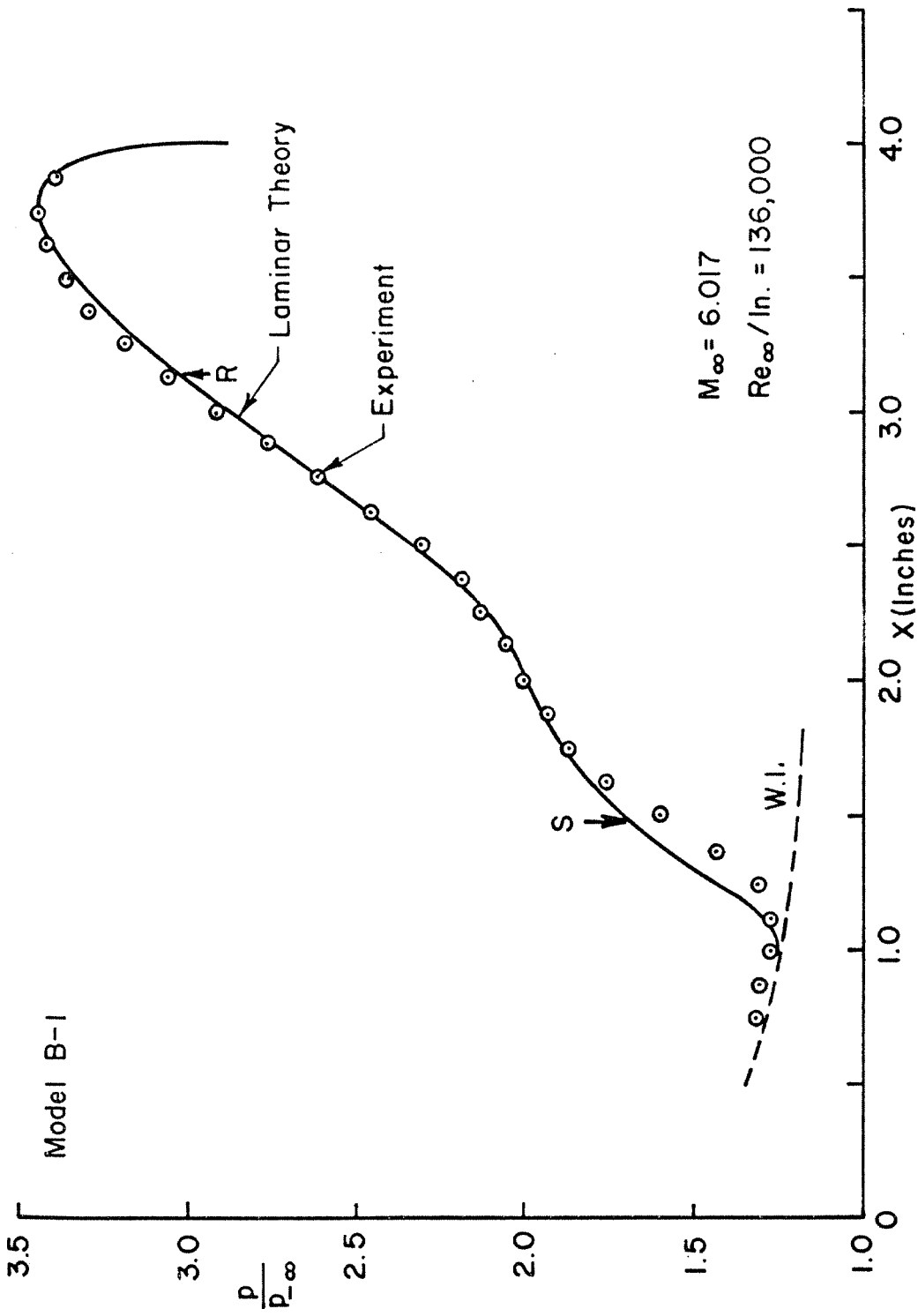

Fig. B5. Static Pressure Distribution for Model B-1 at Re_∞/in. = 136,000

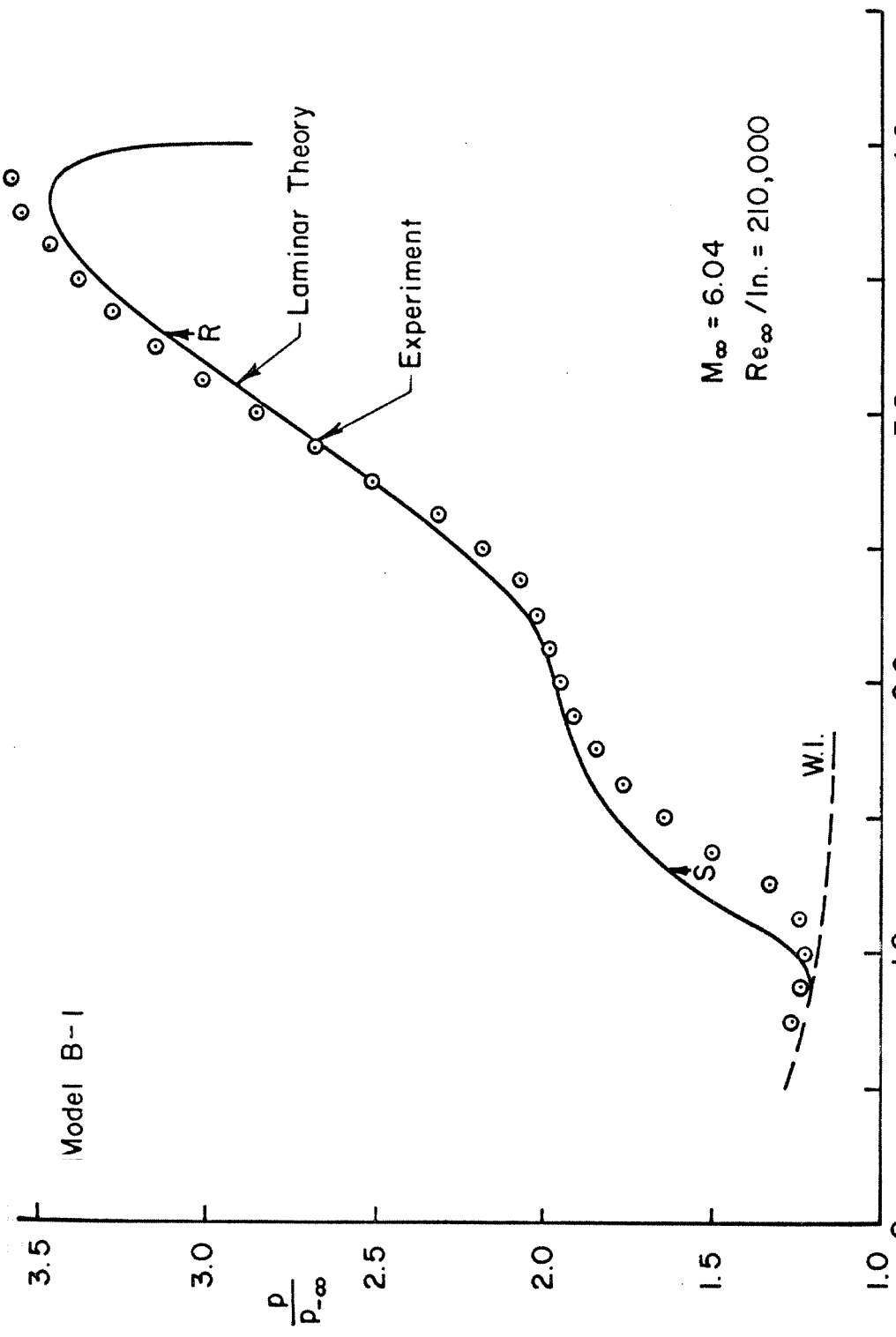

Fig. B6. Static Pressure Distribution for Model B-1 at Re_∞/in. = 210,000

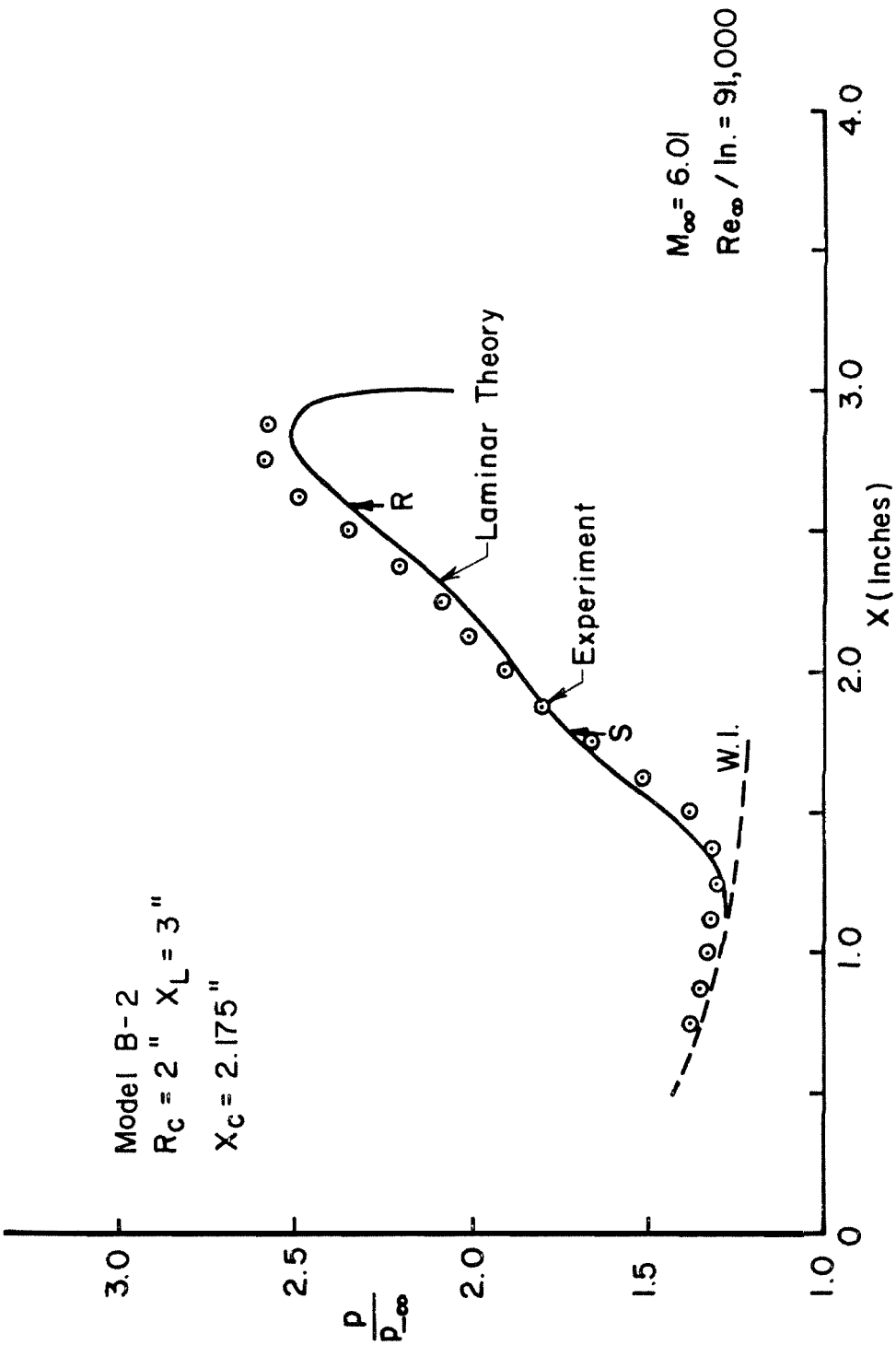

Fig. B7. Static Pressure Distribution for Model B-2 at Re_∞/in. = 91,000

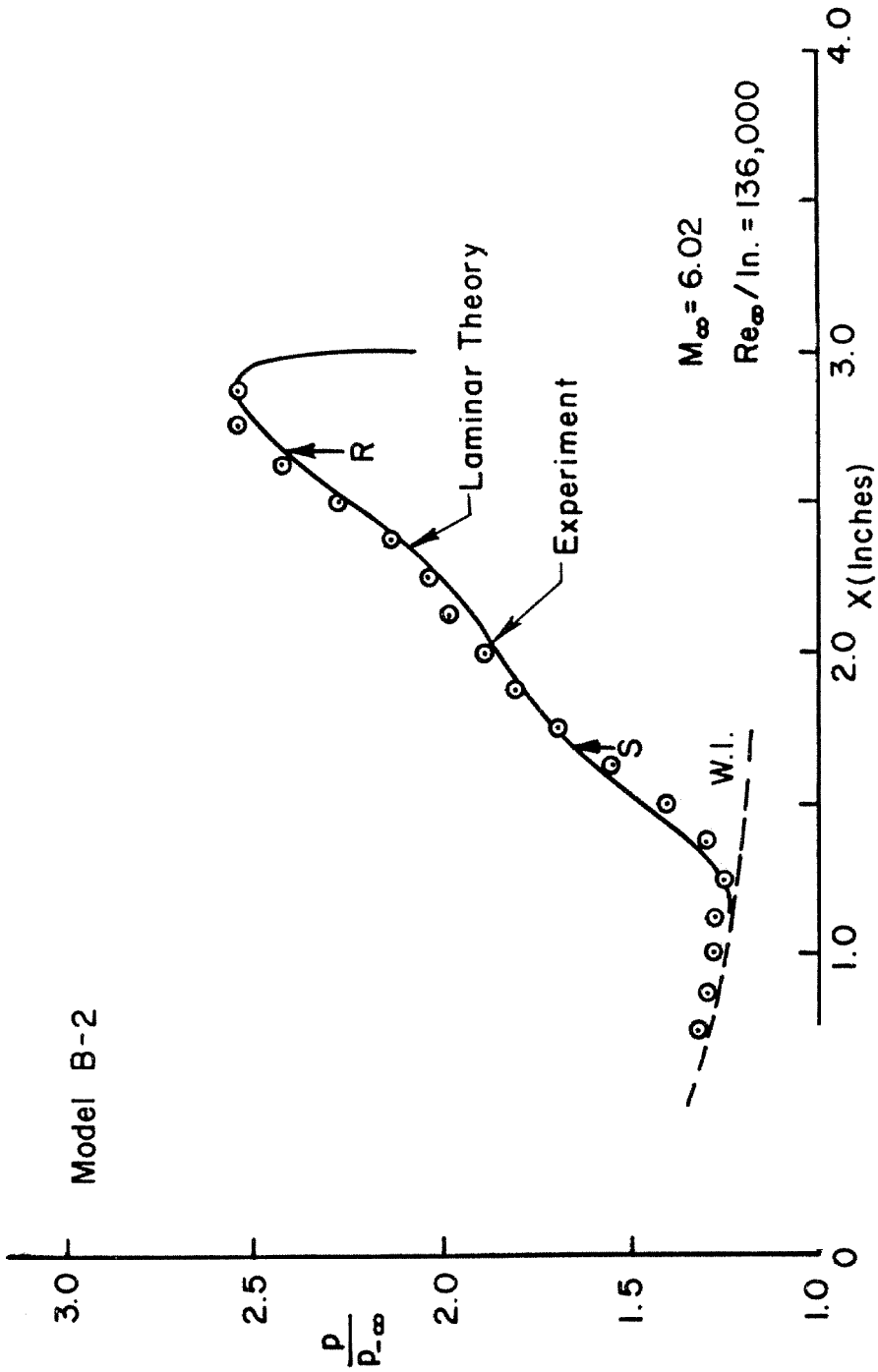

Fig. B8. Static Pressure Distribution for Model B-2 at $Re_\infty/in. = 136,000$

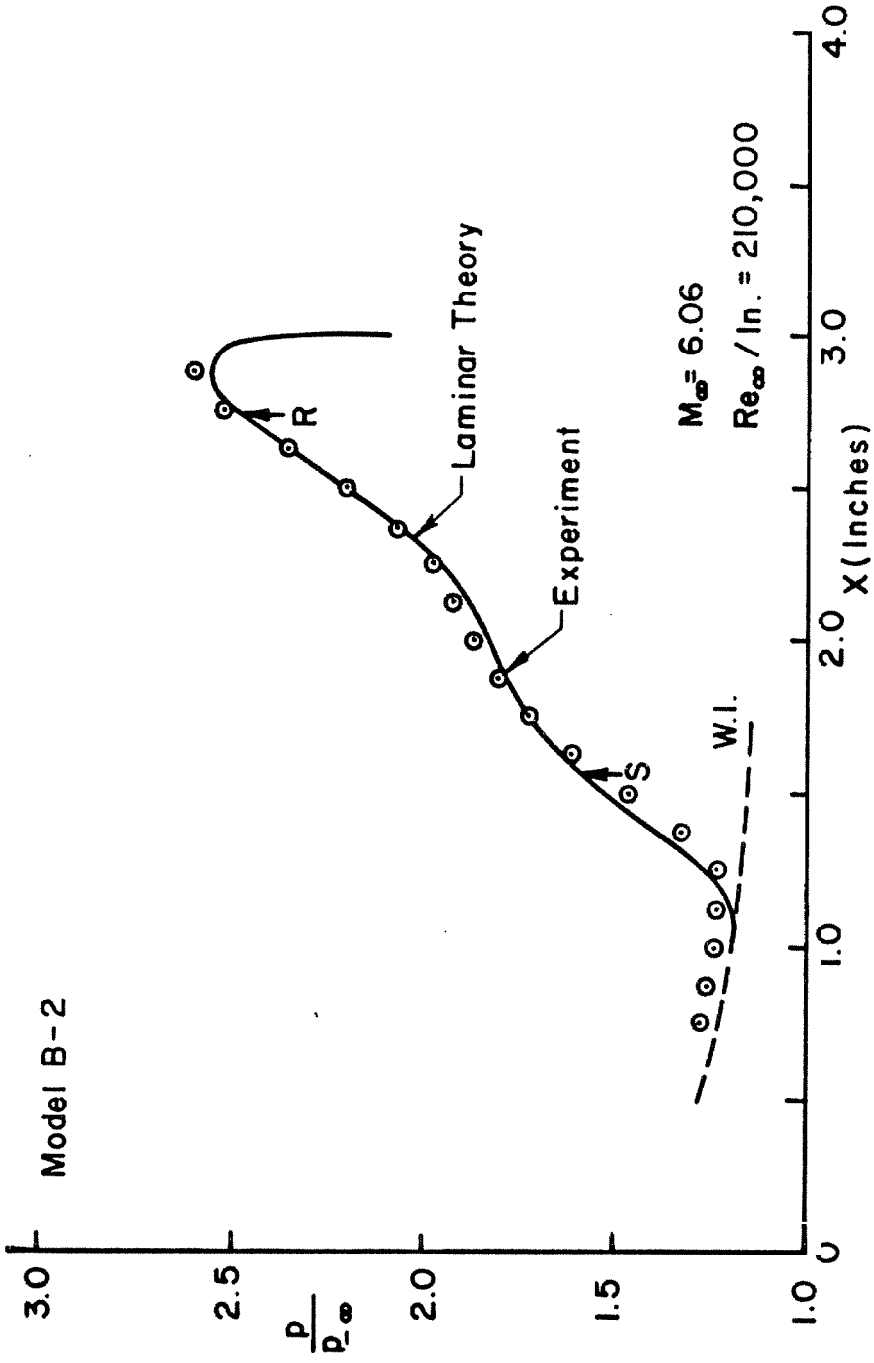

Fig. B9. Static Pressure Distribution for Model B-2 at Re_{∞}/in. = 210,000

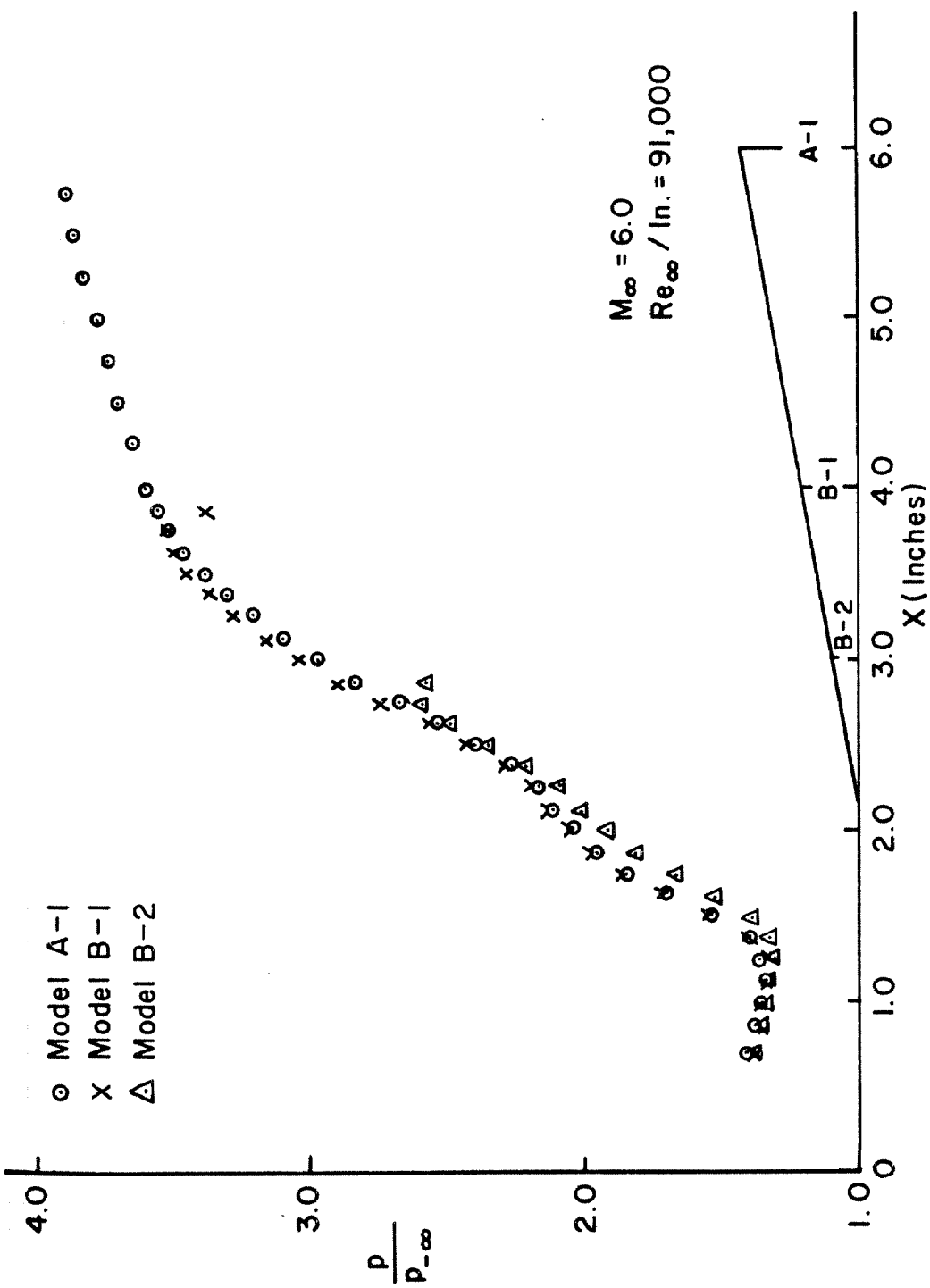

Fig. B10. Effect of Model Length at Re_∞/in. = 91,000

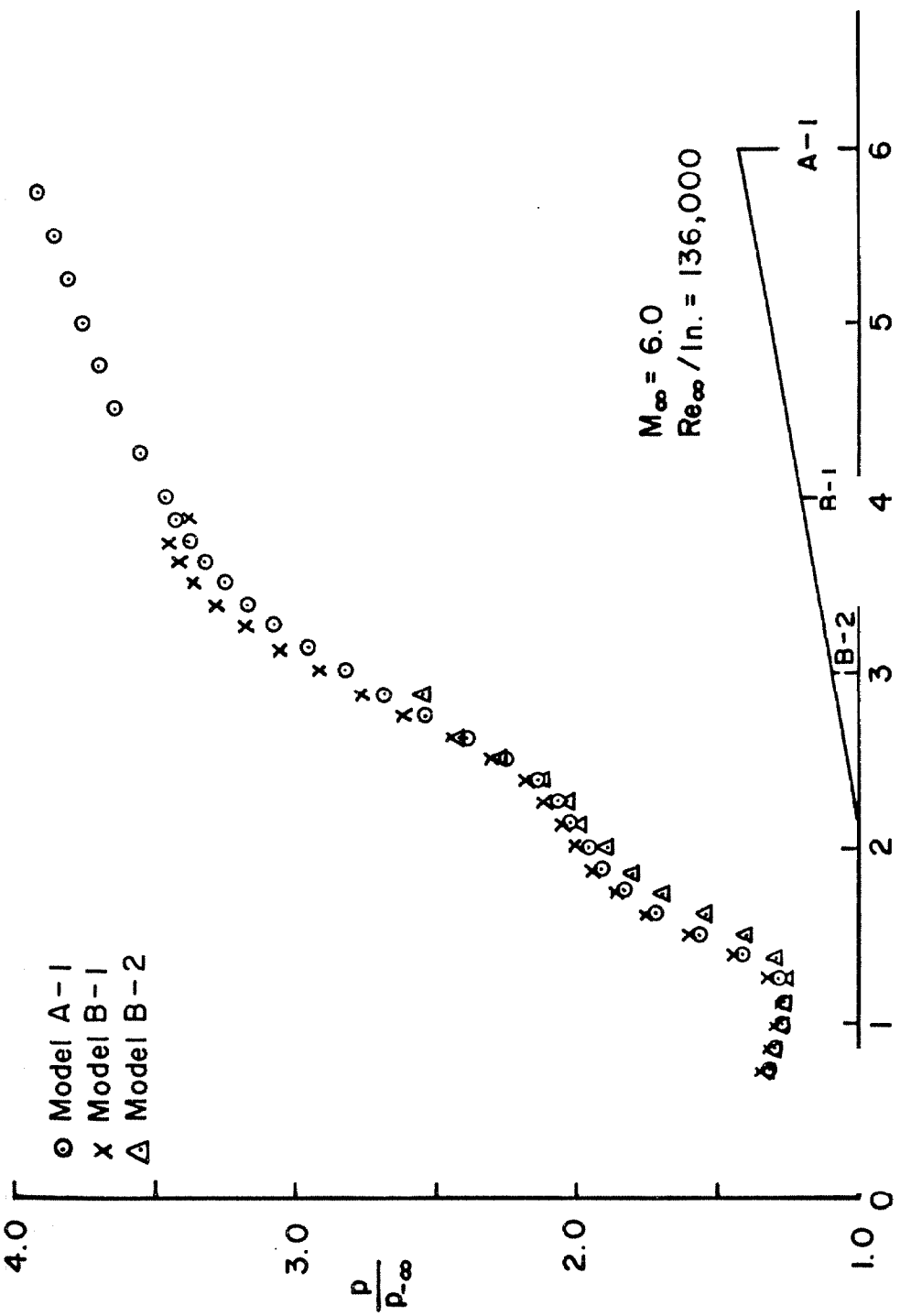

Fig. B11. Effect of Model Length at $Re_\infty/in. = 136,000$

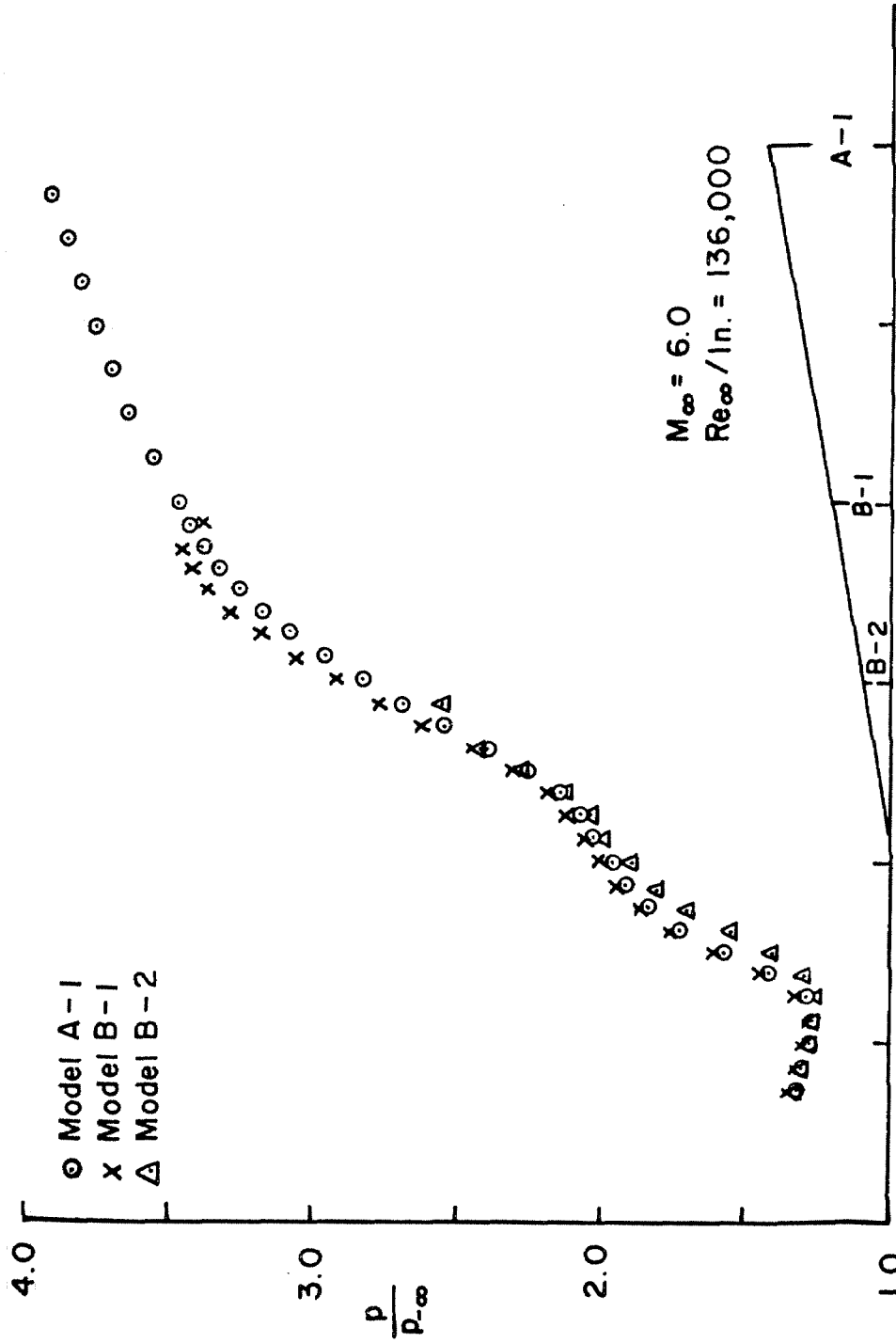

Fig. B11. Effect of Model Length at Re_∞/in. = 136,000

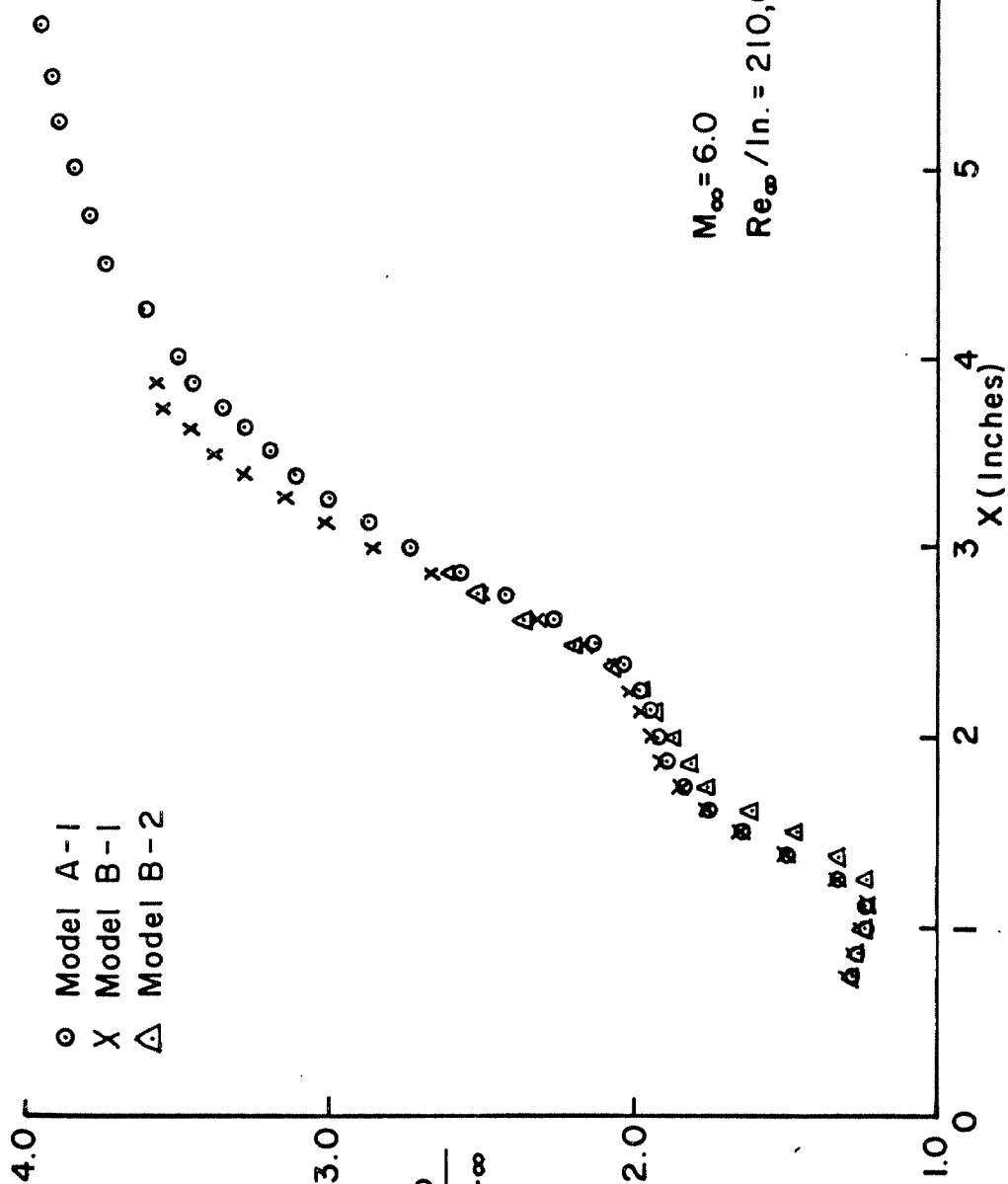

Fig. B12. Effect of Model Length at Re_∞/in. = 210,000

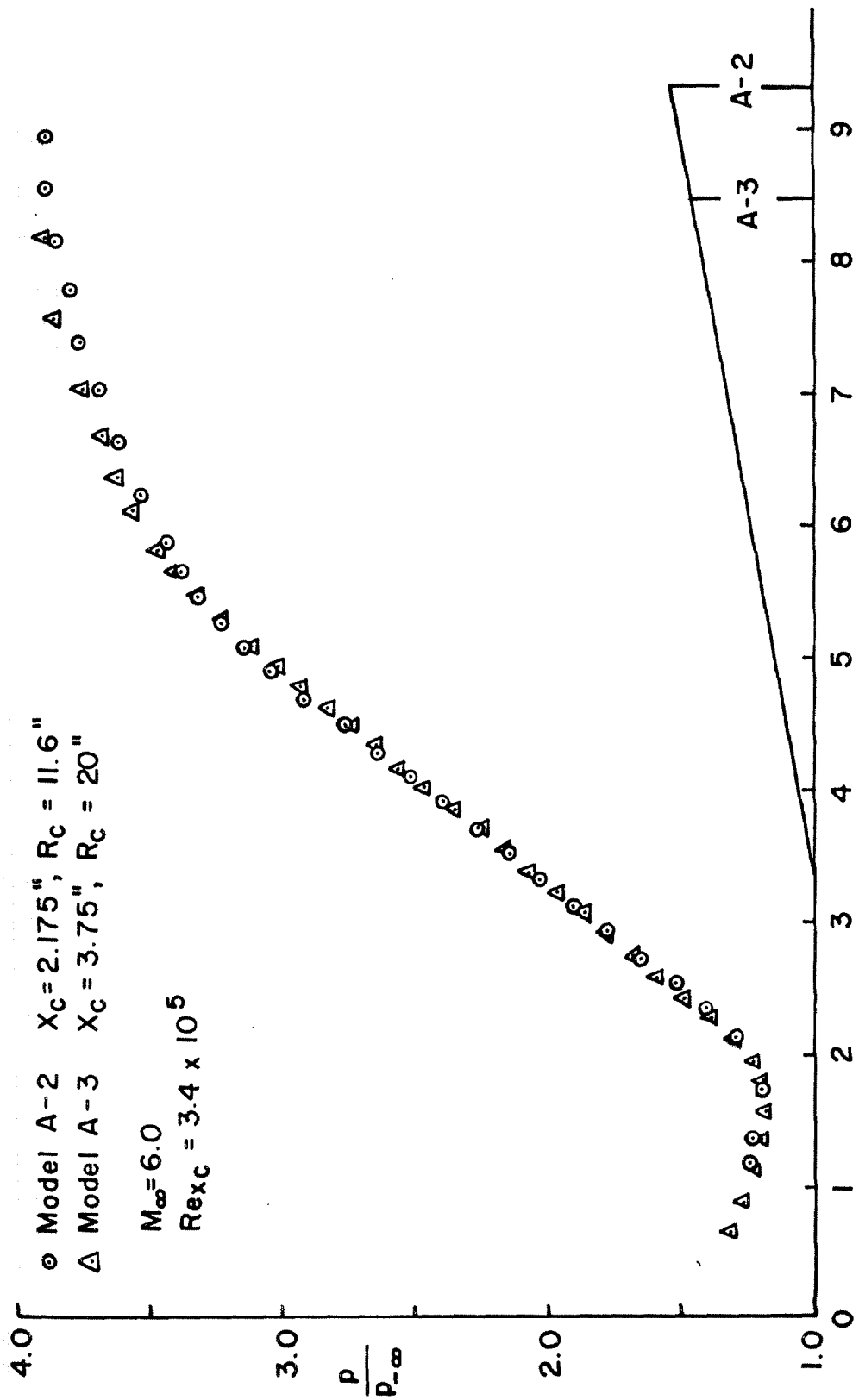

Fig. B13. Reynolds Number Correlation at $Re_{x_c} = 3.4 \times 10^5$

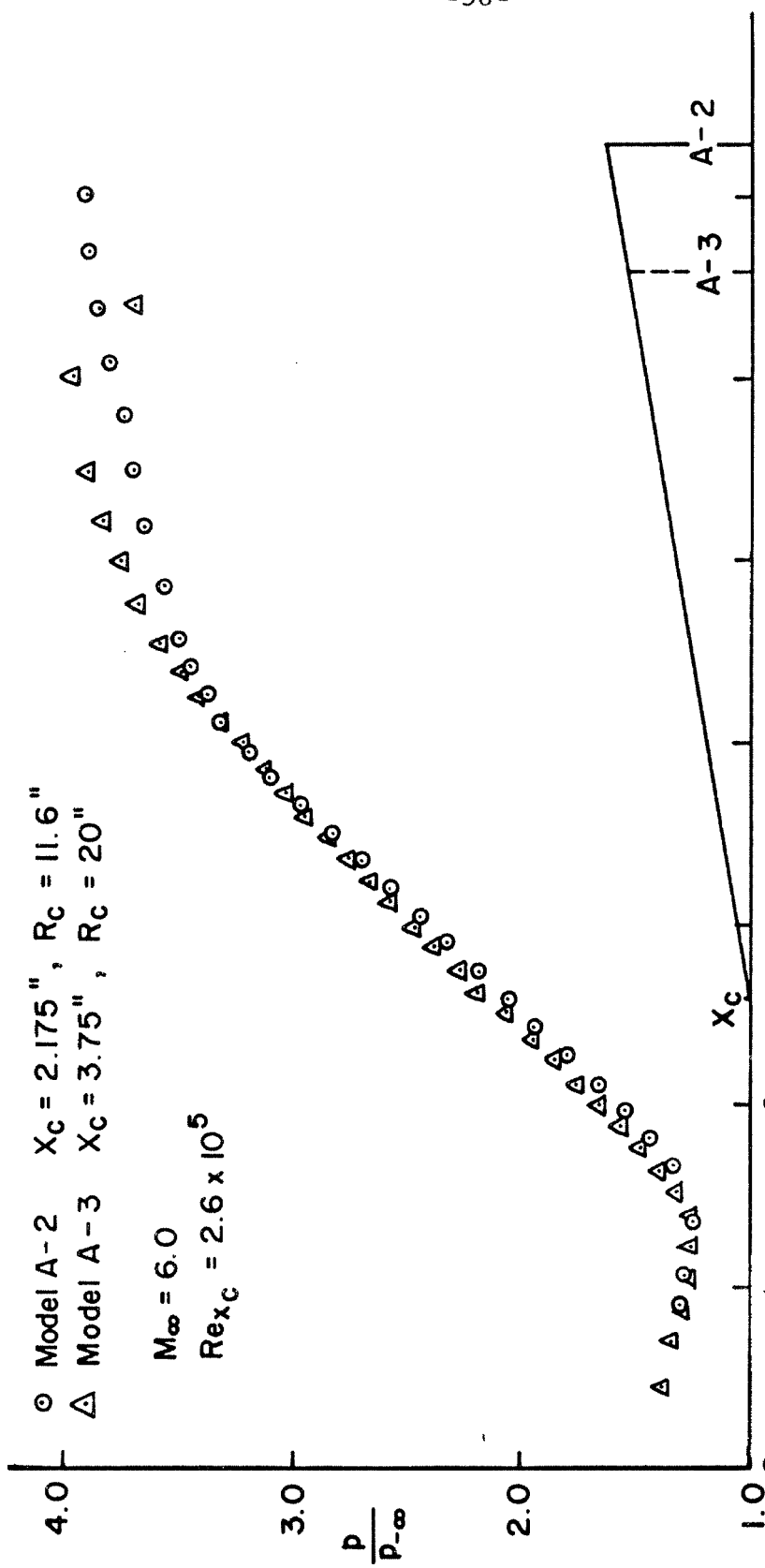

Fig. B14. Reynolds Number Correlation at $Re_{x_c} = 2.6 \times 10^5$

PART II. NON-LINEAR STABILITY THEORY FOR A LAMINAR, INCOMPRESSIBLE WAKE

List of Tables - Part II

List of Figures - Part II

List of Figures - Part II (Cont'd)

List of Figures - Part II (Cont'd)

List of Figures - Part II (Cont'd)

List of Figures - Part II (Cont'd)

List of Figures - Part II (Cont'd)

List of Figures - Part II (Cont'd)

LIST OF SYMBOLS - PART II

A	complex amplitude defined by Eqn. (3.31)
$\|A\|$	magnitude of the amplitude made definite by Eqn. (4.8)
A^*	local complex amplitude of the fluctuation related to A by Eqn. (3.31)
A_u	$\frac{1}{b}\int_0^\infty \overline{u^{*2}}dy$, energy density in u'-component fluctuation normalized by the local velocity
a_m	complex coefficients in the local amplitude equation (3.27)
$\bar{a}_n$	real coefficients in the amplitude equation (4.16)
b	nondimensional wake half-width measured from the wake axis to the half velocity defect point
b_0	value of b at x = 0, trailing edge of the plate
c^*	nondimensional complex phase velocity = ω^*/α^*
$\bar{c}$	phase velocity defined by Eqn. (4.3)
$\bar{c}_1$	phase velocity defined by Eqn. (F.6)
C_{ps}	static pressure coefficient defined by Eqn. (E.2)
D	denominator in Eqn. (4.10)
E_F	total integrated fluctuation energy defined by Eqn. (2.5)
E_f	symbolic fluctuation energy given in Eqn. (4.15b)
	symbolic mean energy given in Eqns. (4.15a) and (2.3)
E_T	total fluctuation energy density defined by Eqn. (2.8)
E_u	fluctuation energy density of u'-component = $\frac{1}{b}\int_0^\infty \overline{u'^2}\,dy$
E_v	fluctuation energy density of v'-component = $\frac{1}{b}\int_0^\infty \overline{v'^2}\,dy$
E_{uf}	fluctuation energy density of u'-component of the fundamental mode *(o)*

E_{u2f} fluctuation energy density of u'-component of the second harmonic (2ω)

E_{u0} initial magnitude of the fluctuation defined by Eqn. (4.14)

F_1 function defined by Eqn. (F.3)

f_0 distribution function of the leading term of the fundamental mode introduced in Eqn. (3.26)

f_1 correction to the distribution function of the fundamental mode introduced in Eqn. (3.26)

G function defined by Eqn. (F.2)

g_0, g_1 the two leading terms for the distribution function of the second harmonic introduced in Eqn. (3.26)

H additional shape parameter for the mean flow defined in Eqn. (3.12), also Eqn. (4.18)

I_i integrals involving fluctuating components defined in Eqns. (3.15) and (3.16)

i $\sqrt{-1}$

$K_{ij}(w_c, Z)$ functions defined by Eqn. (4.10b)

k constant in mean velocity shape function = 0.69315

k_i integrals of functions of f_0 defined by Eqns. (4.7a)

$\bar{k}_{in}$ coefficients in Eqn. (5.1)

k_{ig} integrals of functions of g_0 defined by Eqns. (5.4)

k_{if} integrals of functions of f_0 and f_1 defined by Eqns. (F.8)

k_{iff} integrals of functions of f_1 defined by Eqns. (F.9)

L physical plate length

N_1, N_2 functions defined by Eqns. (4.10a)

p nondimensional static pressure

p^* local fluctuation pressure = p'/w_c^2

p_{10} leading term of the local pressure distribution related to the fundamental mode given by Eqn. (4.1)

p_{20} local pressure distribution related to the second harmonic given by Eqn. (5.2)

p_{11} correction term to the local pressure distribution related to the fundamental mode given by Eqn. (F.5)

R freestream Reynolds number = UL/ν

S function related to the additional shape function $H = w_c H$

T period

T_{12} with subscripts 12, 21, M1, M2, 1M, 2M, indicates the processes between the two modes and the mean flow. Refer to schematic A

T_{R1} contribution to the energy transfer term from the Reynolds stress $\overline{u'v'}$

T_{R2} contribution to the energy transfer term from the normal stress $(\overline{u'^2}-\overline{v'^2})$

T_{Rf} energy transfer term in the fluctuation energy equation (4.15b)

T_{RM} energy transfer term in the mean energy equation (4.15a)

T_{Vf} viscous dissipation term in the fluctuation energy equation (4.15b)

T_{VM} viscous dissipation term in the mean energy equation (4.15a)

t nondimensional time

t^* local time defined by Eqn. (3.17a)

U free stream velocity

U^* universal shape function for the mean velocity given by Eqn. (3.11)

U_1^* additional shape function for the mean velocity given by Eqn. (4.18)

u nondimensional velocity in the x-direction

u^* local fluctuation velocity in the x-direction = u'/w_c

v nondimensional velocity in the y-direction

v^* local fluctuation velocity in the y-direction = v'/w_c

W^* mean velocity shape function defined by Eqn. (C-1)

w_c mean velocity defect on the wake axis = $1-\bar{u}(x, 0)$

w_j coefficients of the expansion for dw_c/dx appearing in Eqn. (B. 3)

x nondimensional streamwise distance measured from the trailing edge of the flat plate

x_0 reference station for local treatment of the fluctuation

x^* local x coordinate defined by Eqn. (3.17a)

$\bar{x}$ normalized distance defined by Eqn. (E. 7)

y nondimensional distance from the wake axis

y^* local y coordinate defined by Eqn. (3.17a)

y_c location of the critical point where $\bar{u} = c^*$

y_δ^* starting station for numerical integration of the Rayleigh equation

y_2 size of the artificial loop taken near the critical point in the complex y*-plane (y_1 and y_3 give the beginning and end of the loop)

Z total energy density of the leading term of the fundamental mode defined by Eqn. (4.9)

a^* complex wave number = $a_r^* + i a_i^*$

β_i integral constants associated with the mean flow shape functions given in Eqn. (3.15)

γ_i constants appear in Eqns. (2.2) and (2.3a)

ϵ complex amplitude associated with the large scale variation appearing in Eqn. (3.31)

ζ_0 initial x of the streamwise integration

θ local phase function = $a_r^* x^* - \omega^* t^*$; phase angle in Figs. 3

λ constant given by Eqn. (F.19)

ν kinematic viscosity

ρ density

φ function defined in Eqn. (F.11)

φ_0 eigenfunction of the adjoint equation of f_0

$\chi_{1,2}$ non-linear quadratic terms in Eqns. (3.4)

χ_3 a solution to Rayleigh equation satisfies the boundary condition (F.17)

ψ^* local stream function defined by Eqn. (3.21)

ψ_n expansion coefficient of the local stream function given by Eqn. (3.22)

ω nondimensional angular frequency of the fundamental mode of fluctuation

ω^* local angular frequency = b_w

Subscripts

e	edge
f	fundamental mode
2f	second harmonic
g	second harmonic
i	imaginary part
ℓ	undisturbed laminar
M	mean flow
r	real part
u	u'-component
v	v'-component
0	initial value

Superscripts

'	fluctuating components; also as $\frac{d}{dy^*}$ when no confusion results
$\bar{}$	time average
*	local variables
~	complex conjugate

1 Introduction

The use of the infinitesimal disturbance theory of hydrodynamic stability for flow in a wake has been studied by various investigators (McKoen[1], Sato-Kuriki[2], Betchov-Criminale[3], et al.) Gold[4] presented a fairly complete formulation of the general problems in the linear stability theory for both the incompressible and compressible wakes. The experiment in the incompressible wake of a thin flat plate reported by Sato and Kuriki[2] has confirmed that the initial stage of the laminar-turbulent transition can be described by the linear stability theory. However, the agreements are usually limited to a relatively small flow region near the beginning of transition. This limited range of applicability of the linear stability theory is expected because the exponentially growing disturbances, no matter how small their initial magnitude may be, will soon invalidate the assumptions made in the linear stability theory. Being encouraged by the relatively orderly behavior of the fluctuations measured by Sato and Kuriki in the "non-linear" region, it is felt that we should be able to extend the theoretical treatment somewhat beyond the linear region before classifying them into the mysterious region of turbulence.

The present study is intended to develop a general theory for considering the effects of the finite amplitude disturbances on a laminar wake, hoping that it may lead to a better understanding on the mechanisms of transition in wakes. But it is by no means intended to offer a possible bridging solution from laminar to turbulent, although non-linearity must be highly responsible for the breakdown of

the laminar flow.

Based on the previous theoretical treatments and experimental findings, it is expected that compressibility will not affect the overall mechanism in an appreciable manner. Thus, only incompressible flow will be studied here.

2 Preliminary Considerations

First of all, in order to devise a non-linear treatment as an improved theory over the linear stability theory, the assumptions usually made in the linear theory will be examined. Secondly, anticipating certain necessary assumptions to be made in the non-linear version, the experimental findings of Sato and Kuriki will be briefly summarized to provide some physical background for better judgements. In Section 2.3, a brief review of the methods used for other types of non-linear stability problems will be made in order to explore certain ideas for the present problem. Finally, the method of solution is discussed and a qualitative discussion of the physical mechanism is made.

2.1 Linear Stability Theory

The most crucial assumption made in the linear stability theory for a wake is the smallness of the amplitude of the disturbances. This assumption of infinitesimal disturbances, which is common to all the linear stability problems, allows the decoupling of the mean flow from the development of the disturbances. Therefore, the mean flow field may be determined independently from the steady laminar equations. For a two-dimensional, incompressible wake behind a flat plate, an exact solution was obtained by Goldstein[5] in 1933 with the additional assumption of a high Reynolds number flow. A general implication of this boundary-layer approximation is that the interaction between the growth of the wake with the external inviscid flow is a higher order effect and may be ignored.

The linear treatment for the disturbance in a wake further assumes a quasi-parallel mean flow; i.e., locally, the mean flow may be taken as constant. With this parallel flow assumption, the linearized equations for disturbance permit a solution of the form

$$\psi = f(y)\exp[ia(x-ct)] \tag{2.1}$$

where ψ = perturbation stream function

a = wave number

ac = angular frequency.

This solution represents a wave train travelling at a phase velocity c. Upon substitution of the above form, the governing equation for the amplitude distribution function f(y) becomes a fourth-order homogeneous ordinary differential equation--the Orr-Sommerfeld equation--which together with the homogeneous boundary conditions constitutes an eigenvalue problem for c when a is given. Two types of disturbances are normally considered.

i) Temporal-mode: a is taken to be real and c complex. When the imaginary part of c is positive, the corresponding disturbance is unstable and grows exponentially with time.

ii) Spatial-mode: ac is taken to be real (which is generally denoted as ω) and a complex. The corresponding disturbance is unstable and grows exponentially with x when the imaginary part of a is negative.

For a complete discussion of the problem, readers may refer to Gold[4] and the references cited there.

2.2 Experimental Evidence

The linear stability theory for the infinitesimal disturbances has been confirmed experimentally in various problems, with or without solid boundaries, to the extent that, by using the local measured mean flow quantities, the most unstable frequency and its exponential growth rate agree satisfactorily with the theoretical predictions. However, the agreements are usually limited to a relatively small region. Both the mean flow and the fluctuations soon cease to follow the undisturbed laminar calculation and the linear stability theory predictions. Frequently, this is defined as the onset of the transition from laminar to turbulent flow.

An excellent experiment for the wake behind a flat plate in an incompressible flow was reported by Sato and Kuriki[2] in 1961, aiming at clarifying the transition mechanism in a wake. Both the free-stream natural fluctuations and the artificial disturbance introduced through a loud speaker were used as the sources of disturbance for the wake. Based on the measured mean flows and fluctuations, they divided the wake into several regions. The main features in those regions which will be of interest to the present investigation are briefly summarized as follows: (Refer to Fig. 1 taken from Sato-Kuriki)

a) Linear region: $x/b_0 \leq 35$, where x denotes the distance from the plate trailing edge and b_0 is the half-width of the wake at x = 0. In this region, the following phenomena were observed.

i) A single-frequency sinusoidal velocity fluctuation was observed which was two-dimensional and antisymmetric with respect to the wake axis.

ii) The measured frequency varied with the free-stream velocity as $U^{3/2}$ in accordance with the dimensional reasoning, and was near the frequency of maximum amplification rate according to the linear stability theory.

iii) The measured radial distributions of the amplitude and the phase were found to agree closely with the eigenfunctions calculated by the linear stability theory using the local measured mean flow.

iv) The measured mean flow quantities agreed with the undisturbed laminar wake calculations of Goldstein.

As a whole, this region demonstrated the validity of the linear stability theory.

b) Non-linear region: $35 \leq x/b_0 \leq 125$

The term "non-linear" was used because of the following facts, which were believed to be the consequences of the finite amplitude of the disturbances.

i) Two-dimensional sinusoidal fluctuations of the same frequency as observed in the linear region were still prominent. However, the growth rate deviated from being a simple exponential, and the amplitude of the disturbance actually decreased in the later stage of this region.

ii) A harmonic at twice the fundamental frequency appeared with measurable amplitude which was symmetric with respect to the wake axis.

iii) The mean flow velocity and the wake width deviated substantially from the undisturbed laminar wake solution.

c) Three-dimensional region: $125 \leqslant x/b_0 \leqslant 250$

The fluctuations became three dimensional and less orderly.

d) Turbulent region: $x/b_0 > 250$

The flow proceeded smoothly to a full turbulent flow. No sudden burst as observed in the wall boundary layers occurred.

As regards the above division, the present study is intended to understand the non-linear region where the fluctuations are still two-dimensional and seem to be dominated by a single frequency and its harmonics.

2.3 Brief Review of the Existing Methods for the Non-linear Stability Theory

An early attempt to include the effects of a finite amplitude disturbance on the stability of flows between two parallel planes was reported by Meksyn and Stuart[6] in 1951. The effect of the finite amplitude disturbance was introduced by including the Reynolds stress term, $\rho\overline{u'v'}$, in the mean equation of motion. Only a single frequency disturbance was considered, and the generation of the

higher harmonics through the non-linear interactions between modes was ignored. The method of solution used was essentially an integral approach. The Reynolds stress was evaluated in terms of a mean flow parameter U_0''/U_0' under the assumption that the distribution of the disturbance was given by the solution of the linearized, Orr-Sommerfeld equation, where $U_0(y)$ is the mean flow velocity and the prime denotes differentiation with respect to y. Using such an approach, the effect of the finite amplitude disturbance on the critical Reynolds number for plane Poiseuille flow was estimated. As to be expected, the results showed that the critical Reynolds number decreased as the amplitude of the disturbances increased. Stuart (1956) [7,8] gave a more rigorous formulation later. The method was applied recently to the non-linear instability of plane Couette flow by Kuwabara[9] (1967) with the aid of the Galerkin's method to determine the mean flow and the disturbance.

An enlarged and more general formulation with calculations along this line of approach was given by Stuart[10] (1958). In this paper, he gave a good discussion of the role of the Reynolds stress in determining the stability of parallel flows. He also described the physical processes associated with the non-linearity as the amplitude of the disturbances grows from an infinitesimal to a finite one. A Fourier series expansion was assumed for the disturbance and an assumption of constant wave velocity c_r for all the Fourier components was implied. It in turn gave the expression for the Reynolds stress, which appeared in the mean equation of motion linking the

mean flow and the disturbance. An approximate energy method was used in which the dominant non-linear interaction was assumed to be that between the mean flow and the fundamental component of the disturbance. The distribution of the disturbance was again taken from the solution of the linearized equation. The governing equation for the evolution of the amplitude as a function of time was then obtained from the integrated disturbance energy equation. This amplitude equation turned out to be of the same form as given without derivation by Landau in 1944[11]. One most important result of Stuart's analysis is the existence of an equilibrium state when the non-linear effect is introduced. The same method was applied to the flow in a small gap between rotating cylinders. Good agreement of the torque required to maintain the cylinders in motion with G. I. Taylor's measurements[49] was indicated.

A more rigorous formulation for the flows between rotating cylinders given by Davey[12] served as an extension and justification of Stuart's result. The second harmonic at twice the fundamental frequency was included and the mechanics of the higher modes were discussed. Davey's analysis was in fact an application to the specific problem of the general theory developed by Stuart[13] (1960) and Watson[14] (1960). In these two papers, a formal expansion in powers of amplitude was employed for the disturbances. Although the integral method was no longer used, the theory was definitely an outgrowth of the previous developments. The physical mechanisms were described by Stuart and the relation to the previous developments was

mentioned. The formal mathematical justification and systematic solution to the higher harmonics were given by Watson. The generalization to a full solution paid the price of having a limitation on the magnitude of the amplitude that restricted the considerations to the disturbances near the neutral case where $ac_i = 0$. Even though, as it was remarked by Watson:[14]

> "there is no guarantee that the series will converge, or even represent a solution asymptotically as $c_i \to 0$, as t becomes large. However, one would expect the theory to be an improvement over linearized theory for a range in time-----"

This theory, as it was further generalized by Eckhaus[15] (1965), is usually termed the "normal mode cascade approach". Applications to inviscid shear layers were reported by Schade[16] (1964) and Stuart[17] (1967). Stuart's analysis was slightly different from the previous ones in showing the explicit dependence of the wave number a and the wave velocity c on the amplitude. The numerical version of Stuart's theory was reported by Reynolds and Potter[18] (1967). The treatment was extended to three-dimensional disturbances and the method was applied to plane Poiseuille flow and a combination of plane Poiseuille and plane Couette flow. The numerical values of each term contributing to the so-called "second Landau constant" in the amplitude equation were obtained in settling the question of stability in the non-linear theory. In all the papers mentioned above, the so-called temporal mode of disturbances were considered; i.e., the disturbance would grow or decay with time. In 1962, Watson[19] formulated in a similar manner a theory for the spatially

growing finite disturbances in plane Poiseuille flow.

It should be mentioned here that some important contributions to the non-linear stability theory were made in a parallel manner by Gorkov, [20] Malkus and Veronis, [21] Joseph, [23] Segel and Stuart, [24] Joseph and Shir, [25] etc., on the thermal-convective instability of a horizontal layer of fluid heated from below (the Bénard problem). In fact, most of the ideas are interchangeable. A good account of all these works and some general discussions on the various methods used were given by Segel. [26]

The methods reported so far have dealt with flows of constant Reynolds number. In all cases, the mean flow remains parallel and its deviation from the laminar flow appears as a power series in the square of the amplitude. In fact, in the case of shear layers (Schade and Stuart) the mean flows were left unperturbed to the order they considered. One exceptional case is the spatially-growing disturbance considered by Watson, where the mean flow is not parallel except as the flow approaches equilibrium amplitude. But the deviation from parallel flow comes in only as a higher order correction. In any case, the interaction with the mean flow may be considered to be a weak one such that the first few terms in the series expansion for fluctuation may be determined with an undisturbed laminar mean flow.

The ideas used to develop the following theory have been extracted from those previous works. The integral method is used to avoid the unrealistic limitation to disturbances of small linear amplification rate imposed by a formal series expansion theory. This

approach is required because the wake is dynamically unstable and disturbances of much larger amplitude than those permitted by the formal expansion solution of Stuart and Watson will appear and dominate the physical process. The approach is analogous to the earlier works of Stuart (e.g., 1958) applying to a non-parallel mean flow.

2.4 Method of Approach and Qualitative Discussions

In this section, the formulation of the method of solution is outlined, and then, a qualitative consideration on the flow field based on the proposed method will be given that may help in understanding the experimental results of Sato and Kuriki. The fundamental difference of the present theory to the formal expansion theory of Stuart and Watson will also be briefly discussed. This section will serve as a prelude as well as an abstract of the detailed formulation of Section 3, and the quantitative discussions of Section 4.

According to the linear stability theory, an unstable disturbance grows exponentially as it proceeds downstream. When the amplification rate is large enough, even if the disturbance is infinitesimally small originally, the amplitude of the disturbance soon reaches a magnitude where the assumptions pertinent to the linear theory become invalid. The finite amplitude disturbance will induce the following non-linear effects: a) Interaction of the disturbances with the mean flow through the Reynolds stresses that are ignored in the linear stability theory, b) Generation of the higher harmonics and their interactions through the non-linear terms. The present study formulates a theoretical approach in general and devises a

method in which these non-linear effects are introduced systematically in order to have some better understanding of the physical mechanisms involved in the transition.

The flow is decomposed into a mean part, which is independent of time, and a fluctuating part, which has a zero mean. Through the mean equations of motion obtained by time-averaging, the effects of finite amplitude disturbances become evident. Because of the Reynolds stresses, the decay of the mean velocity and, therefore, the growth of the wake are expected to be different from a steady laminar wake. Experimentally, a fairly rapid growth of the wake as compared to the steady laminar case is observed in the non-linear region. Hence, the interaction between the fluctuation and the mean flow will be expected to be a strong one. The weak interaction model of Stuart and Watson, where the mean flow to the first order is given by the undisturbed laminar solution, is therefore not applicable. The variation of the mean flow with distance in the flow direction will have to be determined simultaneously with the development of the amplitude of the fluctuation.

In principle, the complete set of the governing partial differential equations may be solved for any given flow conditions. However, it will be an immensely difficult numerical task that will provide little understanding of the non-linear mechanism in the wake. Therefore, in an attempt to bring out the essential effects in the non-linear region, the approximate integral method is adopted for the present investigation. Instead of solving the complete system

of the governing partial differential equations, the flow is required to satisfy the conservation equations of mean momentum, mean energy and fluctuation energy in integral form. The main simplification of the integral method lies in the fact that the unknowns may be approximated by profiles with a few parameters which are then determined by the ordinary differential equations. In the present study, the mean flow profile is assumed to be a Gaussian distribution characterized by two parameters: the mean velocity defect on the wake axis, w_c, and the half-wake width, b. For an integral approach, the details of this distribution generally are not important if it possesses the qualitative characters of the expected solution.

In the case of an unsteady wake with finite amplitude disturbances, the Reynolds stresses couple the mean flow to the fluctuations. Thus, the fluctuations must also be represented in terms of a few governing parameters, A method in obtaining a reasonable representation of the distribution of the amplitude and phase of the fluctuation across the wake is to solve the Orr-Sommerfeld equation of the linear stability theory, based on the local mean flow. This choice has the advantage of representing the proper limit of infinitesimal disturbance. Then, the fluctuation and, therefore, the integrals involving fluctuating components become functions of b, w_c and A, the amplitude of the fluctuation when a single frequency fluctuation is assumed. The integral conservation equations of mean momentum, mean energy and fluctuation energy then provide three ordinary differential equations for the three unknowns b, w_c and **A.**

The use of the linearized Orr-Sommerfeld equation locally to obtain the functionals required in the integral method can he shown to be the first order term of a local power series representation of the fluctuation. The justification will be given through a careful ordering process in the next section. However, it must be emphasized that the method clevised for obtaining the integrals involving fluctuating components as functions of the mean flow parameters and the amplitude is a sufficient but not a necessary one. The integral method does not restrict the means in obtaining the distributions as long as they are good representations of the true distributions. This important idea behind the integral method will have to be stressed in order to understand the method of truncation used in representing the fluctuation. The local power series expansion in the amplitude **A** for the fluctuation is merely a tool to introduce systematically the higher harmonics. Therefore, the method does not restrict to the cases of small linear amplification rate as considered by the analysis of Stuart and Watson.

Based on the first-order terms of the fluctuation, a qualitative understanding of the non-linear region may be achieved. Various crude approximations, which will not affect the qualitative discussion, will be made in arriving at the following model equations. The full detail justifications are given in the next section.

With the assumption that the mean flow may be described by two shape parameters $b(x)$ and $w_c(x)$, the leading terms of the momentum integral equation give

$$bw_c \simeq \gamma_1 R^{-\frac{1}{2}} \tag{2.2}$$

where γ_1 is a constant and R denotes the free-stream Reynolds number based on the plate length. The energy integral equations of the mean flow and the fluctuation, to the first order, may be written as

$$\frac{dE_m}{dx} \simeq - I_6 w_c^3 - \frac{\beta_4 w_c^2}{Rb} \tag{2.3}$$

and

$$\frac{dE_F}{dx} \simeq I_6 w_c^3 - \frac{I_8 w_c^2}{Rb} \tag{2.4}$$

correspondingly. Here E_m denotes the integral energy of the mean flow. For small w_c, since bw_c is nearly constant according to Eqn. (2.2), E_m is linearly proportional to w_c to the first order. E_F in Eqn. (2.4) represents the energy associated with the fluctuations and is defined by

$$E_F = \int_0^\infty (\overline{u'^2} + \overline{v'^2})\, dy \tag{2.5}$$

The first terms on the RHS of Eqns. (2.3) and (2.4) are the same but with an opposite sign. These terms represent an energy transfer between the mean flow and the fluctuations due to the Reynolds stresses. For a locally amplified disturbance, the sign of I_6 is always positive. Therefore, the energy is transferred from the mean to the fluctuation through the Reynolds stress, The remaining terms on the RHS of both equations represent the effect of viscous dissipation. For a given shape function of the mean flow, β_4 is a constant. However, I_6 and I_8 are generally functions of all three

unknowns, b, w_c and the amplitude of the fluctuation. Upon neglecting all the higher harmonics and using Eqn. (2.2), I_6 and I_8 are proportional to the square of the amplitude. We may let

$$I_6 = k_6(w_c)\,|A|^2$$
$$I_8 = k_8(w_c)\,|A|^2 \qquad (2.6)$$

where k_6 and k_8 are functions of w_c only. The amplitude $|A|^2$ is defined in the present formulation as

$$|A|^2 = E_F/(2bw_c^2) \qquad (2.7)$$

Now, Eqns. (2.3) and (2.4) may be rewritten as

$$\gamma_2 R^{-\frac{1}{2}} \frac{dw_c}{dx} = -k_6(w_c)\,|A|^2 w_c^3 - \frac{\beta_4 w_c^3}{\gamma_1 R^{\frac{1}{2}}} \qquad (2.3a)$$

$$2\frac{d}{dx}[b|A|^2 w_c^2] = k_6(w_c)\,|A|^2 w_c^3 - \frac{k_8(w_c)}{\gamma_1 R^{\frac{1}{2}}}\,|A|^2 w_c^3 \qquad (2.4a)$$

A qualitative behavior of the flow field in the non-linear region may be obtained from these two equations. When the amplitude of the fluctuation is small, the first term on the RHS of Eqn. (2.3a) is negligible as compared to the laminar viscous dissipation term. Hence, the mean flow will be closely approximated by the steady laminar solution, and w_c decreases as $x^{-\frac{1}{2}}$. Since w_c changes slowly in this region, Eqn. (2.4a) may be approximately considered as an equation for the amplitude $w_c^2|A|^2$ with constant coefficients. Then, the exponential growth rate of the linear stability theory immediately follows. This region corresponds to the linear

region observed by Sato and Kuriki.

As the amplitude grows, the Reynolds stress term becomes comparable with the viscous term in Eqn. (2.3a), and the mean velocity defect starts deviating from the steady laminar solution. As the fluctuation is further amplified, the Reynolds stress term becomes dominating. The experimentally observed rapid change of the mean velocity and the wake width in the non-linear region may be understood from this consideration. As will be shown through numerical results later, the local amplification rate decreases as w_C decreases if a single frequency fluctuation is followed. In other words, when the fluctuation corresponding to the most unstable frequency in the linear region is taken to represent the fluctuating component, it will approach neutral as w_c decreases. The value of k_6 is positive for a locally amplified disturbance and tends to zero for a neutral one. Thus, when w_C decreases to the value where k_6 becomes small, the laminar viscous term and also all the higher order terms neglected in arriving at Eqn. (2.3a) become important. The mean flow is expected to have a relatively slow variation as observed experimentally.

The behavior of the fluctuation in the non-linear region may be studied qualitatively using Eqn. (2.4a). The total energy of the fluctuation, E_F, as defined by Eqn. (2.5), is expected to increase continuously by extracting energy from the mean flow through the Reynolds stress. This process will be dominated by the first term of Eqn. (2.4a) until k_6 becomes of order $R^{-\frac{1}{2}}$. Then, the viscous

dissipation term and the ignored higher order terms come into effect, Because of the growth of the **wake,** it is more interesting to look at the averaged total energy of the fluctuation. Let E_T be the energy "density" of the fluctuation defined by

$$E_T = \frac{E_F}{b} = 2|A|^2 w_c^2 \tag{2.8}$$

Then, using (2.3a), Eqn. (2.4a) can be written as

$$\frac{dE_T}{dx} = \left(\frac{1}{\gamma_1} - \frac{2}{\gamma_2}|A|^2\right)k_6|A|^2 w_c^4 R^{\frac{1}{2}}$$

$$- \frac{1}{\gamma_1}\left(\frac{k_8}{\gamma_1} + \frac{2\beta_4}{\gamma_2}\right)|A|^2 w_c^4 \tag{2.4b}$$

For $k_6 >> R^{-\frac{1}{2}}$, the first term dominates. The appearance of the $|A|^4$ term with an opposite sign to the $|A|^2$ term is the most interesting feature caused by the growth of the wake, It permits not only a state where $dE_T/dx = 0$, but also a decreasing E_T with x even when the fluctuation under consideration is still amplifying according to the local linear theory ($k_6 > 0$). Experimentally, the maximum amplitude of the fundamental mode grows initially but decreases after reaching a peak value. This fact may now be explained since the energy density E_T is expected to be indicative of the magnitude of fluctuation.

The crucial differences of the present problem from the parallel flow analysis of Stuart and Watson. become evident from the above discussions. The main result of the non-linear analysis of Stuart and Watson is the governing equation for the amplitude of the disturbances and is of the form

$$\frac{1}{|A|^2}\,\frac{d|A|^2}{dx} = \bar{a}_0 + \bar{a}_1\,|A|^2 + \cdots \qquad (2.9)$$

where $\bar{a}_n$'s are constants. The coefficient $\bar{a}_0$ is given by the linear theory with the undisturbed laminar mean flow and $\bar{a}_1$ is a result of three effects; the generation of the second harmonic, the correction of the fundamental and the correction to the laminar mean flow. The amplitude $|A|$ in the Stuart-Watson theory corresponds to the average energy density E_T defined by Eqn. (2.8). Then, an analogous equation of the form of Eqn. (2.9) results with $|A|^2$ being replaced by E_T. However, the coefficients $\bar{a}_0$ and $\bar{a}_1$ are no longer constants but functions of the mean flow and, therefore, functions of x, since the mean flow is not expanded as the undisturbed laminar flow plus a correction in the present problem, but is lumped together to be determined by the integral equations. The so-called "second Landau constant" does have an appreciable magnitude even when the second harmonic is ignored. The sign of $\bar{a}_1$ is opposite to that of $\bar{a}_0$. In the case of a parallel flow, a supercritical equilibrium state may exist. However, the continued variation of the mean flow provides the possibility of a decreasing magnitude of the fluctuation before reaching the final equilibrium state as demonstrated previously. Therefore, the present approach is much more general than the theory of Stuart and Watson. In fact, the parallel flow analysis may be considered as a special case of the present theory.

The above qualitative discussions seem to suggest the model

proposed here to be a plausible one. The formal derivation and numerical solutions are then given in the following sections.

3. Formulation of the Problem

The problem will now be formulated in detail in this section. The difficulties in developing a non-linear theory will be pointed out and the proposed method of solution will be justified in a self-consistent manner.

3.1 Governing Differential Equations

For the two-dimensional flat-plate wake, let x be the non-dimensional distance along the wake axis measured from the trailing edge, and y the non-dimensional distance from the wake axis. Correspondingly, u and v represent the non-dimensional velocity components. Here the reference quantities for the non-dimensionalization are chosen to be

Velocities	U (free stream velocity)
Length	L (plate length)
Time	L/U
Pressure	ρU^2

Then the Navier-Stokes equations in two dimensions can be written as

$$u_x + v_y = 0$$

$$u_t + uu_x + vu_y = -p_x + \frac{1}{R}(u_{xx} + u_{yy}) \qquad (3.1)$$

$$v_t + uv_x + vv_y = -p_y + \frac{1}{R}(v_{xx} + v_{yy})$$

where R is the Reynolds number based on the reference quantities, i.e., $R = UL/\nu$. Now, divide the flow into a mean part independent of time and a fluctuating part with zero mean, i.e.,

$$u(x,y,t) = \bar{u}(x,y) + u'(x,y,t)$$
$$v(x,y,t) = \bar{v}(x,y) + v'(x,y,t) \qquad (3.2)$$
$$p(x,y,t) = \bar{p}(x,y) + p'(x,y,t)$$

where the "bar" indicates a time average according to

$$\bar{Q} = \frac{1}{T}\int_{-T/2}^{T/2} Q\,dt$$

The fluctuations are assumed to be periodic in time with T being the period such that

$$\bar{u}' = \bar{v}' = \bar{p}' = 0$$

For simplicity, the time dependence of the fluctuating quantities will be assumed to be of the form $\sim e^{in\omega t}$ with $w = \frac{2\pi}{T}$, a real quantity, being the frequency and n, an integer.

Substituting (3.2) into (3.1) and integrating over t to separate out the mean and the fluctuating parts, we obtain for the mean flow

$$\bar{u}_x + \bar{v}_y = 0$$
$$\bar{u}\,\bar{u}_x + \bar{v}\,\bar{u}_y + (\overline{u'^2})_x + (\overline{u'v'})_y = -\bar{p}_x + \frac{1}{R}(\bar{u}_{xx} + \bar{u}_{yy}) \qquad (3.3)$$
$$\bar{u}\,\bar{v}_x + \bar{v}\,\bar{v}_y + (\overline{u'v'})_x + (\overline{v'^2})_y = -\bar{p}_y + \frac{1}{R}(\bar{v}_{xx} + \bar{v}_{yy})$$

By subtracting Eqn. (3.3) from Eqn. (3.1), one obtains

$$u'_x + v'_y = 0$$
$$u'_t + \bar{u}\,u'_x + u'\bar{u}_x + \bar{v}\,u'_y + v'\bar{u}_y + \chi_1 = -p'_x + \frac{1}{R}(u'_{xx} + u'_{yy}) \qquad (3.4)$$
$$v'_t + \bar{u}v'_x + u'\bar{v}_x + \bar{v}v'_y + v'\bar{v}_y + \chi_2 = -p'_y + \frac{1}{R}(v'_{xx} + v'_{yy})$$

where

$$\chi_1 = u'u'_x + v'u'_y - (\overline{u'v'})_y - (\overline{u'^2})_x$$

$$\chi_2 = u'v'_x + v'v'_y - (\overline{u'v'})_x - (\overline{v'^2})_y$$

In principle, these six non-linear partial differential equations may be solved for the six unknowns $\bar{p}$, $\bar{u}$, $\bar{v}$, p', u', v' with the proper initial and boundary conditions. However, with the intention of gaining a better understanding of the physical mechanism in the non-linear region of the wake rather than obtaining some numerical values, we will first make the following physically realizable approximations to the mean flow quantities to simplify the analysis.

For the wake flow behind a flat plate, except in the immediate vicinity of the trailing edge, the boundary-layer type approximation is quite satisfactory for a relatively large Reynolds number. In Sato-Kuriki's experiment, the Reynolds numbers are of the order of 10^4 and higher. We will therefore consider flows of large Reynolds number and apply the boundary-layer approximation to the mean flow, which implies

i) $\bar{v}/\bar{u} = O(R^{-\frac{1}{2}}) << 1$

ii) "b", the nondimensional half wake-width much less than 1

iii) $\frac{\partial}{\partial x} / \frac{\partial}{\partial y} = O(R^{-\frac{1}{2}}) << 1$

With these approximations, if the magnitude of the fluctuation is further assumed to be infinitesimal, Eqns. **(3.3)** reduce to the

steady laminar wake equations

$$\bar{u}_x + \bar{v}_y = 0$$

$$\bar{u}\bar{u}_x + \bar{v}\bar{u}_y = -\bar{p}_x + \frac{1}{R}\bar{u}_{yy} \qquad (3.5)$$

$$\bar{p}_y = 0$$

where $\bar{p}_x$ may be set equal to zero with the boundary condition that $\bar{p}_x = 0$ as $y \to \infty$. Eqns. (3.5) were first solved by Goldstein by joining a far-wake solution to a series expansion near-wake solution. This solution of Eqn. (3.5) will be referred to as the "pure laminar wake" solution in this thesis.

The role of the finite amplitude disturbances can be clearly seen from Eqns. (3.3). As the amplitude grows, the Reynolds-stress terms become comparable to the remaining terms in the equation. The experimental results obtained in the non-linear region seem to indicate that the Reynolds-stress terms dominate. If A denotes a measure of the amplitude of the fluctuation, we will expect $A^2\sqrt{R}$ to be of the order one or higher in the non-linear region. In other words, when A^2 becomes $O(\frac{1}{\sqrt{R}})$, the effect of the disturbance on the mean flow can no longer be ignored. Hence, for the non-linear theory, we will tentatively keep the terms involving the fluctuating quantities without exact specification of their relative magnitudes as compared with the remaining terms in the mean flow equations. Then Eqns. (3.3) become

$$\bar{u}_x + \bar{v}_y = 0$$

$$\bar{u}\,\bar{u}_x + \bar{v}\,\bar{u}_y + (\overline{u'v'})_y + (\overline{u'^2})_x = -\bar{p}_x + \frac{1}{R}\,\bar{u}_{yy} \qquad (3.6)$$

$$(\overline{v'^2})_y = -\bar{p}_y$$

Upon the assumption that $\bar{p}_Y$ is an induced quantity which vanishes as the amplitude of the fluctuation becomes infinitesimal, only the leading terms $(\overline{v'^2})_Y$ is kept in the third equation to balance the pressure term. Eqns. (3.6) can be contracted further by integrating out the third equation and substituting into the second one. The equations become

$$\bar{u}_x + \bar{v}_y = 0$$

$$\bar{u}\,\bar{u}_x + \bar{v}\,\bar{u}_Y + (\overline{u'v'})_Y + (\overline{u'^2} - \overline{v'^2})_x = \frac{1}{R}\,\bar{u}_{yy} \qquad (3.7)$$

Eqns. (3.7) further demonstrate that the $(\overline{u'v'})_x$ term neglected in arriving at the third equation of (3.6) is indeed a higher order term compared to the terms remaining.

3.2 Integral Equations

The integral equations of the mean flow are obtained by integrating over the lateral coordinate y. The equations are then reduced to ordinary differential equations in x. They are

Mean Momentum Equation

$$\frac{d}{dx}\int_{-\infty}^{\infty} (\bar{u}^2 - \bar{u} + \overline{u'^2} - \overline{v'^2})\,dy = 0 \qquad (3.8)$$

Mean Mechanical Energy Equation

$$\frac{d}{dx}\int_{-\infty}^{\infty}\left[\tfrac{1}{2}(\bar{u}^3-\bar{u})+\bar{u}(\overline{u'^2}-\overline{v'^2})\right]dy$$

$$=\int_{-\infty}^{\infty}(\overline{u'^2}-\overline{v'^2})\frac{\partial\bar{u}}{\partial x}\,dy+\int_{-\infty}^{\infty}\overline{u'v'}\frac{\partial\bar{u}}{\partial y}\,dy-\frac{1}{R}\int_{-\infty}^{\infty}\left(\frac{\partial\bar{u}}{\partial y}\right)^2 dy \qquad (3.9)$$

An additional equation for the fluctuation is provided by the energy equation of the fluctuation which is obtained by multiplying the second equation of (3.4) by u' and the third one by v' and add. This equation is then integrated over y and averaged over a period T. It yields

$$\tfrac{1}{2}\frac{d}{dx}\int_{-\infty}^{\infty}\left[\bar{u}(\overline{u'^2}+\overline{v'^2})+\overline{u'^3}+\overline{u'v'^2}+2\,\overline{u'p'}\right]dy$$

$$=-\int_{-\infty}^{\infty}(\overline{u'^2}-\overline{v'^2})\frac{\partial\bar{u}}{\partial x}\,dy-\int_{-\infty}^{\infty}\overline{u'v'}\left(\frac{\partial\bar{u}}{\partial y}+\frac{\partial\bar{v}}{\partial x}\right)dy \qquad (3.10)$$

$$+\tfrac{1}{2}\frac{1}{R}\frac{d^2}{dx^2}\int_{-\infty}^{\infty}(\overline{u'^2}+\overline{v'^2})\,dy$$

$$-\frac{1}{R}\int_{-\infty}^{\infty}\left[\overline{\left(\frac{\partial u'}{\partial x}\right)^2}+\overline{\left(\frac{\partial u'}{\partial y}\right)^2}+\overline{\left(\frac{\partial v'}{\partial x}\right)^2}+\overline{\left(\frac{\partial v'}{\partial y}\right)^2}\right]dy$$

The term $\frac{\partial\bar{v}}{\partial x}$ may be neglected as compared to $\frac{\partial\bar{u}}{\partial y}$ with the boundary-layer approximation for the mean flow. Furthermore, the term involving the second derivative in x represents the conduction of the fluctuating energy which is quite small in general and may be ignored.

The great advantage of the integral equations is the apparent display of the energy exchange mechanism because of the conservation

forms. In Eqn. (3.9), the left-hand side terms represent essentially the variation of the mechanical energy associated with the mean flow in the flow direction, while the left-hand side terms in Eqn. (3.10) give the variation of energy associated with the fluctuations. The transfer of energy between the mean flow and the fluctuations is clearly indicated by the two Reynolds-stress terms appearing on the RHS of both equations but with opposite sign. The remaining terms on the RHS of both equations represent the viscous dissipation effect.

3.3 Shape Assumption for the Mean Flow

It is the main implication of using an integral method approach that the unknowns may be approximated by a few shape parameters which will in turn be determined by the integral equations. To simplify the analysis, we will assume the mean velocity profiles to be similar when they are expressed as

$$\frac{1-\bar{u}(x,y)}{1-\bar{u}(x,0)} = \frac{1-\bar{u}}{w_c(x)} = U^*(y^*) \qquad (3.11)$$

where $y^* = y/b(x)$, and b gives a measure of the wake width. $U^*(y^*)$ will be assumed as known from the experiments or some other means. This complete similarity of the mean flow is not quite valid in view of the experimental results of Sato and Kuriki where overshoot of the mean velocity at some stations have been indicated. However, the profiles measured are generally close to a Gaussian distribution, and, therefore, (3.11) may be a fairly good approximation when $U^*(y^*)$ is taken from the averaged experimental data points. The exact form of $U^*(y^*)$ should not be too crucial if the integral method

is a good approximation to the problem. A better approximation to the mean velocity may be obtained by introducing more shape parameters such that

$$\frac{1-\bar{u}(x,y)}{w_c(x)} = U^*(y^*, H_1(x), H_2(x), \text{---}) \tag{3.12}$$

The additional unknowns introduced require additional governing equations which may easily be obtained by using the higher moment equations. The loss of the physical explanation for the higher moment equations is the price we have to pay for more generality of the profile shape, Only (3.11) will be used in most of the following analysis and the effect of using (3.12) will be considered later when one additional shape parameter is allowed in Appendix C.

We transform the equations (3.8), (3.9) and (3.10) from (x, y) to (x,y*) according to the following rules.

$$\begin{aligned} x &= x \\ y^* &= \frac{y}{b(x)} \\ \frac{\partial}{\partial x} &= \frac{\partial}{\partial x} - \frac{y^*}{b}\frac{db}{dx}\frac{\partial}{\partial y^*} \\ \frac{\partial}{\partial y} &= \frac{1}{b}\frac{\partial}{\partial y^*} \end{aligned} \tag{3.13}$$

Now, with $u^* = u'/w_c$, $v^* = v'/w_c$, and $p^* = p'/w_c^2$, together with Eqn. (3.11), Eqns. (3.8) and (3.9) become

$$\frac{d}{dx}\left\{bw_c\left[(\beta_1-\beta_2 w_c)-2w_c(I_1-I_2)\right]\right\} = 0 \tag{3.14a}$$

and

$$\frac{d}{dx}\left\{bw_c^2[\beta_2-\beta_3 w_c-4w_c(I_3-I_4)]\right\}$$

$$= 4w_c^3\frac{db}{dx}I_5 - 4bw_c^2\frac{dw_c}{dx}(I_3-I_4)-Zw_c^3I_6-\frac{2w_c^2}{Rb}\beta_4 \qquad (3.15)$$

where

$$\beta_1 = \int_0^\infty U^*\, dy^*$$

$$\beta_2 = \int_0^\infty U^{*2} dy^*$$

$$\beta_3 = \int_0^\infty U^{*3} dy^*$$

$$\beta_4 = \int_0^\infty \left(\frac{\partial U^*}{\partial y^*}\right)^2 dy^*$$

and

$$I_1 = \frac{1}{2}\int_0^\infty \overline{u^{*2}}\, dy^*$$

$$I_2 = \frac{1}{2}\int_0^\infty \overline{v^{*2}}\, dy^*$$

$$I_3 = \frac{1}{2}\int_0^\infty U^*\,\overline{u^{*2}}\, dy^*$$

$$I_4 = \frac{1}{2}\int_0^\infty U^*\,\overline{v^{*2}}\, dy^*$$

$$I_5 = \frac{1}{2}\int_0^\infty y^*\frac{\partial U^*}{\partial y^*}\left(\overline{u^{*2}} - \overline{v^{*2}}\right) dy^*$$

$$I_6 = \int_0^\infty \overline{u^*v^*}\frac{\partial U^*}{\partial y^*}\, dy^*$$

There will be an additional term of the form $\left[-bw_c^3\int_0^\infty \frac{\partial U^*}{\partial x}\left(\overline{u^{*2}}-\overline{v^{*2}}\right)dy^*\right]$ on the RHS of Eqn. (3.15) when the expression (3.12) is used instead of (3.11). Without losing the main features of the present approach,

we will use (3.11) for the moment. In this case, the β_i's are constants. Moreover, it may be noted that the leading terms of Eqn. (3.15) yield Eqn. (2.3).

For Eqn. (3.10), an additional assumption is made on evaluating the dissipation terms. Looking ahead to obtaining this dissipation integral through solving the fluctuation equation locally, the x-derivative appearing inside this integral will be approximated by its local values. That is

$$\frac{\partial}{\partial x} \approx \frac{1}{b} \frac{\partial}{\partial x^*} \quad \text{for} \quad x^* = \frac{x-x_0}{b(x)}$$

This approximation introduces the same order of error as neglecting the conduction term in Eqn. (3.10). Since both of them are multiplied by (1/R), the error introduced is expected to be very small for the high Reynolds number flow considered here. Equation (3.10) then becomes

$$\begin{aligned} &\frac{d}{dx}\left[bw_c^2\left\{(I_1+I_2)-w_c(I_3+I_4)+w_c(I_7+I_9/2)\right\}\right] \\ &= w_c^3 I_6 - 2w_c^3 \frac{db}{dx} I_5 + 2bw_c^2 \frac{dw_c}{dx}(I_3-I_4) - \frac{w_c^2}{Rb} I_8 \end{aligned} \tag{3.16}$$

where

$$I_7 = \int_0^\infty \overline{u^*p^*}\, dy^*$$

$$I_8 = \int_0^\infty \left[\overline{\left(\frac{\partial u^*}{\partial x^*}\right)^2} + \overline{\left(\frac{\partial u^*}{\partial y^*}\right)^2} + \overline{\left(\frac{\partial v^*}{\partial x^*}\right)^2} + \overline{\left(\frac{\partial v^*}{\partial y^*}\right)^2}\right] dy^*$$

$$I_9 = \int_0^\infty \left(\overline{u^{*3}} + \overline{u^*v^{*2}}\right) dy^*$$

The correspondence of this equation to Eqn. (2.4) may be immediately

established by taking the leading terms.

With $U^*(y^*)$ given, the integrals I_i will be obtained from the solutions of the local disturbance equations to be discussed in the next section. Therefore, in general, the values of I_i depend not only on the amplitude of the disturbances, but also on the local mean flow shape parameters.

Eqn. *(3.*14a) can be immediately integrated to give

$$bw_c\left[(\beta_1-\beta_2 w_c) - 2w_c(I_1-I_2)\right] = \frac{C_D}{2} = \frac{0.664}{\sqrt{R}} \qquad (3.14)$$

where the integration constant has been obtained by assuming a laminar flow over the flat plate. Eqns. *(3.*14), *(3.15)* and *(3.*16) provide the governing equations for the interaction between the mean flow and the fluctuations. When the expression *(3.*12) is used for describing the mean flow, additional equations may be obtained by taking higher moment integral equations.

3. 4 Perturbation Solution of the Local Fluctuation Equations

The integrals I_i appearing in the three integral equations involve the fluctuation components. As far as the integral method is concerned, the integrals I_i may be represented as functions of a few parameters. The proper choice of these parameters depends on the underlying physics of the problem. In order to form a closure of the system without using more integral equations, the integrals I_i are assumed to be functions of the mean flow parameters, b and w_c, as well as the amplitude of the disturbance. The following method is then devised to obtain these functional relations.

The basic idea is to apply a two length-scale expansion procedure to the fluctuation equation (3.4) in order to obtain a good representation of the fluctuating components in terms of the parameters. Locally, the fluctuation is assumed to be expanded in an ascending power of amplitude to account for the non-linear interaction between modes and the generation of the higher harmonics. The series representation will be truncated at various terms to bring in the higher order effects systematically. However, the expression for the fluctuation is not intended to be a series expansion of the exact solution but merely as a technique for introducing the high order effects. Hence, the limitation of being close to the neutral disturbance imposed in the Stuart's theory for parallel flows may be ignored.

Before formulating the method of solution, it should be noted that the experiment of Sato-Kuriki had indicated the domination of one fundamental mode in the earlier stage of the wake instability. This is believed to be the result of the highly selective amplification of the small disturbances in the boundary layer preceding the wake and the linear region of the wake. Therefore, we assume that $u', v' \sim e^{in\omega t}$, $n = \pm 1, \pm 2 \ldots$ where ω = real angular frequency corresponding to the fundamental mode. The higher harmonics are the results of non-linear interaction.

First of all, the existence of two length scales for the longitudinal distance x in this problem should be noted. They are

i) $x \sim O(1)$ over which the mean flow quantities will vary by an appreciable amount, and

ii) $x^* = \frac{x-x_0}{b(x_0)}$, a local length scale associated with the fluctuations. Where x_0 is the coordinate of some reference station which depends on the local mean flow variation near x such that the mean flow may be considered as parallel to the first approximation in x* coordinates, e. g., $\frac{(x-x_0)}{b}\left(\frac{db}{dx}\right)_{x_0} << 1$. Therefore, x_0 is generally a function of x. It differs from x by a small amount of the order b.

The existence of these two different scales may be realized by assuming that the disturbance locally displays the wave characteristics having a local wave length of the order b, which is much smaller than 1 in the high Reynolds number case. Therefore, the mean flow may be considered as slowly varying as compared to the variation of the fluctuating quantities.

Since the wake thickness is of the order of $R^{-\frac{1}{2}}$ as indicated by Eqn. (3.14), we introduce the following new variables to bring out the above-mentioned order of magnitude more clearly. Let

$$\begin{aligned} t^* &= tR^{\frac{1}{2}} \\ x^* &= (x-x_0)R^{\frac{1}{2}} \\ y^* &= yR^{\frac{1}{2}} \end{aligned} \tag{3.17}$$

We further assume the fluctuating quantities to be functions of x, t*, x* and y* by letting

$$\begin{aligned} u' &= w_c(x)u^*(t^*, x^*, y^*, x) \\ v' &= w_c(x)v^*(t^*, x^*, y^*, x) \\ p' &= w_c^2(x)p^*(t^*, x^*, y^*, x) \end{aligned} \tag{3.18}$$

where $w_c(x) = 1-\bar{u}(x, 0)$ is the mean velocity defect along the wake axis that serves as a proper measure of the local mean velocity. Then one gets, e. g. ,

$$\frac{\partial u'}{\partial x} = R^{\frac{1}{2}} w_c \frac{\partial u^*}{\partial x^*} + w_c \frac{\partial u^*}{\partial x} + u^* \frac{dw_c}{dx}$$

The other derivatives are calculated in the same manner. Upon substitution of these results into Eqn. (3.4), one obtains

$$\frac{\partial u^*}{\partial x^*} + \frac{\partial v^*}{\partial y^*} = -R^{-\frac{1}{2}} \left(\frac{\partial u^*}{\partial x} + \frac{u^*}{w_c} \frac{dw_c}{dx}\right)$$

$$\frac{\partial u^*}{\partial t^*} + \bar{u} \frac{\partial u^*}{\partial x^*} + \bar{u}_{y^*} v^* + w_c \frac{\partial p^*}{\partial x^*} + w_c \chi_1^*$$

$$= R^{-\frac{1}{2}} \left[\left(\frac{\partial^2 u^*}{\partial x^{*2}} + \frac{\partial^2 u^*}{\partial y^{*2}}\right) - \left(\bar{u} \frac{\partial u^*}{\partial x} + \frac{dw_c}{dx} \frac{\bar{u} u^*}{w_c} + R^{\frac{1}{2}} \bar{v} \frac{\partial u^*}{\partial y^*} \right.\right.$$

$$\left.\left. + \frac{\partial \bar{u}}{\partial x} u^* + w_c \frac{\partial p^*}{\partial x} + 2 \frac{dw_c}{dx} p^*\right)\right] + O(R^{-1}) \qquad (3.19)$$

$$\frac{\partial v^*}{\partial t^*} + \bar{u} \frac{\partial v^*}{\partial x^*} + w_c \frac{\partial p^*}{\partial y^*} + w_c \chi_2 = R^{-\frac{1}{2}} \left[\left(\frac{\partial^2 v^*}{\partial x^{*2}} + \frac{\partial^2 v^*}{\partial y^{*2}}\right) \right.$$

$$\left. - \left(\bar{u} \frac{\partial v^*}{ax} \mathbf{t} R^{\bar{2}} \bar{v} \frac{\partial v^*}{\hat{a} y^*} + \frac{dw_c}{dx} \frac{\bar{u} v^*}{w_c} + R^{\frac{1}{2}} v^* \frac{\partial \bar{v}}{\partial y^*}\right)\right] + O(R^{-1})$$

where

$$\chi_1^* = u^* \frac{\partial u^*}{\partial x^*} + v^* \frac{\partial u^*}{\partial y^*} - \frac{\partial}{\partial x^*} \overline{u^{*2}} - \frac{\partial}{\partial y^*} \overline{u^* v^*} + O(R^{-\frac{1}{2}})$$

$$\chi_2^* = u^* \frac{\partial v^*}{\partial x^*} + v^* \frac{\partial v^*}{\partial y^*} - \frac{\partial}{\partial x^*} \overline{u^* v^*} - \frac{\partial}{\partial y^*} \overline{v^{*2}} + O(R^{-\frac{1}{2}}) \qquad (3.19a)$$

These equations then describe the local behavior of the fluctuating quantities for x near x_0. The terms of the same order in $R^{-\frac{1}{2}}$ have

been grouped together in the above equations. For R>>1, it may seem to be plausible in neglecting terms of $O(R^{-\frac{1}{2}})$ to obtain

$$\frac{\partial u^*}{\partial x^*} + \frac{\partial v^*}{\partial y^*} = 0$$

$$\frac{\partial u^*}{\partial t^*} + \bar{u}\frac{\partial u^*}{\partial x^*} + \bar{u}_{y^*} v^* + w_c \frac{\partial p^*}{\partial x^*} + w_c \chi_1^* = 0 \qquad (3.20)$$

$$\frac{\partial v^*}{\partial t^*} + \bar{u}\frac{\partial v^*}{\partial x^*} \quad \text{t } w_c \frac{\partial p^*}{\partial y^*} + w_e \chi_2^* = 0$$

where χ_1^* and χ_2^* are given by (3.19a) with the terms of $O(R^{-\frac{1}{2}})$ neglected. However, a careful examination of the terms will reveal the inadequacy of such an approximation in a complete non-linear analysis. In fact, two independent small parameters appear in this problem: the amplitude of the fluctuation and $R^{-\frac{1}{2}}$ for large Reynolds number. Even for an arbitrary large Reynolds number, the terms on the RHS of Eqns. (3.19) are not negligible when the amplitude of the fluctuation becomes finite. This fact may be readily revealed by examining the leading terms on the RHS of Eqns. (3.19). Two types of terms appear; the Laplacian terms which indicate the viscous dissipation effect existed in all viscous fluid, and the terms originated from non-parallel mean flow. For a wake which is dynamically unstable, the viscous dissipation terms may be ignored in general for large R except for a few occasions in which the viscous terms are needed to smooth out singularity. But the terms resulting from the variation of the mean flow are in fact of a different nature. The leading terms are proportional to $(R^{-\frac{1}{2}} \frac{ciw_c}{dx} u^*)$ which can be immediately shown by using Eqn. (2.3a) to be of the order $(A|A|^2 j$ for large

R. Now, we note that the leading terms of χ_1^* and χ_2^* are of the order (A^2). Since the solution of Eqns. (3.19) will be sought in an ascending power series of A, the effect of the non-parallel mean flow will have to be included when terms of order higher than A^2 are intended. Appendix B gives further discussions on this point and indicates the approach to include these effects for the higher order terms.

For the present investigation, the higher order terms will not be intended numerically. Therefore, Eqns. (3.20) are used in place of the full equations without inconsistency. To this order, the local mean flow is considered to be parallel, and the transformation (3.17) may be replaced by

$$t^* = t/b(x)$$
$$x^* = (x-x_0)/b(x) \qquad (3.17a)$$
$$y^* = y/b(x)$$

which provides a consistent definition for the "*" variables with the expression (3.13). Equations (3.20) remain the same under this change. The differences between (3.17) and (3.17a) are of the same order of the terms ignored in arriving at Eqns. (3.20).

The first equation in (3.20) is satisfied by introducing a local stream function $\psi^*(x^*, y^*, t^*, x)$ such that

$$u^* = \frac{\partial \psi^*}{\partial y^*}, \quad v^* = -\frac{\partial \psi^*}{\partial x^*} \qquad (3.21)$$

Now, let

$$\psi^* = \sum_{n=1}^{\infty} [\, \psi_n(x^*, y^*; x)\, e^{-in\omega^* t^*} + \tilde{\psi}_n(x^*, y^*; x)\, e^{in\omega^* t^*}] \qquad (3.22)$$

where "~" denotes the complex conjugate and $\omega^* = b\omega$, a local angular frequency. The implicit dependence on x for both the amplitude and the distribution through the local mean flow quantities is also indicated. With Eqns. (3.21) and (3.22), after eliminating p* in the last two equations in (3.20), one obtains

$$\begin{aligned} &\bar{u}\frac{\partial}{\partial x^*}\nabla^2\psi_n - in\omega^*\nabla^2\psi_n - \bar{u}_{y^*y^*}\frac{\partial\psi_n}{\partial x^*} \\ &= -w_c \sum_{m=1}^{\infty} \left[\left(\frac{\partial\tilde{\psi}_m}{\partial y^*}\frac{\partial}{\partial x^*} - \frac{\partial\tilde{\psi}_m}{\partial x^*}\frac{\partial}{\partial y^*}\right)\nabla^2\psi_{m+n} \right. \\ &\left. + \left(\frac{\partial\psi_{m+n}}{\partial y^*}\frac{\partial}{\partial x^*} - \frac{\partial\psi_{m+n}}{\partial x^*}\frac{\partial}{\partial y^*}\right)\nabla^2\tilde{\psi}_m \right] \\ &+ \begin{cases} 0, & n = 1 \\ -w_c \sum_{m=1}^{n-1} \left(\frac{\partial\psi_m}{\partial y^*}\frac{\partial}{\partial x^*} - \frac{\partial\psi_m}{\partial x^*}\frac{\partial}{\partial y^*}\right)\nabla^2\psi_{n-m}, & n \geq 2 \end{cases} \end{aligned} \qquad (3.23)$$

where $\nabla^2 = \frac{\partial^2}{\partial x^{*2}} + \frac{\partial^2}{\partial y^{*2}}$.

This is a system of infinite numbers of coupled non-linear partial differential equations whose solutions are difficult to obtain in general. However, since the fundamental and the second harmonic are observed to be prominent in the "non-linear" region of Sato-Kuriki's experiment, the higher harmonics are not expected to play any essential role in this region. In order to simplify the analysis, we

truncate the series at n = 2, and obtain four coupled non-linear equations:

$$\bar{u}\frac{\partial}{\partial x^*}\nabla^2\psi_1 - i\omega^*\nabla^2\psi_1 - \bar{u}_{y^*y^*}\frac{\partial\psi_1}{\partial x^*}$$

$$= -w_c\left[\left(\frac{\partial\tilde{\psi}_1}{\partial y^*}\frac{\partial}{\partial x^*} - \frac{\partial\tilde{\psi}_1}{\partial x^*}\frac{\partial}{\partial y^*}\right)\nabla^2\psi_2\right.$$

$$\left. + \left(\frac{\partial\psi_2}{\partial y^*}\frac{\partial}{\partial x^*} - \frac{\partial\psi_2}{\partial x^*}\frac{\partial}{\partial y^*}\right)\nabla^2\tilde{\psi}_1\right] \qquad (3.24)$$

$$\bar{u}\frac{\partial}{\partial x^*}\nabla^2\psi_2 - 2i\omega^*\nabla^2\psi_2 - \bar{u}_{y^*y^*}\frac{\partial\psi_2}{\partial x^*}$$

$$= -w_c\left(\frac{\partial\psi_1}{\partial y^*}\frac{\partial}{\partial x^*} - \frac{\partial\psi_1}{\partial x^*}\frac{\partial}{\partial y^*}\right)\nabla^2\psi_1$$

and the complex conjugate of the above equations lor $\tilde{\psi}_1$ and $\tilde{\psi}_2$. For an antisymmetrical fundamental mode,† the second harmonic will be symmetric from Eqn. (3.24). Thus, the boundary conditions at $y^* = 0$ are:

$$\frac{\partial\psi_1}{\partial y^*} = 0 \quad \text{and} \quad \psi_2 = 0 \qquad (3.25a)$$

At large distances from the wake axis, the fluctuations should vanish. Therefore as $y^* \to \infty$

$$\psi_1,\ \psi_2 \to 0 \qquad (3.25b)$$

---

† The fundamental mode is chosen to be antisymmetric because the result of linear stability theory indicates that an antisymmetric fluctuation is more unstable than a symmetric one in the wake.

Then the solution to the above system becomes a non-linear eigenvalue problem. Since, however, we are not interested in the exact solution of these equations but in generating reasonable profiles for the use in the integral method, we adopt a small perturbation method for the solution of this problem. Even though in actual application, the amplitude of the fluctuations are not necessarily small.

Following Stuart and Watson, the following form is assumed for the solution of Eqn. (3.24)

$$\psi_1 = A^*(x^*;x)[f_0(y^*;x) + |A^*|^2 f_1(y^*;x) + \cdots]$$
$$\psi_2 = A^*(x^*;x)[g_0(y^*;x) + |A^*|^2 g_1(y^*;x) + \cdots] \qquad (3.26)$$

and

$$\frac{dA^*}{dx^*} = A^* \sum_{m=0}^{\infty} a_m |A^*|^{2m} \quad (a_0 = i\alpha^*) \qquad (3.27)$$

then

$$\frac{d|A^*|^2}{dx^*} = 2|A^*|^2 \sum_{m=0}^{\infty} a_{mr} |A^*|^{2m} \quad (a_m = a_{mr} + i a_{mi}) \qquad (3.27a)$$

As shown by Stuart and Watson, this form of solution leads to no inconsistency with Eqn. (3.24)† Upon substitution of Eqns. (3.26) and (3.27) into Eqn. (3.24), a set of ordinary differential equations can be obtained after equating terms of like powers in A^*. For the

---

†It should be noted that for the terms of order higher than A^2 in the above expressions, Eqns. (3.24) will have to be modified according to Appendix B.

leading term of the fundamental mode, $f_0(y^*)$, one obtains the Rayleigh equation

$$(\bar{u} - \frac{\omega^*}{a^*}) (\frac{d^2}{dy^{*2}} - a^{*2}) f_0 - \bar{u}_{y^*y^*} f_0 = 0 \qquad (3.28)$$

and its conjugate.

Here we have considered the so-called ''spatial mode'' of amplification as against the more commonly used ''temporal mode''. That is, with ω^* real, we take $a^* = ab = a_r^* + ia_i^*$, a complex wave number whose imaginary part gives the local spatial rate of amplification or decay depending on its sign, It has certainly a closer resemblance to the experimental situations than the temporal mode, and their interrelation, to the first order, is provided by the group velocity as shown by Gaster(27, 28)

Eqn. (3.28) may be solved together with the appropriate homogeneous boundary conditions. This constitutes an eigenvalue problem and a^* will be determined which in turn fixes the value of a_0 in Eqn. (3.27). However, it should be noted here that, being a solution to the homogeneous problem, f_0 may be multiplied by an arbitrary complex constant. Although this constant may be included in the amplitude A^*, which is not exactly defined yet, it may still have a dependence on the large length scale. This fact is indicated by the dependence of A^* on x in Eqn. *(3.26)*.

The equation for g_0 may be written as

$$(\bar{u} - \frac{\omega^*}{a^*}) (\frac{d^2}{dy^{*2}} - 4a^{*2}) g_0 - \bar{u}_{y^*y^*} g_0 = \frac{f_0^2}{2} w_c \frac{d}{dy^*} (\frac{\bar{u}_{y^*y^*}}{\bar{u} - \omega^*/a^*}) \qquad (3.29)$$

It should be mentioned that, in general, the solution to g_0 consists of **two** parts:

i) the homogeneous solution which satisfies the Rayleigh equation corresponding to an angular frequency $2\omega^*$, and

ii) the particular solution which depends on the forcing terms on the RHS of Eqn. (3.29) as a result of the non-linear interaction of the fundamental modes.

The homogeneous solution will introduce a new measure for its magnitude, say B^*, which is independent from **A*.** Therefore, an equation of an analogous form to Eqn. **(3.** 27) will have to be introduced. The theory of Stuart and Watson has completely ignored this contribution to the solution. Although this situation may be handled by the present method, as will be seen later, the algebra will become increasingly tedious and will tend to cover up the real physics. To simplify the calculations, we note that, as shown by Sato **and** Kuriki, the fundamental mode observed experimentally in the linear region is very close to the peak amplification rate predicted by the linear stability theory. Then, also from the linear stability theory (refer to Gold[4]), we will expect the disturbance at twice the fundamental frequency to be much less amplified or even damped, Therefore, it seems to be plausible to ignore the contribution to g_0 from the homogeneous part and use the particular solution of Eqn. *(3.* 29) as the sole representation for the leading term of the second harmonic.

In order to obtain the equation for $f_1(y^*)$, the correction term to the fundamental mode, the terms ignored in arriving at Eqns. **(3.** 20) must be included. Appendix F gives an approximate numerical

investigation of the effects of $f_1(y^*)$ on the complete flow based on Eqns. (3.20). The approach for an exact treatment of $f_1(y^*)$ is also discussed in Appendix F.

The solutions of f_0 and g_0 may be obtained numerically without much difficulty in general. However, an additional difficulty is encountered when $\alpha_i^* = 0$. In this case, the wave speed $c^* = \omega^*/\alpha^*$ is a real number, and there exists in the flow a critical point $y^* = y_c$ where $(\bar{u}-c^*)$ vanishes. For a wake, $\bar{u}_{y^*y^*}$ also vanishes at this point. Therefore, the equation for f_0 is regular. However, unless the RHS of Eqn. (3.29) for g_0 also vanishes as in the case of a shear layer considered by Stuart,[17] a singularity exists in Eqn. (3.29). For a wake, the singularity exists, hence the viscous terms will have to be retained in the neighborhood of the critical point in order to obtain a solution for g_0.†

To summarize, up to the order retained including the approximate solution of f_1 in Appendix F, the local stream-function is given by

$$\psi^* = \left\{ A(f_0 + |A|^2 f_1)\, e^{i\theta} + A^2 g_0 e^{i2\theta} \right\} + \text{conj.} \qquad (3.30)$$

where $\theta = \alpha_r^* x^* - \omega^* t^*$,

and $$A(x) = \epsilon(x) e^{-\alpha_i^* x^*} = A^* e^{-i\alpha_r^* x^*} \qquad (3.31)$$

with $\epsilon(x)$ denoting the slowly varying complex "constant" mentioned in discussing Eqn. (3.28). Thus, $A(x)$ represents the complex

---

† An alternate method to avoid the numerical difficulty is by taking a distorted contour around the critical point in the artificial complex y^*-plane.

amplitude of the fluctuation, still undefined so far. The expressions for u*, v* and p* can be easily obtained from (3.30).

If desired, the higher order solutions may be obtained similarly through this cascade process where the higher harmonics are generated as a result of the interaction of the lower harmonics and in return the lower harmonics are modified by the higher harmonics. The inclusion of f_0, g_0 and the discussion of f_1 in Appendix F in the present study demonstrate the essentials of these processes.

When the local mean flow conditions are known, Eqn. (3.30) will determine the distribution of the fluctuations when A is found. Because of the effects of the Reynolds stress and the non-parallel mean flow, a strong non-linear coupling exists between the growth of the wake (variation of the mean flow) and the variation of the fluctuation amplitude. The relations among the unknowns are obtained from the integral equations (3.14), (3.15) and (3.16). The expression (3.30) is used only to systematically introduce the higher harmonics into consideration. It provides a method to obtain the local distribution of the fluctuations and, therefore, the evaluation of the integrals, I_i, appearing in the governing equations (3.14), (3.15) and (3.16).

The complete interaction mechanism may be briefly illustrated in the schematic below.

The mean flow, being characterized by the centerline velocity defect $w_c(x)$ and the wake half-width $b(x)$ under the shape assumption (3.11), interacts with the fluctuating components through the Reynolds stress. The cascade process for generating the higher harmonics

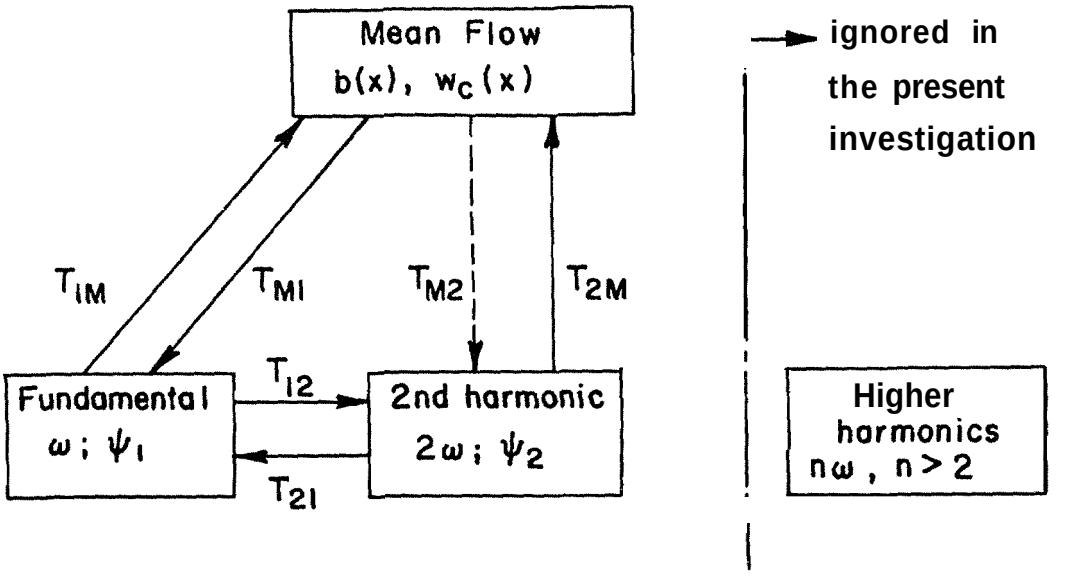

Schematic A of the Non-linear Interaction

and the corrections back to the lower harmonics seems, at least superficially, to limit the interaction of the mean flow with the higher harmonics to unidirectional. For example, the second harmonic (2ω), being generated by the interaction of the fundamental components, will have an effect on the mean flow through modifying the Reynolds stress. However, it seems to extract energy from the fundamental instead of directly from the mean flow because of the close link s f the second harmonic to the fundamental. This is the usual criticism on the cascade model (ref. to Yih[29]). But, because of the dependence of the integrals, I_i, on the local mean flow quantities, the mean flow in fact has a direct influence on the development of the second harmonic. So, basically, the present model does include all the essentials of the interacting mechanism. In the next

section, we will discuss the numerical treatment and will try to understand the various mechanisms by using the truncational approach discussed in this section to bring in the different effects in sequence.

4. First Order Results and Discussions; Case A

The present study is intended to bring out the main effects of the following two mechanisms in the transition region when the amplitude of the fluctuation can no longer be considered as infinitesimal;

a) the interaction between the growth of the wake and the growth of the amplitude of the fluctuation,

b) the generation of the higher harmonics and the interaction between modes.

It is therefore desirable to separate out the effects of these two mechanisms when we try to understand the processes numerically. This is done by truncating the expression **(3. 30)** for the perturbation stream function at various orders such that their effects may be isolated. Three cases are considered numerically in this investigation.

i) Case **A:** Eqn. **(3.** 30) is truncated after the first term by assuming that the fluctuation may be represented by the fundamental mode alone. This study is intended to understand the role of the Reynolds-stress in the energy exchange between the mean flow and the fluctuation. Since the higher harmonics are ignored, this case will bring out the effect of the first mechanism discussed above, This case is considered as the first order effect and will be discussed in this section.

ii) Case B: Both f_0 and g_0 remain in Eqn. **(3. 30)** to represent the fluctuation. This case allows a study of the

generation of the second harmonic through the non-linear terms and its interaction with the mean flow. By comparing with the results of case A in the next section, the effect of tne second harmonic may be separated out.

iii) Case C: All three terms in Eqn. (3.30) arc retained. The f_1 term, representing the feed-back to the fundamental mode, is generally considered as one basic feature of the non-linear interaction between modes. The study of this case is expected to bring out such an effect on the complete interaction. An approximate treatment is made in Appendix F.

These three cases, basically, include the essentials of the non-linear interaction mechanisms in the wake. Similar processes at much higher complexity are expected to be present in the wake where all the higher harmonics and other disturbances of different frequency exist. However, no deeper understanding of the transition of the wake is expected from the additional complexity, even though the evolution into a fully developed turbulent wake may be visualized as a result of such interaction.

4.1 Formulation

By truncating the expression (3.30) after the first term, this case considers only the processes T_{M1} and T_{1M} indicated in the schematic A representing the interaction between the mean flow and the fundamental mode.

From (3.30), the local fluctuating velocity components are

simply given by

$$u^* = A(x) f_0'(y^*) e^{i\theta} + \text{conj}$$

$$v^* = -i[A(x)\alpha^* f_0(y^*) e^{i\theta} - \text{conj}] \qquad (4.1)$$

$$p^* = A(x) p_{10}(y^*) e^{i\theta} + \text{conj}$$

Here "'" indicates differentiation with respect to y*. The solutions to the linear equation (3.28) have been studied by many investigators and show no conceptual difficulties. For a wake, $\bar{u}_{Y^*Y^*}$ vanishes at the critical point for the neutrally stable case. Therefore, no true singularity exists in Eqn. (3.28) even in the case of $\alpha_i^* = 0$. However, numerically, the error is enlarged when α_i^* becomes small. One method to overcome this difficulty is to include the viscous term partially such that Eqn. (3.28) is replaced by the Orr-Sommerfeld equation. But, even with the accuracy of the modern computing machines, special schemes (e.g., Kaplan's method[30]) have to be devised for obtaining a solution because of the presence of the rapidly growing exponential solutions (refer to Betchov and Crirninale)[31]. One possible way to avoid such an elaborated numerical scheme is discussed in Appendix D. The other method, which is used in the present investigation, is based on the findings of Lin[32-34]. Lin showed that, by taking an appropriate artificial complex contour near the critical point, the inviscid solution gave a good approximation to the full solution for the near neutral and slightly damped cases.

Using Eqn. (3.11) for the mean velocity, we can rewrite Eqn. (3.28) in the form

$$(U^*-\bar{c})\left(\frac{d^2}{dy^{*2}} - \alpha^{*2}\right) f_0 - \frac{d^2U^*}{dy^{*2}} f_0 = 0 \qquad (4.2)$$

where $\bar{c} = \frac{1}{w_c}\left(1 - \frac{\omega^*}{\alpha^*}\right)$ (4.3)

The appropriate boundary conditions lor the antisymmetric mode of disturbance are

$$f_0'(0) = 0$$
$$f_0'(\infty) + \alpha^* f_0(\infty) = 0 \qquad (4.2a)$$

Eqn. (4.2), together with the homogeneous boundary conditions (4.2a), constitute an eigenvalue problem. When the mean flow is given, Eqn. (4.2) can be solvecl numerically to obtain the eigenvalue and the corresponding eigenfunction $f_0(y^*)$. The details of the method of solution are given in Appendix A. It will only be noted here that, in general, for a given $U^*(y^*)$, we have

$$\alpha^* = \alpha^*(w_c, \omega^*)$$

and (4.4)

$$f_0 = f_0(y^*;\ w_c,\ \omega^*)$$

which indicates the iunctional dependence of the eigenvalue and the eigenfunction. Now, using (4.1), all integrals appearing in Eqns. (3.14), (3.15) and (3.16) can be expressed in terms of $f_0(y^*)$ and evaluated. The pressure is related to $f_0(y^*)$ by

$$p_{10}(y^*) = (U^*-\bar{c})f_0' - \frac{dU^*}{dy^*} f_0 \qquad (4.5)$$

It should be noted that the formulation so far has reduced the integrals I_i to a two-parameter representation aside from the direct square dependence on the amplitude A. Further approximation will now be made to simplify the analysis. We observe that, in general, the fluctuating components are much smaller than the mean, and since both I_1 and I_2 are positive and of the same order, the contributions from the fluctuations in Eqn. (3.14) may be ignored as a first approximation. This approximation allows the decoupling of the amplitude of the fluctuation from the relation between b and w_c, thus,

$$b = \frac{C_D/2}{w_c(\beta_1 - \beta_2 w_c)} \qquad (4.6)$$

Using (4.6), the integrals are then simplified to be functions of a single parameter w_c when the physical angular frequency and the free stream Reynolds number are given. Of course, the validity of this assumption will have to be examined a posteriori. It may be noted that for w_c small, Eqn. (4.6) reduces to Eqn. (2.2).

Using (4.1), the integrals can be written as

$$I_i = k_i(w_c)|A|^2 \qquad (4.7)$$

for i = 1, 2, ... 9. The k_i's are integrals of functions of $f_0(y^*)$ and, therefore, they are functions of one parameter $w_c(x)$ only. They are given by

$$k_1(w_c) = \int_0^\infty |f_0'|^2 \, dy^*$$

$$k_2(w_c) = \int_0^\infty |a^*|^2 \, |f_0|^2 \, dy^*$$

$$k_3(w_c) = \int_0^\infty U^* \, |f_0'|^2 \, dy^*$$

$$k_4(w_c) = \int_0^\infty U^* |a^*|^2 \, |f_0|^2 \, dy^*$$

$$k_5(w_c) = \int_0^\infty y^* \frac{dU^*}{dy^*} (|f_0'|^2 - |a^*|^2 \, |f_0|^2) dy^*$$

$$k_6(w_c) = -i \int_0^\infty [a^* f_0 \tilde{f}_0' - \tilde{a}^* \tilde{f}_0 f_0'] \frac{dU^*}{dy^*} dy^* \qquad (4.7a)$$

$$k_7(w_c) = \int_0^\infty [f_0' \tilde{p}_{10} + \tilde{f}_0' p_{10}] \, dy^*$$

$$k_8(w_c) = \int_0^\infty [2|a^*|^2 (a_i^{*2} - a_r^{*2}) |f_0|^2 + (a^{*2} f_0 \tilde{f}_0'' + \tilde{a}^{*2} \tilde{f}_0 f_0'') - |f_0''|^2 - |a^*|^2 \, |f_0'|^2] \, dy^*$$

$$k_9(w_c) \equiv 0$$

Then by using (4.6), Eqns. (3.15) and (3.16) can be written as two first order ordinary differential equations for $w_c(x)$ and $|A|^2(x)$. The exact definition of A will now be given by setting

$$k_1 + k_2 = \int_0^\infty [|f_0'|^2 + |a^*|^2 \, |f_0|^2] \, dy^* = 1 \qquad (4.8)$$

This definition seems to be an appropriate one since both the governing equations are for the energy and (4.8) identifies one of the unknowns, $|A|^2(x)$, as the averaged energy of the fluctuating components nondimensionalized by the local mean velocity defect. Because of the quantities $|A|^2$ and w_c^2 always appearing together, it is more convenient to use $Z = 2|A|^2 w_c^2$ as one dependent variable instead of $|A|^2$. The physical significance of Z to this order can be easily seen to be the total energy density of the fluctuation, because

$$Z = \frac{1}{b}\int_0^{\infty} (\overline{u'^2} + \overline{v'^2})dy \tag{4.9}$$

The set of equations can now be written in the form

$$K_{11}(w_c, Z)\frac{dw_c}{dx} + K_{12}(w_c, Z)\frac{dZ}{dx} = K_{13}(w_c, Z) \tag{3.15a}$$

$$K_{21}(w_c, Z)\frac{dw_c}{dx} + K_{22}(w_c, Z)\frac{dZ}{dx} = K_{23}(w_c, Z) \tag{3.16a}$$

or, solving for the derivatives algebraically, one obtains

$$\frac{dw_c}{dx} = \frac{N_1(w_c, Z)}{D(w_c, Z)}$$

$$\frac{dZ}{dx} = \frac{N_2(w_c, Z)}{D(w_c, Z)} \tag{4.10}$$

with

$$N_1 = K_{13}K_{22} - K_{12}K_{23}$$

$$N_2 = K_{23}K_{11} - K_{13}K_{21} \tag{4.10a}$$

$$D = K_{11}K_{22} - K_{21}K_{12}$$

and

$$K_{11} = b[2\beta_2 - 3\beta_3 w_c - 2Z(\frac{dk_3}{dw_c} - \frac{dk_4}{dw_c})]$$

$$+ \frac{db}{dw_c}[\beta_2 w_c - \beta_3 w_c^2 - 2Z(k_3 + k_5 - k_4)]$$

$$K_{12} = -2(k_3 - k_4)b$$

$$K_{13} = -k_6 Z - \frac{2\beta_4 w_c}{Rb}$$

(4.10b)

$$K_{21} = Z\left\{b(k_7 - 3k_3 + k_4) + bw_c \frac{d}{dw_c}(k_7 - k_3 - k_4)\right.$$

$$\left. + \frac{db}{dw_c}[1 + w_c(k_7 - k_3 - k_4 + 2k_5)]\right\}$$

$$K_{22} = b[1 + (k_7 - k_3 - k_4)w_c]$$

$$K_{23} = Z[k_6 w_c + \frac{k_8}{Rb}]$$

Eqns. (4.10) are then solved as an initial value problem. However, since the initial magnitude of the fluctuation will be different for different testing conditions, it should be left as a parameter to be specified for each problem. It is, therefore, first proposed to solve this initial valued problem in the following manner.

In the limiting case of zero amplitude of the fluctuation, the set reduces to the integral equations of a steady laminar wake. Eqn. (3.16) is identically satisfied and Eqn. (3.15) becomes

$$\frac{dw_{c_\ell}}{dx} = \frac{-\beta_4 w_{c_\ell}/(Rb)}{b(\beta_2 - 1.5\beta_3 w_{c_\ell}) + \frac{w_{c_\ell}}{2}\frac{db}{dw_c}(\beta_2 - \beta_3 w_{c_\ell})} \qquad (4.11)$$

with b given by (4.6) exactly. The solution of (4.11) can he obtained once and for all by starting the numerical integration from a far wake solution at some large distance x. The additional subscript "ℓ" is used to designate this solution which corresponds to no disturbance case.

In general, to solve Eqns. (4.10), a set of initial conditions, $w_{c\theta}$ and Z_0, has to be given at some initial station ζ_0. Then, it seems to require two free parameters for the problem. However, if ζ_0 is taken to be somewhere near the beginning of the wake (but not right at the vicinity of the plate trailing edge where the boundary layer approximations are invalidated), the magnitude of Z_0 is expected to be very small if a laminar boundary layer exists on the plate. Then Z_0 and w_{co} are not independent but connected by the governing equations. If we let

$$w_{c0} = w_{c_\ell} + \Delta w,$$

then apply linearization, Δw and Z_0 satisfy a set of homogeneous ordinary differential equations. The condition on the existence of a solution yields a relation of the form

$$\frac{\Delta w}{Z_0} = \text{function } (w_{c_\ell}) \qquad (4.12)$$

Eqn. (4.12) reduces the problem to one initial parameter.

Integration of Eqns. (4.10) can then be started by picking an initial station ξ_0 and specifying an initial magnitude $Z_{0'}$

Since Δw is generally very small when Z_0 is small, it has been found numerically that the solutions are quite insensitive to the value of Δw as long as Z_0 is small. For a qualitative understanding of the problem, this small difference in the solutions may be ignored. Thus, most of the results to be presented in the next section have been obtained by using $w_{c0} \equiv w_{c_\ell}$ at the initial station. Its effect on the solutions will be discussed later.

4.2 Results and Discussions

For the purpose of comparison with the experimental results of Sato and Kuriki, [2] the numerical calculations have been performed corresponding closely to the experimental conditions. The mean velocity function, $U^*(y^*)$, used for the calculation is taken to be the one used by Sato and Kuriki in the linear region, i.e.,

$$U^*(y^*) = \exp(-0.69315\, y^{*2}) \tag{4.13}$$

Eqn. (4.13) also gives the exact definition of the half-wake width b as the distance from the wake axis to the half velocity defect point where $U^* = 0.5$. The physical angular frequency of the fundamental mode used in the calculation is also taken from the experiment of Sato and Kuriki to be 730 cps at $R = 2 \times 10^5$.

The preliminary numerical work for case **A,** where the non-linear terms in the local disturbance equations are neglected, amounts to solving the Rayleigh equation and obtaining the integrals. Using the method discussed in Appendix **A,** we find that the frequency

observed experimentally does correspond to the one receiving nearly maximum amplification rate in the linear region as indicated by the temporal mode calculation of Sato and Kuriki. Following this frequency, the variation of the local amplification rate as a function of the mean velocity defect along the wake axis, w_c, is shown in Fig. 2. As the value of w_c decreases, the disturbance becomes less amplified. At $w_c \approx .147$, $a_i^* = 0$; the given frequency corresponds to a neutrally stable solution according to the linear theory. Further decrease of the mean flow parameter w_c will make this frequency a damped disturbance ($a_I^* > 0$) according to the linear theory.

A few typical distributions of the magnitude and phase of the eigenfunction $f_0(y^*)$ and its derivative $f_0'(y^*)$, corresponding to a range of eigenvalues between the most amplified and the nearly neutral ones, are shown in Figs. 3a-j. It may be interesting to note the fairly drastic variation of the phase of f_0 with the mean flow parameter as it approaches the neutral case.

The eigenvalues and the corresponding integrals, k_i, as functions of the parameter, w_c, are given in Tables I and II. Calculations have been performed only for those listed cases. A complete curve for each integral as a function of w_c is generated by curve-fitting through those points. The derivatives (dk_i/dw_c), when required, are obtained by differentiating the curve-fit. In general, the integral curves are sufficiently smooth to permit such an operation, and check well with the slopes obtained graphically.

With all the functions appearing in Eqns. (4.10) determined, the equations may be integrated for each given set of initial conditions.

4.2.1 Comparison with Experiment

Most of the experimental results presented by Sato and Kuriki were measured with a free stream velocity U = 10m/sec. and a plate length L = 30 cm. These conditions co respond to a free stream Reynolds number of 2×10^5. From the experimental evidences, laminar Blasius velocity profile was established on the wall near the end of the plate, and a nearly laminar region of small amplitude disturbances existed at the beginning of the wake, The calculations are therefore started at an initial station $\zeta_0 = .05$ using the appropriate initial conditions. Two initial parameters are at our disposal. The centerline velocity defect w_{c0} at ζ_0 can be taken from either the exact solution of Goldstein or the integral solution of an undisturbed laminar wake in the present formulation which is not very accurate there in view of the decreasing validity of the boundary-layer approximation as ζ_0 decreases. For the present comparison purposes, it is decided to use $w_{co} = 0.7$ at $\zeta_0 = .05$ because of the closer agreement with the experiment at that point.

Another initial parameter is chosen to be the initial integrated energy content in the u'-component; i. e. ,

$$E_{u0} = \left(\frac{1}{b} \int_0^{\infty} \overline{u'^2}\, dy \right)_{\zeta_0} = k_1 (w_{c0}) Z_0 \qquad (4.14)$$

where the subscript "0" refers to value at ζ_0. The use of this free parameter seems to be justifiable because of the different flow conditions encountered in each experiment, e. g. , the free stream turbulence intensity level, the physical dimension of the plate trailing edge, etc.

As we have mentioned previously, these two initial parameters are not independent for small E_{uo} and only one free parameter exists. But, for the purpose of a qualitative understanding of the transition mechanisms in the wake, they are chosen somewhat arbitrarily in performing the following calculations. The effects of each of the initial parameters on the complete solutions will of course be investigated later,

Fig. 4 shows a comparison of the measured centerline velocity defect w_C with the present calculation. The value of E_{u0} has been taken as 1×10^{-5} for obtaining the curve. The result is quite satisfactory and seems to provide the explanation for the rapid breakaway from the pure laminar wake solution of Goldstein which is also shown in the same figure for comparison.

Only those data and calculated curve for $x \leq 0.5$ are presented because the three-dimensional effects observed experimentally at larger x are not included in the present formulation. Theoretical calculation for $x > 0.5$ stays practically unchanged near the value of $w_C = .148$. It is also interesting to note that this asymptotic value of w_c corresponds closely to the value where $\alpha_1^* = 0$. This value seems to indicate a balance between the various mechanisms which are responsible for changing the mean flow. A detailed discussion of the physical mechanisms involved will be given later. We will just note that, although it may be somewhat fortuitous, the measured w_C has never become smaller than this value before the turbulent region for all the tests.

Fig. 5 shows the comparison of the measured wake half-width with the one calculated by using Eqn. (4.6). The general trend is still satisfactory but not as good as w_c. This disagreement tends to suggest the approximation used in leading to (4.6) may not be appropriate if a better calculation is required. In such cases, the exact relation (3.14) will have to be used which couples the growth of the wake directly to the amplitude of the disturbance. An attempt to include this effect will be discussed in Section 4.2.6. Also shown on the same plot is the growth of the purely laminar wake. The strong interaction effect induced by the Reynolds stresses is evident from this comparison where the wake width has increased by more than a factor of two.

Fig. 6 gives the theoretically calculated variation of the integrated fluctuation energy, $E_u = \frac{1}{b}\int_0^{\infty} \overline{u'^2}\, dy$. Since no quantitative measurement of the magnitude of the fluctuating components has been reported by Sato and Kuriki, a direct comparison with the experiment is not possible. However, the variation of the maximum of $(\overline{u_f^2})^{\frac{1}{2}}$ given by Sato-Kuriki on an arbitrary scale (Fig. 1) does yield the similar relative development of the fluctuation. Experimentally, the magnitude of the fundamental mode grows initially according to the exponential law of the linear stability theory but it soon reaches a maximum and then decreases. This fact, which cannot be explained by the linear stability theory alone, may be understood now from the present calculation. However, it should be pointed out that the rapid decrease of E_u does not imply the same variation of the total fluctuation energy. This is seen in Fig. 7 where

$$E_F = \int_0^\infty (\overline{u'^2} + \overline{v'^2})dy,$$

are plotted. The variation of E_F is related to the local amplification rate a_1^* given by the linear theory with some correction due to the variation of the mean flow as demonstrated in Section 2.4. The rate of change of the amplitude will therefore start out in the linear region with a nearly maximum exponential growth and decreases as it moves downstream. The fluctuation reaches an equilibrium amplitude somewhere near $a_1^* = 0$ when the mean flow ceases to vary, and then slowly decays because of the viscous dissipating effect. Because of the growth of the wake, a more appropriate measure of the magnitude of the disturbance is the total energy density E_T defined by Eqn. (2.8). The variation of E_T is shown in Fig. 7a. The reason for the sharp decrease of E_u in contrast to a relatively slower variation of the total fluctuation energy density as shown in Fig, 7a is given by Fig. 8 where the ratio of the integrated energy content in u' to that in v',

$$k_1/k_2 = \int_0^\infty \overline{u'^2}\, dy^*/\int_0^\infty \overline{v'^2}\, dy^*,$$

is plotted against w_c. The ratio varies by more than a factor of six for the range of w_c encountered here. Therefore, we may conclude that the redistribution of the fluctuation energy between the two components u' and v', together with the change of mean flow are responsible for the experimentally observed abnormal phenomena.

The non-dimensional wave propagation velocity, taken as the real part of $c^* = \omega^*/\alpha^*$, measured by Sato-Kuriki, can also be obtained from the present calculation and the comparison is shown in

Fig. 9. The scatter of the experimental data suggests that the agreement is acceptable. The variation of the wave speed is again a consequence of the changing mean flow.

In view of the expansion series in $|A|^2$ used in the present formulation, the variation of $|A|^2$ with x is shown in Fig. 10. This variation should follow closely the local amplification rate except for a small correction caused by the changing mean flow indicated by $\epsilon(x)$ in Eqn. (3.33) and the viscous damping effect which has been ignored in the local calculation. The maximum value reached, 0.8, is certainly too large for justifying the truncation of the higher order terms. However, it should be emphasized again that the error induced by the truncation would be minimized by the use of the integral method.

Another indication of the need for the inclusion of the higher order terms is seen in Fig. 11 where the variation of the integrated fluctuation energy in u'-component divided by the square of the local mean velocity defect, $A_u = \int_0^\infty \overline{u^{*2}}\, dy^*$, is shown. This quantity, which is usually used by the experimentalists as a measure of the intensity of the fluctuation, seems to be too high from the calculation. This discrepancy may be a result of the truncation. However, it should be noted that, in the present formulation we have assumed that only a single frequency dominates and the higher harmonics, as a consequence of the non-linear interactions, only appear at integer multiples of this frequency. In the real situation, a spectrum of all frequency exists. Individually the fluctuation with frequency other

than ω may have negligible amplitude as compared to the one at ω, but their integrated effect may not be ignored. The present formulation has included practically all the energy in a single frequency; hence we shall expect a higher level than that being observed in the experiments. A further discussion on this point will have to be made after the completion of the calculations including the higher harmonics. We will first accept this first order truncational approach and proceed to study the physical interaction mechanisms in the wake through the numerical results.

4.2.2 Physical Mechanisms of Energy Balance

This section will recapitulate and justify quantitatively the qualitative discussions given in Section 2.4. As we have discussed previously, the energy equations for the mean flow and for the fluctuation written in the form of (3.15) and (3.16) indicate clearly the governing energy transfer mechanisms. The left hand side of both equations represent essentially the rate of change of the energy which are balanced by the terms representing the Reynolds stresses and the viscous dissipation on the right. We may rewrite Eqns. (3.15) and (3.16) symbolically as

$$\frac{dE_m}{dx} = - T_{RM} - T_{VM} \tag{4.15a}$$

$$\frac{dE_f}{dx} = T_{Rf} - T_{Vf} \tag{4.15b}$$

where

$$T_{RM} = T_{Rf} = I_6 w_c^3 - 2w_c^2 [I_5 w_c \frac{db}{dx} + (I_4 - I_3) b \frac{dw_c}{dx}]$$

and

$$T_{VM} = \beta_4 \frac{w_c^2}{Rb}$$

$$T_{Vf} = I_8 \frac{w_c^2}{Rb}$$

E_m and E_f, to the leading order, represent the energy content of the mean flow and the fluctuation correspondingly. Both T_{VM} and T_{Vf} are always positive and represent the loss of energy by viscous dissipation. We will expect the sign of T_{RM} or T_{Rf} to be positive in general such that the energy is taken from the mean flow and fed into the fluctuation through the Reynolds stresses.

It is appropriate to note here that Eqn. (4.15b) may be written in the form of a governing equation for the amplitude of the fluctuation, which gives

$$\frac{d|A|^2}{dx} = |A|^2 [\overline{a_0}(x) + \sum_{n=1}^{\infty} \overline{a_n}(x) |A|^{2n}] \qquad (4.16)$$

This is analogous to the amplitude equation obtained in the non-linear stability theory for parallel flows (e.g., Watson[19]). The main difference is in the dependence of the coefficients $\overline{a_n}(x)$, on the mean flow quantities instead of being constants as in the case of parallel flows. In fact this is the feature which brings out a much larger deviation from the linear stability theory. The coefficient $\overline{a_0}(x)$ in Eqn. (4.16) is proportional to the local amplification rate which is equal to $(-\alpha_i^*)$

in the present spatial mode approach. The coefficient $\overline{a_1}(x)$ which is generally referred to as the second Landau "constant" in the parallel flow theory, is no longer a constant here. And because of the changing mean flow, $\overline{a_1}$ is non-zero even when the higher harmonics apart from the fundamental mode are ignored.

With the numerical results obtained, a detailed numerical breakdown of the variations of the terms which appear in Eqns. (4.15) should be helpful in understanding the physical processes in the transition region. The result is shown in Fig. 12. The following physical picture is evident if we refer simultaneously to Figs. 4 and 7, where w_c gives a measure of the energy of the mean flow while E_F is certainly the correct representation of the fluctuation energy.

When the amplitude of the fluctuation is small in the initial stage of the wake, the magnitude of T_{RM} is quite small as compared to the viscous term T_{VM}. Eqn. (4.15a) is not much different from the integral energy equations for a steady laminar wake and the solution for w_c follows closely the solution of Goldstein. As to Eqn. (4.15b), it can be shown that for Z small, where the variation of mean flow may be ignored, the equation gives a nearly constant rate of exponential growth predicted by the linear stability theory for the infinitesimal disturbances as it should. Moreover, the viscous dissipation term T_{Vf} is of an order of magnitude smaller than T_{Rf} which supports the fact that the instability of a wake is basically an inviscid phenomenon. In this region, the energy transfer terms, whose leading order is proportional to the square of the amplitude of the fluctuation, are so small that the transfer of energy may be

ignored as assumed in the linear stability theory. However, as the amplitude grows, the energy transfer by the Reynolds stresses, T_{RM}, becomes of comparable magnitude to the laminar viscous dissipating term T_{VM}, and may no longer be ignored. The effect appears on the noticeable branching away of the mean velocity from the steady laminar wake solution. The continuing near exponential increase of the magnitude of this energy transfer term causes the complete wake to be quickly dominated by the energy transfer between the mean and the fluctuation. The energy is continuously extracted from the mean flow and fed into the fluctuating components. In the meantime, because of the rapid growth of the wake, the disturbance is driven away from the maximum amplification rate and becomes less amplified. This fact is clearly shown in Fig. 12a where the variation of the local spatial amplification rate, $-\alpha_i^*$, is plotted. As a result, the rate of energy transfer from the mean flow soon becomes saturated and decreases. This point of saturation corresponds approximately to the location of maximum slope (dw_c/dx). From this point on, the fluctuating component continues to take energy out from the mean flow but at a decreasing rate until it reaches the value w_c for the mean flow, where the local linear solution gives a very small negative value of α_i^*. At this point, the Reynolds stresses term becomes vanishingly small and because of the higher order terms, which appeared as a result of interpreting part of E_m as the energy of the mean flow, the energy is feeding, though slowly, back to the mean flow. When this energy transfer is just right to balance the laminar viscous dissipation

term, T_{VM}, the mean flow reaches an equilibrium, i.e., the asymptotic value of w_c obtained numerically. Meanwhile, the magnitude of T_{Vf} becomes comparable to T_{Rf} and dominates the fluctuation development. The energy is then dissipated from the fluctuation which causes the amplitude of the fluctuation to decrease at a small rate.

Calculations have been carried out to a much larger x that shows practically no change from the picture described above. Because of the viscous dissipation terms, eventually the amplitude goes back down to a very small value where the laminar viscous term in the mean flow equation takes over again. This is a slow process and we have known from the experiments that both the higher harmonics and the three-dimensional effect, even turbulence, will set in long before then. Therefore, no emphasis will be placed on the results at large x.

It may be noted here that the terms which have been generally termed as the "Reynolds stresses" effect in Eqns. (4.15) are actually composed of two parts: one is the usual Reynolds stress $(\overline{u'v'})\frac{\partial \bar{u}}{\partial y}$, and the other originates from the normal stresses, $(\overline{u'^2} - \overline{v'^2})\frac{\partial u}{\partial x}$. The latter will not appear in a strictly parallel flow. A further breakdown of the contributions to T_{RM} or T_{Rf} is shown in Fig. 13, where T_{R1} denotes the contribution from $(\overline{u'v'})\frac{\partial \bar{u}}{\partial y}$ and T_{R2} gives the direct effect of the non-zero mean flow gradient on the energy exchange. It is clear that the contribution of T_{R2} is small in general except near equilibrium. This is in agreement with the large Reynolds number boundary layer approximation used in the present analysis.

However, it should be noted that, if there were an axial mean pressure gradient, its effects would appear mainly through T_{R2} as seen from the derivation leading to the equation. This point will be discussed further through additional numerical calculations in Appendix E, to investigate the effect of dp/dx.

4.2.3 Effects of the Initial Values

Although no special attempt has been made in obtaining the theoretical curves discussed in this section to match the experimental data, the arbitrariness in getting the set of initial values warrants an investigation of their effects. We will study the effects of the two initial values, w_{co} and E_{u0}, separately in the following.

(A) Effects of w_{co}

We first notice that the integral solution of Eqn. (4.11) does not agree exactly with the solution of Goldstein. Curve 1 in Fig. 14 corresponds to the solution of Goldstein. Curve 2 is obtained by starting the integration of Eqn. (4.11) at a large value of x, using the far wake solution of Goldstein at that point, integrating backward toward the origin. The curve deviates from the solution of Goldstein in the near wake region as a result of the integral approximation. Curve 3 is obtained by using the exact value of Goldstein at ζ_0 and integrating downstream. This gives a closer agreement with the solution of Goldstein in the region where the main interest of our present investigation rests, but it gives a consistently higher w_c than curve 1. Curve 3 can in fact be obtained by shifting the origin of curve 2. Physically, curve 3 corresponds to a thinner wake than the other two at

corresponding stations. For consistency of the integral approach the value from curve 2 should be used for the calculation. However, since all integrals are taken as functions of w_c alone, it is also desirable to use the result closest to the exact solution. This fatter choice has been used in obtaining the previous calculations because of the closer agreement of curve 3 to the exact solution in the region of interest ($.05 \leq x \leq .30$). It is therefore necessary to investigate the effect of varying w_{c0} in the solutions.

Three cases of variation of w_c corresponding to the initial values w_{co} being 0.7, 0.675, and 0.6386 are shown in Fig. 15. The value $w_{c0} = 0.6386$ corresponds to the steady laminar wake solution of curve 2 in Fig. 14 at $\zeta_0 = .05$. The same value of E_{u0} has been used for all three curves which seem to give qualitatively the same variation of w_c and asymptote to the same value of w_c. The effect of w_{c0} appears mainly in the maximum value of dw_c/dx reached such that a smoother variation is obtained for a lower value of w_{c0}. A few experimental data points are also shown there for comparison. Using the location of maximum dw_c/dx as a point of demarcation, it seems to indicate that the experimental data agree better with the result of smaller w_{c0} in the rear portion of x, but a closer agreement is seen with the larger w_{c0} case for the front portion. This is expected because of the implications of different initial wake thicknesses for the different values of w_{c0}.

Figs. 16 and 17 give the variations of the integrated fluctuation energy for the three cases. The general variation is again qualitatively unchanged except for the different locations and levels

of the maximum value reached. This difference can also be understood from the fact that a higher w_{c0} implies a thinner wake and therefore a higher amplification rate locally. This finding explains in a small part the high peak energy obtained by the calculations using $w_{c0} = 0.7$ as compared to the experiments.

An additional test has been made by varying the values of w_{c0} by a small amount according to Eqn. (4.12) when w_{co} is linked to the initial disturbance energy level E_{u0}. The results show practically the same solutions. Therefore, no attempt has been made to use Eqn. (4.12) for all the calculations.

In conclusion, the effect of w_{co} is not very important when the purpose of the study is a qualitative understanding of the transition mechanism in a wake. However, the indicated effects should be borne in mind when any quantitative comparison is intended,

(B) Effects of E_{u0}

To investigate the effect of E_{u0} on the solutions, a few cases were calculated for $R = 2 \times 10^5$ with the same value of w_{co} but different E_{u0}. Fig. 18 shows the variations of w_c for three initial values $E_{u0} = 0.1,\ 1.0,\ 3.0 \times 10^{-5}$. The shape of the curves remains practically unchanged. Changing the initial value of E_{u0} amounts only to a shift of the curve. It is expected from the previous discussions of the physical mechanisms that the magnitude of the disturbance required to cause a sensible deviation of the solution from the undisturbed case is approximately the same over a range of w_c where the laminar viscous term is of the same order. Therefore a smaller

initial magnitude of the disturbance will cause the mean flow to be well approximated by the laminar solution for a longer distance, while the disturbance grows exponentially without much influence on the mean flow, till it reaches the magnitude where the interaction becomes important. This is further illustrated by the variations of the integrated fluctuation energy, E_u, shown on Fig. 19. The shapes are again similar with merely a shift in abscissa. It should be noted that, with the variation of a factor **30** in E_{u0}, the maximum values of E_u reached are nearly the same and the difference in the "equilibrium" magnitude is negligible, The slight difference in the peak values of E_u is caused by the slight change in the magnitude of the laminar viscous term when the interaction becomes important. In principle, if the initial magnitude of the fluctuation is small enough, the solution will approach the steady laminar wake solution corresponding to $E_{u0} \equiv 0$ which is also shown in Fig. 18 for comparison.

The magnitude of the disturbances existing at the initial stage of the wake depends on many factors which vary from experiment to experiment. These factors include both controllable, e. g. , an artificial source of disturbance, and partially controllable, e. g. , roughness of the plate, wind tunnel noise level, etc. If any quantitative calculations are needed, it will be necessary to have some measure of the magnitude of E_{u0}. This fact is further demonstrated by the two sets of experimental data points also shown on Fig. 18 taken from the paper of Sato-Kuriki. The data points correspond to two different plate models tested under the same free stream conditions. Model I has a sharp trailing edge but Model II has a blunt one. As to be

expected, a larger E_{uo} will be associated with Model II which shows the right trend as indicated by the calculations.

As a whole, we may conclude that the initial values will affect the solutions quantitatively but with the qualitative mechanisms in the non-linear region remaining practically unchanged. This insensitivity is to be expected when the non-linear effects are important; the memory of the initial values should be mostly erased.

4.2.4 Reynolds Number Effect

A wake is dynamically unstable because of the inflected mean velocity profile. The linear stability theory indicates that the effect of Reynolds number on the stability of the free shear flow is negligibly small for sufficiently large Reynolds number. It has been shown that the effect of $(1/R)$ terms in the equation is small everywhere except in a small region near the critical layer for the amplified and neutral disturbances. In general, the viscous effect does not affect the eigenvalues which may be determined from the inviscid equation, The amplification rate given by the linear stability theory is therefore unaffected by the Reynolds number. For the non-linear approach here, it is certainly desirable to find out the effects of Reynolds number on the transition of the wake, which is defined here as the deviation from a pure laminar wake.

Since the inviscid Rayleigh equation has been used to obtain the local solutions for the fluctuation, the integrals, k_i, are universal functions of w_C for all Reynolds numbers. This may be seen from Eqn. (4.4) where the eigenvalue and the corresponding eigenfunction are indicated to be functions of w_c' and ω^*. The non-dimensional

frequency ω^* is related to the physical angular frequency by

$$\omega^* = \omega b = \frac{bL}{U} \times (\text{physical frequency}) \qquad (4.17)$$

It was found experimentally by Sato and Kuriki that the physical frequency of the most unstable sinusoidal fluctuation observed in the linear region of the wake follows a 3/2 power law as the Reynolds number varies. Furthermore, the half-width, b, is clearly seen from Eqn. (3.14) to be varying with the drag coefficient which is proportional to $R^{-\frac{1}{2}}$. Therefore, if we chose to follow the most unstable frequency at various free stream Reynolds numbers, the value of w^* is a constant which is independent of R. Thus, the same functional relations $k_i(w_c)$ may be used for different Reynolds numbers that greatly simplify the investigation of the effects of Reynolds number.

Fig. 20 shows the variations of w_c for four values of Reynolds numbers. The same set of initial values, $w_{co} = 0.7$ and $E_{u0} = 1 \times 10^{-5}$ has been used in obtaining the curves, in order to isolate the effects of Reynolds number. The effect on the solution is somewhat similar to the effect of changing the initial magnitude of the fluctuation E_{u0}. In fact, it may be seen from Eqn. (4.15a) that the ratio of the Reynolds stresses term to the laminar viscous term is of the order $|A|^2\sqrt{R}$. Hence, the effect of R on the beginning of transition is similar to the effect of E_{u0}. However, the effect of R differs through its persistent influence over the whole non-linear region other than a mere shift of the abscissa. When the

Reynolds number decreases, the viscous damping term becomes more important in the non-linear region, therefore the overall transition becomes smoother. The pure laminar wake solution also shown on the same plot, in principle, gives the limiting case of very small Reynolds number. But this interpretation of the pure laminar wake solution is merely an ideal one and the one corresponding to zero amplitude disturbance is preferred in the present high Reynolds number approach.

Also shown in Fig. 20 are two sets of experimental data of Sato and Kuriki at $R = 2 \times 10^5$, 1×10^5 correspondingly. The agreement in the trend and even the quantitative effect are fairly good considering the fact that if $E_{u0} = 1 \times 10^{-5}$ were correct for the case of $R = 2 \times 10^5$, the same value of E_{u0} would have been too large for the smaller Reynolds number case.

Because of the persistent influence of the Reynolds number on the interaction, its effect on the fluctuation energy is more pronounced than the effect of E_{u0}. The result is shown on Fig. 21 where it may also be noted that the final equilibrium amplitudes reached are different because of the effect of Reynolds number appearing through the term T_{Vf} in Eqn. (4.15b). This result is also different from the effect of E_{u0} which leaves the final equilibrium amplitude of the fluctuation practically unchanged.

4.2.5 Effect of the Viscous Dissipation Term T_{Vf}

The effect of the viscous dissipating term T_{Vf} in the development of the disturbances can be studied by simply setting $I_8 \equiv 0$.

Comparison is made on Figs. 22 and 23 for the case of $R = 2 \times 10^5$. With identical initial conditions, Fig. 22 shows that the effect of T_{Vf} on the mean flow is quite small as one would expect. Figs. 23 and 23a show that if the viscous dissipation term were absent, a final equilibrium amplitude would have been achieved, and therefore another laminar oscillatory flow. However, because of the effect of the viscous dissipation, this equilibrium condition cannot maintain itself and the amplitude decays slowly as it proceeds further downstream to account for the energy loss.

4.2.6 Effect of Coupling b to w_c

The assumption of neglecting the contribution from the fluctuating components in the integrated momentum equation, which leads to a simple relation (4.6) between b and w_c, will now be examined. From the calculated results, it is found that the terms, which have been neglected to arrive at the expression (4.6), are indeed small compared to the remaining terms in the initial stage but increase to about 20 percent of the sum of the remaining terms when the amplitude of the fluctuation reaches a maximum, It is therefore desirable to investigate the effect of using the full integral momentum equation.

An exact formulation will require the generation of the integrals, k_i, as functions of two parameters, b and w_c. To simplify the analysis, we assume that the integrals may still be taken as functions of w_c only, but the integral momentum, Eqn. (3.14), is used instead of the approximated Eqn. (4.6). Then, the wake half-width b is a function of w_c as well as the amplitude of the fluctuation.

The results of such an integration are shown in Figs. 24 to 26 for the case of $R = 2 \times 10^5$. It is clear that the effect on the mean flow velocity variation is quite small. Since a relatively thinner wake is obtained when b is decoupled from w_c, it does make a difference on the variation of the fluctuation energy and the final level approached. The variation of wake half-width b for the two cases are shown in Fig. 26 together with the measured results of Sato and Kuriki. The decoupled result does seem to agree better with the measurements, especially in the "equilibrium" wake width.

In any case, a conclusive discussion on this effect can only be made after an exact formulation with $k_i = k_i(w_c, b)$. Depending on the sensitivity of these integrals to the variation of b, the actual effect may be significant, since a careful examination of the Rayleigh equation will immediately reveal that the change of b for a given w_c is equivalent to a change of the physical frequency. (Refer to Eqn. (4. 4).) Based on the result of the linear stability theory, this change of the physical frequency amounts to a shift on the eigenvalues which will then cause the disturbance to become more or less amplified locally according to the direction of the change.

4. 2. 7 Effect of the Shape Assumption for the Mean Flow Velocity

It is learned from the experimental results of Sato and Kuriki that the mean velocity profiles at various x-stations are not completely similar in non-dimensional form. Even an overshoot in the mean velocity profile has been observed at a station which makes the distribution quite different from the Gaussian assumed in the present

calculation. Although this abnormal mean velocity clistribution may be caused by some other effects which are not accounted for in the present analysis, it is still desirable to study the effect on the solution when the mean flow velocity distribution is modified. For this purpose, we assume the simplest possible form for the mean flow other than Eqn. (3.11) as follows,

$$\frac{1-\bar{u}(x,y)}{w_c(x)} = U^*(y^*) + H(x)\, U_1^*(y^*) \qquad (4.18)$$

where $U^*(y^*)$ is taken to be the same Gaussian distribution as given by (4.13) and $U_1^*(y^*)$, a correction function for the distribution, is assumed to be the second Hermite polynomial multiplying the Gaussian such that U^* and U_1^* are orthogonal. The use of Eqn. (4.18) implies that the mean flow is described by three parameters: b, w_c and H. Because of the appearance of this additional unknown H(x), one more governing equation is needed. The second moment equation, obtained by multiplying the mean momentum equation by $\bar{u}^2$ and integrating over y, is used,

For simplicity, the integrals appearing in the I_i's, are assumed to be functions of the centerline velocity defect alone which is $(w_c - S)$, if we define $S(x) = w_c(x)H(x)$. This assumption is a good one only if H is very much smaller than one and, in general, the solutions to the local Rayleigh equation will depend on both parameters and so do the integrals. The details are given in Appendix C and only the results of the calculation will be presented here.

In this case, one additional initial condition S_0, or H_0, at

$x = \zeta_0$ must be given. The initial values have been obtained at $\zeta_0 = 0.1$, where the measured distribution is very close to the calculation of Goldstein, by finding the set of w_c and H which gives the minimum mean square error fit for the profiles of Goldstein. The values found are $w_{co} = 0.63047$ and $S_0 = -.00103$. The initial value of E_u was taken to be .001 at $\zeta_0 = 0.1$. Fig. 27 shows the result of the centerline velocity variation of this calculation together with the result of the previous two-parameter calculation for comparison. Fig. 28 gives the comparison of the variation of E_u. The differences in both figures are quite small and seem to yield the same qualitative picture. The lower maximum fluctuation energy level reached in this calculation is favorable in view of the experimentally encountered magnitudes.

Fig. 29 gives the variation of S with x which terminates at $x = 0.33$ where S is approaching zero, since for S equal to zero, one of the governing equations is redundant and numerical difficulty results. The fact that S shows a rather peculiar variation and decreases rapidly to zero may be caused by the inaccuracy in the integral quantities in that region where the given frequency corresponds closely to the neutral solution of the local linear stability equation. Of course, it may also be an indication that a three-parameter mean velocity profile is no longer needed as to be expected when the additional interaction effect is diminishing.

The extraordinary mean velocity distributions observed may be somewhat understood if we rewrite Eqn. (4.18) as

$$\frac{1-\bar{u}(x,y)}{w_c-S} = e^{-ky^{*2}}\left[1 + \frac{S}{w_c-S}\,4\,ky^{*2}\right] \qquad (4.18a)$$

where k = 0.69315. Fig. 30 shows a plot of $S/(w_c-S)$ vs. x. The region of large, negative $S/(w_c-S)$ may be realized as to where the overshoot in velocity may be observed. However, the magnitude obtained in the calculation seems to be too small to have a noticeable overshoot as observed experimentally.

Again, the comparisons presented here give only a qualitative indication of the effect which seems to be small. The calculation using a two-parameter representation of the integrals is needed before any definite statement about the effects of non-Gaussian mean flow can be made.

5. Effects of the Second Harmonic; Case B

Because of the nonlinear terms χ_1 and χ_2 in Eqn. (3.4), the higher harmonics are generated and become of appreciable magnitude. Within the framework of the integral method, these higher order effects amount to an improved representation of the integrals I_i's. In other words, the integrals are assumed to be given by

$$I_i(w_c, |A|^2) = \sum_{n=1}^{\infty} \bar{k}_{in}(w_c) \, |A|^{2n} \tag{5.1}$$

The local-quasi-parallel flow treatment of Section 3.4 is only a method devised to evaluate the coefficients $\bar{k}_{in}$ as functions of w_c. Case A, considered in Section 4, has included $\bar{k}_{11}$ only. This section will study the effects of the second harmonic by including the coefficient $\bar{k}_{i2}$ partially. Physically, when the second harmonic is included, referring to the schematic A, the additional processes T_{12}, T_{2M}, T_{M2} are introduced which modify the processes T_{1M} and T_{M1} as well.

From Eqn. (3.30), including the second harmonic, the fluctuating quantities are represented by

$$\begin{aligned} u^* &= [A(x) f_0'(y^*) e^{i\theta} + A^2 g_0(y^*) e^{i2\theta}] + \text{conj} \\ v^* &= -i\{[A(x) \alpha^* f_0(y^*) e^{i\theta} + 2\alpha^* A^2 g_0 e^{i2\theta}] - \text{conj}\} \\ p^* &= [A(x) p_{10} e^{i\theta} + A^2 p_{20} e^{i2\theta}] + \text{conj} \end{aligned} \tag{5.2}$$

$g_0(y^*)$ satisfies Eqn. (3.29) which, after using Eqn. (3,11), can be Written as

$$(U^*-\bar{c})\left(\frac{d^2}{dy^{*2}} - 4a^{*2}\right)g_0 - \frac{d^2U^*}{dy^{*2}}\,g_0 = \frac{f_0''}{2}\,\frac{d}{dy^*}\left(\frac{U^{*\prime\prime}}{U^*-\bar{c}}\right) \qquad (5.3)$$

where $\bar{c}$ is again given by (4.3). The boundary conditions are

$$g_0(0) = 0$$

$$g_0'(\infty) + 2a^*g_0(\infty) = 0 \qquad (5.3a)$$

The method of solution is also given in Appendix A. In general, no particular difficulty is involved in getting the solution for g_0 when $f_0(y^*)$ is known from solving (4.2). However, as $\bar{c}_i$ (or a_1^*) approaches zero, singularity exists in the flow as discussed in Section 4. Therefore, the viscous terms, which have been neglected in obtaining (5.3), must be included when a_1^* is small in order to avoid excessive errors in the solutions.† However, as discussed briefly in Appendix A, the inclusion of the viscous terms will make the numerical calculations much more difficult. Thus, aiming at a primitive and qualitative investigation of the non-linear mechanisms in a wake, the numerical calculations will be carried out using the inviscid equation only. Inevitably, this approximation limits the calculations to values of a_i^* away from the neutrally stable case, and some unknown errors are introduced in the evaluation of the integrals when a_i^* becomes small. This fact should be kept in mind when the numerical results of this section are discussed.

---

† Or alternatively, a close approximation to the true solution may be obtained by taking an appropriate contour in the artificial complex plane for small $\bar{c}_i$.

Using the present cascade model for the local generation of the higher harmonics, the effects are reflected through the representations of the integral quantities I_i. They are now modified to

$$I_1 = k_i |A|^2 + k_{ig} |A|^4 \qquad \text{(5. 1a)}$$

where the k_i's are the contributions from the fundamental as given by (4. 7a) and k_{ig}'s are the corrections to the integrals because of the presence of the second harmonic. They are given by

$$\begin{aligned}
k_{1g}(w_c) &= \int_0^\infty |g_0'|^2 \, dy^* \\
k_{2g}(w_c) &= 4|a^*|^2 \int_0^\infty |g_0|^2 \, dy^* \\
k_{3g}(w_c) &= \int_0^\infty U^* |g_0'|^2 \, dy^* \\
k_{4g}(w_c) &= \int_0^\infty 4|a^*|^2 U^* |g_0|^2 \, dy^* \\
k_{5g}(w_c) &= \int_0^\infty y^* \frac{dU^*}{dy^*} (|g_0'|^2 - 4|a^*|^2 |g_0|^2) dy^* \\
k_{6g}(w_c) &= -2i \int_0^\infty \frac{dU^*}{dy^*} (a^* g_0 g_0' - \bar{a}^* g_0 g_0') dy^* \\
k_{7g}(w_c) &= \int_0^\infty (g_0' \tilde{P}_{20} + \tilde{g}_0' P_{20}) \, dy^* \\
k_{8g}(w_c) &= -\int_0^\infty [4(a^{*2} + \bar{a}^{*2})(|g_0'|^2 + 4 |a^*|^2 |g_0|^2) \\
&\quad + 2|g_0''|^2 + 8|a^*|^2 |g_0'|^2] \, dy^* \\
k_{9g}(w_c) &= 3\int_0^\infty (f_0'^2 \tilde{g}_0' + \tilde{f}_0'^2 g_0') dy^* + 4|a^*|^2 \int_0^\infty (f_0 f_0' \tilde{g}_0 + \tilde{f}_0 \tilde{f}_0' g_0) dy^* \\
&\quad - \int_0^\infty (a^{*2} f_0^2 \tilde{g}_0' + \tilde{a}^{*2} \tilde{f}_0^2 g_0') dy^*
\end{aligned} \qquad \text{(5. 4)}$$

When the magnitude of $|A|^2$ increases, the effect of the second harmonic is expected to appear. The relative magnitude of k_{ig}/k_i, to be determined from the numerical calculations, will decide the magnitude of $|A|^2$ at which the effect of the second harmonic may not be ignored. Since this ratio is a function of $w_c(x)$, the development of the second harmonic and its effects on the mean flow are not completely linked to the first harmonic as being usually criticized.

The definition for A remains unchanged by imposing (4.8), which is now interpreted as the total non-dimensional energy of the fundamental fluctuation. The governing equations can be reduced to the same form as Eqns. (4.10) with the functions K_{ij} modified by the additional terms in the integrals. The solutions can be obtained without much difficulty with given initial conditions at ζ_0 similar to case A.

The inclusion of the second harmonic in the representation for the fluctuation requires the solution of $g_0(y^*)$ for evaluating the additional integrals k_{ig}. With the solution of f_0 obtained, the forcing function on the right hand side of Eqn. (5.3) may be readily calculated. Figs. 31a-e show a few examples of the variation of the forcing function F with y^* using w_c as the parameter, where F represents the RHS of Eqn. (5.3). It is apparent that the forcing function becomes more concentrated and highly oscillating when the values of w_c approach the one which gives the neutral solution locally. As discussed previously, the use of the local inviscid equation, which is singular at the critical point for the neutral case, may induce a

large error in the solution near this region. Nevertheless, the solutions have been attempted as close to the neutral solution as possible.

Figs. 32a-h give a few typical results of the solution g_0 and its derivative. The integrals k_{ig} are then evaluated and tabulated on Table III. The comparatively rapid increase in the relative magnitude of all the integrals near $w_c = .16$, where α_1^* is very small, is believed to be a result of the inaccuracy in obtaining g_0 and its derivatives.

Fig. 33 gives a comparison of the calculated w_c of the present case to case A at $R = 2 \times 10^5$. The agreement between cases A and B is very good in the initial stage of the wake. This agreement is expected because of the domination of the fundamental mode in this part of the wake. The solution curves start deviating from each other when the magnitude of the second harmonic becomes noticeable in the latter portion. The smoother variation in w_c is somewhat surprising since we intuitively expect the inclusion of the second harmonic will tend to extract more energy from the mean flow and, therefore, a faster decay of w_c. The possible explanation can be seen on Fig. 34 where the variations of the magnitude of the terms in Eqns. (4.15) are plotted for both cases A and B for comparison. The introduction of the second harmonic has apparently modified the relative magnitude of the various terms in Eqns. (4.15). This modification results in a lower peak value of the main energy transfer term T_{RM} and, hence, a smoother variation of the mean flow. However, the qualitative nature seems to remain unchanged.

The large difference in the magnitude of T_{Vf} is believed to be an error in calculating the viscous dissipating integral, k_{8g}, which will be further discussed later.

Fig. 35 gives the variations of the averaged energy in the fundamental component, E_{uf}, and the second harmonic, E_{u2f}. Again, we are unable to compare this result with the experimental data. However, the calculation shows that the magnitude of the fundamental mode first reaches a peak and then decreases while the magnitude of the second harmonic is still increasing. The magnitude of the second harmonic will reach its maximum at a distance further downstream. Referring to the results of Sato-Kuriki shown in Fig. 1, this behavior seems to agree perfectly with the experiment, and if the two arbitrary scales used on that figure were comparable, even the ratio of the two maximum magnitudes would have been nearly correct. This result will help to explain the intuitive expectation of concurrent development if the second harmonic is solely generated by the nonlinear interaction of the fundamental mode with itself. It is clear now that the variation of the mean flow serves as a mechanism for redistributing the energy contents not only between the two components of velocity, but also between the various fluctuating modes. This result is evidence that, in the present formulation, the higher harmonics are not strictly linked to the lower ones. In other words, the present theory does take into account the direct interaction between the higher harmonics and the mean flow, e.g., the process T_{M2} indicated in the schematic A.

Fig. 36 shows the comparison of the variations of the total energy density E_T for cases A and B. Fig. 36a gives the corresponding variations of the integrated energy in the fundamental mode. The variations of E_T are practically identical in the front portion. The higher peak of E_T reached when the second harmonic is included justifies the intuition that more energy is taken from the mean flow and fed into the fluctuations. This fact may seem to be a contradiction to the result of Fig. 34. The explanation is again given by the higher order differences between E_f and E_T, and also between E_m and w_c. The fairly rapid decrease in E_T and E_{uf} at larger x for case B, as compared to the result of case **A** where a nearly constant value is maintained, is a consequence of the large magnitude of the viscous dissipation term T_{Vf} shown in Fig. **34.** This difference is more prominent when the non-dimensional energy of the fundamental mode, A_{uf}, is plotted in Fig. 36b for the two cases.

The variation of $|A|^2$ is shown on Fig. **37.** The maximum has decreased from case **A** by more than half. The inclusion of the higher harmonics is expected to cause a further decrease of the maximum of $|A|^2$, although it is not of much concern to the truncational approach adopted here.

The general behavior of the disturbance when the second harmonic is included shows a fairly rapid decrease in magnitude to a much smaller value than the result of case **A.** This behavior is believed to be caused by the fact that the viscous dissipating integral, k_{8g}, which requires the evaluation of the second derivative of g_0, is

subjected to maximum possible numerical error when the viscous terms are ignored in the local disturbance equation. The evidence of this statement may be seen from the rapidly growing magnitude of k_{8g} in Table III for small w_c and also from Fig. 34. Another clue to support this conjecture is furnished by the result of Section 4. 2. 5. It was found there that the viscous dissipation term T_{Vf} had a relatively small effect on the solutions. Two numerical computations are now performed to study this effect. One result is obtained by setting $I_8 \equiv 0$ which ignores the viscous dissipation terms in the fluctuation energy equation completely; the other keeps the contribution from the fundamental mode to the T_{Vf} term by setting $k_{8g} \equiv 0$ only. The results are presented in Figs. 38 and 39a-c. Fig. 38 shows the effect on the w_c variation that seems to be quite small especially when k_8 is left in the equation to account partially for the viscous damping effect. However, the effect on the integrated fluctuation energy is quite large, as shown on Figs. 39a-c, particularly at larger x.

By comparing the results, it may be seen that the effect of the viscous dissipation term due to the harmonic component, k_{8g}, is negligible for $x < 0.2$. But for large x, because of the inaccuracy in evaluating the integral k_{8g} at the corresponding values of w_c, the effect of k_{8g} is hard to assess correctly. A crude approximation is to assume the effect of k_{8g} is always small and may be neglected. Then the result obtained should be more representative except in the final stage where the corrections due to k_{8g} will undoubtedly modify the solutions. The exact effect of this approximation can only be

estimated after the integrals are correctly evaluated by solving the local viscous equations.

It is also interesting to note that, assuming the actual solution is closely represented by the approximate result when k_{8g} is set to be identically zero, the relative variation of E_{uf} and E_{u2f}, shown in Figs. 39a and *c*, is quite similar to the measured results of Sato-Kuriki. The relative maximum magnitude of the second harmonic to the fundamental component may seem to be slightly too high but is expected to be modified when the correction to the fundamental mode is included as considered in Appendix F.

6. Summary and Concluding Remarks

Based on the comparison of the numerical calculations with the experimental data discussed in Sections 4 and 5, the following concluding remarks may be drawn:

(1) In spite of the assumptions made in the present theory and the approximate methods of solution, the present approach does seem to bring out the essentials of the non-linear interacting mechanisms in a laminar wake.

(2) The theory shows that the relatively fast break-away of the mean flow velocity along the wake axis from the steady laminar case and, therefore, the rapid growth of the wake width observed experimentally in the transition region are the consequences of the non-linear effects induced by the finite amplitude disturbances.

(3) The effects of the free stream Reynolds number on the transition (defined as deviation from a steady laminar solution) can be predicted and agree quite well with the experiments.

(4) Two main non-linear mechanisms are responsible for the transition of the wake from one laminar state to another. They are,

   (a) the interaction between the mean flow and the fluctuation through the mean Reynolds stresses, and

   (b) the generation of the higher harmonics and the modification of the lower ones caused by the non-linear interaction between modes.

Based on the numerical results by introducing the above-mentioned effects successively, the first mechanism seems to play the dominant role in explaining the experimentally observed mean flow and fluctuation variations. The inclusion of the second harmonic and the modification of the fundamental mode do not alter the qualitative behaviors except to provide the relative development of the fundamental and the second harmonic. The relatively small influence of the higher harmonics in the early stage of transition, where the amplitude of fluctuation is small, is understandable in view of the power series expansion in the amplitude **A** assumed for the solution of the local stream function. However, it is somewhat surprising that their effects do not show up in the calculated results as the fundamental mode approaches the local neutral solution, because, near the equilibrium region, the calculation indicates that the mean flow remains practically unchanged and the local eigenvalues are very close to the neutral solution. The strictly parallel flow analysis of Stuart and Watson should be a good approximation to this situation. In their terminology, it corresponds to a supercritical case where the fluctuation, being amplified according to the linear theory, will approach a new equilibrium amplitude when the higher order terms are included. In view of

the definite role of the second mechanism played in their analysis, we intuitively expect to observe a larger effect on the solutions than we have obtained. The reason that the effect is not prominent even after the first mechanism weakens may be a result of the present approximate numerical approach. However, this speculation will have to be justified after a more accurate calculation being carried out.

(5) The experimentally observed neck-down of the wake, accompanying reacceleration of the mean flow, is not predicted by the present model (refer to Fig. 1 around x = 70 mm.). These phenomena may be a result of the static pressure distribution induced by the rapid growth of the wake in the non-linear region. To answer this question, a model including the interaction between the growth of the wake with its external flow will have to be taken into consideration. Methods for including this effect for the mean flow in a steady incompressible wake have been outlined by Alber.[35] The basic idea there is, again, the use of the integral moment method which is in line with the present formulation. Therefore, it should be feasible to incorporate this effect into the present analysis.

(6) The calculations show that the general behavior of the variations of the magnitude of the fluctuations, including

both the fundamental and the harmonic modes, is in accord with the relative variations observed experimentally and has been considered as "abnormal" in view of the linear stability theory. However, no quantitative experimental data is available for comparison, although the maximum magnitude calculated seems to be higher than the expected value in this type of flow. It is felt that the static pressure gradient induced or caused by the experimental environment may be responsible for this discrepancy. A numerical study of this effect is presented in Appendix E. The results obtained there give the indication that the effect of the static pressure gradient does reflect strongly on the magnitude of the fluctuations.

In conclusion, the approach proposed here, despite its simplicity, does seem to provide the correct model for the wake flow in the transition region where three-dimensional effects may still be neglected. The method of solution provides a mean for extending and applying the classical hydrodynamic stability theory to a real problem. The strong interaction model of the present theory is preferable to the weak interaction model of Stuart and Watson because of the following reasons:

i) It is capable of treating problems having large deviations in mean flow from the steady laminar case.

ii) It accounts for the divergence of the mean flow and gives

the results of Stuart and Watson in the limit of parallel flows.

iii) Since the integral method is used, the details of the distribution of the fluctuation are not vital in the analysis. Therefore, truncation of the local series representation of the fluctuation does not require a strict convergence of the solution. Hence, disturbances of much larger amplitude than those allowed in the theory of Stuart and Watson may exist in the present theory. This absence of limitation in the magnitude of the fluctuation is certainly desirable for practical applications.

7. Future Work

In view of the success of this approach, further work is suggested for the following three reasons: (i)to clear up the remaining uncertainties caused by the approximations made in the present numerical treatments; (ii)to study some additional effects on the transition mechanisms of the wake; (iii)to extend the present approach to problems of similar nature.

(i) From the discussions of the last section, there remain a few immediate tasks, mostly numerical, to provide the required answers to those uncertainties.

(a) The use of the full viscous Orr-Sommerfeld operator instead of the inviscid Rayleigh operator for the calculations of f_0, g_0 and f_1. This calculation will provide the correct integrals up to case B considered here as we have discussed previously. The numerical difficulties involved are mentioned in Appendix A and the method of a viscous bridging solution discussed in Appendix D may be used. Completion of this work should settle the effect of the second harmonic completely using the truncational approach.

(b) The calculation of f_1 near $a_i^* = 0$ using the reformulation of Appendix F to provide the complete correct integral functions appearing in the I_i's as functions of w_c over the whole range of interest. This result will provide the correct estimate of the effects of f_1 we set out to study in case C discussed in Appendix F.

(c) Using a formal three or more mean flow parameter approach by calculating the integrals as functions of those parameters. This effect may be significant as we mentioned previously. No essential difficulties are encountered in this work, but time and labor are certainly needed because of the lengthy algebra involved.

(d) The effect of the local-quasi-parallel flow approximation. The leading effect can be obtained following the discussion of Appendix B. It may be noted that the effect only appears on the determination of f_1 and the higher order terms.

(e) The inclusion of the non-linear interaction of the growth of the wake with the external flow.

(ii) (a) Using the present method of approach, an interesting study on the interaction between modes with non-commensurable frequencies may be made. Sato and Kuriki have shown experimentally that when an artificial disturbance at different frequency from the natural one is introduced, it shows a "suppressing effect" on the natural disturbance (Fig. 24 in Sato-Kuriki's paper).[2] This type of interaction is interesting in the sense that it may provide the explanation as to why only a nearly single frequency fluctuation exists in the initial stage of the wake. This study requires an additional governing equation for the amplitude of the additional fluctuation. In the first approximation, they are independent and each

may be required to satisfy the integrated fluctuation energy equation. The interaction between them is provided through the mean flow. Since the main energy transfer mechanism is proportional to the square of the amplitude of the disturbances, if one disturbance has more energy initially (therefore a larger amplitude), it will absorb a larger portion of the energy taken from the mean flow which consequently makes it grow faster than the other. This self-propelling process will soon make this frequency completely dominate the other one.

(b) The discussion given above does not apply when two or more frequencies at integer multiples of each other exist initially in the wake. Then resonance will occur which will undoubtedly have a much larger effect than the cascade-generated higher harmonics discussed here. Again additional equations are needed for the additional unknown amplitudes. In this case, we will have to use the higher moment equations of the fluctuation or some other physically meaningful equations.

It will be interesting to consider the case where a frequency corresponding to the maximum local amplification rate exists simultaneously with another one at half of this frequency at the beginning of the wake. Both have a comparable magnitude initially. From the nurner ical results obtained for the present single-frequency

case we have learned that as the flow proceeds downstream the fundamental mode is driving toward the neutral solution. Therefore, when another disturhance at half the frequency exists, it will be near the maximum amplification rate according to the linear stability theory when the fundamental mode is approaching zero amplification rate. The complete non-linear interaction will be very interesting not only because of this feature but also because of the beating effect. This type of study of interaction between various frequencies may serve as a guide to the occurrence of turbulence.

(iii) Using the same idea, several practically important problems of transition involving the interaction of the disturbances with a laminar mean flow may be considered. The following gives a few possible applications.

(a) Study of the non-linear stability of an oblique wave to find out if there is an equivalent to the Squire theorem in the linear stability theory. Also it would be of interest to study the role of the oblique waves when they appear simultaneously with the plane wave in the wake. Because of the varying wake widths experienced by the front of the oblique wave, their interaction with each other and with the mean flow should show some very interesting phenomena.

(b) Consideration of a three-dimensional disturbance. Although the present approach is dealing with the laminar wake, it is hoped that certain clues as to the origin of turbulence may be found. In that respect, a study of the stability of three-dimensional disturbances is essential since turbulence is basically three-dimensional.. Besides, the consideration of the three-dimensional disturbance should extend the region of validity of the present approach in regard to the simulation of experimental or practical situations.

(c) Applying to the axisymmetric wakes. Here the fundamental frequency seems to play a dominant role and also has greater practical significance.

(d) =tension to the compressible wakes. Experimentally, similar structures in the transition region from laminar to turbulent have been observed in a compressible wake. [41, 42] The effects of the additional fluctuation of temperature or density on the stability of the wake and the interaction with the compressible mean flow should be investigated.

(e) Considering cases with the initial fluctuation having a continuous energy spectrum. In the case of the compressible wakes, experimentally, a spectrum of frequencies dominates instead of a single frequency as being closely approximated in the incompressible case. A

new approach should be formulated to handle this type of fluctuation. It is not clear at the present time as to how to proceed with this project. The generalized group velocity concept used successfully in the water-wave theory (e.g., Whitham[36-39]) may find some application here. In the present approach, it has basically assumed a slowly varying wave train, with fixed frequency but varying wave number, travelling in a slowly varying mean flow. The generalization to a slowly varying frequency will be able to include this effe'ct. However, the present system is not conservative, which may form some additional difficulties in applying the method. This line of thinking is still primitive and requires a more sophisticated consideration.

(f) Unsymmetric wakes. Experimentally,[40] it has been observed that the wake becomes exceedingly unstable when the symmetry is destroyed. A study of the stability of a disturbance in the wake with an asymmetric mean flow is needed.

(g) Application to other types of flows without boundaries such as jets and mixing layers.

Appendix A

Numerical Method of Solution of the Differential Equations

Since only the inviscid equations are used in performing the numerical integration in the present study, the discussion given here will be restricted to the inviscid second order operator. Difficulty in numerical integration of the viscous equations because of large R has been discussed by various investigators (e.g., refer to Betchov and Criminale).[31] Special techniques are needed to obtain numerical solution even with the modern computer capacity. Only a brief discussion on the possible techniques is given at the end of this appendix. We will first desc ibe the method used for solving the homogeneous Rayleigh equation; the determination of the eigenvalues as well as the eigenfunctions. The method for solving the differential equation for g_0 and f_1 with known forcing terms on the right is then given in Section (A-2).

A-1) Rayleigh Equation

The methods of solution of the inviscid Rayleigh equation (4.2)

$$(U^*-\bar{c})\left(\frac{d^2}{dy^{*2}} - a^{*2}\right) f_0 - \frac{d^2U^*}{dy^{*2}} f_0 = 0 \qquad (A.1)$$

with the homogeneous antisymmetric boundary conditions

$$f_0'(0) = 0; \quad f_0'(\infty) + a^* f_0(\infty) = 0 \qquad (A.2)$$

have been reported elsewhere. As to the present specific problem for an incompressible wake behind a flat plate, the numerical method of solution developed by L. Mac (e.g., refer to (43))for a compressible boundary layer, modified by T. Kubota[44] for a compressible

wake, is further simplified for the present incompressible case. Certain modifications have been made in order to perform the required spatial mode calculations. The method of solution is briefly described as follows:

It is first desirable to indicate the dependence of the eigenvalues and the eigenfunctions of Eqn. (A. 1) on the local mean flow quantities when the shape of the mean velocity, $U^*(y^*)$, is given. With $a^* = \overset{*}{a}_r + i a_i^*$, a simple manipulation shows

$$\bar{c}_r = \frac{1}{w_c}\left(1 - \frac{\omega b}{|a^*|^2}\, a_r^*\right)$$
$$\bar{c}_i = \frac{\omega b}{w_c}\, \frac{a_i^*}{|a^*|^2} \qquad \text{(A. 3)}$$

where ω is the given nondimensional frequency of the fundamental disturbance. Therefore, with the approximation that $b = b(w_c)$, the remaining task is to obtain the eigenvalue a^* and the corresponding eigenfunction $f_0(y^*)$ for each given value of w_c.

Eqn. (A. 1) can also be written as a pair of first order ordinary differential equations of the form

$$\frac{dp_{10}}{dy^*} = a^{*2}\,(U^* - \bar{c})\, f_0$$
$$\frac{df_0}{dy^*} = \frac{1}{U^* - \bar{c}}\left(\frac{dU^*}{dy^*} f_0 + p_{10}\right) \qquad \text{(A. 4)}$$

The boundary condition at the axis is

$$p_{10}(0) = 0 \qquad \text{(A. 5)}$$

and the corresponding condition as $y^* \to \infty$ can be immediately deduced from the equation to be

$$f_0 \to \text{const} \cdot e^{-a^* y^*}$$

and then (A. 6)

$$f_0' \to -a^* f_0$$

$$p_{10} \to \bar{c}\, a^* f_0$$

The numerical integration is then started at some large value of y^*, say y_δ^*, where (A. 6) is a good approximation (i.e., where $\frac{d^2U}{dy^{*2}}$ and $\frac{dU^*}{dy^*}$ are vanishingly small). Because of the homogeneity of the system, we set

$$f_0(y_\delta^*) = 1.0 \qquad (A.7)$$

to make the solution definite.

For a given set of a_r^* and a_i^*, there will be no difficulty in integrating the equation to $y^* = 0$ when the corresponding $\bar{c}_i$ is not small. In general, a non-zero p_{10} will be obtained at $y^* = 0$ for an arbitrary set of a_r^* and a_i^*. In order to satisfy the boundary condition $p_{10}(0) = 0$, a set of eigenvalues must be found. For this purpose, the linear search method discussed by Mac is used. The method requires a simultaneous integration of the differential equations which yield the variations of the dependent variables as the eigenvalue varies. They may be easily obtained by differentiating Eqn. (A. 4) with respect to a^*, which gives,

$$\frac{d}{dy^*}(p_{10,a^*}) = a^{*2}(U^*-\bar{c})f_{0,a^*} + \left[2a^*(U^*-\bar{c}) - \frac{\omega^*}{w_c}\right]f_0$$

$$\frac{d}{dy^*}(f_{0,a^*}) = \frac{1}{U^*-\bar{c}}\left(\frac{dU^*}{dy^*}f_{0,a^*} + p_{10,a^*}\right) + \frac{\omega^*}{w_c a^{*2}}\frac{\left(\frac{dU^*}{dy^*}f_0 + p_{10}\right)}{(U^*-\bar{c})^2}$$

(A. 8)

where the subscript a* indicates partial differentiation with respect to a*.

The "initial" condition at $y^* = y^*_\delta$ for Eqn. (A. 8) are

$$p_{10,a^*}(y^*_\delta) = \bar{c} + \frac{\omega^*}{w_c a^*}$$

(A. 9)

$$f_{0,a^*}(y^*_\delta) = 0$$

Eqns. (A. 4) and (A. 8) are then integrated simultaneously on the IBM 7094 computer toward $y^* = 0$ with the initial values at some large station y^*_δ given by (A. 6) and (A. 9). The boundary condition (A 5) is not satisfied in general for an initial guess of the eigenvalues a^s_r and a^*_i. A new set of a''_r and a^*_i is then obtained by solving

$$p_{10}(0) = p_{10,a^*}(0)\,\Delta a^* \qquad \text{(A. 10)}$$

for the correction ha*. The values of $p_{10}(0)$ and p_{10,a^*} are taken from the results of the last integration. This is a complex algebraic equation, which may also be written as

$$p_{10r}(0) = (p_{10,a^*})_r\,\Delta a^*_r - (p_{10,a^*})_i\,\Delta a^*_i$$

$$p_{10i}(0) = (p_{10,a^*})_i\,\Delta a^*_r + (p_{10,a^*})_r\,\Delta a^*_i \qquad \text{(A. 10a)}$$

With this estimated correction to the eigenvalues, the integration can be restarted at $y^*_{6'}$. This procedure is repeated until both a^*_r and a^*_i converge. With a fairly good initial guess of the eigenvalues, this search procedure for the eigenvalues converges in a few iterations. The eigenfunctions f_0, as well as its derivatives and the required integrals for the present investigation are then calculated. The complete calculation, including iterations, takes about thirty seconds or less for a step size of 0.05 with $y^*_\delta = 5.5$.

In the case of a small $\bar{c}_i$, the existence of a simple pole at the point y_c where $U^* = \bar{c}$ (critical point) prevents a straightforward numerical integration along the real axis. However, as shown by Lin[32] and used by Zaat[45] and Mac[43], we can get around this difficulty by changing the integration contour to an indented one on the artificial complex y*-plane (Fig. A-1). This is done by analytically continuing the mean velocity U^* and its derivatives into the complex y*-plane by using a truncated Taylor series expansion (up to the third order) around the point y_c where $U^* = \bar{c}$. Details of the method may be referred to Mac.

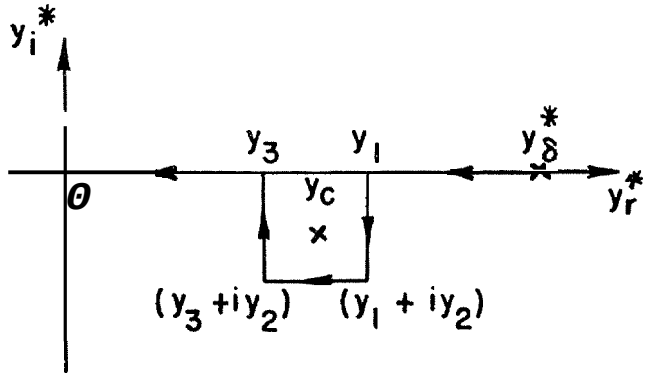

Fig. A1. Schematic of the Integration Contour

For the cases of highly amplified solutions, the point $U^* = \bar{c}$ located far above the real y*-axis, the integration starts at $y^*_{6'}$ and

proceeds directly to $y^* = 0$ (i.e., set $y_2 \equiv 0$). But, for the near neutral and all the darnped disturbances, an indented contour as shown in Fig. A-1 will be taken. The size of the indention has been somewhat arbitrarily taken to keep the integration path a few integration step sizes away from the location of the critical point. The contributions of this indented contour to the integrals have been evaluated by calculating the integrals for several different values of $(y_1 - y_3)$ and extrapolating to zero. Therefore, the values of those integrals for the damped disturbances are of less accuracy than the others. Luckily, it turns out that they are not essential to the present investigation as indicated in the numerical results. If higher accuracy is needed, the integration of the full viscous Orr-Sommerfeld equation will have to be performed.

A-2) The Inhomogeneous Differential Equations

The governing differential equations for g_0, f_1 and the higher order terms in the expansion for the disturbance are of the form (when the viscous terms are included)

$$(L_I + \frac{1}{R} L_V)\varphi = F \qquad \text{(A. 11)}$$

where L_I is the second order linear inviscid operator and L_V is the fourth order linear viscous operator. F is a known forcing function and φ is the unknown. The solutions of **(A.** 11) are subjected to the corresponding homogeneous boundary conditions (symmetric or anti-symmetric).

In the present numerical calculations, the viscous terms have been neglected by assuming large Reynolds number flow which makes

(A.11) a second order equation. Thus, the method of solution is to obtain two linearly independent solutions to (A.11), say φ_1 and φ_2, which satisfy the boundary condition at ∞. The complete solution to (A.11) is then obtained from a linear combination of these two, i.e.,

$$\varphi = K\varphi_1 + (1-K)\varphi_2 \qquad (A.12)$$

where K is a complex constant to be determined by satisfying the boundary condition for φ at $y^* = 0$. Numerically, the two solutions, φ_1 and φ_2, are obtained by two different sets of arbitrary given initial conditions at y^*_δ.

This procedure, in general, provides the solution of the inviscid equation which is a close approximation to the solution of (A.11). However, when $\bar{c}_i$ is small, difficulties arise. Specifically, for the integration of g_0, the operator, L_I is approaching zero but F is not. This causes a large error in obtaining the solution for g_0 because of the difficulties in finding the two linearly independent solutions numerically. It is clear that this difficulty can be removed by including the viscous operator, L_V, at least near the critical layer, or taking an indented contour as shown in Fig. A-1. A different kind of trouble occurs for the integration of f_1 near the neutral case. As $\bar{c}_i$ becomes smaller, the complete operator on the left hand side of (A.11) approaches the homogeneous eigen-operator. Thus, the numerical solution will contain a large unknown contribution of the homogeneous solution which means resonance. As we have remarked in Appendix F, this is a consequence of the formulation. The alternate formulation discussed in section F.4 of Appendix F will have to be

used to iron out this difficulty.

A-3) Viscous Operator

From the previous discussions we learn that the inclusion of the fourth order viscous operator in Eqns, **(A.1)** and **(A.11)** is necessary if improved calculations are to be performed. Although we will not include this numerical calculation in the present work, it is desirable to point out briefly here some of the difficulties involved and the possible methods of solution.

The problem introduced by the viscous operator is not just a higher order system but rather the highly singular behavior due to the largeness of R. The existence of a rapidly growing homogeneous solution makes the numerical integration of the system a challenge to an applied mathematician in numerical analysis even with the help of the modern large capacity computers, Various attempts have been made to cope with these difficulties. The most successful one and commonly used is the suppression scheme of Kaplan.[30] Either this scheme or a straightforward integration with double precision may be used. Further details may be referred to the original paper of Kaplan or the book by Betchov and Criminale.[31] The treatment of Eqn. **(A.11)** in the case of Poiseuille flow has been reported recently by Reynolds and Potter[18] using the scheme of Kaplan. An alternative analytical approach to include the viscous effect near the critical layer is suggested in Appendix D.

Appendix B

Examination of the Approximation Made in the Local Parallel Flow Assumption

The use of the two-length scale concept in Section 3 that leads to a local parallel flow treatment for the disturbances, has much simplified the analysis. But, from the calculated results, we learn that the wake in fact grows quite rapidly in the non-linear region. Therefore, it is necessary to examine in some detail the implications of the assumptions which lead to Eqns. (3.20). This may be achieved by examining the terms neglected in Eqns. (3.19).

The terms multiplied by $R^{-\frac{1}{2}}$ in Eqns. (3.19) may be grouped into two types: the Laplacian terms which arise from viscous effect, and the remaining terms ensuing as a result of the non-parallel mean flow. When the non-linear interaction between the mean flow and the fluctuation is not important, they are of the same order and appear together as the viscous correction terms to the inviscid Rayleigh equation in the linear case. This fact has been pointed out by S. I. Cheng[46] in 1953 and may be easily seen in Eqns. (3.19), e.g., $(R^{\frac{1}{2}}\overline{v}) \sim O(1)$. However, this type of correction is not of much concern to the investigation here, This is because we have shown in the previous analysis that these terms can in fact be completely ignored for most cases except near the neutral solution of the linear stability theory. When the non-linear interaction is included, a different nature of approximation is involved in neglecting terms of the second types. It may be found immediately that the leading terms on the

RHS of Eqns. (3.19) are of the order of $(R^{-\frac{1}{2}} \frac{dw_c}{dx}$. To estimate the order of magnitude of the error made in neglecting these terms, we choose to use a simpler, though less accurate, equation; the mean momentum equation along the centerline of the wake,† which is given by

$$(1-w_c)\frac{dw_c}{dx} = \frac{w_c}{Rb^2}\left.\frac{d^2U^*}{dy^{*2}}\right|_{y^*=0} + \frac{w_c^2}{b}\left(\frac{\partial}{\partial y^*}\overline{u^*v^*}\right)_{y^*=0} + \frac{\partial}{\partial x}\left[w_c^2(\overline{u^{*2}} - \overline{v^{*2}})\right]_{y^*=0} \qquad (B.1)$$

The first term on the right represents the laminar viscous dissipating effect which is O(1), and the remaining terms represent the Reynolds stresses which are important in the non-linear region and are of the order ($|A|^2 R^{\frac{1}{2}}$). It is therefore clear that the terms ignored in the local parallel mean flow assumption are of the order

$$R^{-\frac{1}{2}}\frac{dw_c}{dx} \sim O(R^{-\frac{1}{2}}) + O(|A|^2) \qquad (B.2)$$

The first term will modify the viscous correction term in Eqns. (3.19) and may be ignored in the present high Reynolds number consideration. However, the correction appearing as $O(|A|^2)$ will have certain effects on the present investigation in view of the expansion in amplitude assumed for the local stream function. But, this correction will not affect the determination of f_0 and g_0 because of the appearance as $O(|A|^2)$. The first term in the expansion being affected by this

---

†Similar estimates may be obtained by using Eqn. (2.3) of Section 2A, which gives the leading order terms without using Eqn. (B.1).

correction is f_1, the correction term to the fundamental. To include this effect in the local calculation of the disturbance, a possible method of solution is briefly proposed in the following.

Guided by the discussions leading to Eq. (B.2), we let

$$R^{-\frac{1}{2}} \frac{dw_c}{dx} = w_0(x)\, R^{-\frac{1}{2}} + \sum_{j=1}^{\infty} w_j(x)\, |A|^{2j} \qquad (B.3)$$

The coefficient $w_0(x)$ may be taken as zero because of its small effect on the local calculation discussed previously. And w_j's may be obtained either from Eqn. (B.1) or a similar equation to (4.10). In general, w_j's are functions of w_c only when b is linked to w_c by Eqn. (4.6). Incorporating the expression (B.3) with the expansion (3.26), we find that the governing equations for f_0 and g_0 remain unchanged and their solutions may be obtained as discussed previously. The equation for $f_1(y^*)$ will now include the coefficient $w_1(x)$ of Eqn. (B.3). However, it may be shown from the equation for w_c that $w_1(x)$ is a function of w_c and the integrals of $f_0(y^*)$ only. Therefore, with f_0 known, w_1 is completely determined in terms of w_c. Thus, the solution of $f_1(y^*)$ may be determined with w_1 modifying the forcing terms. Similarly, $w_2(x)$ will only need the determination of g_0 and f_1 which can then be used for higher order calculations. The complete expansion solution can, in principle, be determined in this step-by-step manner. The actual effect on the calculation of the mean flow and the growth of the disturbance through the modification of the integrals involving f_1 will have to be determined numerically.

It should be pointed out here that although this effect is of the

same order as the one discussed in Appendix F for the near neutral solutions, they are of a completely different character. In Eqn. (3.27), the coefficient a_m is not completely determined when they appear in the equation. For example, a_1, which appears in the equation for f_1, cannot be determined from the integral equations, since the terms contributing to $\bar{a}_1(x)$ in Eqn. (4.16) involve certain integrals of f_1 and, moreover, $\bar{a}_1$ is not identical to a_1. Therefore, the a_m's may either be set as zero when α_i^* is large or be determined from the method of Appendix F for the local disturbance calculation. On the other hand, the w_j's are completely known functions of w_c when they appear, and their appearance does not prevent the resonance from occurring. If desired, both effects can be included simultaneously, using the methods outlined.

It should also be pointed out that the relation of f_1 to the velocity components would be modified in this formal approach, because of the terms on the RHS of the first equation of Eqn. (3.19).

Appendix C

Approach for Using a Multi-Parameter Mean Velocity Profile

For certain purposes, the shape assumption (3.11) for the mean velocity may have to be relaxed to allow for a closer approximation to the actual mean velocity distributions. The use of a more general formula (3.12) can in principle be treated with the integral approach suggested here without any conceptual difficulties. The additional governing equations required may be obtained from the higher moment equations, It is to be expected that a higher degree of flexibility in the representation of the mean velocity profile will improve the accuracy of the present approach. However, the increasing numerical work prevents further study along this line. Instead, we will indicate briefly in the following the approximate method of solution when the mean velocity profiles deviate only slightly from the expression (3.11).

The mean velocity distribution is assumed to be represented by the form

$$W^* = \frac{1-\bar{u}(x,y)}{w_c(x)} = U^*(y^*) + H(x)U_1^*(y^*) \qquad (C.1)$$

where H(x) is the additional shape parameter which will be assumed to be small as compared to 1. Following previous formulation, three of the four governing equations needed are obtained from the integrated mean momentum equation, the first integral rnoment equation (the mean energy equation) and the fluctuation energy equation. They

are again given in the form of Eqns. (3.14a), (3.15) and (3.16) with the expressions for some of the integrals being modified by replacing U^* by W^* given by (C.1). The fourth equation may be taken to be the second integral moment equation which is obtained by multiplying the mean momentum equation (3.7) by $\bar{u}^2$ and integrating over y^*. This equation may be written in the form

$$\frac{2}{3}\frac{d}{dx}\left[bw_c^3(\beta_3-\beta_5 w_c-3w_c I_{10})\right] = w_c^4 I_{11}\frac{db}{dx} - bw_c^3 I_{10}\frac{dw_c}{dx} - bw_c^4 I_{12}\frac{dH}{dx} - w_c^4 I_{13} - \frac{w_c^3}{Rb}\beta_6 \qquad (C.2)$$

where

$$\beta_5(H) = \int_0^\infty W^{*4}\, dy^*$$

$$\beta_6(H) = \int_0^\infty W^* \left(\frac{\partial W^*}{\partial y^*}\right)^2 dy^*$$

$$I_{10} = \int_0^\infty W^{*2}\,(\overline{u^{*2}} - \overline{v^{*2}})dy^*$$

$$I_{11} = \int_0^\infty y^* W^* \frac{\partial W^*}{\partial y^*}\,(\overline{u^{*2}} - \overline{v^{*2}})dy^*$$

$$I_{12} = \int_0^\infty U_1^* W^*(\overline{u^{*2}} - \overline{v^{*2}})dy^*$$

$$I_{13} = \int_0^\infty W^* \frac{\partial W^*}{\partial y^*}\,\overline{u^*v^*}\, dy^*$$

Thus, we have four equations for four unknowns, $w_c(x)$, $H(x)$, $b(x)$ and $|A|^2(x)$. The integrals, I_i, are in general functions of all these four unknowns. For the case A discussed in Section 4 where only the fundamental mode is used for representing the fluctuation, one can again write

$$I_i = |A|^2 k_i \qquad (C.3)$$

Now k_i's depend on the solution of the local Rayleigh equation which is, in general, a function of the three quantities w_c, H, and b prescribing the local mean flow, To simplify the analysis, we again assume b to be approximately related to w_c by Eqn. (4.6) which reduces the dependence down to two quantities. If we further assume H to be so small that the local eigenfunctions will not be greatly altered by the value of H in (C.1), then we can bring out the dependence on H explicitly in the k_i's with the remaining integrals being a function of w_c only. The integrals are then evaluated and the solutions to this set of equations are obtained for a few cases discussed in Section (4.2.7).

If more shape functions are required to represent the mean velocity profiles, similar approach may be used with the additional equations being obtained by taking the higher moments of the momentum equation.

Appendix D

Viscous Correction to the Local Disturbance Equation

As we have discussed in the main text, the viscous terms will have to be included when a_i^* is small for any finite Reynolds number. It was suggested that the full fourth order Orr-Sommerfeld operator be used instead of the second order Rayleigh operator to overcome this difficulty. However, that approach will generally require a special elaborated numerical scheme (e.g., Kaplan's method) to suppress the undesired exponentially growing solution. An alternative approach is, therefore, proposed here in an attempt to reduce the problem to a numerically simpler one.

The method of solution follows quite closely the scheme of Graebel[47] by use of the inner-outer expansion theory. Only the homogeneous equation for f_0 will be considered here. Similar treatment may be used for the inhomogeneous equation with known forcing terms on the right. For convenience, the notation used here will be self-explanatory and independent of those in the main text.

Consider the Orr-Sommerfeld equation.

$$\left(\frac{1}{\alpha R}\right)\left(D^2-\alpha^2\right)^2 v = iW\left(D^2-\alpha^2\right)v - ivD^2W \qquad (D.1)$$

where $W \equiv U(y)-C$, C and a are the corresponding complex wave speed and wave number, R is the Reynolds number and D denotes differentiation with respect to y. v represents the vertical component of the disturbance velocity and is proportional to the disturbance

stream function f_0 in the main text. The boundary conditions for an antisymmetric disturbance in the wake are given by

$$\begin{aligned} Dv = D^3v = 0 \qquad & \text{on } y = 0 \\ v,\ Dv \to 0 \qquad & \text{as } y \to \infty \end{aligned} \tag{D. 2}$$

The critical point is defined as the location y_c where $W(y_c)=0$. y_c is generally complex for non-zero imaginary part of C. For sufficiently large C_i, the inviscid Rayleigh equation, obtained by setting the RHS of Eqn. (D. 1) to zero, does not have a singularity on the real y-axis. Integration along the real y-axis can proceed smoothly and the viscous correction, if any, will be quite small. However, as C_i approaches zero, the error in the solution introduced by such an approximation increases. The following approach is intended to cope with the solutions having an eigenvalue in this region.

The classical treatment of Heisenberg[48], being corrected and clarified by Lin[34], has shown that a Stokes' region with radius of the order $(\alpha R)^{-1/3}$ exists near the critical point. Outside this region, for large αR, the flow is essentially inviscid and the Rayleigh equation is appropriate. Using the WKBJ method, Lin was able to obtain an analytically continuous solution through the critical point. However, the method proposed by Graebel[47] seems to simplify the analysis and will be used here by treating it as a singular perturbation problem.

For the outer region, the independent variable y remains unchanged and the dependent variable v has the form

$$\bar{v}(y,\mu) \sim \sum_{n=0}^{\infty} \bar{\epsilon}_n(\mu)\, \bar{v}_n(y) \tag{D. 3}$$

where $\mu = (\alpha R)^{-1/3}$, a small parameter.

The inner variable is suitably taken to be

$$\eta = \frac{y-y_c}{\mu} \sim O(1) \tag{D. 4}$$

and the corresponding inner expansion for v is

$$v^*(\eta,\mu) = \sum_{n=0}^{\infty} \epsilon_n^*(\mu)\, v_n^*(\eta) \tag{D. 5}$$

The forms of $\bar{\epsilon}_n$ and ϵ_n^* will be determined by matching. The only restriction on them is

$$\lim \frac{\bar{\epsilon}_{n+1}}{\epsilon_n} = \lim_{\mu \to 0} \frac{\epsilon_{n+1}^*}{\epsilon_n^*} = 0 \tag{D. 6}$$

Substituting (D. 3) into (D. 1), we get

$$WD^2 \bar{v}_n - (D^2W + \alpha^2 W)\, \bar{v}_n = 0 \tag{D. 7}$$

for n such that $\bar{\epsilon}_n > 0\ (\mu^3 \epsilon_0)$. This is exactly the inviscid Rayleigh equation used in the present numerical analysis and its solution may be considered as known. But for matching purposes, an analytical form near the critical point is desirable. A power series representation of the two independent solutions near y_c, corresponding to Tollmien's[50] (1935) solutions, is given by Graebel as

$$\varphi_1(z) = z + \frac{1}{2}\left(\frac{D^2W}{DW}\right)_{c} z^2 + \frac{1}{6}\left[\left(\frac{D^3W}{DW}\right)_{c} - \left(\frac{D^2W}{DW}\right)_{c}^2 + \alpha^2\right] z^3 + \ldots \tag{D. 8}$$

$$\varphi_2(z) = \varphi_1(z) \ln z + \frac{DW_c}{D^2W_c} + \frac{1}{2}\left[\frac{DW_c}{D^2W_c}\alpha^2 + \frac{D^3W_c}{D^2W_c} - \frac{3}{2}\frac{D^2W_c}{DW_c}\right]z^2 + \ldots \qquad (D.9)$$

where $z = y - y_c$, and subscript c indicates a value at $y = y_c$. These representations are acceptable as long as $D^2W_c \neq 0$. In the case of a wake with Gaussian mean velocity profile, it turns out that $D^2W_c = 0$ when $C_i = 0$. However, in such a case corresponding to a neutral disturbance, the inviscid equation may again be used to give an analytic solution through y_c without using the viscous terms. We will therefore exclude the case $D^2W_c = 0$ and assume the analyticity of expression (D.9).

Without loss of generality, we set $\bar{\epsilon}_0 = 1$. To the first order, the outer inviscid solution may be approximated by $\bar{v}_0$ which is given by

$$\bar{v}_0(y) = a_1\varphi_1(z) + a_2\varphi_2(z) \qquad (D.10)$$

The complex constants a_1 and a_2 can be determined from the machine calculated values of $\bar{v}$ and $(D\bar{v})$ at some location near the critical point on the real y-axis.

For the purpose of matching, we rewrite (D.10) in the inner variable $\eta = z/\mu$

$$\bar{v}_0 = a_2 \frac{DW_c}{D^2W_c} + \mu\eta(a_1 + a_2 \ell n\eta) + (\mu \ell n\mu)\, a_2\, \eta$$

$$+ \frac{\mu^2}{2}\, \eta^2 \left[\frac{D^2W_c}{DW_c} (a_1 + a_2 \ell n\, \eta) + a_2 \left(\frac{DW_c}{D^2W_c} a^2 + \frac{D^3W_c}{DW_c} - \frac{3}{2} \frac{D^2W_c}{DW_c} \right) \right]$$

$$+ (\mu^2 \ell n\mu) \frac{a_2}{2}\, \eta^2 \left(\frac{D^2W_c}{DW_c} \right) + O(\mu^3) \qquad \text{(D. 11)}$$

Substitution of the inner expansion (D. 5) into (D. 1) gives to the leading order

$$\frac{d^4}{d\eta^4}\, v_0^* - i\eta\, DW_c \frac{d^2 v_0^*}{d\eta^2} = 0 \qquad \text{(D. 12)}$$

Referring to (D. 1), the leading term is O(1). Hence,

$$\epsilon_0^* = 1 \qquad \text{(D. 13)}$$

The solution to (D. 12) which matches with (D. 11) is readily found to be

$$v_0^* = a_2 \frac{DW_c}{D^2W_c} \qquad \text{(D. 14)}$$

In order to match the $O(\mu)$ term in (D. 11), we take

$$\epsilon_1^* = \mu \qquad \text{(D. 15)}$$

The governing equation for v_1^* is given by

$$\left(\frac{d^4}{d\eta^4} - i\eta\, DW_c \frac{d^2}{d\eta^2} \right) v_1^* = \frac{i}{2} \eta^2 (D^2W_c) \frac{d^2 v_0^*}{d\eta^2} - i v_0^* D^2W_c \qquad \text{(D. 16)}$$

and using (D. 15), this becomes

$$\left(\frac{d^4}{d\eta^4} - i\eta\, DW_c \frac{d^2}{d\eta^2} \right) v_1^* = -i a_2 DW_c \qquad \text{(D. 17)}$$

To put this equation in a more tractable form, we introduce a new variable

$$\xi = (i\,D\,W_c)^{1/3}\,\eta \tag{D.18}$$

Then, Eqn. (D.17) becomes

$$\frac{d^4 v_1^*}{d\xi^4} - \frac{d^2 v_1^*}{d\xi^2} = -\,(i\,DW_c)^{-1/3}\,a_2 \tag{D.19}$$

The solution to (D.19) which will not grow exponentially as $\xi \to \pm\infty$ may be written, back in η variable, as

$$v_1^* = A_1 + A_2\eta + (iDW_c)^{1/3}\,a_2 (v_1^*)_{part} \tag{D.20}$$

with $(v_1^*)_{part}$ being the particular solution of (D.19) given by

$$(v_1^*)_{part} = \pi \int_0^\eta \int_0^\eta G\left[(iDW_c)^{1/3}\eta\right] d\eta\, d\eta$$

$$= -\eta (iDW_c)^{-1/3} + \pi\eta \int_0^\eta G\left[(iDW_c)^{1/3}\eta\right] d\eta$$

$$+ \pi (iDW_c)^{1/3} \left[\left(\frac{dG}{d\eta}\right)_{\eta=0} - \left(\frac{dG}{d\eta}\right)\right] \tag{D.20a}$$

and

$$G(\xi) = \frac{i}{\pi} \int_0^\infty \exp\left[-i\left(\xi t + \frac{1}{3}t^3\right)\right] dt$$

$$\frac{dG}{d\eta} = \frac{(iDW_c)^{1/3}}{\pi} \int_0^\infty t \exp\left[-i\left(\xi t + \frac{1}{3}t^3\right)\right] dt$$

then

$$\left(\frac{dG}{d\eta}\right)_{\eta=0} = \frac{(iDW_c)^{1/3}}{\pi} \int_0^\infty t \exp\left(-\frac{1}{3}t^3\right) dt$$

$$= \left(\frac{iDW_c}{3}\right)^{1/3} \frac{\Gamma(2/3)}{\pi}$$

The asymptotic behavior of the function $G(\xi)$ and its integrals may be obtained from Luke[51]. For $-\pi<\arg(\xi)<\frac{1}{3}a$, as $|\xi| \to \infty$

$$\int_0^\xi \int_0^\xi G(\xi)d\xi d\xi \sim \frac{\xi}{\pi}\left[\ell n\xi + \frac{1}{3}(\ln 3 + 2\gamma - 3 + i\pi)\right.$$

$$+ \frac{\pi 3^{-5/6}}{\xi\Gamma(\frac{1}{3})}(1 - i\sqrt{3}) + \frac{1}{\xi^2}\ {}_3F_0\left(1, \frac{2}{3}, \frac{4}{3}; \frac{9}{\xi^3}\right)$$

$$\left. + \frac{2}{3\xi^3}\ {}_4F_1\left(1, 1, \frac{4}{3}, \frac{5}{3}; 2; \frac{9}{\xi^3}\right)\right] \qquad \text{(D. 21)}$$

Therefore, for $-\pi < \arg(iDW_c)^{1/3}\eta < {}^1 a$, as $|\eta| \to \infty$

$$(v_1^*)_{part} \sim (iDW_c)^{-1/3}\eta\left[\ell n(iDW_c)^{1/3} + \ell n\ \eta + \frac{1}{3}(\ell n3 + 2\gamma - 3 + i\pi)\right.$$

$$\left. + \frac{\pi 3^{-5/6}(iDW_c)^{-1/3}}{\eta\Gamma(1/3)}(1 - i\sqrt{3}) + O(\frac{1}{\eta^2})\right] \qquad \text{(D. 22)}$$

The correct branch of $(iDW_c)^{1/3}$ may be determined from the asymptotic behavior of the solutions.

Now, we are in a position to determine the constants A_1 and A_2 through matching by comparing (D. 11) and {D. 20) for the terms of $O(\mu)$. Since no $O(\eta^0)$ term appears in (D. 11), it requires,

$$A_1 = \frac{\pi 3^{-5/6}(iDW_c)^{-1/3}}{\Gamma(1/3)}\ (\sqrt{3}\,i - 1)\ a_2 \qquad \text{(D. 23a)}$$

Comparing terms of $O(\eta)$, gives

$$A_2 = a_1 - a_2[\ell n\ (iDW_c)^{1/3} + \tfrac{1}{2}\ (\ell n\ 3\ t\ 2\gamma - 3\ t\ in)] \qquad (D.23b)$$

The term of $O(\eta \ell n\ \eta)$ is completely matched. Therefore, the solution v_1^* is completely determined with (D. 23).

To match the $(\mu \ell n \mu)$ term in the outer expansion (D. 11), we take

$$\epsilon_2^* = \mu \ell n \mu \qquad (D.24)$$

The governing equation for v_2^* is again given in the form of (D. 12), i. e. ,

$$\frac{d^4}{d\eta^4} v_2^* - i\ \eta\ DW_c \frac{d^2 v_2^*}{d\eta^2} = 0 \qquad (D.25)$$

By matching with the outer expansion, we have the solution to (D. 25) as

$$v_2^* = a_2 \eta \qquad (D.26)$$

Therefore, the full inner expansion up to $O(\mu^2)$ is

$$v^* \sim a_2 \frac{DW_c}{D^2 W_c} + \mu \Bigg\{ a_2 \left[\frac{\pi 3^{-5/6} (iDW_c)^{-1/3}}{\Gamma(1/3)} (\sqrt{3}\, i - 1) \right] + \left[a_1 - a_2 (\ell n\ (iDW_c)^{1/3} + \tfrac{1}{3}\ (\ell n\ 3 + 2\gamma\ t\ in)) \right] \eta + a_2 \Bigg[\pi (iDW_c)^{1/3}\ \eta \int_0^\eta G\left[(iDW_c)^{1/3} \eta \right] d\eta + \pi (iDW_c)^{2/3} \left\{ \left(\frac{dG}{d\eta} \right)_{\eta=0} - \frac{dG}{d\eta} \right\} \Bigg] \Bigg\} + (\mu \ell n \mu)\ a_2 \eta + O(\mu^2) \qquad (D.27)$$

Terms of higher order in both the inner and the outer expansions may be analogously determined, if desired.

Two possible ways of applying these results to the actual calculations are given as follows:

(i) Stop the numerical integration of the approximated inviscid equation at some point on one side near the critical point y_c. The constants a_1 and a_2 are then evaluated from the numerical solution. Then, the composite expansion

$$v_{composite} = \bar{v} + v^* - v_{common} \tag{D. 28}$$

is used for calculating the solution in this region and providing the initial conditions for starting integration on the other side of the critical point. The common part of the inner and outer expansion up to the order considered is given by

$$v_{common} = a_2 \frac{DW_c}{D^2W_c} + \mu a_1 \eta + (\mu \ell n \mu)\, a_2 \eta + O(\mu^2) \tag{D. 29}$$

(ii) Obtain the solution of the inviscid equation throughout the whole range by machine integration. The correction obtained from

$$v_{corr.} = v^* - v_{common} \tag{D. 30}$$

is then added to the numerically integrated solution to yield the full solution.

The difficulty in the application of such a solution to the problem is the evaluation of the function $G(\xi)$, its derivatives and integrals, for the complex argument ξ appearing in the present problem. Only

part of these desired functions are tabulated for a certain range of ξ, and they may be found or referred to in the book by Luke. Thus, a preliminary task for applying this solution will be a collection and numerical generation s f all the functions needed. Because of the highly oscillatory behavior of those functions, the numerical generation of the table is certainly a non-trivial matter. For such a purpose, the method of evaluating the Tietjens function (which is of a similar character to the functions here) as the ratio of two rapidly convergent power series given by Chen et al. [52] and a different approach by Huppert[53] may be referred to.

Appendix E

Effects of the Static Pressure Gradient

In the present model, the static pressure at free stream infinity has been assumed to be uniform. Experimentally, the wind tunnel walls were adjusted to provide a nearly constant static pressure on the wall as reported by Sato and Kuriki. However, the static pressure gradients in both the axial and the radial directions are not zero inside the wake, Physically, this pressure gradient is induced by two main effects. The first one is the effect of finite amplitude disturbances which induce both $\partial\bar{p}/\partial x$ and $\partial\bar{p}/\partial y$. This effect is included in the integral sense in the present model. The second effect is due to the interaction of the wake with the external flow which has been neglected in the calculations by setting the static pressure at the edge of the wake, $\bar{p}_e$, equal to $\bar{p}_\infty$. Hence, $\partial\bar{p}_e/\partial x \equiv 0$ is the approximation made to simplify the analysis. This appendix is aimed at considering qualitatively this effect on the numerical solutions.

First of all, the present formulation gives

$$\bar{p} - \bar{p}_e = \overline{-v'^2} \tag{E. 1}$$

And by assuming $\bar{p}_e = \bar{p}_\infty$ = constant, this yields the static pressure coefficient

$$C_{ps} = 2(\bar{p} - \bar{p}_\infty) = -2\,\overline{v'^2} \tag{E. 2}$$

This is generally a function of both x and y. For the case A considered numerically where only the fundamental mode is included,

the static pressure coefficient along the wake axis is given by

$$C_{ps}\,(y^* = 0) = -2Z\,[\,|a^*|^2\,|f_0|^2\,]_{y^*=0} \qquad \text{(E. 3)}$$

The quantity $(|a^*)^2\,|f_0|^2)_{y^*=0}$ is a function of w_c under the assumptions made in carrying out the calculations of case **A.** This function is plotted in Fig. E. 1. The variation of C_{ps} along the wake axis can therefore be calculated and is compared with the measured result of: Sato-Kuriki* in Fig. E. *2*. The agreement is generally fair. The discrepancy in the detail distribution is believed to be at least partially, the consequence of setting $\bar{p}_e \equiv \bar{p}_\infty$. This may be seen qualitatively as follows:

The velocity $\bar{v}$ at the edge of the wake is proportional to the quantity $[d(bw_c)/dx]$ from the continuity equation. But, from the integral momentum equation (3, 14), neglecting the fluctuation terms, the quantity (bw_c), being proportional to the displacement thickness, is decreasing for decreasing w_c. The displacement effect of the wake, therefore, appears to the external flow as a distributed sink. The non-linear effect induced by the finite amplitude disturbances investigated here has effectively concentrated the strength of this sink distribution. The interaction with the external flow may therefore become important. Now, if the small perturbation theory is used and the interaction is introduced by using the calculated sink distribution, it is not hard to visualize a static pressure distribution which may be added to the one shown in Fig. E. *2* to give a

*The author is grateful to Dr. Sato for making those test results available for comparison.

distribution similar to the experimental result.

Without carrying out the complete interaction with the external flow in the present numerical investigations, it is decided to consider, in the simplest possible way, the qualitative effects of the mean static pressure gradient on the solutions.

The approach adopted is to ignore the y-momentum equation completely. This is equivalent to assuming the existence of a static pressure distribution in both x and y which will be just enough to offset the induced static pressure by the finite amplitude effect given by Eqn. (E. 2). The governing equations stay nearly the same with slight modification caused by the disappearance of the $(\partial \overline{v'^2}/\partial x)$ term in Eqns. (4. 7) and (4. 8). The numerical integration can be immediately performed as before. Calculation has been carried out corresponding to case **A** including only the fundamental mode of the fluctuation at $R = 2 \times 10^5$. The same initial conditions, $w_{co} = 0.7$ and $E_{u0} = 1 \times 10^{-5}$, have been used in obtaining the following results for comparison.

Fig. E. 3 shows the effect of the imposed fictitious positive static pressure gradient on the variation of w_c. Some experimental points are also shown there for comparison. Since we expect the induced static pressure gradient, caused by the interaction, to be opposite from this fictitious one, at least at the front portion of the wake, the trend of the solution seems to favor a better agreement with the experimental results.

Figs. E. 4 to E. 6 show the effects on the variations of the

total fluctuation energy density, E_T, the energy in the u'-component, and the non-dimensional amplitude of the fluctuation $|A|^2$. The general variations remain qualitatively unchanged but the maximum and the final equilibrium magnitudes are greatly influenced. An increase of factor two in the peak values results when the fictitious positive pressure gradient is imposed. This fact is again very much in favor of the explanation of the seemingly higher peak values of the fluctuation magnitude calculated. Based on this result, the induced negative external pressure gradient in the front portion of the wake, when included, is expected to further cut down the peak values obtained.

The explanation of these effects may be seen when we consider the governing equations in the form of Eqns. (4.15)

$$\frac{dE_m}{dx} = - T_{RM} - T_{VM} \tag{E.4a}$$

$$\frac{dE_f}{dx} = T_{Rf} - T_{Vf} \tag{E.4b}$$

with T_{VM}, T_{Vf}, T_{Rf} being the same as given in Eqns. (4.15). However, because of the existence of an external pressure field, either imposed or induced, T_{RM} is no longer identical to T_{Rf}. Again, let us split the energy transfer term T_{RM} into two parts: T_{R1}, the contribution from the usual Reynolds stress, $\overline{u'v'}$, and T_{R2}, the term resulting from the mean flow variation. T_{R1} being the main mechanism of the energy transfer, remains unchanged and is given as

$$T_{R1} = I_6 w_c^3 \tag{E.5a}$$

However, T_{R2} is now modified by the external pressure field and becomes

$$T_{R2} = -2 w_c^2 [I_5 w_c \frac{db}{dx} t \ (I_4 - I_3) b \frac{d w_c}{dx}]$$

$$- (\text{External Pressure Term}) \qquad \text{(E.5b)}$$

Since $T_{Rf} = T_{RM} + (\text{External pressure term})$, it is clear that part of the mean energy variation appears as the work done on or by the fluid because of the external pressure field. The energy exchange between the mean and the fluctuations is therefore modified. Depending on the sign of the external pressure gradient, the onset of transition (the location where T_{RM} becomes the same order of T_{VM}) will move correspondingly.

In the simplified case considered here, the imposed static pressure field is positive as given by the negative of the values shown on Fig. E. 2. Eqn. (E. 5b), then, becomes

$$T_{R2} = 2 w_c^2 [I_3 b \frac{dw_c}{dx} - I_5 w_c \frac{db}{dx}] \qquad \text{(E. 6)}$$

Numerical calculation shows that the values of T_{R2} are now generally of opposite sign to T_{R1} as against the results shown in Fig. **13** where T_{R2} and T_{R1} have the same sign. Since the interaction between the mean and the fluctuation is relatively weak at the initial state of the wake where the mean flow is varying slowly resembling the pure laminar solution, the fluctuation grows near exponentially as given by the linear theory. This weak-coupling development will cease to exist when T_{RM}, which is proportional to $|A|^2$ to the first order,

becomes of appreciable magnitude as compared to T_{VM}. Because of the present imposed static pressure field, a much higher magnitude disturbance is required. This implies a delay of the onset of transition as compared to the case of no external pressure gradient. This fact is clearly indicated in Fig. E. 3. The much higher peak values and a different equilibrium magnitude reached can also be understood from Eqns. (E. 4).

Although the effects of the external mean static pressure field on the calculation is qualitatively known, it remains to obtain an estimate on the magnitude and distribution of the actual interaction induced static pressure field. This estimate is especially needed in view of the present arbitrary imposed pressure gradient.

First of all, we may note from Fig. E. 3 that the mean flow is not greatly affected by the external static pressure gradient. If we assume that the induced pressure field will have a smaller pressure level than the one imposed here, we can use the calculated mean flow to estimate the external induced pressure. This assumption will have to be justified later and, for the time being, we will ignore the interaction between the growth of the wake and the external flow.

Integrating the mean continuity equation to the distance y^*_e where $U^*(y^*_e)$ is nearly zero, we get

$$v_e = \beta_1 \frac{d(b\, w_c)}{dx} \qquad \text{(E. 7)}$$

Furthermore, using the approximate integrated mean momentum equation (4.6), Eqn. (E. 7) becomes

$$\bar{v}_e = \frac{\beta_1 \beta_2 b w_c}{\beta_1 - \beta_2 w_c} \frac{dw_c}{dx} \qquad (E.8)$$

Since $dw_c/dx < 0$, this appears to the external flow as a sink. The distribution of $\bar{v}_e$ calculated for case **A** at $R = 2 \times 10^5$ is shown in Fig. E.7, together with the calculated result of a pure laminar wake for the purpose of comparison. The non-linear effect induced by the finite amplitude disturbances has effectively replaced the distributed sinks of small slowly varying strength by a much more concentrated distribution. Since the total strength is the same, the latter will have a generally larger strength as indicated in Fig. E.7. Thus, the induced external pressure field will be much more important and interaction effects may not be ignored as is usually the case in an undisturbed laminar wake.

With the calculated magnitude of the vertical velocity component $\bar{v}_e$, it seems justifiable to use the linearized small perturbation theory for calculating the induced pressure field. The induced static pressure coefficient along the wake axis is then given by

$$C_{ps}(x, y = 0) = -\frac{2}{\pi} \int_{-\infty}^{\infty} \frac{\bar{v}_e(\xi)}{x - \xi} d\xi \qquad (E.9)$$

When the interaction is neglected, we may use the calculated $\bar{v}_e$ in Eqn. (E.9) to evaluate the induced pressure coefficient. However, for the purpose of obtaining a rough estimate of the magnitude and the variation of the induced pressure field, an approximate distribution of the form

$$\frac{\bar{v}_e}{0.0172} = -\left[1 - \left(\frac{x-0.154}{0.079}\right)^2\right]^5 \qquad \text{(E.10)}$$

is used instead of the true calculated distribution. Eqn. (E.10) is plotted on Fig. E.7 for comparison with the true distribution. Using Eqn. (E.10) for $\bar{v}_e$, Eqn. (E.9) may be readily integrated to obtain

$$C_{ps}(X,0) = 2\bar{x}^9 - 9.333\bar{x}^7 + 17.067\bar{x}^5 - 15.0476\bar{x}^3 + 6.127\bar{x} + (1-\bar{x}^2)^5 \ln\left|\frac{\bar{x}+1}{\bar{x}-1}\right| \qquad \text{(E.11)}$$

where $\bar{x} = \frac{x-0.154}{0.079}$

This distribution of pressure coefficient is plotted in Fig. E.8 against the normalized variable $\bar{x}$. It is added to the expression (E.3) assuming that the two induced pressure fields do not interact with each other. The result is shown in Fig. E.2 to indicate the effect. It is evident that the combined result does give a closer resemblance to the experimentally observed distribution. The deviation at x greater than 0.25 may be attributed partially to the assumption that the two effects are additive, because, for $x > 0.25$, the mean flow remains practically unchanged. From Eqn. (E.3), we can see that the static pressure level beyond this point is strictly proportional to $|A|^2$. Therefore, because of the favorable pressure induced by the interaction near the beginning of the wake, we will expect a lower final equilibrium amplitude from the numerical results of this Appendix. Hence, the static pressure coefficients at $x > 0.25$ will be expected to come closer than indicated to the experimental results when the complete interaction is included.

However, it may be noticed that the station where C_{ps} starts deviating from the theoretical prediction is near the same location where the re-acceleration of the mean flow and the rather sudden decrease of the amplitude of fundamental mode take place experimentally. All these phenomena cannot be predicted by the present theory, but they are consistent in the light of the numerical investigations obtained so far.

Appendix F

Effects of f_1; Case C

F. 1 General Formulation

As previously discussed in the main text, Eqns. (3. 20) need to be modified when the correction term to the fundamental mode, $f_1(y^*)$, is included. The method proposed in Appendix B to include the effect of the mean flow variation in the x direction should be incorporated to obtain a solution for $f_1(y^*)$. Without involving such a modification, this appendix will assume that the solution of f_1 may be approximately obtained by using Eqns. (3. 20) alone. This parallel mean flow assumption will undoubtedly induce errors in the estimation of the integrals I_i by ignoring the history effect on f_1. However, the numerical complexity is greatly reduced, and the approximation will not affect a qualitative study of the effect and allows a discussion of the problems associated with f_1.

Using Eqns. (3. 20), the governing equation of $f_1(y^*)$ may be written in the form

$$\left[\left(\bar{u} - \frac{\omega^*}{a^*}\right)\left(\frac{d^2}{dy^{*2}} - a^{*2}\right) - \bar{u}_{y^*y^*}\right] f_1 - \left(\frac{2ia_i^*}{a^*}\right) G(f_1)$$

$$= -\frac{ia_1}{a^*} G(f_0) + w_c F_1(f_0, g_0; a^*) \qquad \text{(F. 1)}$$

where

$$G(f) = -\bar{u} f'' + \left[\bar{u}(3a^{*2} + 6ia^* a_i^* - 4a_i^{*2})\right.$$

$$\left. -2\omega^*(a^* + ia_i^*) + \bar{u}''\right] f \qquad \text{(F. 2)}$$

and

$$F_1 = \frac{1}{a^*}\left[2a^*(g_0\tilde{f}_0''' - g_0'\tilde{f}_0') + \tilde{a}^*(\tilde{f}_0''g_0' - \tilde{f}_0 g_0''') \right.$$
$$\left. + (4a^{*2} - \tilde{a}^{*2})(2a^*\tilde{f}_0' g_0 + \tilde{a}^*\tilde{f}_0 g_0') \right] \qquad \text{(F. 3)}$$

with the superscript " ' " denoting differentiation with respect to y*.

When a_i^* is not small, the solution of Eqn. (F.1) may be obtained for any value of a_1. Since no particular choice of the value of a_1 is required, we can specify a_1 to be zero. The significance of this choice may be seen from Eqn. (3.27). Since a_r^* is generally of order one, when a_i^* is not small, the leading term of Eqn. (3.27) or (3.27a) is sufficient to describe the local spatial variation of the phase and the amplitude. Therefore, the correction given by a_1 may be ignored.

On the other hand, when a_i^* is identically zero, i.e., the fundamental mode is neutrally stable, a resonance occurs. The operator on the left of Eqn. (F.1) becomes identical to the eigenoperator. In order to assure the existence of a solution for f_1, a_1 must take a special value. The value of a_1 is determined so that the RHS of Eqn. (F.1) is orthogonal to the eigensolution of the adjoint of Eqn. (3.28). Namely,

$$a_1 = -iw_c a^* \frac{\int_0^\infty F_1 \varphi_0 dy^*}{\int_0^\infty G\varphi_0 dy^*} \qquad \text{(F. 4)}$$

where φ_0 is the eigensolution of the adjoint equation of f_0. For the near resonance cases, i.e., when a_i^* is small, the same procedure

is applied to insure a bounded solution. The solution may be obtained following the method of Watson by forming a series solution in a_1^* for f_1. This will be discussed in section F. 4 of this appendix.

F. 2 Numerical Treatments

This case differs from case B by including the process T_{21} shown in the schematic A. The inclusion of this new non-linear . feature will modify the other processes and, therefore, affects the complete interaction.

Using all three terms in Eqn. (3.30), the fluctuations are given by

$$u^* = \{A[f_0' + |A|^2 f_1'] e^{i\theta} t A^2 g_0' e^{2i\theta}\} + \text{conj.}$$

$$v^* = -i\{A[a^* f_0 + a_1^* |A|^2 f_1] e^{ie} + 2a^* A^2 g_0 e^{2i\theta}\} + \text{conj.} \quad (F.5)$$

$$p^* = [A(p_{10} + |A|^2 p_{11}) e^{i\theta} + A^2 p_{20} e^{2i\theta}] t \text{ conj.}$$

Using (3.11) and writing out $F_1(f_0, g_0, a^*)$ explicitly, Eqn. (F.1) with $a_1 = 0$ becomes,

$$(U^* - \bar{c}_1)\left(\frac{d^2}{dy^{*2}} - a_1^{*2}\right) f_1 - \frac{d^2 U^*}{dy^{*2}} f_1$$

$$= -(2a^* + \tilde{a}^*)(2a^* g_0 \tilde{f}_0' + \tilde{a}^* \tilde{f}_0 g_0') \quad (F.6)$$

$$+ \frac{2a^*}{a_1^*}(g_0'' \tilde{f}_0' - g_0 \tilde{f}_0''') + \frac{\tilde{a}^*}{a_1^*}(\tilde{f}_0 g_0''' - \tilde{f}_0'' g_0')$$

where $a_1^* = 2a^* - \tilde{a}^*$ and $\bar{c}_1 = \frac{1}{w_c}\left(1 - \frac{w^*}{a_1^*}\right)$.

The boundary conditions are

$$f_0'(0) = 0$$

$$f_1'(m) + a_1^* f_1(m) = 0 \qquad \text{(F. 6a)}$$

The solutions to (F.6) can again be obtained by the method given in Appendix **A** when the forcing terms on the right are known from the solutions of f_0 and $g_{0'}$ However, solutions near $a_i^* = 0$ are difficult to obtain and possess a high degree of uncertainty. This difficulty is different from the one mentioned in getting the solutions for $g_{0'}$ The inclusion of the viscous terms will not prevent its occurrence. A method of obtaining a bounded solution near $a_i^* = 0$ with a non-zero a_1 is given in section F. 4. Numerically, the solution to Eqn. (F.6) will be intended without making such a modification as close to the neutral case as possible. The difficulty mentioned above will become obvious when the numerical results are discussed in the next section.

The effects of f_1 on the flow development again appeared on the representations of the integral quantities I_i as given by Eqn. (5.1). It essentially modifies the Reynolds stress and the relative energy content in the fundamental and the second harmonics. For purposes of comparison and for simplicity, the same definition for A, as given by (4. 8), is used. In this case, the integrals are given by

$$I_i = k_i |A|^2 + (k_{ig} + k_{if}) |A|^4 + k_{iff} |A|^6 \qquad \text{(F. 7)}$$

$$\text{for } i = 1, \text{ ---- } 8$$

For i = 9

$$I_9 = k_{9g} |A|^4 + k_{9f} |A|^6 + k_{9ff} |A|^8 \qquad \textbf{(F.7a)}$$

where the k_{if}'s and k_{iff}'s are the results of f_1. They are given by

$$k_{1f}(w_c) = \int_0^\infty (\tilde{f}'_0 f'_1 + f'_0 \tilde{f}'_1)dy^*$$

$$k_{2f}(w_c) = \int_0^\infty (a^* \tilde{a}^*_1 f_0\tilde{f}_1 + \tilde{a}^* a^*_1 \tilde{f}_0 f_1)dy^*$$

$$k_{3f}(w_c) = \int_0^\infty U^*(\tilde{f}'_0 f'_1 + f'_0 \tilde{f}'_1)dy^*$$

$$k_{4f}(w_c) = \int_0^\infty U^*(a^* \tilde{a}^*_1 f_0\tilde{f}_1 + \tilde{a}^* a^*_1 \tilde{f}_0 f_1)dy^*$$

$$k_{5f}(w_c) = \int_0^\infty y^* \frac{dU^*}{dy^*} [(\tilde{f}'_0 f'_1 + f'_0 \tilde{f}'_1) - (a^*\tilde{a}^*_1 f_0\tilde{f}_1 + \tilde{a}^* a^*_1 \tilde{f}_0 f_1)]\, dy^*$$

$$k_{6f}(w_c) = -i \int_0^\infty \frac{dU^*}{dy^*} [(a^* f_0 \tilde{f}'_1 - \tilde{a}^* \tilde{f}_0 f'_1) + (a^*_1 \tilde{f}'_0 f_1 - \tilde{a}^*_1 f'_0 \tilde{f}_1)]\, dy^* \qquad \text{(F. 8)}$$

$$k_{7f}(w_c) = \int_0^\infty [(\tilde{p}_{10} f'_1 + p_{10}\tilde{f}'_1) + (f'_0 \tilde{p}_{11} + \tilde{f}'_0 p_{11})]\, dy^*$$

$$k_{8f}(w_c) = -\int_0^\infty \{4(\tilde{a}^{*2} f'_0 \tilde{f}'_1 + a^{*2} \tilde{f}'_0 f'_1) + 2(f''_0 \tilde{f}''_1 + \tilde{f}''_0 f''_1)$$
$$+ [(\tilde{a}^{*2}_1 + a^{*2}) a^* \tilde{a}^*_1 f_0 \tilde{f}_1 + (a^{*2}_1 + \tilde{a}^{*2}) \tilde{a}^* a^*_1 \tilde{f}_0 f_1]\}dy^*$$

$$k_{9f}(w_c) = \int_0^\infty \{6(f'_0 f'_1 \tilde{g}'_0 + \tilde{f}'_0 \tilde{f}'_1 g'_0) + 4[\tilde{a}^* \tilde{g}_0 (a^* f_0 f'_1 + a^*_1 f_1 f'_0)$$
$$+ a^* g_0 (\tilde{a}^* \tilde{f}_0 \tilde{f}'_1 + \tilde{a}^*_1 \tilde{f}_1 \tilde{f}'_0)] - 2(\tilde{a}^* \tilde{a}^*_1 \tilde{f}_0 \tilde{f}_1 g'_0$$
$$+ a^* a^*_1 f_0 f_1 \tilde{g}'_0)\}\, dy^*$$

and

$$k_{1ff}(w_c) = \int_0^\infty |f_1'|^2 \, dy^*$$

$$k_{2ff}(w_c) = \int_0^\infty |a_1^*|^2 \, |f_1|^2 \, dy^*$$

$$k_{3ff}(w_c) = \int_0^\infty U^* \, |f_1'|^2 \, dy^*$$

$$k_{4ff}(w_c) = \int_0^\infty U^* \, |a_1^*|^2 \, |f_1|^2 dy^*$$

$$k_{5ff}(w_c) = \int_0^\infty y^* \frac{dU^*}{dy^*} \, [\, |f_1'|^2 - |a_1^*|^2 \, |f_1|^2] \, dy^*$$

$$k_{6ff}(w_c) = -i \int_0^\infty \frac{dU^*}{dy^*} (a_1^* f_1 \tilde{f}_1' - \tilde{a}_1^* \tilde{f}_1 f_1') dy^* \qquad \text{(F. 9)}$$

$$k_{7ff}(w_c) = \int_0^\infty (f_1' \tilde{p}_{11} + \tilde{f}_1' p_{11}) dy^*$$

$$k_{8ff}(w_c) = -\int_0^\infty \{(a_1^{*2} + \tilde{a}_1^{*2}) (|f_1'|^2 + |a_1^*|^2 |f_1|^2) + 2(|f_1'|^2 + |a_1^*|^2 |f_1'|^2)\} dy^*$$

$$k_{9ff}(w_c) = \int_0^\infty \{3(f_1'^2 \tilde{g}_0' + \tilde{f}_1'^2 g_0') + 4(\tilde{a}^* a_1^* f_1 f_1' \tilde{g}_0 + a^* \tilde{a}_1^* \tilde{f}_1 \tilde{f}_1' g_0) - (\tilde{a}_1^{*2} \tilde{f}_1^2 g_0' + a_1^{*2} f_1^2 \tilde{g}_0')\} dy^*$$

The governing equations for $|A|^2$ and w_c can again be written in the form sf Eqn. (4. 10) with different expressions for the functions K_{ij}. The solutions can be readily obtained similarly as for **case A,**

F. 3 Results and Discussion

A few typical distributions of the forcing function, $F_1(y^*)$, are shown in Figs. F. la-d. It may be noticed that the variation of the magnitude becomes increasingly large as a_i^* tends to zero. The difficulties are enhanced by the inaccuracy in calculating the derivatives of g_0 when a_i^* is small, because of the use of the inviscid Rayleigh operator. Therefore, errors in the derivatives of g_0 are amplified in this stage of calculation through $F_1(y^*)$. These numerical difficulties will result in a much less accurate estimate on the integrals k_{if} and k_{iff} for small a_i^*. This situation is further complicated by the resonance behavior in the solution of f_1 near $a_i^* = 0$, since, in this case, the operator on the left-hand side is nearly the eigen-operator and causes the numerical solutions of f_1 obtained by the method of Appendix A to be completely dominated by the undesirable homogeneous solution. As we have discussed previously, the reformulation given in section F. 4 with non-zero a_1 is needed for this case.

Disregarding these difficulties, the solutions for f_1 have been intended for fairly small values of a_i^* using the inviscid equation (F.6). The integrals, k_{if} and k_{iff}, are then evaluated and listed in Tables IV and V. The extremely large values of the integrals for small values of w_c are believed to be numerical errors induced by the above-mentioned difficulties, However, it is not possible to estimate exactly at what value of w_c, or a_i^*, that these errors will be large enough to affect the solution. A more accurate calculation, using the full viscous operator and the reformulation of section F. 4, is needed to justify this approximation.

A few typical distributions of f_1 and its derivative are shown in Figs. F. 2a-h. The extremely large scale used for the cases of small w_c (thus, small a_i^*) indicates that a large unknown contribution from the homogeneous solution is dominating. According to the present formulation, this distribution, multiplied by $|A|^2$, is added to $f_0(y^*)$ to obtain the real distribution of the fundamental mode. Therefore, the measured distributions of the amplitude and phase of the fundamental mode shown by Sato and Kuriki in Figs. 18 and 19 of their paper at various x-stations may be realized through these results. But, since no emphasis should be placed on the local distributions when the integral method is used, and, moreover, the solutions of f_1 are subject to a large source of error in the present approximation, we will not attempt to make such a representation here.

The calculated variation of w_c for the present case at $R = 2 \times 10^5$ is compared with the results of cases A and B in Fig. F. 3. The general trend again remains unchanged, but the curve levels out at a higher value of w_c, i.e., a larger value of a_i^*. However, this near "equilibrium" result may be caused by the inaccuracy in the integrals k_{if} and k_{iff}. This fact may be further illustrated by the variations of the total energy density shown in Fig. F. 4. The results of cases A and B are also shown on the same plot for comparison. From Fig. F. 3, we may see that the mean flow velocity is varying quite slowly for all three cases for $x > 0.2$. Thus, the rapid decrease in the fluctuation energy for case C is believed to

be caused by the same reason discussed for case B: the overestimated viscous damping effect due to the inaccuracy in evaluating the integrals causes the rapid energy loss by dissipation.

Fig. F. 5 shows the variations of the fluctuation energy in the fundamental and the second harmonic. As expected, the result indicates a lower ratio of $(E_{u2f})_{max}$ to $(E_{uf})_{max}$ than the result obtained in case B. However, the relatively small energy content of the second harmonic, as well as the continuous decrease in magnitude at large x are believed to be the consequences of the difficulties mentioned in obtaining the integrals.

Similar to the treatment of case B, we will try to remedy this difficulty by setting both k_{8g}, k_{8f} and k_{8ff} identically zero. This treatment will tend to eliminate the maximum possible source of error by accepting some uncertainties in including the correct viscous damping effect. (Only the contribution from f_0 is included.) However, the improvement in the solution for this case will not be expected to be as good as for case B. In fact, a large unknown error still remains in all the integrals for small a_i^* on account of the error in the forcing function F_1 and the resonance behavior of the solutions. Some of the results of this calculation will indicate this difficulty.

Fig. F. 6 gives the effect of k_{8g}, k_{8f} and k_{8ff} on the w_c variation. Assuming that the result obtained when k_{8g}, k_{8f} and k_{8ff} are set to be identically zero is more representative of the actual solution, comparison between the three cases may be made. Using the results of Fig. F. 6, it may be seen from Fig. F. 3 that the general behavior

for the three cases remains the same. However, the asymptotic values of w_c seem to be increasing when more terms in the local series expansion of the fluctuation stream function are included. This trend implies that the flow is equilibrated at a larger value of $-a_i^*$ which is in contrast to the linear theory, where equilibrium is only possible at $a_i^* = 0$.

Fig. F. 7 shows the effect of the viscous dissipation terms on the total fluctuation energy density. The large effect at large x indicates the domination of the erroneous viscous dissipation terms on the solutions. Fig. F. 8 gives the corresponding development of E_{uf} and E_{u2f}. The variation of E_{uf} is somewhat peculiar judging from the previous results of cases A and B. It is again believed to be caused by the errors in the integrals.

Fig. F. 9 gives the variation of $|A|^2$ for case C. Notice that the maximum value reached is further decreased from case B. This result gives additional confidence in using the amplitude expansion proposed together with the truncational approach.

Before leaving this section, it should be mentioned that the results of case C are not conclusive because of the uncertainty in the numerical results. It is merely included here for a qualitative reference. For a more accurate estimate on its effects, the reformulation of section F. 4 will be needed and the integrals may be evaluated for the range of small a_i^*. The results may then be patched with the present integrals to provide the complete curves as functions of w_c over the whole range of a_i^*, even for slightly damped cases.

F. 4 Solution of f_1 near $a_i^* = 0$

When the eigenvalues a*, found by solving the local Rayleigh equation, possess a small imaginary part, a straightforward numerical integration of f_1 will cause a large unknown error in the solution. The method of Watson may be used to obtain the solution.

Rewrite Eqn. (F.1) in the form

$$L(\omega^*, a^*) f_1 - \left(\frac{2ia_i^*}{w_c a^*}\right) G(f_1) = -\frac{ia_1}{w_c a^*} G(f_0) + F_1 \qquad (F.10)$$

where

$$L(\omega^*, a^*) = \frac{1}{w_c}\left[(\bar{u} - \frac{\omega^*}{a^*})\left(\frac{d^2}{dy^{*2}} - a^{*2}\right) - \frac{d^2\bar{u}}{dy^{*2}}\right]$$

and G, F_1 are given by Eqns. (F.2) and (F.3). It should be noted that, if the non-parallelness of the mean flow is taken into account as discussed in Appendix B, the additional terms will appear in F_1. The present analysis can be easily modified to incorporate this effect. In the following, the procedure of Watson for finding the solution to Eqn. (F.10) for a small a_i^* will be recapitulated.

We first write f_1 in the form

$$f_1 = \left(\frac{a_1}{2a_i^*}\right) f_0 + \varphi \qquad (F.11)$$

then, φ satisfies

$$L(\omega^*, a^*)\,\varphi - \left(\frac{2ia_i^*}{w_c a^*}\right) G(\varphi) = F_1 \qquad (F.12)$$

with the boundary conditions

$$\varphi'(0) = 0$$

$$\varphi'(\infty) + a_1^* \varphi\ (\infty) = 0 \qquad \text{(F.13)}$$

with $\quad a_1^* = 2a^* - \tilde{a}^*$

Since a_i^* is small for the cases considered here, the operator on the LHS of (F.12) is almost the inviscid Rayleigh operator. Hence we may choose two independent parts of the complementary function, one of which will almost be the eigenfunction f_0. It follows from this that the highest order term in φ is probably a multiple of f_0 and moreover that the multiple will tend to infinity as $a_i^* \to 0$. Following the arguments of Watson, we assumed that the most probable case does occur, then φ may be expanded in the series

$$\varphi = \frac{1}{a_i^*} \varphi^{(-1)} + \varphi^{(0)} + a_i^* \varphi^{(1)} + \text{----} \qquad \text{(F.14)}$$

Substituting (F.14) into Eqn. (F.12), we obtain the equations for $\varphi^{(r)}$. They are

$$L(\omega^*, a^*)\, \varphi^{(-1)} = 0 \qquad \text{(F.15)}$$

$$L(\omega^*, a^*)\, \varphi^{(0)} = \frac{2i}{wca^*}\ G(\varphi^{(-1)}) + F_1 \qquad \text{(F.16)}$$

$$L(\omega^*, a^*)\, \varphi^{(r)} = \frac{2i}{w_c a^*} G(\varphi^{(r-1)}) \qquad (r \geq 1) \qquad \text{(F.17)}$$

The corresponding boundary conditions are

$$\begin{cases} \varphi^{(-1)'}(0) = 0 \\ \varphi^{(-1)'}(\infty) + a^* \varphi^{(-1)}(\infty) = 0 \end{cases} \qquad \text{(F.15a)}$$

The solution to (F.15) is $\varphi^{(-1)} = Xf_0$, where X is an arbitrary constant. On substituting this solution into the right-hand side of (F.16), λ appears explicitly in the equation for $\varphi^{(0)}$. The solvability condition (ref. Ince, p. 214) will then determine λ. Following Stuart and Watson, we define χ_3 to be the solution of the Rayleigh equation satisfying the even boundary conditions.

$$\chi_3' = 0, \quad \chi_3 = 1 \qquad \text{at } y^* = 0 \tag{F.17}$$

Then, let φ_0 be the solution of the adjoint equation of the Rayleigh equation, which satisfies

$$L^*(\omega^*, a^*)\,\varphi_0 = \frac{1}{w_c}\left[\left(\bar{u} - \frac{\omega^*}{a^*}\right)\left(\frac{d^2}{dy^{*2}} - a^{*2}\right)\varphi_0 + 2\,\frac{d\bar{u}}{dy^*}\,\frac{d\varphi_0}{dy^*}\right] = 0 \tag{F.18}$$

with the same boundary conditions (F.15a). By multiplying (F.16) with φ_0 and integrating with respect to y* between 0 and ∞, we get

$$\lambda = -\frac{w_c \int_0^\infty \varphi_0 F_1 dy^*}{2i \int_0^\infty \varphi_0 (f_0'' - a^{*2} f_0) dy^*} \tag{F.19}$$

The solution to (F.7) may then be written as

$$\varphi^{(0)} = B_1 f_0 + B_2 \chi_3 + P \tag{F.20}$$

where P is any even particular integral of (F.16) with X known from (F.19). Then the condition at ∞, (F.16a), can be applied to determine B_2. The determination of the constant B_1 will have to go to one higher order equation by the same procedure used in determining X. The solutions for any r can be found in a similar manner. Since the

value of a_1 is arbitrary, if we choose

$$a_1 = -2\lambda \tag{F.21}$$

Then

$$f_1 = \varphi^{(0)} + a_i^* \varphi^{(1)} + \text{---} \tag{F.22}$$

(F.21) makes the function f_1 bounded even when $a_i^* \to 0$. If only the leading term of (F.22) is used to represent the solution, $\varphi^{(0)}$ gives the required solution for f_1. In this case, the determination of B_1 is not necessary and may be set to be zero. This only amounts to a redefinition of the amplitude function **A***.

The determination of the local solutions for ψ^* near $a_i^* \simeq 0$, together with the results obtained for large a_i^*, allows the evaluation of the integrals required in the integral equations over the complete range of a_i^*. (The highly damped case will be ignored and is expected to be of little interest in the practical case.) It should be noted here that the use of the integral method has provided the means to determine the governing equations for the amplitude and the mean flow shape-parameters. The introduction of a_n in (3.27) gives a bounded solution for f_1, etc., but is only used locally to provide a good estimate of the integrals. Therefore, they do not play a central role in the present theory as they do in the theory proposed by Stuart and Watson. Hence, the limitation on the magnitude of a_i^* (or $\bar{c}_i$) placed on their theory does not apply to the present formulation. In fact, the estimate of Watson provides a means to determine the

smallest value of a_1^*, beyond which the procedure discussed in this section is needed.

References

1. McKoen, C. H.: "On the Stability of a Laminar Wake," ARC CP 303 (1955).
2. Sato, H. and Kuriki, K.: "The Mechanism of Transition in the Wake of a Thin Flat Plate Placed Parallel to a Uniform Flow," JFM 11, 321-352 (1961).
3. Betchov, R. and Criminale, W. O., Jr.: "Spatial Instability of the Inviscid Jet and Wake," Phys. of Fl. 9:2, 359-362 (1966).
4. Gold, H.: "Stability of Laminar Wakes," California Institute of Technology, Ph. D. Thesis (1963).
5. Goldstein, S.: "On the Two-Dimensional Steady Flow of a Viscous Fluid Behind a Solid Body. Part I," Proc. Roy. Soc. A, 142, 545-562 (1933).
6. Meksyn, D. and Stuart, J. T.: "Stability of Viscous Motion Between Parallel Planes for Finite Disturbances," Proc. Roy. Soc. A, 208, 517-526 (1951).
7. Stuart, J. T.: "On the Role of the Reynolds Stresses in Stability Theory," J. Aero. Sci. 23, 86 (1956).
8. Stuart, J. T.: "On the Effects of the Reynolds Stress on Hydrodynamic Stability," Z. angew. Math. Mech., Sonderheft, pp. 932-938 (1956).
9. Kuwabara, S.: "Nonlinear Instability of Plane Couette Flow," Phys. of Fluid. Supplement copy on Boundary Layer and Turbulence, 10:9, Part II, S115-116 (1967).
10. Stuart, J. T.: "On the Non-linear Mechanics of Hydrodynamic Stability," JFM 4, 1-21 (1958).

11. Landau, L. :C. R. (Doklady) Acad. Sci. U. R. S.S. 44, 311 (1944). May also refer to Landau and Lifshitz, "Fluid Mechanics," Chapter III, Section 27. Pergamon Press (1959).

12. Davey, A.: "The Growth of Taylor Vortices in Flow Between Rotating Cylinders," JFM 14, 336-368 (1962).

13. Stuart, J. T.: "On the Non-linear Mechanics of Wave Disturbances in Stable and Unstable Parallel Flows. Part I. The Basic Behavior in Plane Poiseuille Flow," JFM 9, 353-370 (1960).

14. Watson, J.: "On the Non-linear Mechanics of Wave Disturbances in Stable and Unstable Parallel Flows. Part 2. The Development of a Solution for Plane Poiseuille Flow and for Plane Couette Flow," JFM 9, 371-389 (1960).

15. Eckhaus, W.: "Studies in Non-linear Stability Theory," Springer Tracts in Natural Phil. Vol. 6. Edited by C. Truesdell et al. (1965).

16. Schade, H.: "Contribution to the Non-linear Stability Theory of Inviscid Shear Layers," Phys. of Fluids 7, 623-628 (1964).

17. Stuart, J. T.: "On Finite Amplitude Oscillations in Laminar Mixing Layers," JFM 29, 417-440 (1967).

18. Reynolds, W. C. and Potter, M. C.: "Finite Amplitude Instability of Parallel Flows," JFM 27, 465-492 (1967).

19. Watson, J.: "On Spatially-growing Finite Disturbances in Plane Poiseuille Flow," JFM 14, 211-221 (1962).

20. Gorkov. L. P.: "Steadv Convection in a Plane Liquid Layer

Near the Critical Heat Transfer Point," Sov. Phys. J. E. T. P., 6(33), 311 (1958).

21. Malkus, W. V. R. and Veronis, G.: "Finite Amplitude Cellular Convection," JFM 4, 225 (1958).

22. Veronis, G.: "Cellular Convection with a Finite Amplitude in a Rotating Fluid," JFM 5, 401 (1959).

23. Joseph, D. D.: "On the Stability of the Boussinesq Equations;" Arch. Rat. Mech. Anal. (1965).

24. Segel, L. A. and Stuart, J. T.: "On the Question of the Preferred Mode in Cellular Thermal Convection," JFM 13, 289-306, (1962).

25. Joseph, D. D. and Shir, C. C.: "Nonlinear Stability of the Boussinesq Equations by the Method of Energy," Rept. of Univ. of Minn., Dept. of Aeronautics and Eng. Mech. (1965).

26. Segel, L. A.: "Nan-linear Hydrodynamic Stability Theory and its Applications to Thermal Convection and Curved Flows," Paper #10 in "Non-equilibrium Thermodynamics, Variational Techniques and Stability," Edited by Donnelly, R. J. et al. Univ. of Chicago Press (1965).

27. Gaster, M.: "A Note on the Relation Between Temporally-Increasing and Spatially-Increasing Disturbances in Hydrodynamic Stability," JFM 14, 222-224 (1962).

28. Gaster, M.: "The Role of Spatially-Growing Waves in the Theory of Hydrodynamic Stability," Prog. Aer. Sci. Sec. 6, 251-270 (1965).

29. Yih, C. S.: Review #3078 in Math. Rev. 29, 589 (1965).

30. Kaplan, R. E.: "The Stability of Laminar Incompressible Boundary Layers in the Presence of Compliant Boundaries," Mass. Inst. of Tech., Aero-Elastic and Structure Research Lab., ASRL-TR 116-1 (1964).

31. Betchov, R. and Criminale, W. O., Jr.: "Stability of Parallel Flows," Academic Press (1967).

32. Lin, C. C.: "The Theory of Hydrodynamic Stability," Camb. Monographs of Mech. and Appl. Mech. (1955).

33. Lin, C. C.: "On Uniformly Valid Asymptotic Solutions of the Orr-Sommerfeld Equation," Proc. 9th Intern. Congr. Appl. Mech. 2, 136-148 (1957).

34. Lin, C. C.: "On the Stability of Two-Dimensional Parallel Flows, Part I," Quarterly of Appl. Math., 3, 117-142 (1945).

35. Alber, I. E.: "Integral Theory for Turbulent Base Flows at Subsonic and Supersonic Speeds," Californa Institute of Technology, Ph. D. Thesis (1967).

36. Whitham, G. B.: "Non-linear Dispersive Waves," Proc. Roy. Soc. Vol. 283, 238-261 (1965).

37. Whitham, G. B.: "A General Approach to Linear and Non-linear Dispersive Waves Using a Lagrangian," JFM, 22, 273-283 (1965).

38. Whitham, G. B.: "Variational Methods and Applications to Water Waves," Proc. Roy. Soc. 299, 6-25 (1967).

39. Whitham, G. B.: "Non-linear Dispersion of Water Waves," JFM 27, Part 2, 399-412 (1967).

40. Behrens, W.: Private Communication.

41. Behrens, W.: "Flow Field and Stability of the Far Wake Behind Cylinders at Hypersonic Speeds," Calif. Inst. of Tech., Ph. D. Thesis (1966).

42. Batt, R. G.: "Experimental Investigation of Wakes Behind Two-Dimensional Slender Bodies at M = 6," Calif. Inst. of Tech., Ph. D. Thesis (1967).

43. Mac, L. M.: "Computation of the Stability of the Laminar Compressible Boundary Layer," Methods in Computational Physics, Vol. 4, pp. 247-299, Academic Press, 1965.

44. Kubota, T.: Private Communication.

45. Zaat, J. A.: In "Boundary Layer Research" (H. Görtler ed.), p. 127. Springer-Verlag, Berlin (1958).

46. Cheng, S. I.: "On the Stability of Laminar Boundary Layer Flow," Princeton Univ. Aero. Eng. Lab. Rept. No. 211 (1953).

47. Graebel, W. P.: "On Determination of the Characteristic Equations for the Stability of Parallel Flows," JFM Vol. 24, Part 3, pp. 497-508 (1966).

48. Heisenberg, W.: "Über Stabilität und Turbulenz von Flüssigkeitsströmen." Ann. Phys. Lpz., 74, 577-627.

49. Taylor, G. I.: "Stability of a Viscous Liquid Contained between Two Rotating Cylinders," Phil. Trans. A, 223, 289 (1923).

50. Tollmien, W. : "Ein Allgemeines Kritcrium der Instabilität Laminarer Geschwindigkeitsverteilungen," Nachr. Ges. Wiss. Göttingen, Math. -phys. Klasse, 50, 79-114. (1935). (English translation in NACA TM No. 792 (1936).)

51. Luke, Y. L. : "Integrals of Bessel Functions:' McGraw-Hill, New York, 1962.

52. Chen, T. S. , Joseph, D. D. , and Sparrow. : "Evaluation of Tietjens Function in S bility Calculations." The Phys. of Fluids. Vol. 9, No. 12. pp. 2519-2521 (1966).

53. Huppert, H. E. : "Numerical Evaluation of the Tietjens Function." The Phys. of Fluids, Vol. 11, No. 3, p. 673 (1968).

TABLE I

EIGENVALUES FOR $R = 2 \times 10^5$, Frequency = 730 cps

w_c	α_r^*	α_i^*	$\bar{c}_r$	$\bar{c}_i$
0.800	0.8431305	-0.2988252	0.4775625	0.2578652
0.750	0.7852360	-0.2461871	0.5090417	0.2641013
0.720	0.7627364	-0.2215836	0.5229835	0.2649093
0.692	0.7474712	-0.2019754	0.5334500	0.2644119
0.650	0.7328011	-0.1771193	0.5453891	0.2619686
0.600	0.7259882	-0.1527365	0.5547822	0.2569737
0.550	0.7294632	-0.1323420	0.5597915	0.2499972
0.500	0.7431208	-0.1147266	0.5609112	0.2409811
0.450	0.7679713	-0.0990128	0.5583199	0.2295612
0.400	0.8063129	-0.0844994	0.5519111	0.2150348
0.375	0.8317493	-0.0774926	0.5471513	0.2062574
0.350	0.8623357	-0.0705436	0.5412335	0.1961997
0.325	0.8991122	-0.0635626	0.5340145	0.1845799
0.300	0.9434874	-0.0564478	0.5252864	0.1710281
0.275	0.9974048	-0.0490771	0.5147428	0.1550497
0.260	1.0354333	-0.0444703	0.5073585	0.1440284
0.250	1.0636119	-0.0412986	0.5019113	0.1359743
0.240	1.0943756	-0.0380309	0.4959810	0.1272814
0.235	1.1108299	-0.0363537	0.4928108	0.1226637
0.230	1.1280579	-0.034652	0.4894985	0.1178765
0.225	1.1461145	-0.0329160	0.4860241	0.1128816

TABLE I (Cont'd)

w_c	α_r^*	α_i^*	$\overline{c}_r$	$\overline{c}_i$
0.220	1.1650544	-0.0311456	0.4823782	0.1076768
0.215	1.1849333	-0.0293387	0.4785683	0.1022513
0.210	1.2058391	-0.0274927	0.4745068	0.0965888
0.205	1.2278256	-0.0256051	0.4702467	0.0906793
0.200	1.2509819	-0.0236730	0.4657424	0.0845077
0.195	1.2753993	-0.0216939	0.4609683	0.0780596
0.190	1.3011783	-0.0196650	0.4558958	0.0713199
0.185	1.3284309	-0.0175835	0.4504911	0.0642742
0.180	1.357284	-0.0154441	0.4447099	0.0568963
0.175	1.3878723	-0.0132532	0.4385217	0.0492057
0.170	1.4203575	-0.0110005	0.4318583	0.0411580
0.165	1.4549144	-0.0086882	0.4246612	0.0327560
0.160	1.4917420	-0.0063177	0.4168583	0.0239998
0.150	1.5731355	-0.0014032	0.3991021	0.0054105
0.145	1.6181980	+0.0011050	0.3889018	-0.0042920
0.140	1.6666878	+0.0036450	0.3776987	-0.0142604
0.135	1.7189451	0.0061911	0.3652805	-0.0243933
0.130	1.7753981	0.0086994	0.351528	-0.0345145
0.125	1.8365481	0.0111242	0.3362865	-0.0444368
0.120	1.9029672	0.0133860	0.3194294	-0.0538316

TABLE II. INTEGRALS k_i **vs.** w_c for $U^* = e^{-0.69315\, y^{*2}}$

w_c	k_1	k_2	k_3	k_4	k_5	k_6	k_7	k_8	k_9
0.800	0.465875	0.534125	0.265706	0.368559	-0.058021	0.181380	-0.312384	-4.60218	
0.750	0.499914	0.500086	0.283472	0.336153	-0.085131	0.204147	-0.299369	-4.55099	
0.720	0.514533	0.485467	0.291352	0.322654	-0.097145	0.214471	-0.291304	-4.54622	
0.692	0.525022	0.474978	0.297119	0.313024	-0.105889	0.222693	-0.284110	-4.55098	
0.650	0.535780	0.464220	0.303187	0.302977	-0.114924	0.233313	-0.274246	-4.56898	
0.600	0.541570	0.458430	0.306658	0.296829	-0.119700	0.244282	-0.264215	-4.60189	
0.550	0.540124	0.459876	0.306152	0.296339	-0.118121	0.254194	-0.256135	-4.64452	$k_9 \equiv 0$
0.500	0.531287	0.468713	0.301487	0.301409	-0.109930	0.263402	-0.249990	-4.69685	
0.450	0.514330	0.485670	0.292155	0.312500	-0.094414	0.271818	-0.245742	-4.76090	
0.400	0.487847	0.512153	0.277216	0.330698	-0.070304	0.278750	-0.243378	-4.84084	
0.375	0.470366	0.529634	0.267195	0.343025	-0.054448	0.281170	-0.242913	-4.88889	
0.350	0.449575	0.550425	0.255140	0.357941	-0.035756	0.282409	-0.242940	-4.94402	
0.325	0.425020	0.574980	0.240727	0.375892	-0.013568	0.281871	-0.243473	-5.00812	
0.300	0.396174	0.603826	0.223568	0.397442	+0.012200	0.278640	-0.244527	-5.08378	
0.275	0.362469	0.637531	0.203214	0.423304	0.041989	0.271294	-0.246109	-5.17470	

TABLE II (Continued)

w_c	k_1	k_2	k_3	k_4	k_5	k_6	k_7	k_8	k_9
0.260	0.339689	0.660311	0.189273	0.441245	0.061875	0.264019	-0.247300	-5.23874	
0.250	0.323386	0.676614	0.179203	0.454344	0.075956	0.257569	-0.248184	-5.28635	
0.240	0.306182	0.693818	0.168493	0.468430	0.090652	0.249535	-0.249124	-5.33858	
0.235	0.297240	0.702760	0.162889	0.475859	0.098218	0.244835	-0.249607	-5.36676	
0.230	0.288094	0.711906	0.157138	0.483564	0.105888	0.239588	-0.250111	-5.39619	
0.225	0.278734	0.721266	0.151224	0.491543	0.113672	0.233775	-0.250592	-5.42724	
0.220	0.269180	0.730820	0.145161	0.499802	0.121536	0.227327	-0.251077	-5.46000	
0.215	0.259479	0.740521	0.138985	0.508331	0.129423	0.220197	-0.251518	-5.49441	$k_9 \equiv 0$
0.210	0.249551	0.750449	0.132616	0.517182	0.137391	0.212247	-0.252001	-5.53118	
0.205	0.239527	0.760473	0.126165	0.526303	0.145302	0.203462	-0.252418	-5.56994	
0.200	0.229413	0.770587	0.119626	0.535707	0.153132	0.193731	-0.252783	-5.61106	
0.195	0.219254	0.780746	0.113028	0.545383	0.160814	0.182949	-0.253080	-5.65478	
0.190	0.209114	0.790886	0.106413	0.555314	0.168264	0.171007	-0.253283	-5.70133	
0.185	0.199073	0.800927	0.099836	0.565473	0.175381	0.157780	-0.253361	-5.75599	
0.180	0.189221	0.810779	0.093357	0.575818	0.182051	0.143132	-0.253279	-5.80410	

TABLE II (Continued)

w_c	k_1	k_2	k_3	k_4	k_5	k_6	k_7	k_8	k_9
0.175	0.179721	0.820279	0.087105	0.586307	0.188069	0.126910	-0.252967	-5.86097	
0.170	0.170735	0.829265	0.081187	0.596813	0.193272	0.108945	-0.252391	-5.92200	
0.165	0.162469	0.837531	0.075763	0.607258	0.197417	0.089067	-0.251439	-5.99058	
0.160	0.155238	0.844762	0.071070	0.617453	0.200175	0.067111	-0.250008	-6.05751	
0.150	0.14575	0.85425	0.06530	0.63582	0.19975	0.01634	-0.24512	-6.2340	
0.145	0.14450	0.85550	0.06520	0.64350	0.19560	-0.01134	-0.2411	-6.4380	$k_9 \equiv 0$
0.140	0.14650	0.85350	0.06665	0.6500	0.18850	-0.03898	-0.2357	-6.790	
0.135	0.1502	0.8498	0.07035	0.6556	0.1796	-0.0702	-0.2263	-7.240	
0.130	0.1553	0.8447	0.07630	0.6598	0.1682	-0.0979	-0.2134	-7.800	
0.125	0.1619	0.8381	0.08425	0.6630	0.1560	-0.1203	-0.1975	-8.430	
0.120	0.1700	0.8300	0.09550	0.6647	0.1430	-0.1347	-0.1750	-9.102	

$\beta_1 = 1.064465$ $\beta_2 = 0.752690$

$\beta_3 = 0.614569$ $\beta_4 = 0.521727$

TABLE III. INTEGRALS k_{ig}

w_c	k_{1g}	k_{2g}	k_{3g}	k_{4g}	$-k_{5g}$	$-k_{6g}$	$-k_{7g}$	$-k_{8g}$	$-k_{9g}$
0.800	0.375555	0.265361	0.284088	0.182140	0.002012	0.093371	0.153854	12.8349	0.889406
0.750	0.411035	0.267177	0.305579	0.178800	0.011347	0.088477	0.158850	12.3849	0.856113
0.720	0.429341	0.268156	0.316426	0.177532	0.016910	0.087768	0.159992	12.3465	0.839136
0.692	0.444293	0.269130	0.325067	0.176767	0.021812	0.088146	0.160231	12.4027	0.824707
0.650	0.462958	0.270825	0.335378	0.176306	0.028534	0.090304	0.159517	12.6193	0.805333
0.600	0.479598	0.273516	0.343660	0.176822	0.035442	0.095130	0.157479	13.0721	0.785026
0.550	0.490596	0.277024	0.347790	0.178415	0.041366	0.102538	0.154465	13.7751	0.766949
0.500	0.496534	0.281367	0.348022	0.181015	0.046732	0.112882	0.150548	14.8385	0.750017
0.450	0.498205	0.286189	0.344684	0.184382	0.052427	0.126925	0.145547	16.4936	0.732588
0.400	0.497175	0.290724	0.338511	0.188036	0.060104	0.145760	0.138991	19.2453	0.711985
0.375	0.496630	0.292374	0.334863	0.189661	0.065673	0.157513	0.134871	21.3647	0.699219
0.350	0.497072	0.293181	0.331385	0.190873	0.073297	0.171146	0.129986	24.3463	0.683810
0.325	0.499886	0.292567	0.328851	0.191309	0.084172	0.187093	0.124092	28.7461	0.664641
0.300	0.507459	0.289830	0.328627	0.190483	0.100137	0.205705	0.116885	35.6612	0.640219
0.275	0.524190	0.283750	0.333265	0.187575	0.124527	0.227618	0.107933	47.5127	0.608500

TABLE III (ontinued)

w_c	k_{1g}	k_{2g}	k_{3g}	k_{4g}	$-k_{5g}$	$-k_{6g}$	$-k_{7g}$	$-k_{8g}$	$-k_{9g}$
0. 260	0. 541952	0. 277793	0. 340322	0. 184330	0. 145596	0. 242653	0. 101485	59. 2482	0. 584688
0. 250	0. 558872	0. 272621	0. 347909	0. 181368	0. 163564	0. 253548	0. 096631	70. 5346	0. 566395
0. 240	0. 581581	0. 266191	0. 358805	0. 177549	0. 185897	0. 265271	0. 091262	86. 3118	0. 545717
0. 235	0. 595917	0. 262482	0. 365974	0. 175298	0. 199198	0. 271517	0. 088367	96. 6960	0. 534375
0. 230	0. 612418	0. 258329	0. 374410	0. 172749	0. 214089	0. 277899	0. 085329	109. 3048	0. 522469
0. 225	0. 631932	0. 253798	0. 384582	0 169920	0. 231068	0. 284641	0. 082093	124. 9474	0. 509477
0. 220	0. 654955	0. 248710	0. 396820	0. 166717	0. 250516	0. 291599	0. 078711	144. 6143	0. 496020
0. 215	0. 682245	0. 243185	0. 411516	0. 163182	0. 272866	0. 298903	0. 075111	169. 7491	0. 481177
0. 210	0. 714870	0. 237055	0. 429386	0. 159232	0. 298821	0. 306407	0. 071345	202. 6444	0. 465783
0. 205	0. 754445	0. 230336	0. 451333	0. 154849	0. 329384	0. 314357	0. 067362	246. 6160	0. 449181
0. 200	0. 803108	0. 222927	0. 478645	0. 149965	0. 365908	0. 322866	0. 063128	307. 1230	0. 431336
0. 195	0. 863397	0. 214985	0. 512814	0. 144653	0. 409901	0. 331896	0. 058644	393. 2041	0. 411625
0. 190	0. 939974	0. 205967	0. 556641	0. 138572	0. 464492	0. 341629	0. 053845	520. 7157	0. 390340
0. 185	1. 038883	0. 195965	0. 613714	0. 131799	0. 533420	0. 351783	0. 048788	719. 0307	0. 368068
0. 180	1. 171356	0. 184864	0. 690821	0. 124174	0. 623510	0. 363317	0. 043355	1048. 871	0. 342648

TABLE III Continued)

w_c	k_1	k_{2g}	k_{3g}	k_{4g}	$-k_{5g}$	$-k_{6g}$	$-k_{7g}$	$-k_{8g}$	$-k_{9g}$
0.175	1.355137	0.172547	0.798471	0.115687	0.745914	0.375219	0 037951	1649.858	0 317303
0.170	1.644331	0.158768	0.968724	0.106072	0.934243	0.391199	0 033748	2963.320	0 293002
0.165	2.092171	0.143671	1.232649	0.095539	1.221866	0.397606	0 029242	6140.617	0 268321
0.160	2.846623	0.126888	1.686796	0.083714	1.692602	0.426316	0 019438	15063.00	0 221242

TABLE IV. INTEGRALS k_{if}

w_c	k_{1f}	k_{2f}	k_{3f}	k_{4f}	k_{5f}	k_{6f}	$-k_{7f}$	k_{8f}	k_{9f}
0.800	1.82337	1.20111	0.79765	0.41220	-0.25503	0.83950	1.56080	4.00838	-2.24582
0.750	1.12596	0.67845	0.41760	0.12441	-0.12782	0.72000	1.26052	5.97721	-0.97830
0.720	0.87924	0.55769	0.29048	0.07497	-0.05953	0.68829	1.18931	6.52356	-0.50688
0.692	0.70521	0.49433	0.20304	0.05568	-0.00182	0.67124	1.15420	6.93091	-0.15316
0.650	0.50349	0.44372	0.10371	0.04726	0.07684	0.65785	1.12813	7.52137	0.29771
0.600	0.31590	0.41765	0.01281	0.04926	0.16318	0.65130	1.10948	8.33115	0.78358
0.550	0.15941	0.41018	-0.06222	0.05507	0.24654	0.64911	1.08449	9.37064	1.27301
0.500	0.01950	0.41317	-0.12876	0.06122	0.33101	0.64819	1.04161	10.7839	1.81429
0.450	-0.11231	0.42339	-0.19082	0.06650	0.42036	0.64666	0.97423	12.8188	2.46530
0.400	-0.24231	0.43958	-0.25140	0.07027	0.51877	0.64242	0.87915	15.9944	3.31539
0.375	-0.30914	0.44937	-0.28245	0.07116	0.57318	0.63788	0.82967	18.3506	3.86587
0.350	-0.37980	0.45905	-0.31558	0.07047	0.63237	0.62976	0.75592	21.5994	4.54938
0.325	-0.46013	0.46311	-0.35423	0.06454	0.69773	0.61301	0.68328	26.3408	5.43962
0.300	-0.56751	0.43736	-0.40815	0.03765	0.76947	0.57096	0.59671	33.8436	6.67636
0.275	-0.76166	0.26540	-0.50760	-0.08539	0.83531	0.44046	0.45670	47.2816	8.59623

TABLE **IV** (Continued)

w_c	k_{1f}	k_{2f}	k_{3f}	k_{4f}	k_{5f}	k_{6f}	k_{7f}	k_{8f}	k_{9f}
0.260	-0.99224	-0.09744	-0.62122	-0.32768	0.83928	0.23554	0.27669	61.5985	10.4333
0.250	-1.24208	-0.62238	-0.73654	-0.67203	0.78667	-0.01667	0.04919	76.2899	12.2198
0.240	-1.60025	-1.57473	-0.88609	-1.29101	0.63478	-0.41250	-0.34409	97.8813	14.7925
0.235	-1.82011	-2.28411	-0.96652	-1.74917	0.49349	-0.67241	-0.63307	112.411	16.5312
0.230	-2.05011	-3.17046	-1.03602	-2.31807	0.29184	-0.96100	-0.99480	130.005	18.6803
0.225	-2.26176	-4.22653	-1.07349	-2.98929	0.01739	-1.25128	-1.43093	151.278	17.5149
0.220	-2.38762	-5.35266	-1.03694	-3.69035	-0.32957	-1.47211	-1.91281	176.366	24.7799
0.215	-2.30869	-6.29492	-0.85775	-4.24161	-0.72009	-1.49127	-2.36091	204.793	29.0698
0.210	-1.78155	-6.39507	-0.40554	-4.18317	-1.04529	-1.02902	-2.56585	234.178	34.5020
0.205	-0.40380	-4.32953	0.52070	-2.59324	-1.04281	0.38624	-2.09993	258.828	41.2886
0.200	2.56844	2.71191	2.27089	2.48213	-0.10046	3.63146	-0.06083	265.461	49.5903
0.195	8.43582	20.3372	5.41901	14.9446	3.09209	10.2297	5.33606	225.751	59.3026
0.190	19.5998	59.9006	10.9809	42.7220	11.2879	22.9167	17.6500	76.6481	69.5039
0.185	41.6243	148.362	21.2915	104.689	31.0677	47.8484	45.1956	-351.243	75.9843
0.180	91.3916	371.816	42.9807	260.514	84.3043	103.892	114.157	-1608.21	57.2655

TABLE V. INTEGRALS k_{iff}

w_c	k_{1ff}	k_{2ff}	k_{3ff}	k_{4ff}	$-k_{5ff}$	k_{6ff}	k_{7ff}	$-k_{8ff}$	$-k_{9ff}$
0.800	10.8067	9.17985	6.71923	6.21525	1.65073	1.88165	0.49287	292.894	2.81390
0.750	7.72743	4.92637	4.80180	3.13896	1.68448	1.51013	1.45379	230.382	4.04396
0.720	6.74822	3.69404	4.19462	2.27877	1.68215	1.34032	1.69921	214.098	4.54817
0.692	6.11901	2.93734	3.80280	1.76143	1.68122	1.20547	1.82512	206.454	4.90793
0.650	5.48731	2.19804	3.40415	1.26652	1.69140	1.03128	1.90830	204.830	5.32727
0.600	5.04553	1.66010	3.11378	0.91460	1.73449	0.84903	1.91894	216.310	5.74602
0.550	4.84855	1.32706	2.96435	0.70042	1.83076	0.67743	1.88773	244.832	6.18205
0.500	4.88890	1.11701	2.94669	0.56612	2.01594	0.50092	1.85152	299.975	6.75070
0.450	5.24565	0.99220	3.09979	0.48508	2.36137	0.29981	1.84072	406.245	7.62269
0.400	6.15905	0.94151	3.54863	0.44859	3.03161	0.04001	1.89079	630.901	9.14147
0.375	7.00521	0.94811	3.97899	0.44916	3.60616	-0.13318	1.95554	843.498	10.37605
0.350	8.33270	0.98514	4.66366	0.46774	4.48287	-0.35786	2.06251	1201.13	12.2086
0.325	10.5148	1.06976	5.80024	0.51529	5.90187	-0.66886	2.23376	1856.65	15.1360
0.300	14.3720	1.24139	7.82364	0.61936	8.39384	-1.13582	2.51115	3205.98	20.3463
0.275	21.9418	1.59280	11.8140	0.85589	12.2966	-1.93000	2.98055	6475.44	30.9578

TABLE V. (CONTINUED)

w_c	k_{1ff}	k_{2ff}	k_{3ff}	k_{4ff}	$-k_{5ff}$	k_{6ff}	k_{7ff}	$-k_{8ff}$	$-k_{9ff}$
0.260	30.3616	1.97495	16.2611	1.14684	18.7988	-2.75618	3.42166	10976.6	42.6144
0.250	39.1290	2.37166	20.8927	1.47785	24.5713	-3.60655	3.80765	16560.2	53.3410
0.240	52.2727	3.05226	27.8334	2.05964	33.2314	-4.24375	4.24375	26534.9	64.6114
0.235	61.4340	3.67993	32.6687	2.56914	39.2054	-5.67372	4.43325	34536.1	68.1859
0.230	73.0964	4.78639	38.8226	3.40559	46.6536	-6.57596	4.51352	45852.9	66.9308
0.225	88.4657	6.99925	46.9279	4.95734	56.0695	-7.40169	4.30506	62404.1	55.0931
0.220	109.426	11.7934	57.9723	8.12849	67.9664	-7.64491	3.37605	87307.5	20.3563
0.215	139.525	22.9032	73.7976	15.2288	82.8643	-5.86745	0.66116	126064.	-63.2909
0.210	186.152	49.9467	98.2334	32.2672	101.007	1.77249	-5.55671	189070.	-256.536
0.205	265.585	119.310	139.574	75.9974	120.813	26.0560	-25.6412	296221.	-692.002
0.200	418.271	307.482	218.241	195.763	134.177	97.9584	-77.8302	489192.	-1675.85
0.195	754.837	854.944	389.460	549.271	107.780	312.818	-229.811	861055.	-3919.72
0.190	1624.03	2618.46	825.883	1707.31	-96.9325	1000.85	-719.794	1638767.	-9213.32
0.185	4420.33	9409.12	2209.44	6243.20	-1161.79	3589.32	-2612.16	3441062.	-22644.5
0.180	17156.5	45223.2	8426.80	30523.4	-7697.47	16754.4	-12626.9	8291290.	-55798.7

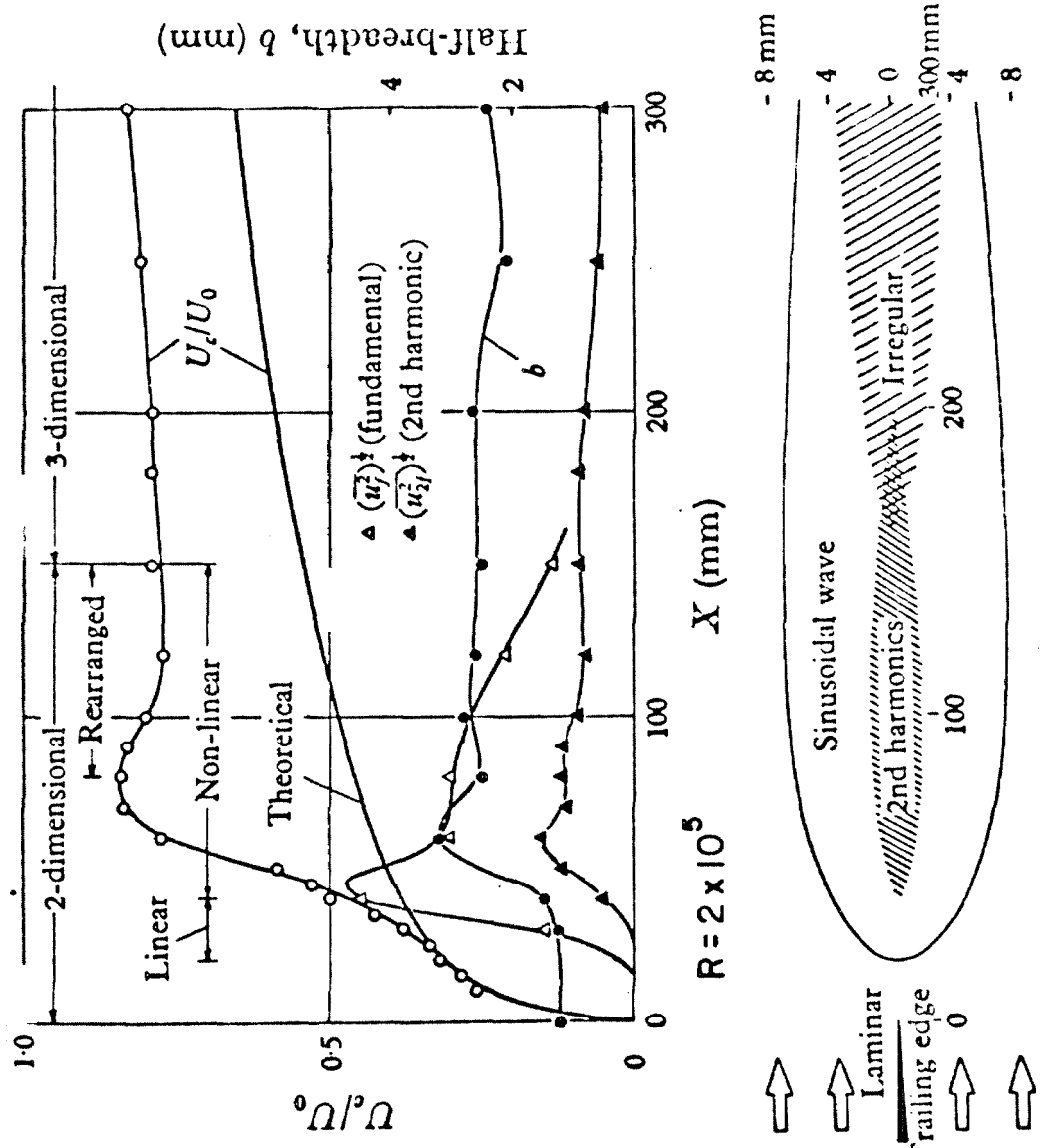

Fig. 1 Experimental Results of Sato-Kuriki for the Wake Behind a Flat Plate

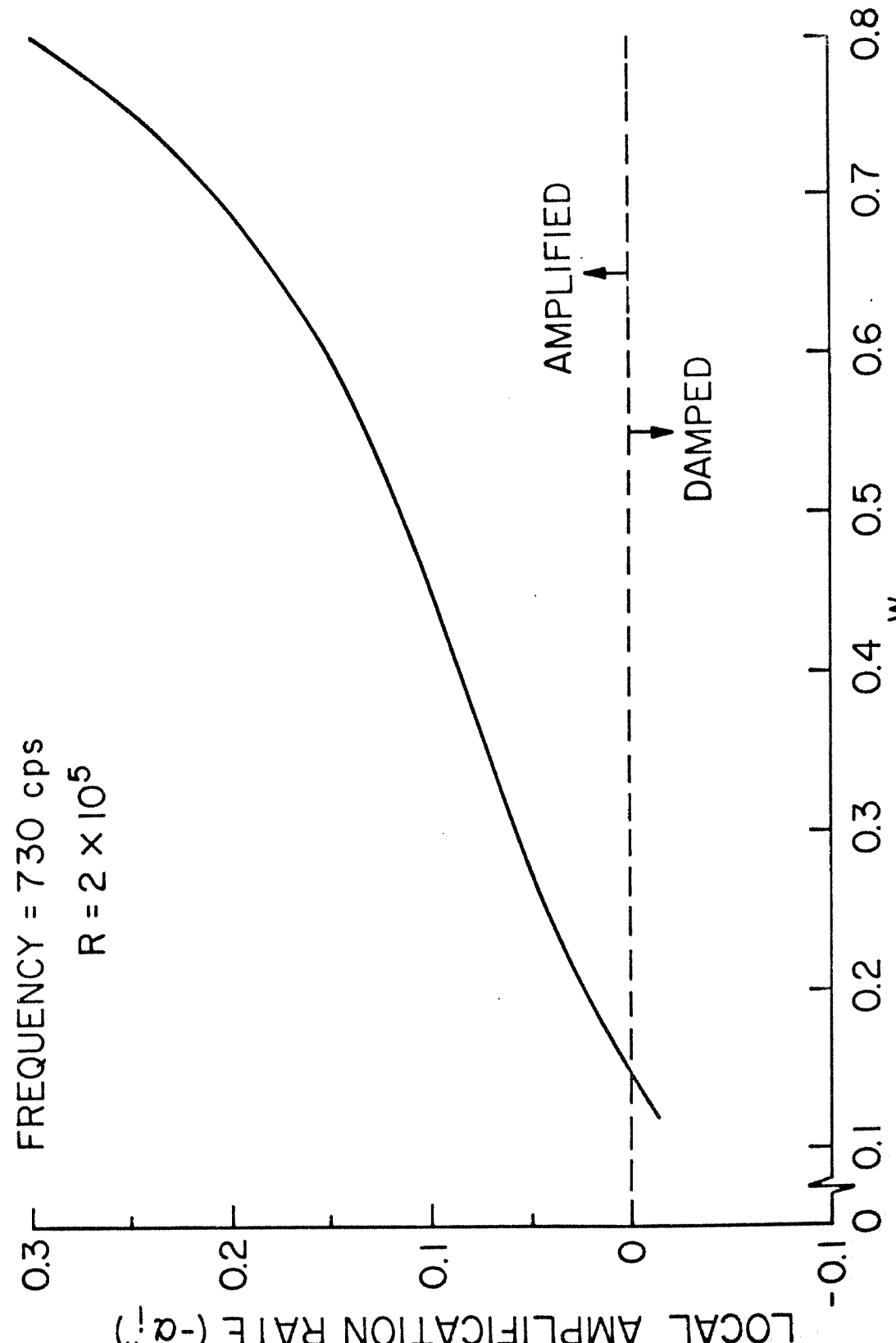

Fig. 2 Local Spatial Amplification Rate as a Function of w_c

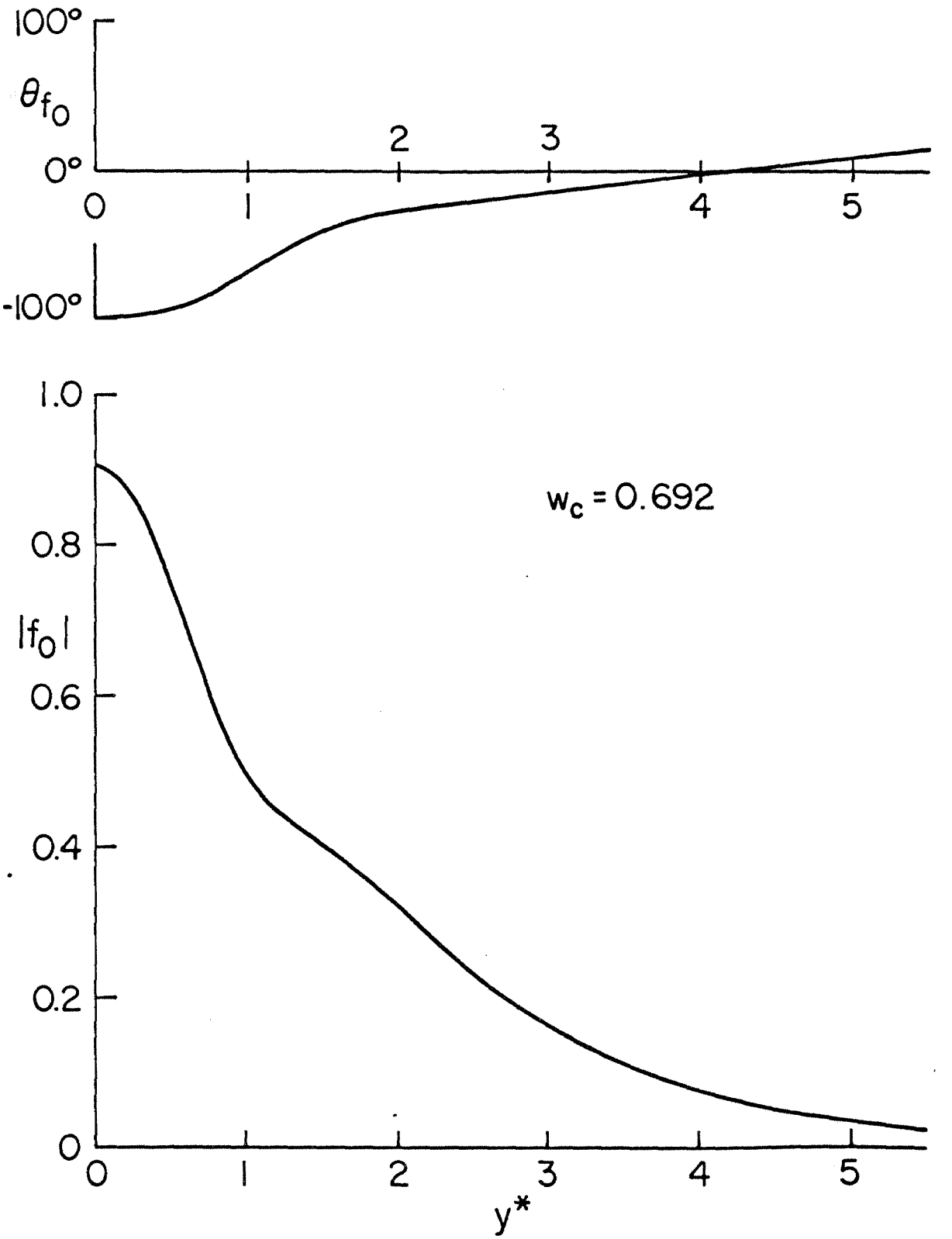

Fig. 3a Distribution of Amplitude and Phase of f_0 at $w_c = 0.692$

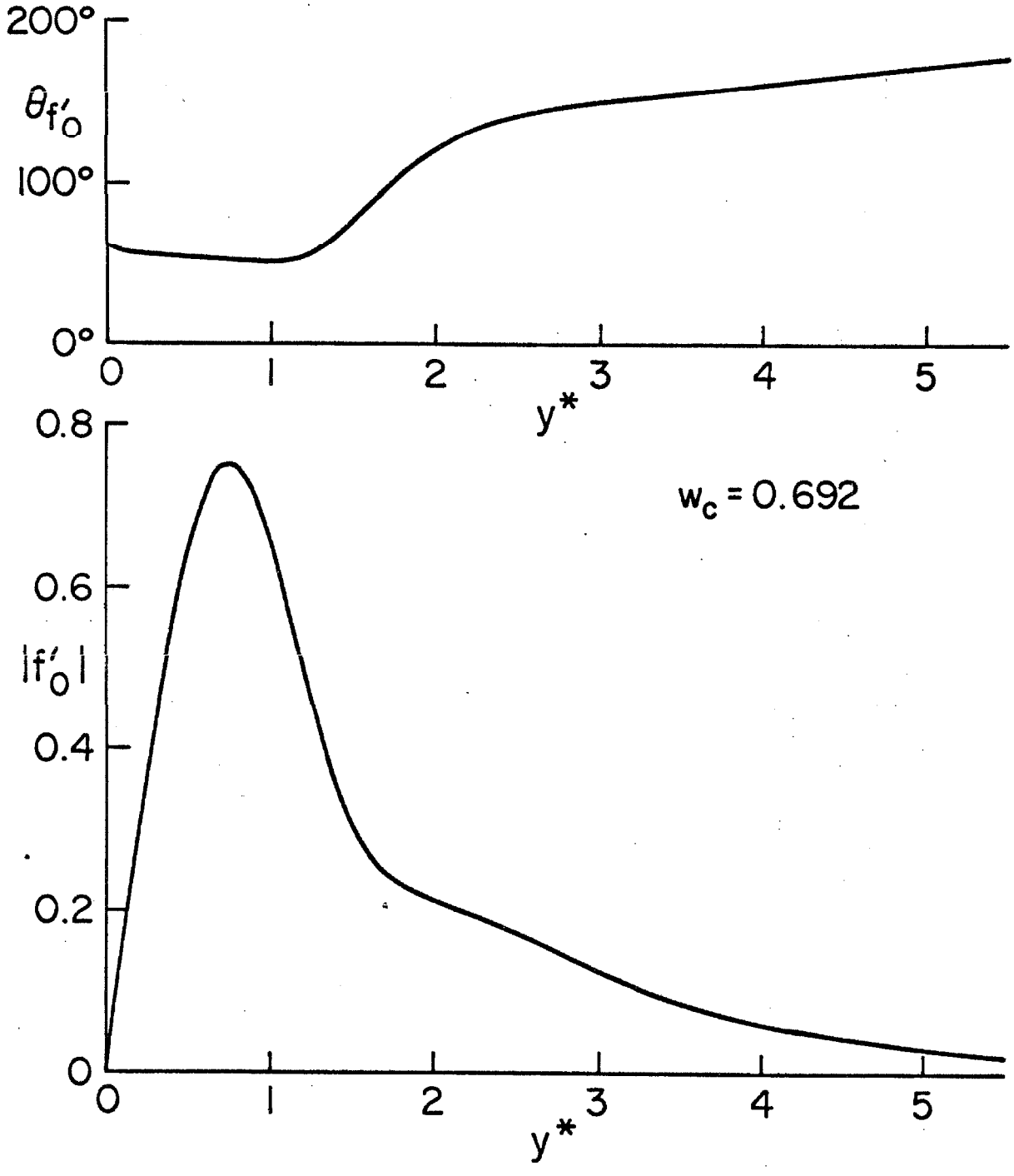

Fig. 3b Distribution of Amplitude and Phase of f'_0 at $w_c = 0.692$

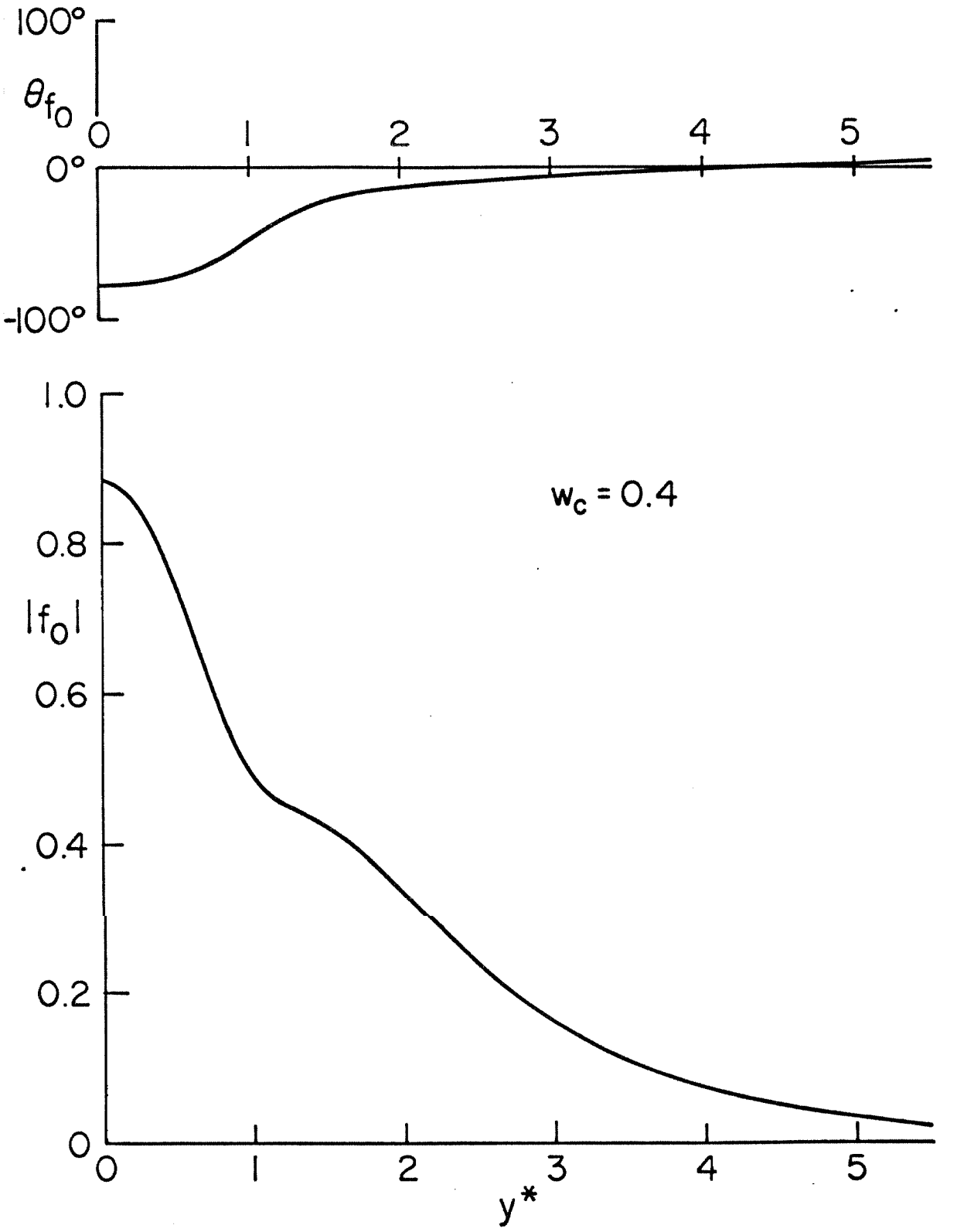

Fig. 3c Distribution of Amplitude and Phase of f_0 at $w_c = 0.40$

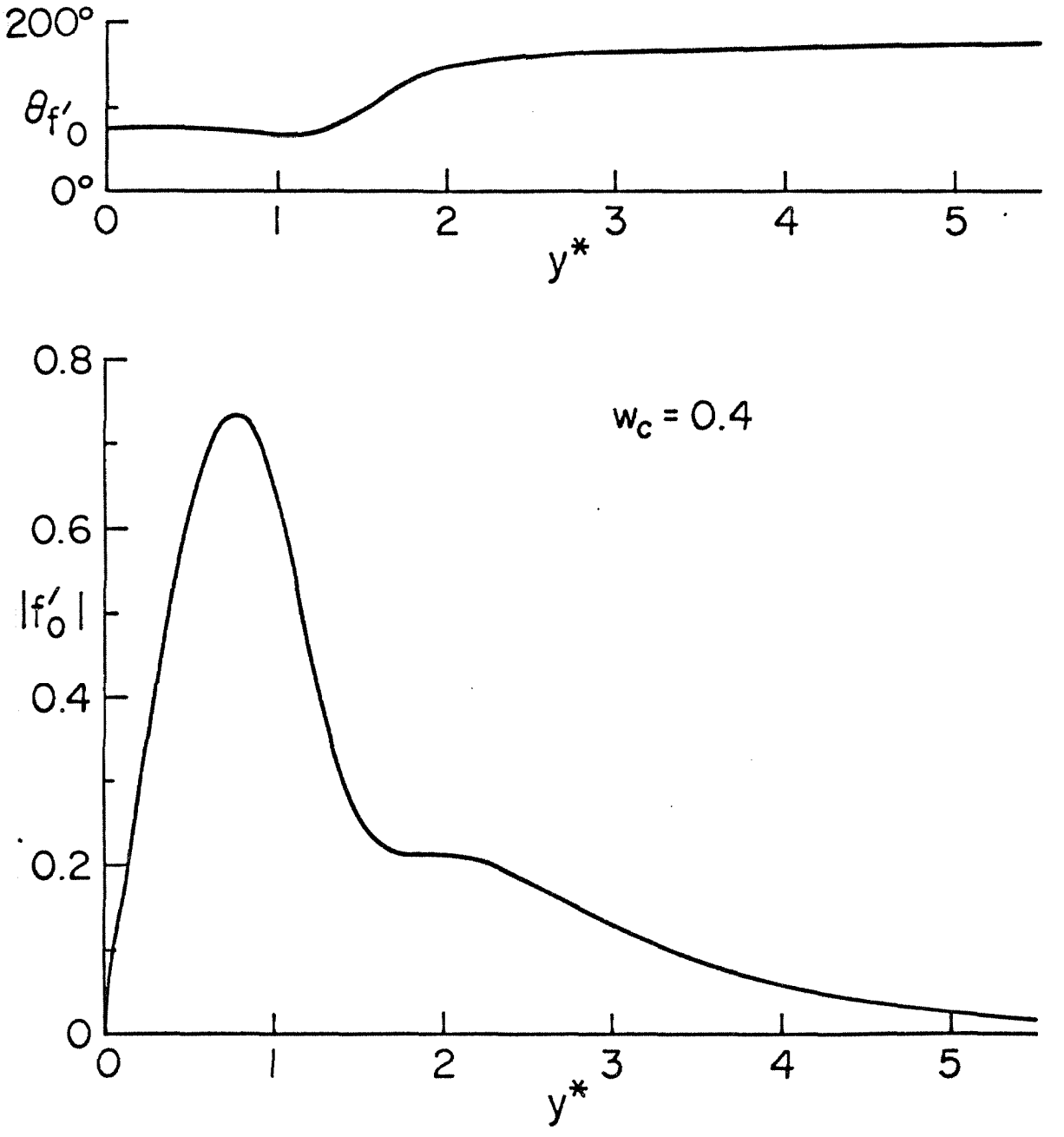

Fig. 3d Distribution of Amplitude and Phase of f'_0 at $w_c = 0.40$

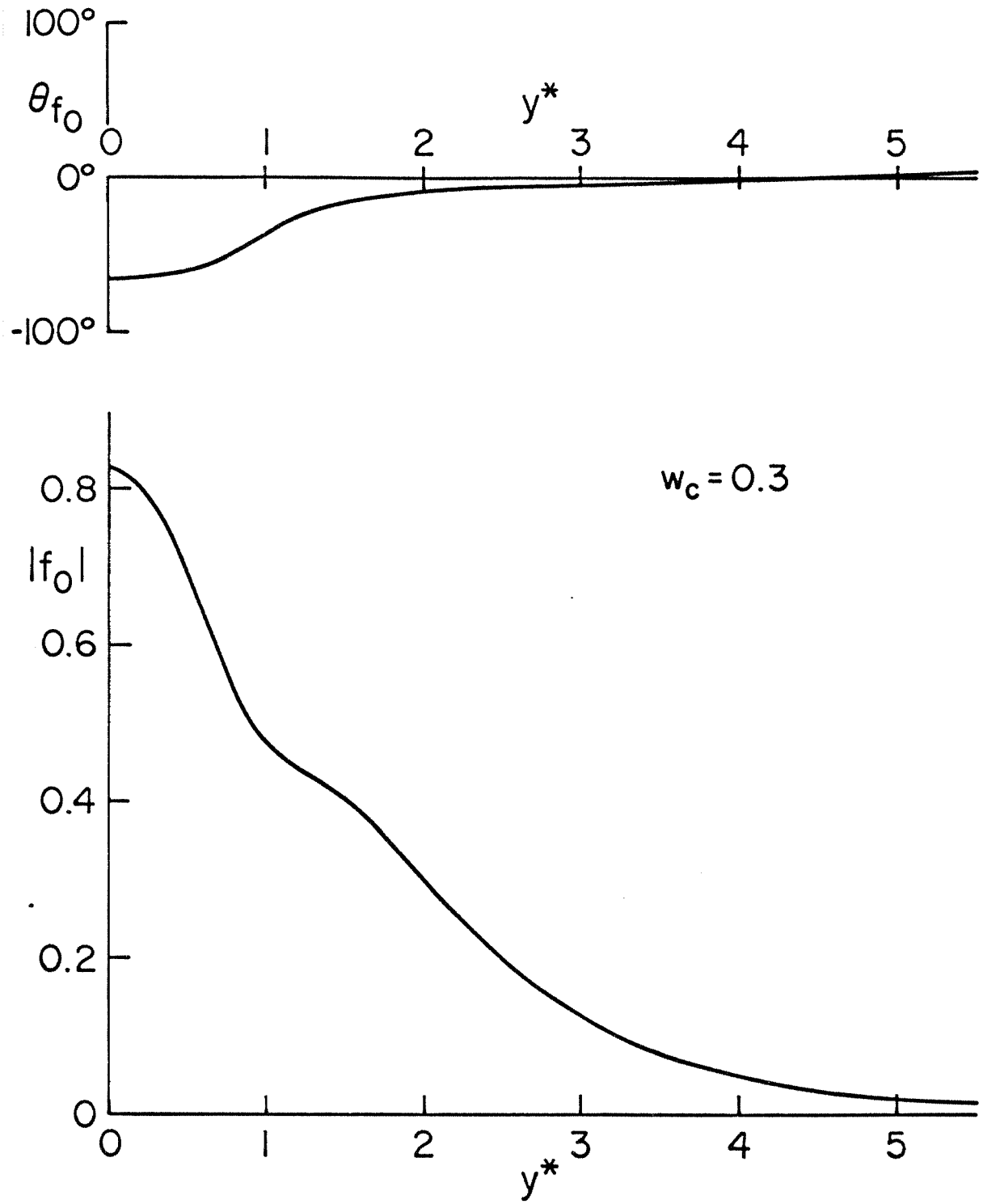

Fig. 3e Distribution of Amplitude and Phase of f_0 at $w_c = 0.30$

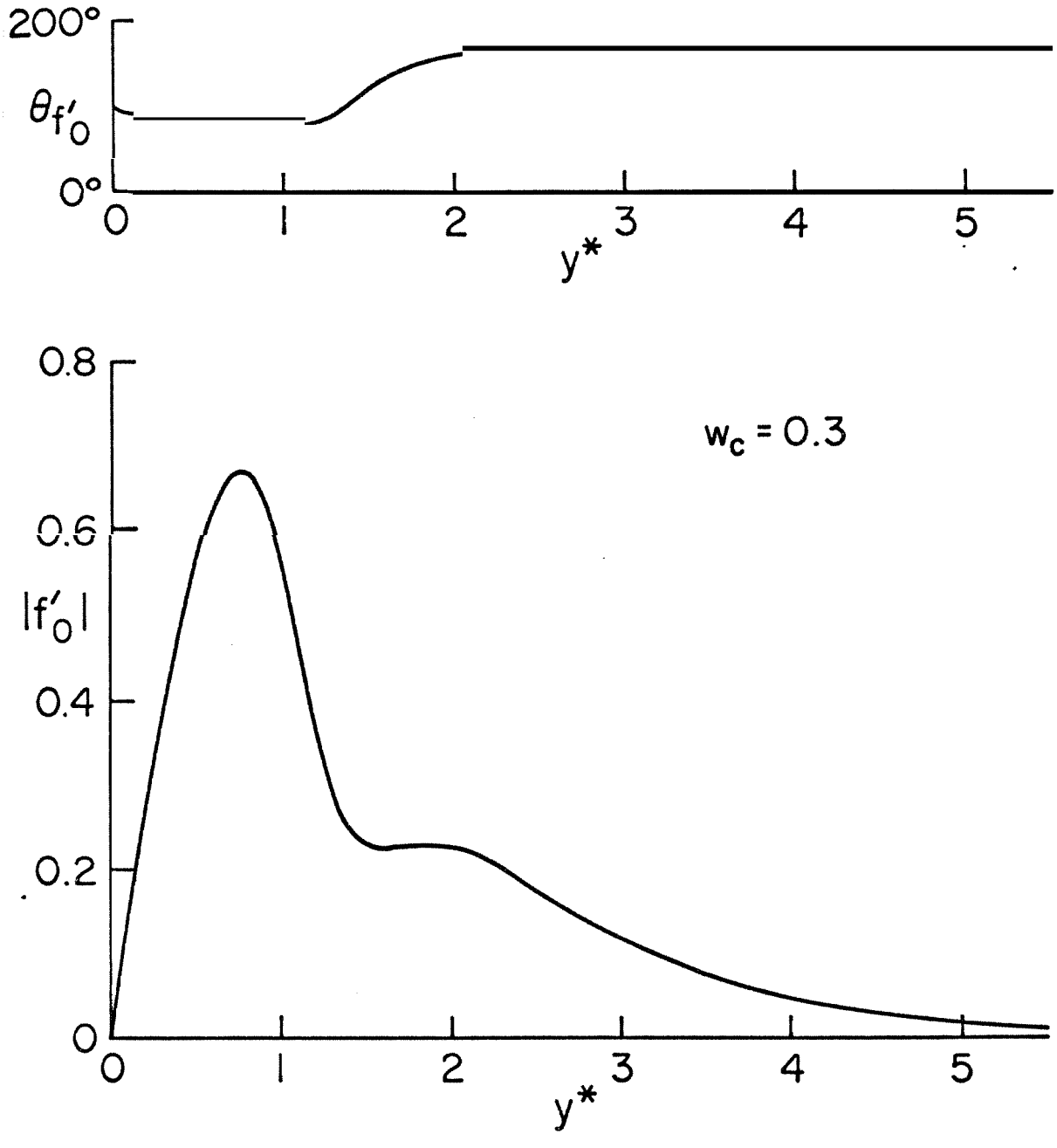

Fig. 3f Distribution of Amplitude and Phase of f'_0 at $w_c = 0.30$

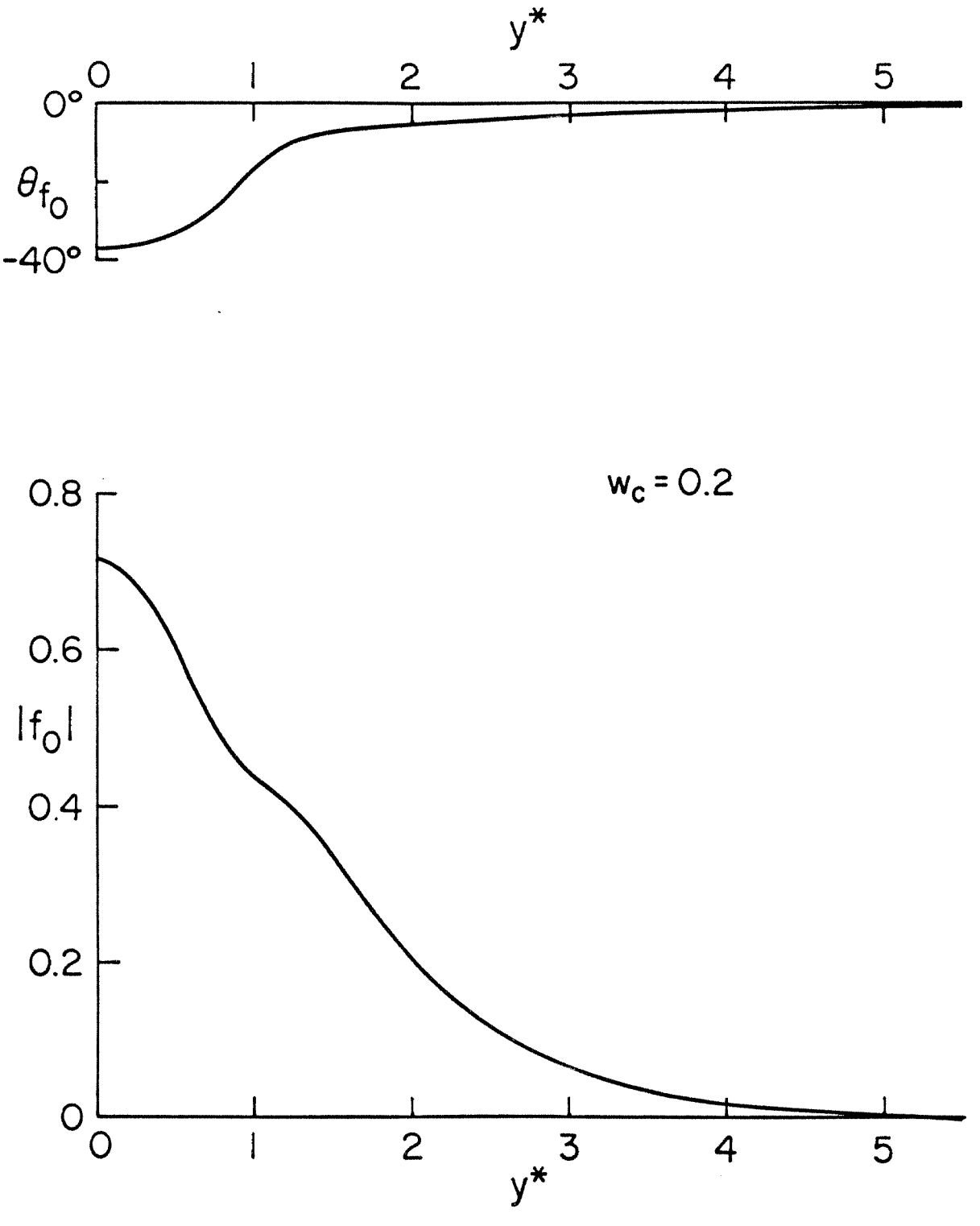

Fig. 3g Distribution of Amplitude and Phase of f_0 at $w_c = 0.20$

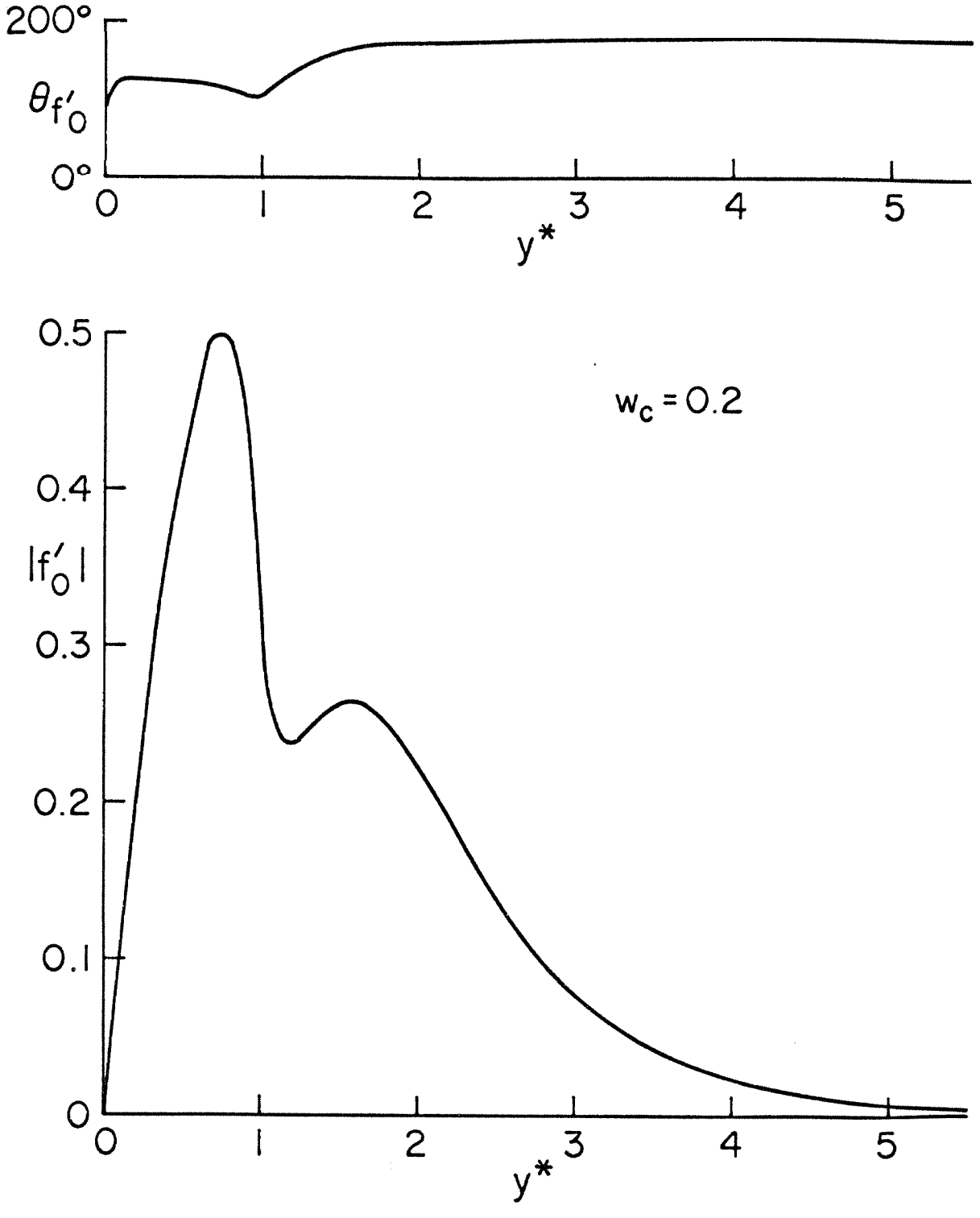

Fig. 3h Distribution of Amplitude and Phase of f'_0 at $w_c = 0.20$

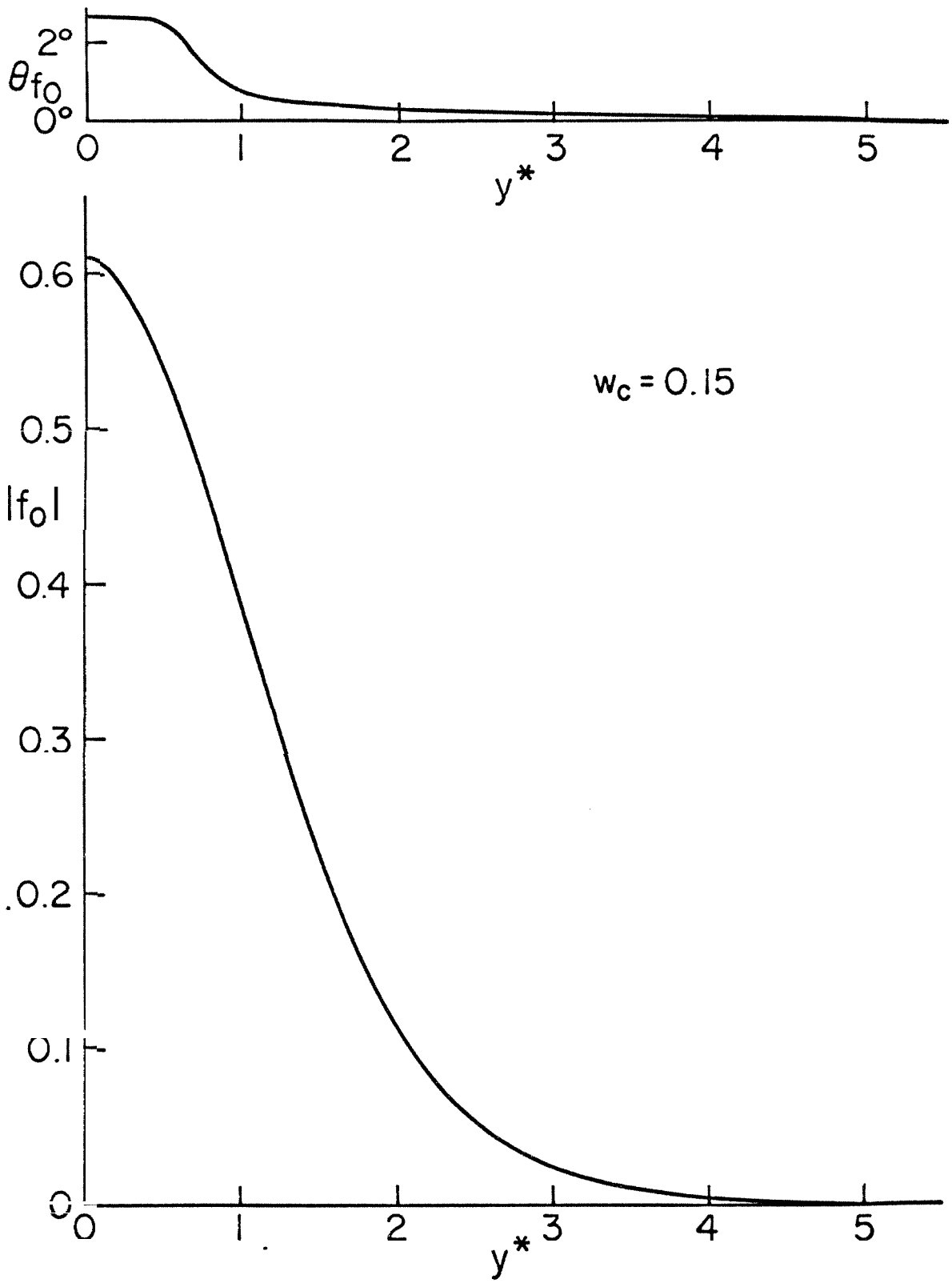

Fig. 3i Distribution of Amplitude and Phase of f_0 at $w_c = 0.15$

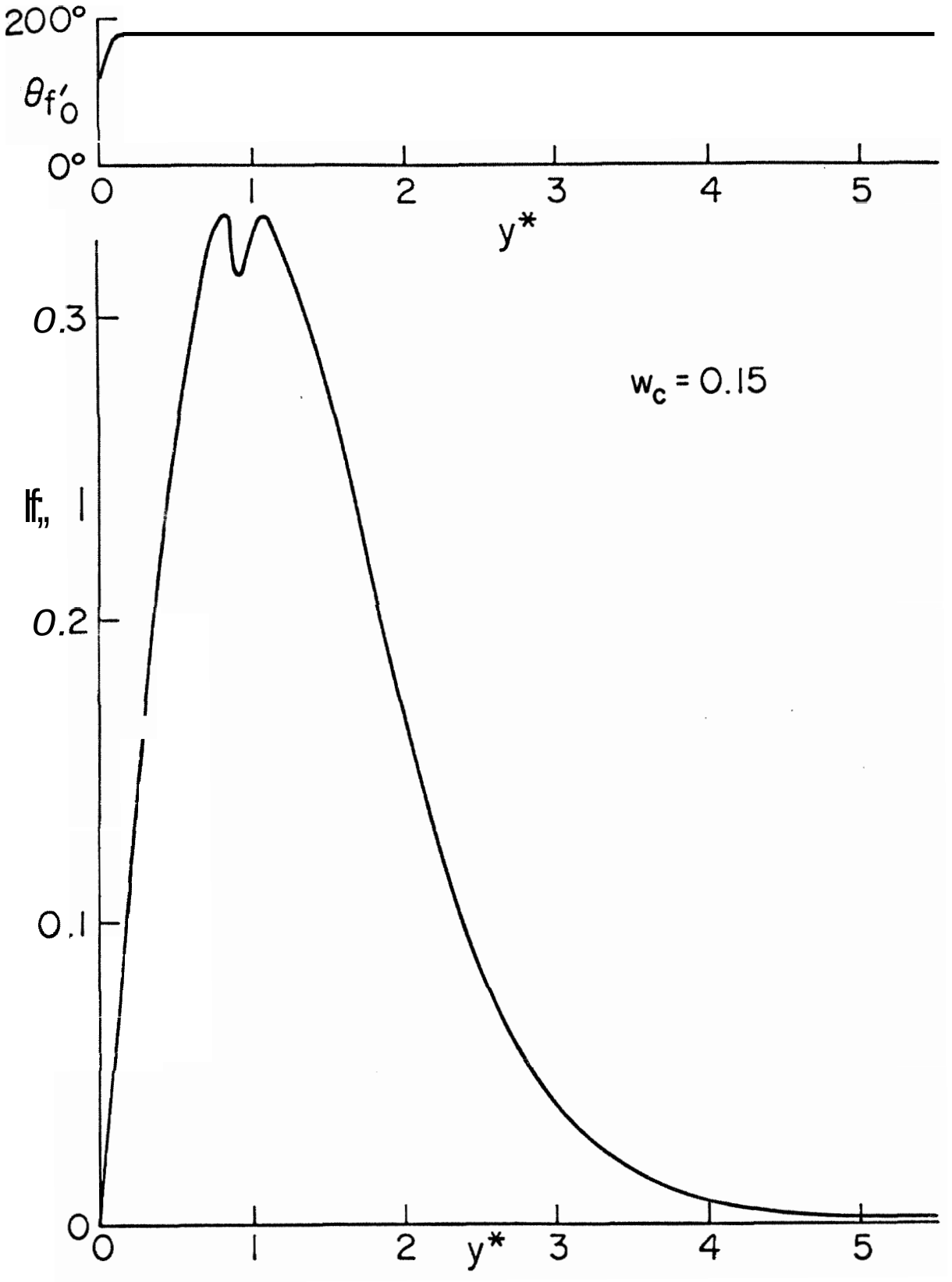

Fig. 3j Distribution of Amplitude and Phase of f'_0 at $w_c = 0.15$

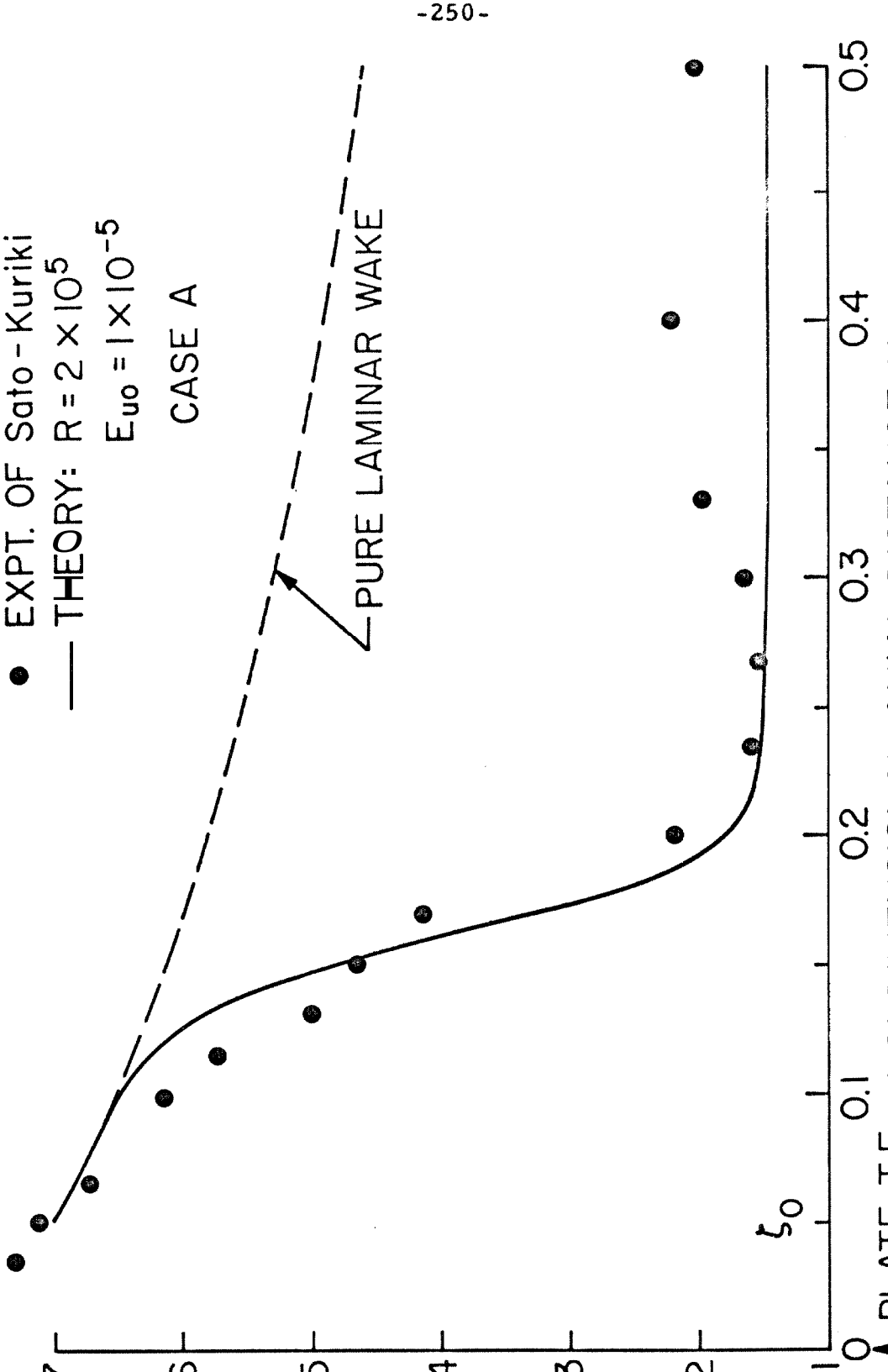

Fig. 4 Comparison of the Mean Centerline Velocity Defect, w_c

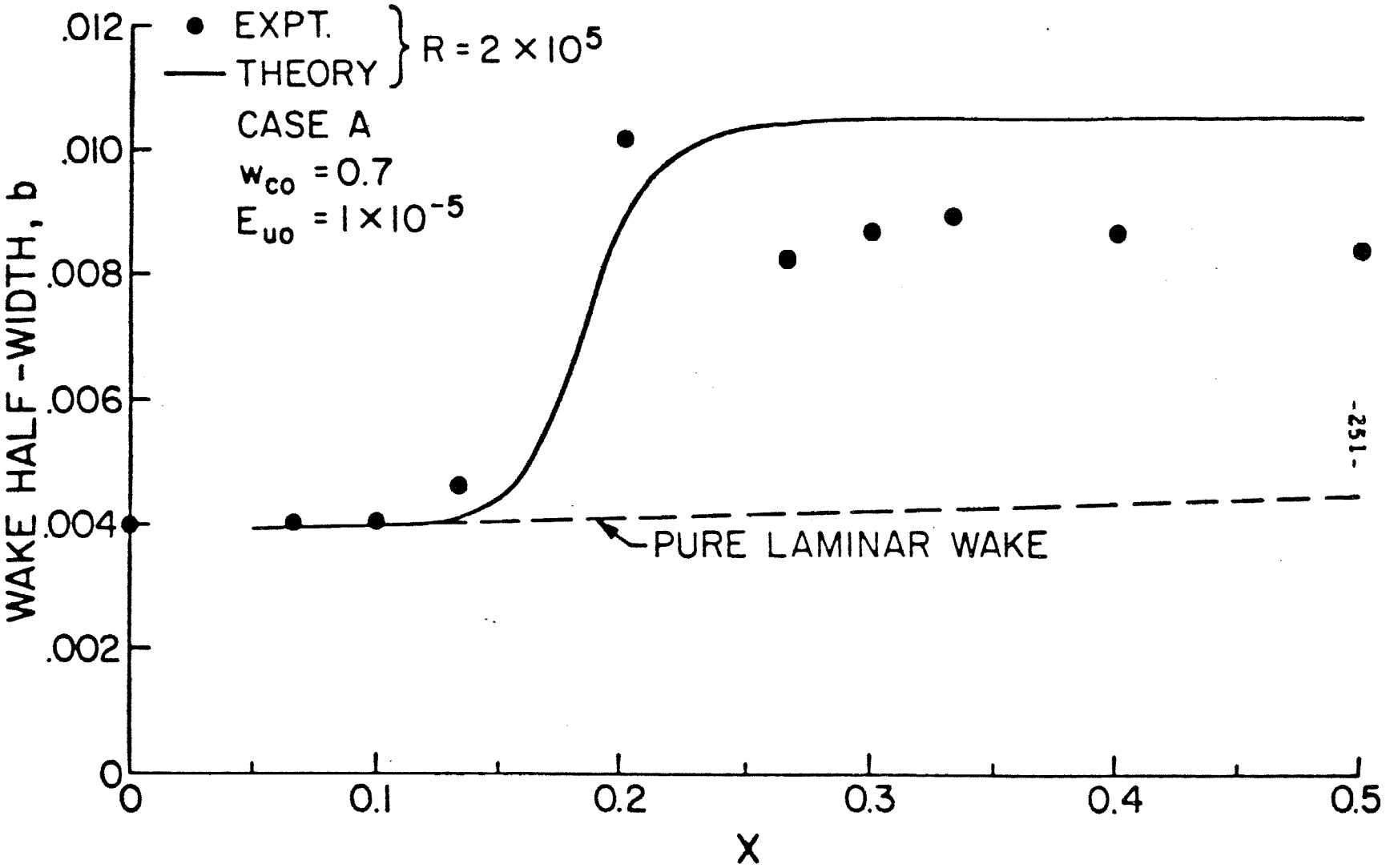

Fig. 5 Comparison of the Wake Half-width b

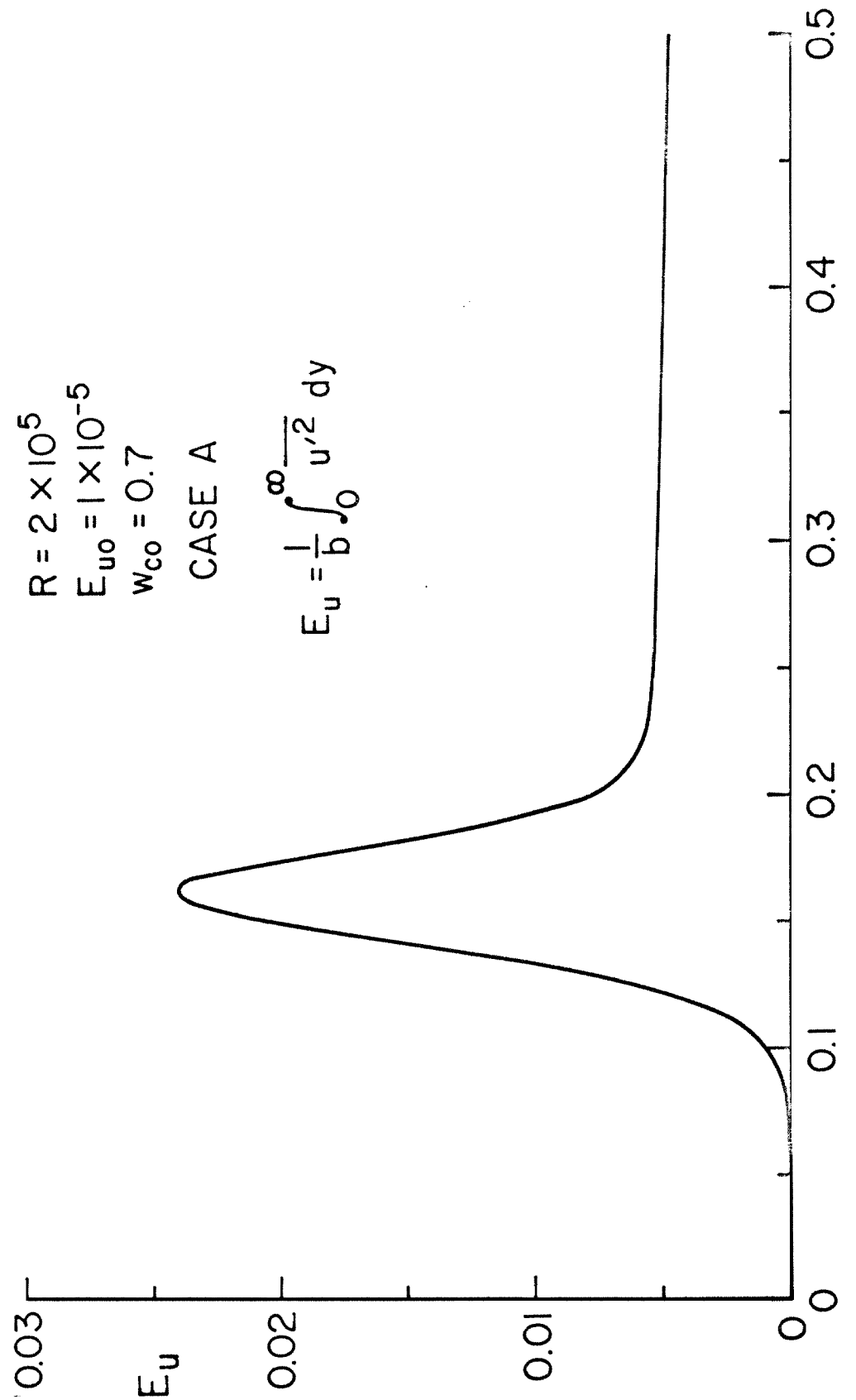

Fig. 6 Calculated Variation of the Integrated Fluctuation Energy in the u'-component E_u

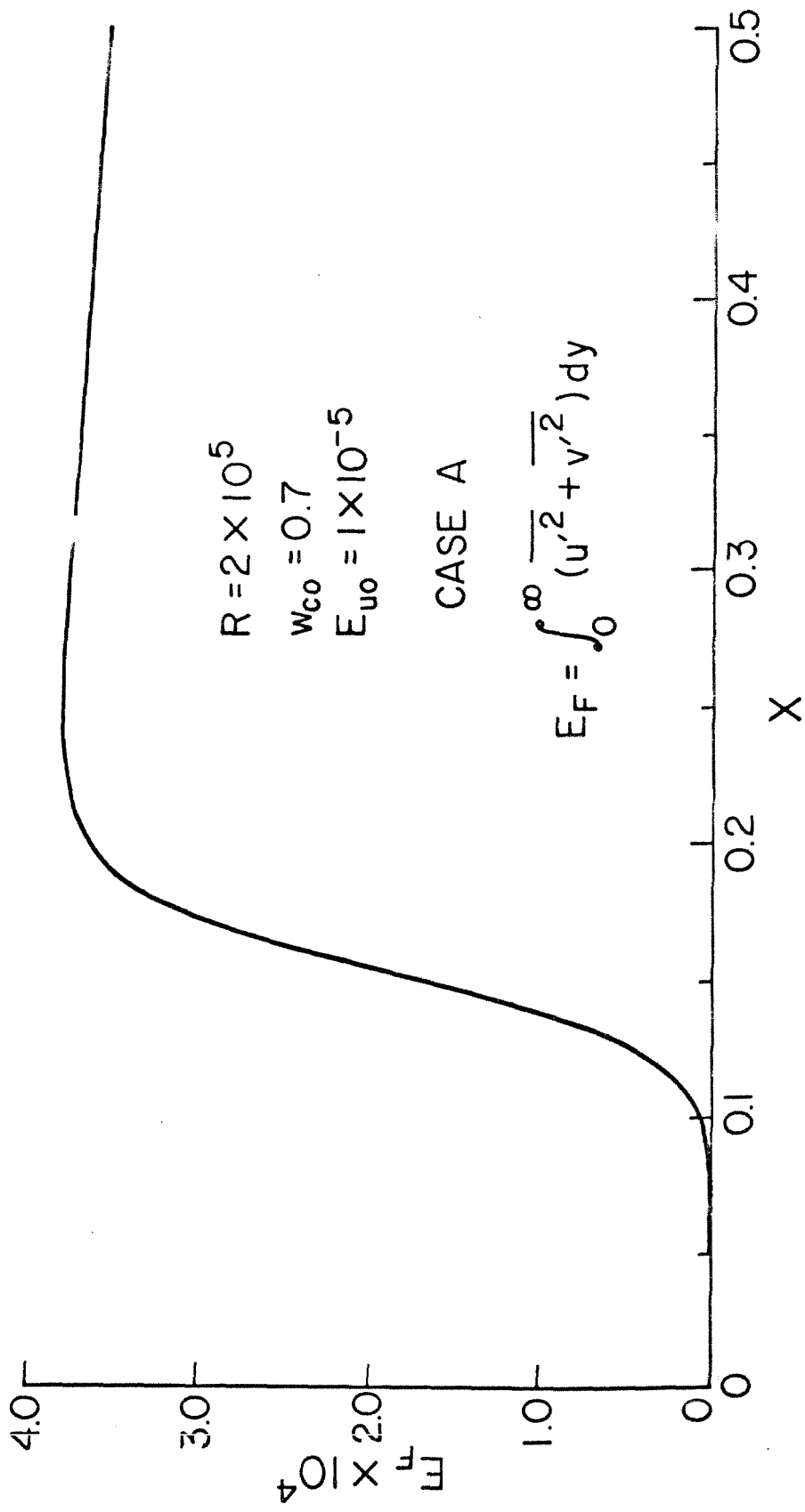

Fig. 7 Variation of the Total Integrated Fluctuation Energy E_F

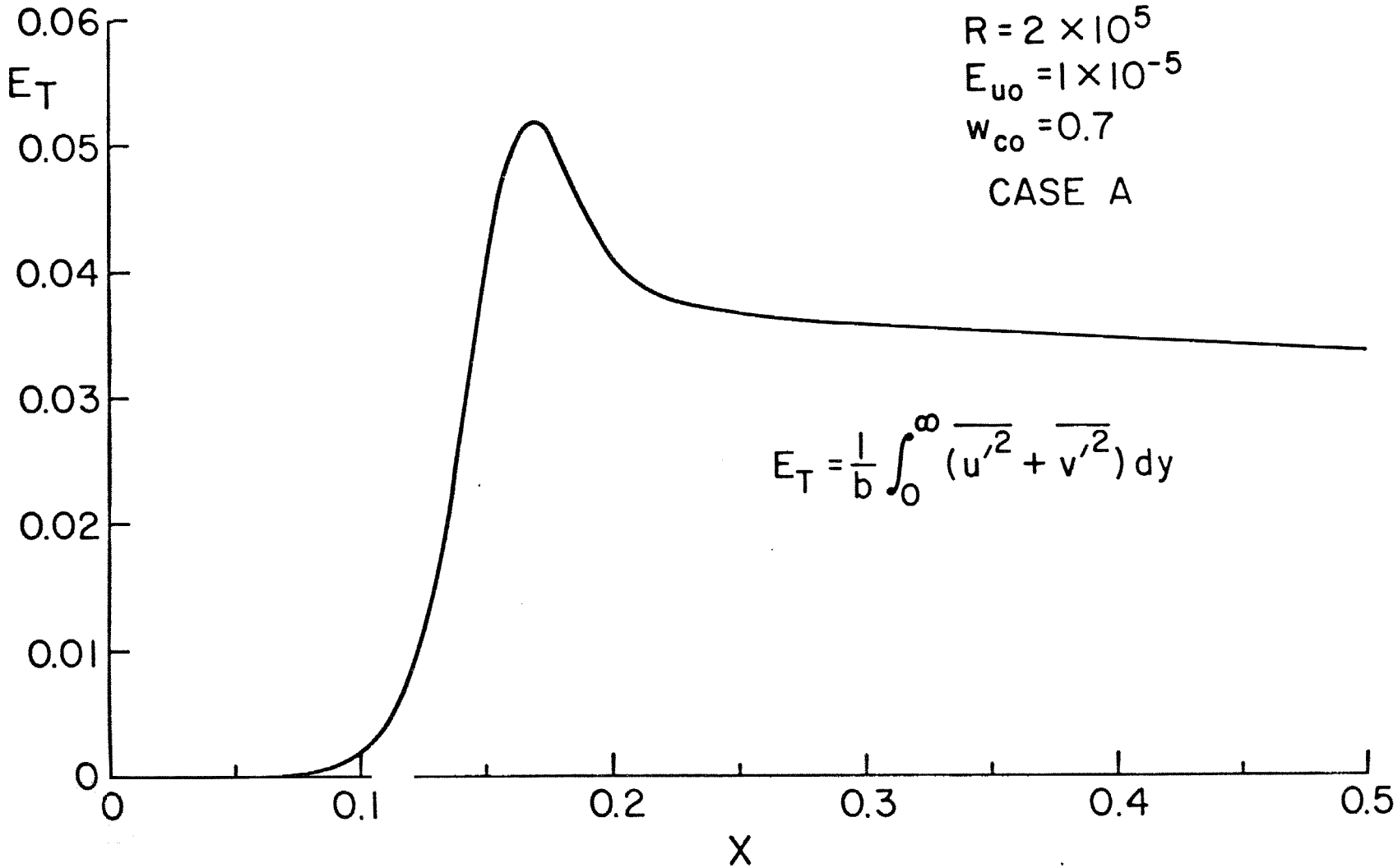

Fig. 7a Variation of the Total Integrated Fluctuation Energy Density E_T

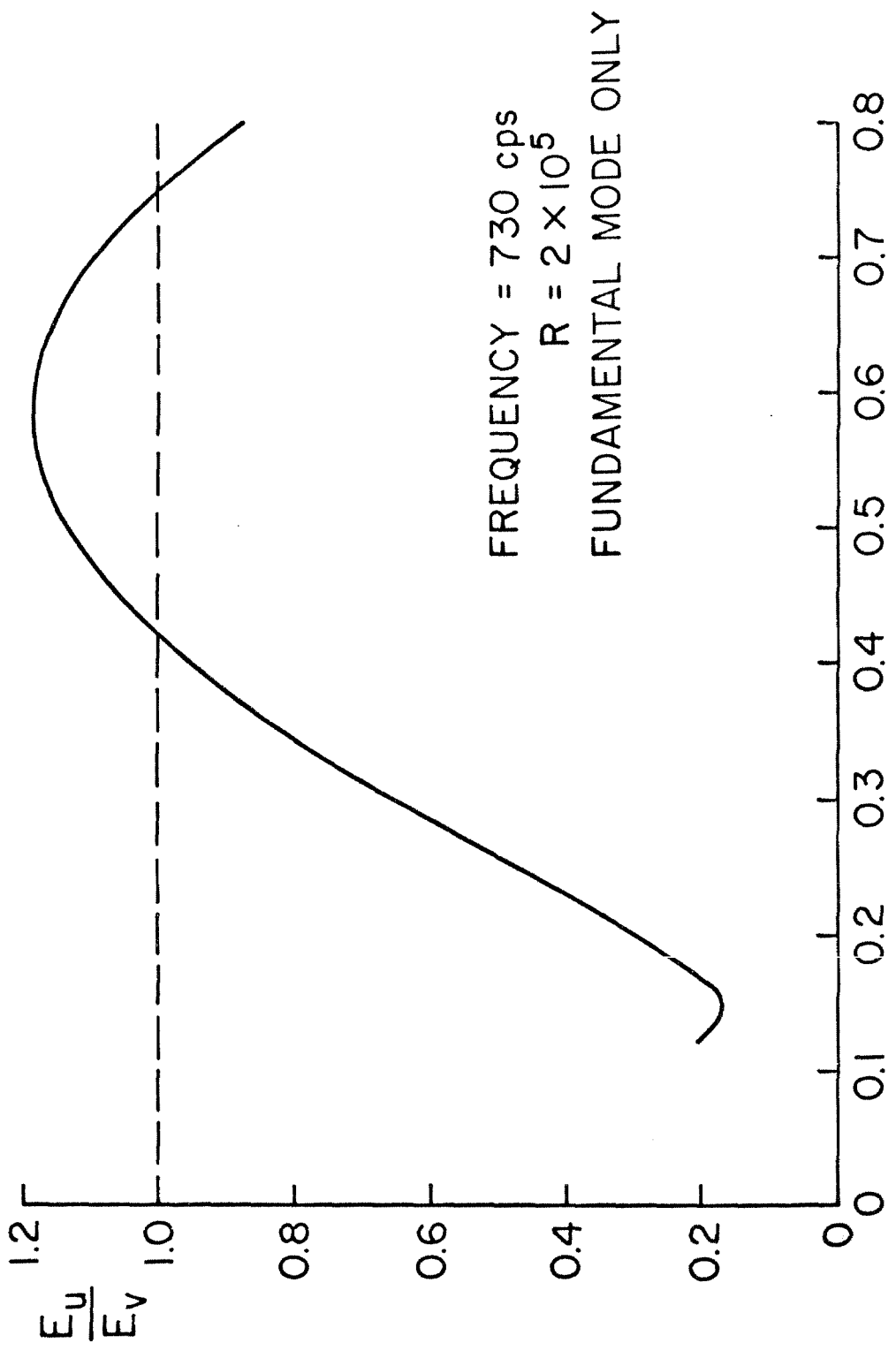

Fig. 8 Relative Energy Content in the u' and v' Components as Function of w_c

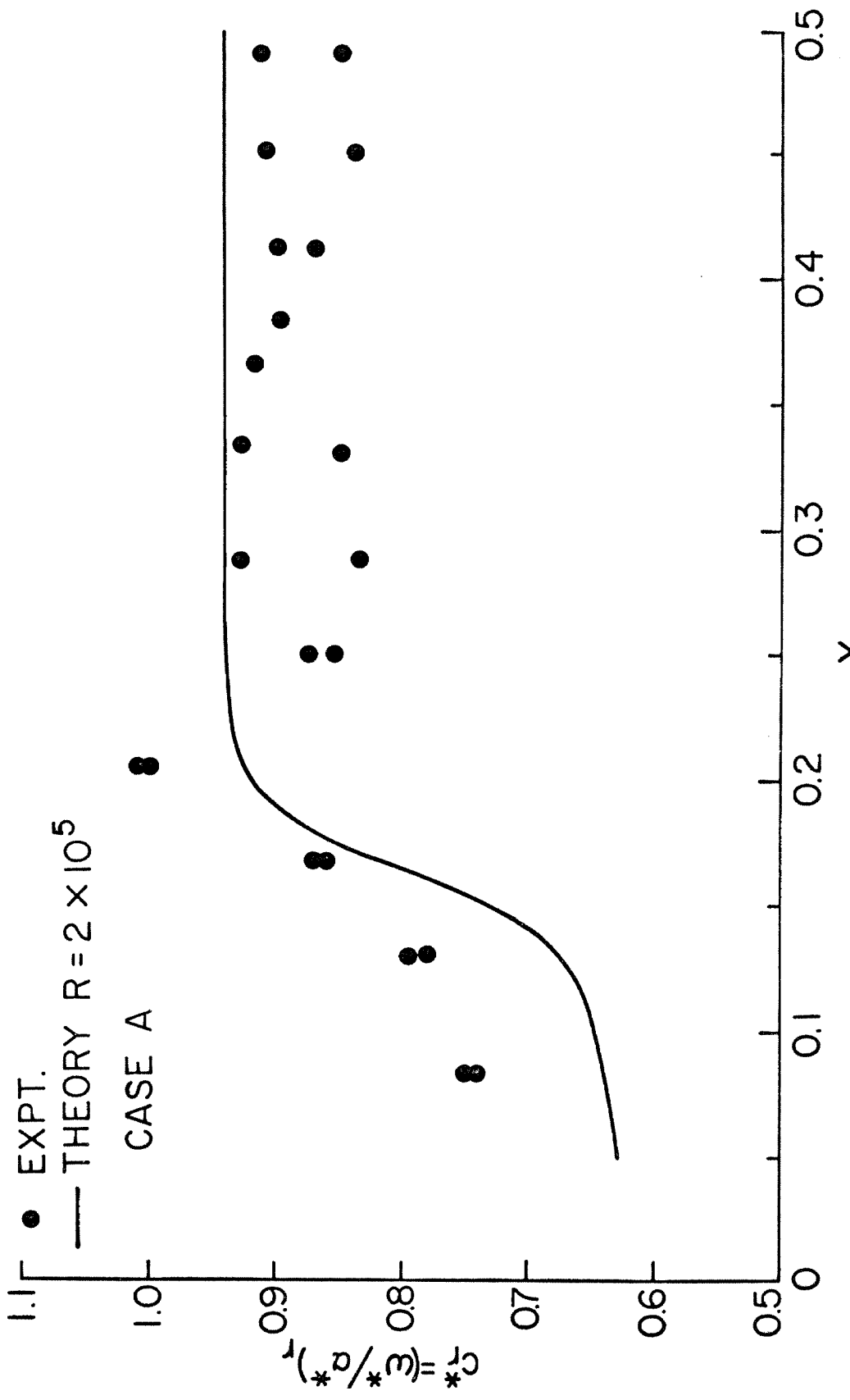

Fig. 9 Comparison of the Non-dimensional Wave Propagation Velocity c_r^*

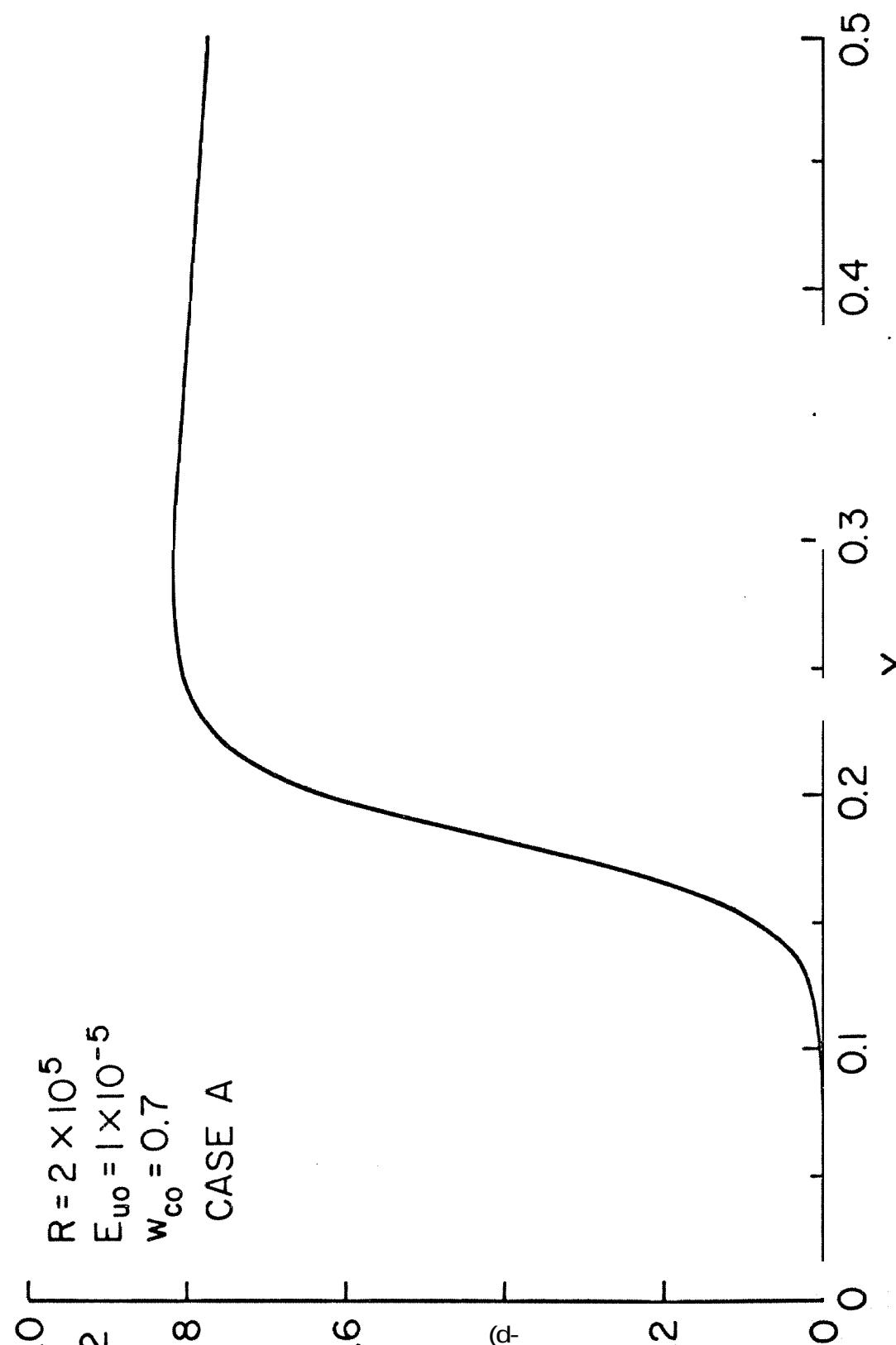

Fig. 10 Variation of the Normalized Amplitude $|A|^2$

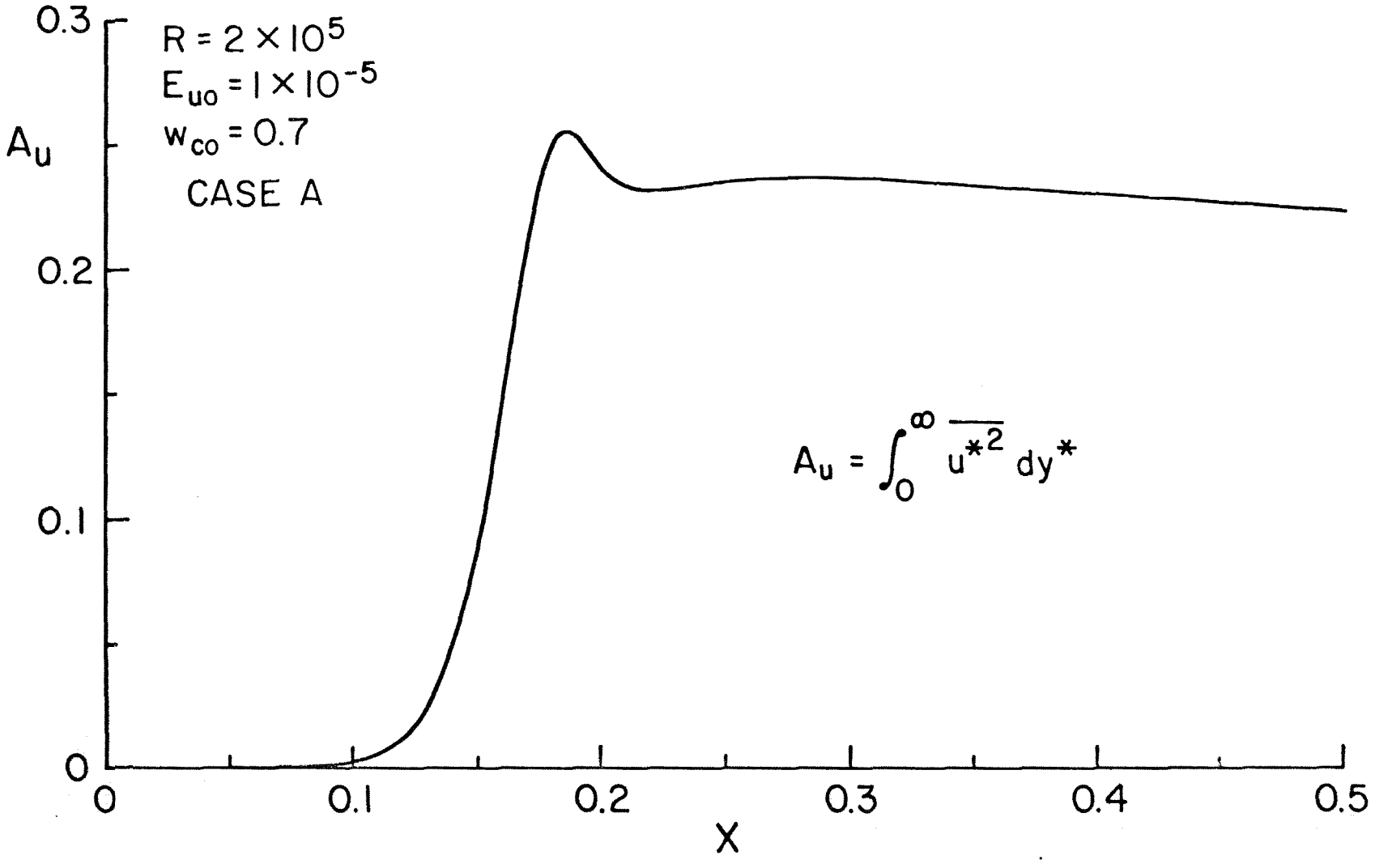

Fig. 11 Variation of the Normalized Integral Fluctuation Energy in the u'-component A_u

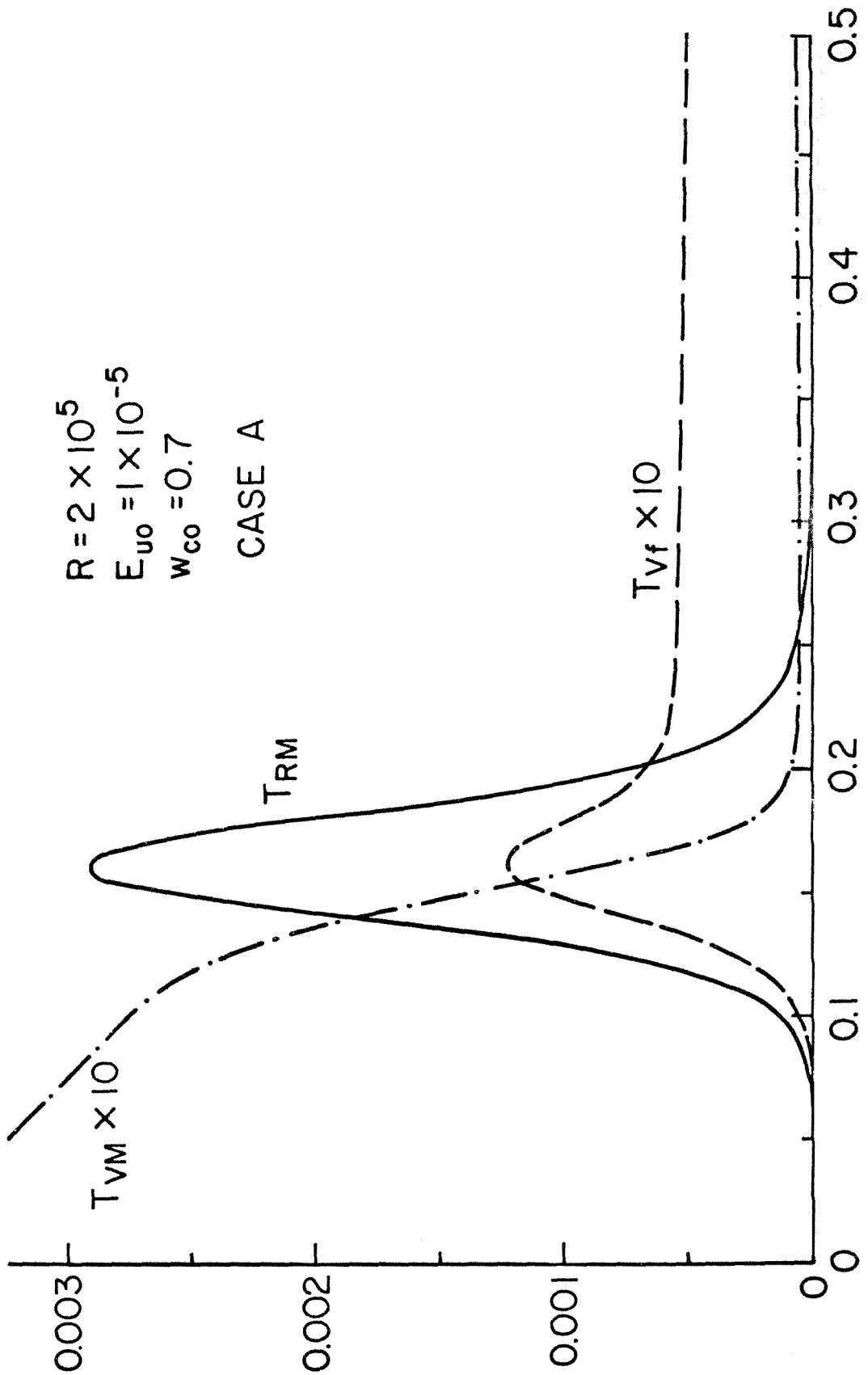

Fig. 12 Variation of the Magnitude of the Various Interacting Mechanisms

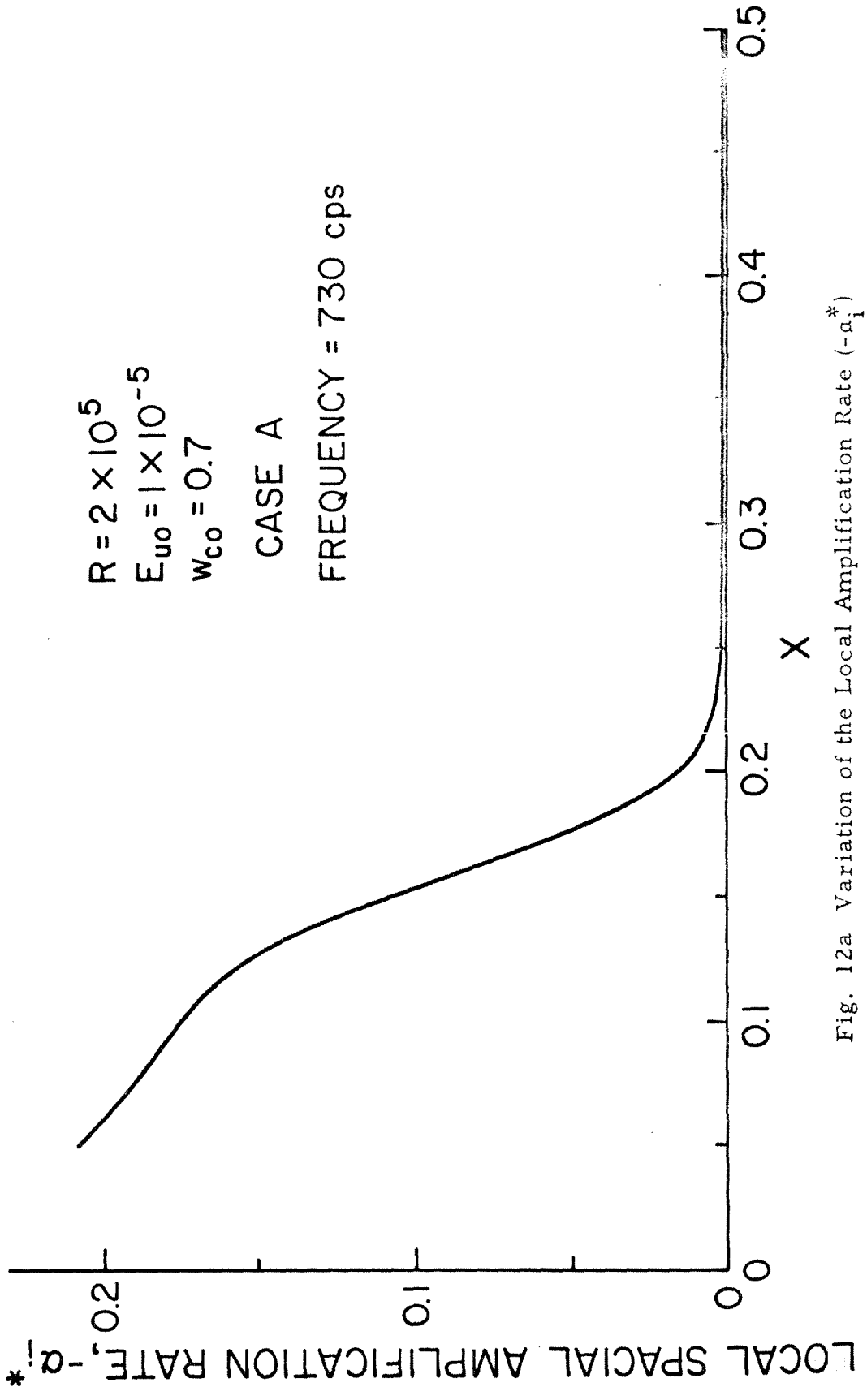

Fig. 12a Variation of the Local Amplification Rate ($-\alpha_i^*$)

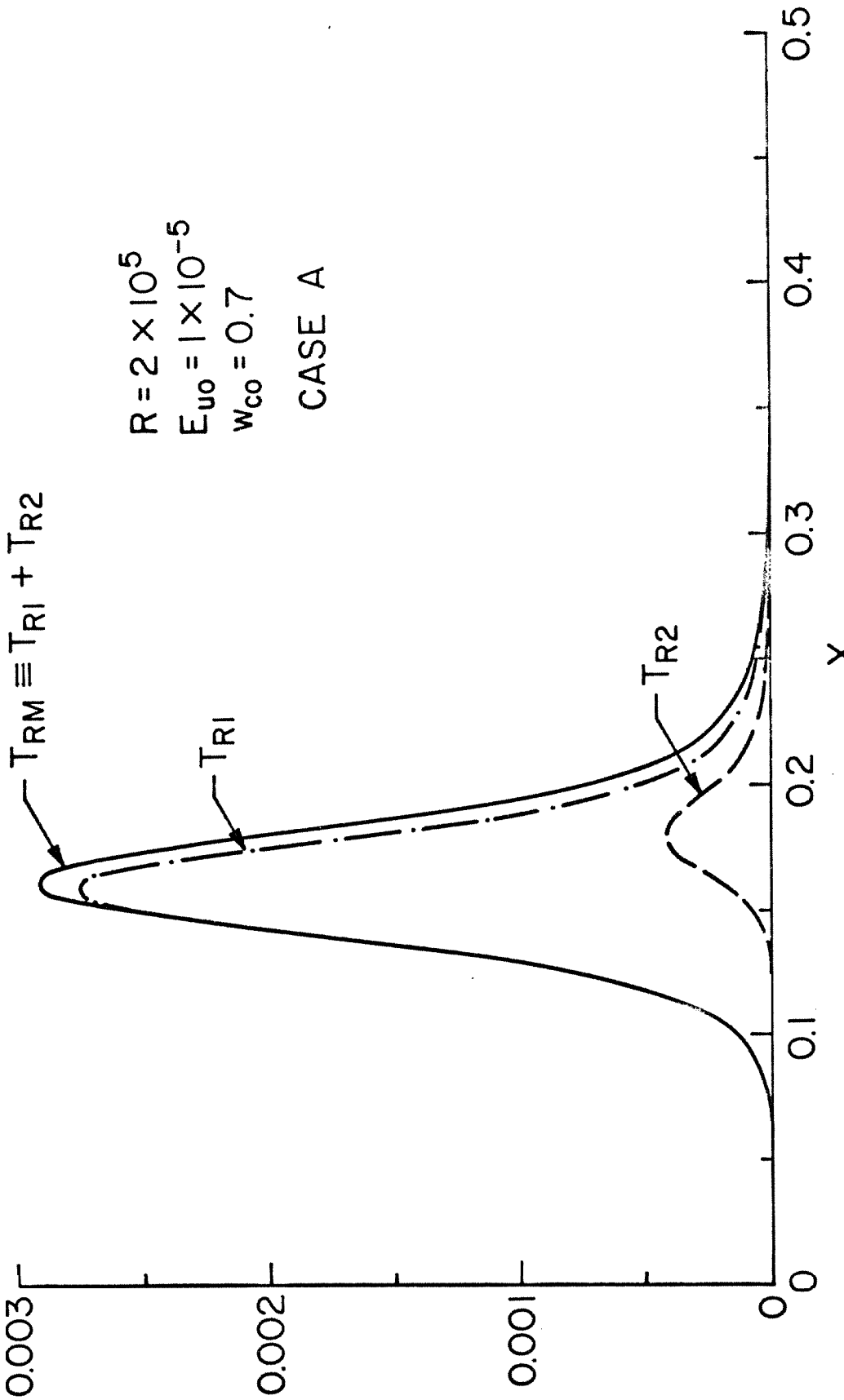

Fig. 13 Breakdown of the Energy Transferring Mechanism T_{RM}

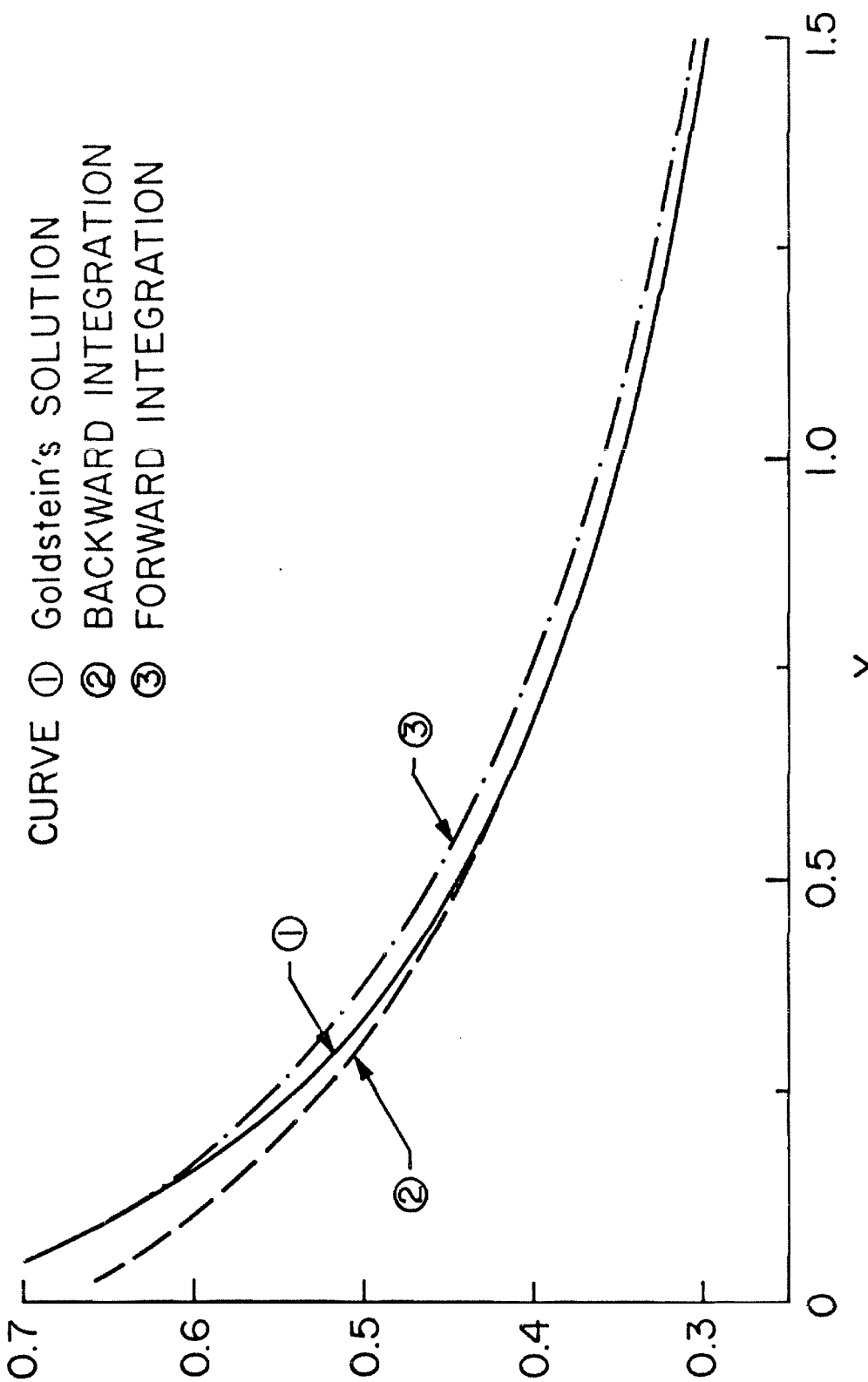

Fig. 14 Comparison of the Steady Laminar Wake Solutions

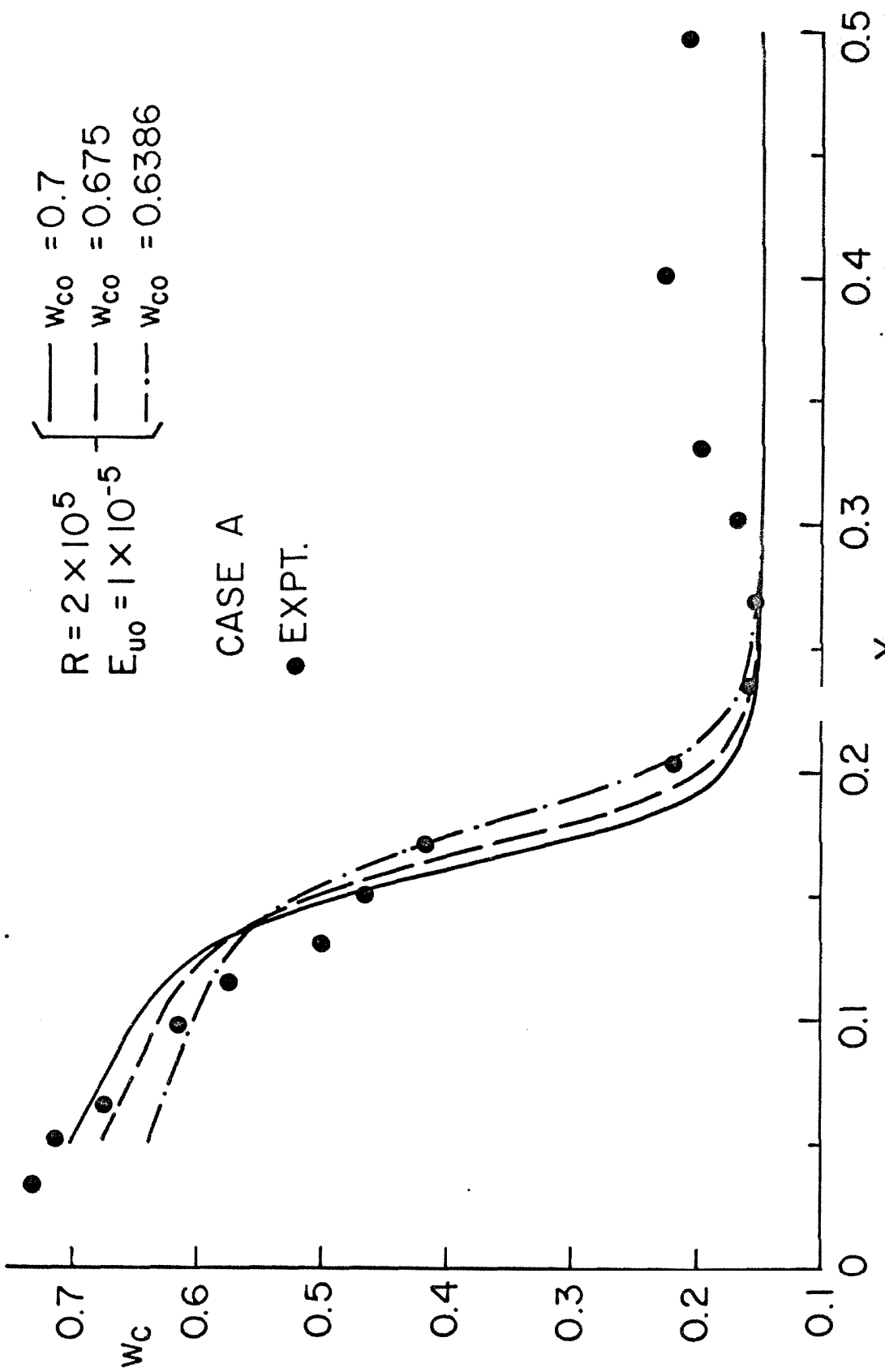

Fig. 15 Effect of w_{c0} on the Variation of w_c

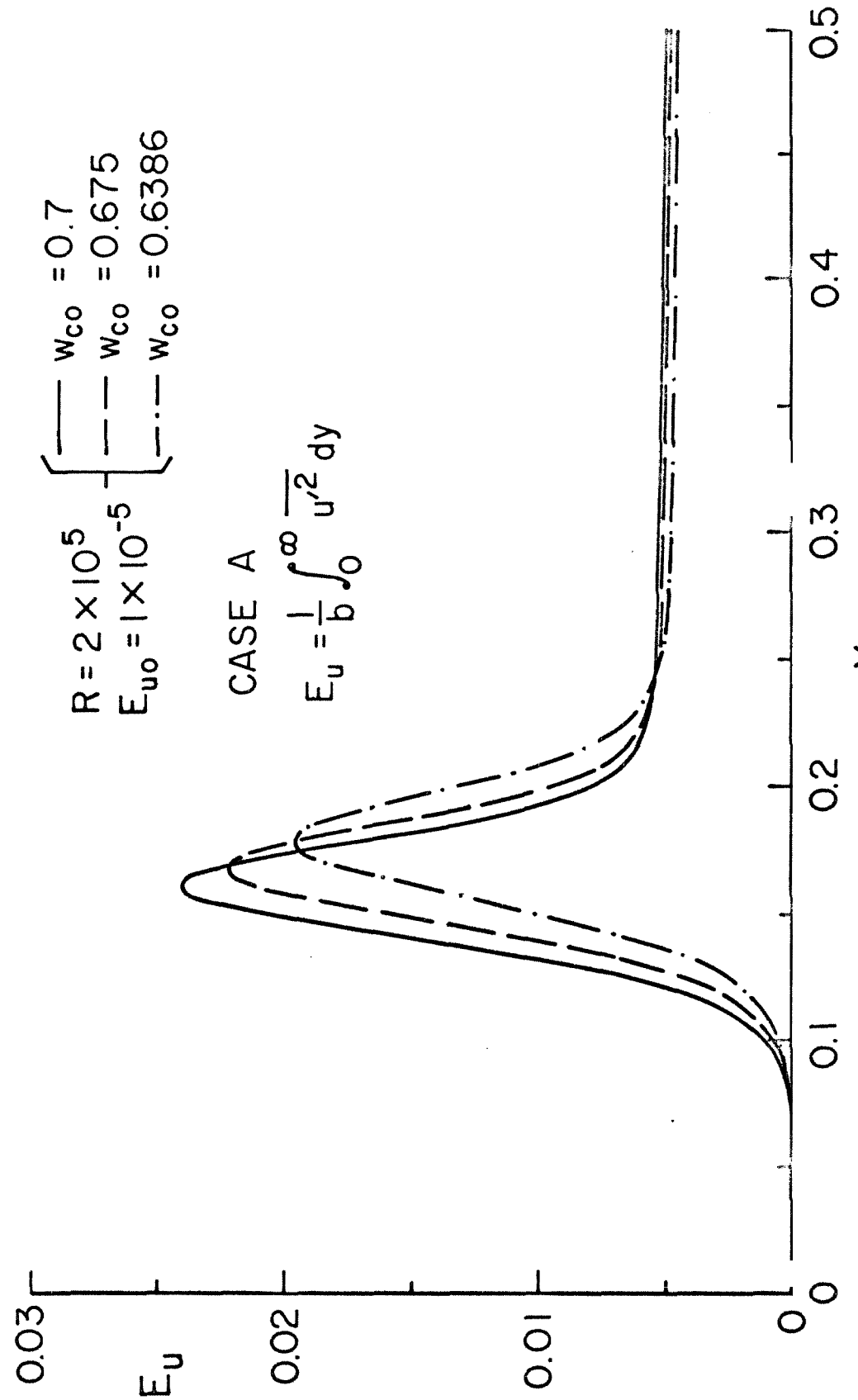

Fig. 16 Effect of w_{c0} on the Variation of E_u

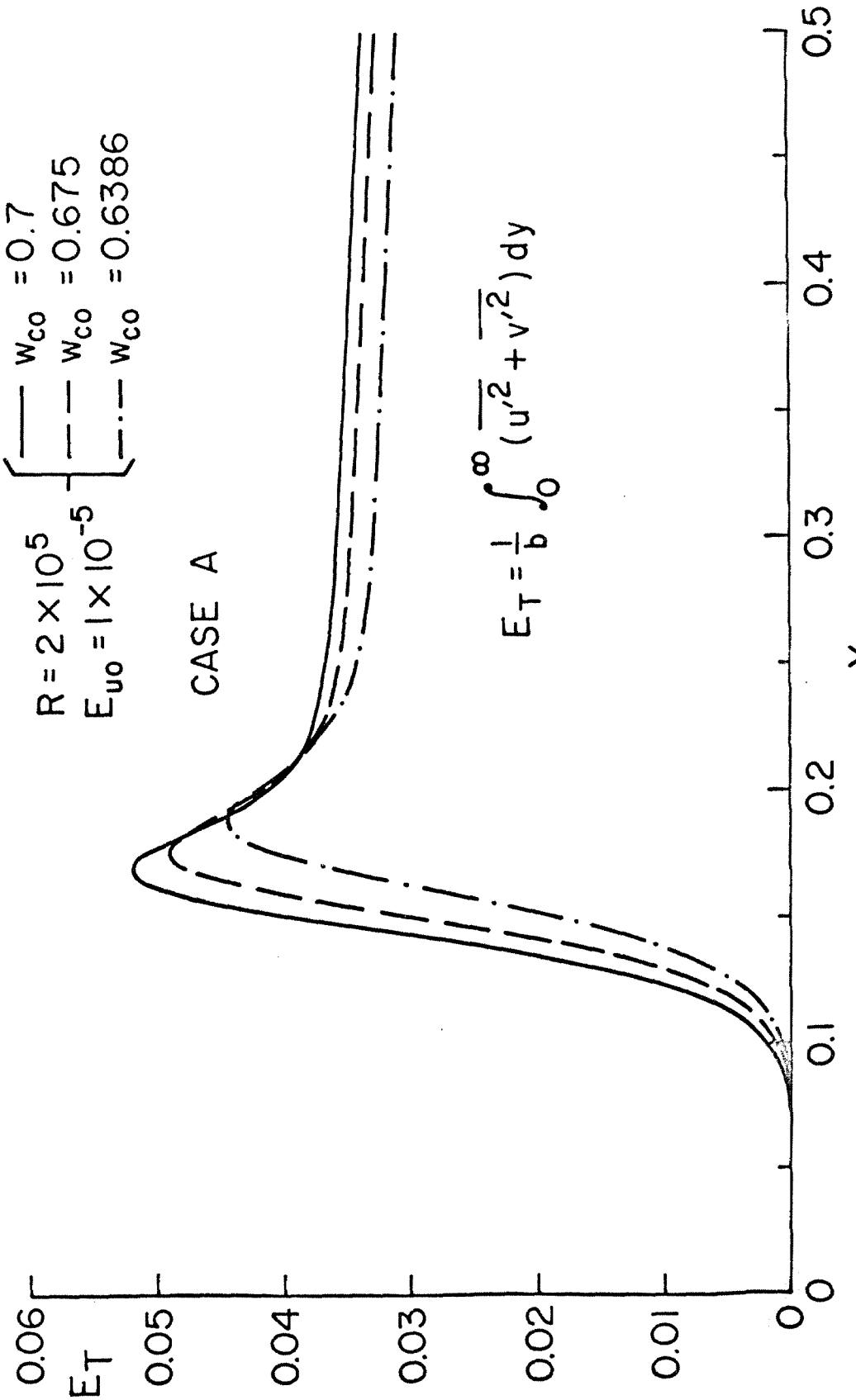

Fig. 17 Effect of w_{c0} on the Variation of E_T

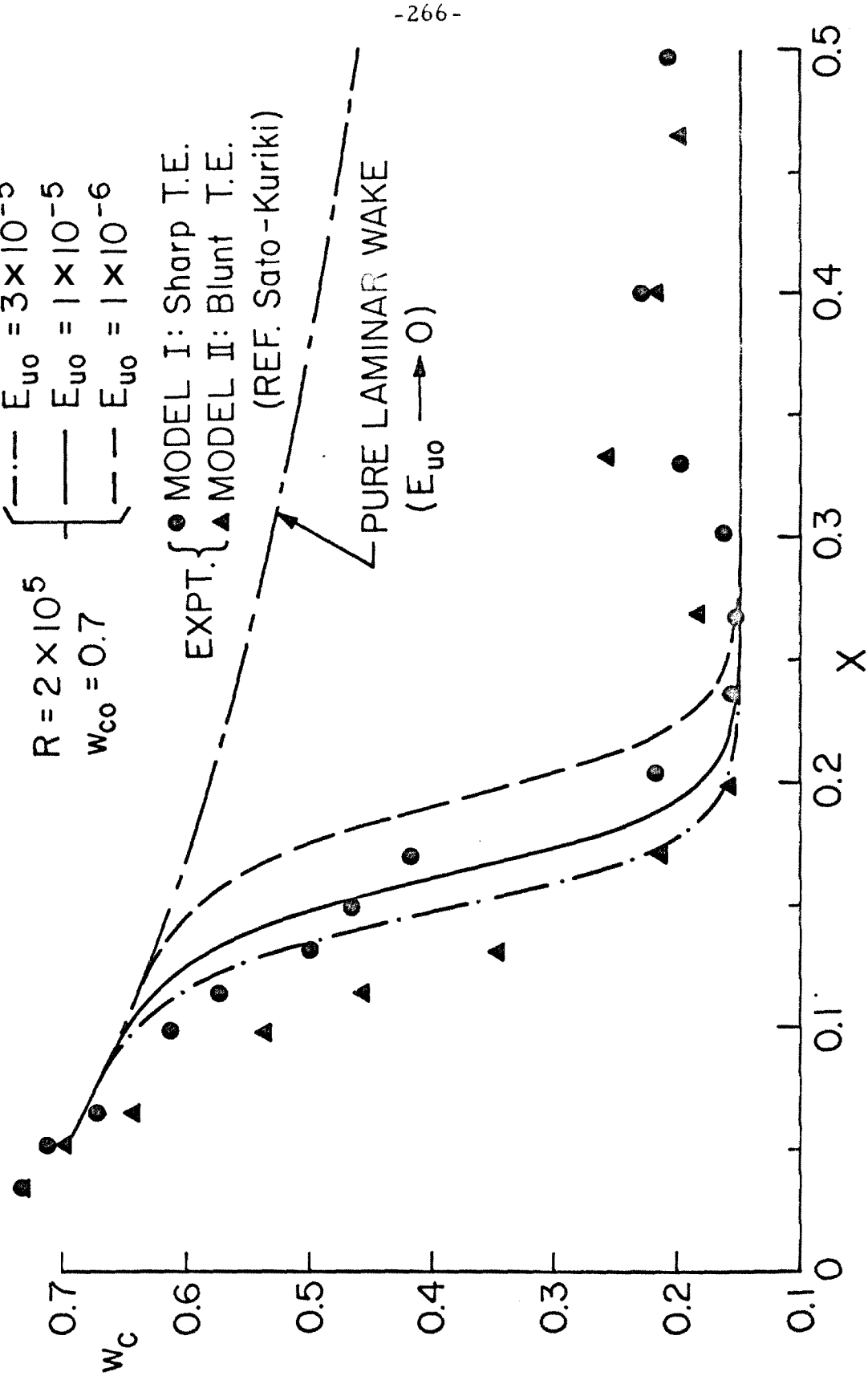

Fig. 18 Effect of E_{u0} on the Variation of w_c

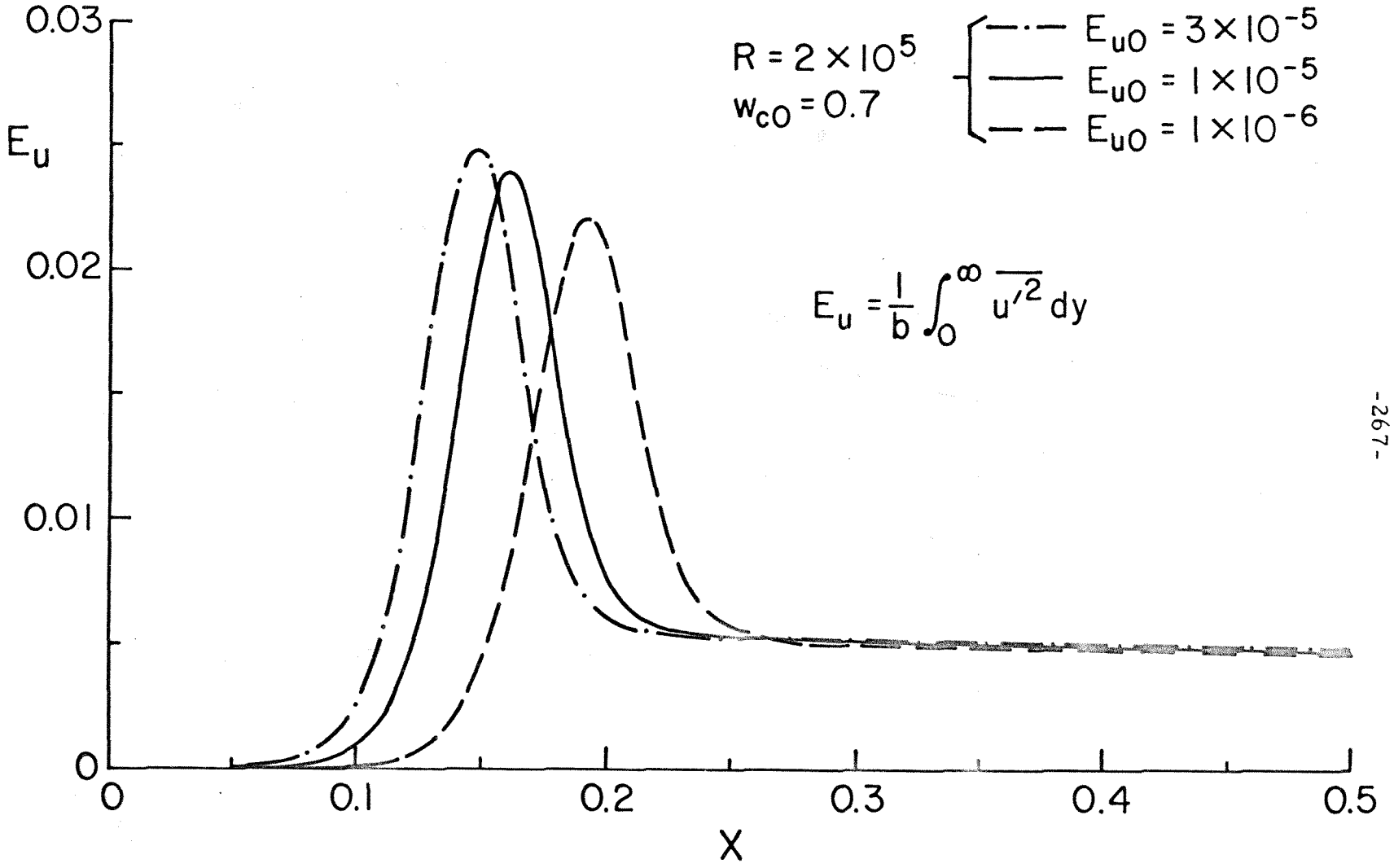

Fig. 19 Effect of E_{u0} on the Variation of E_u

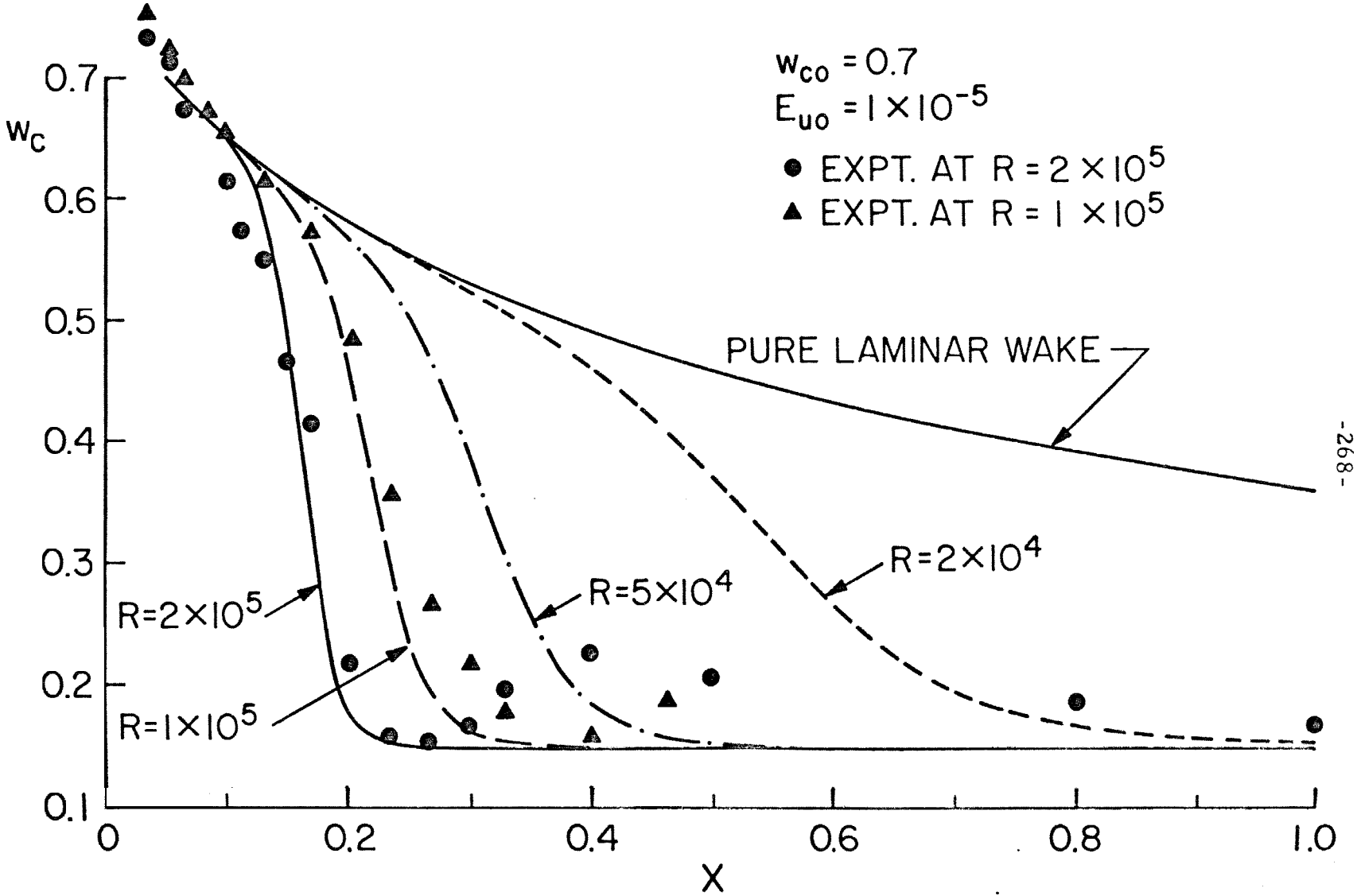

Fig. 20 Reynolds Number Effect on w_c (Case A) and Comparison with the Experiments

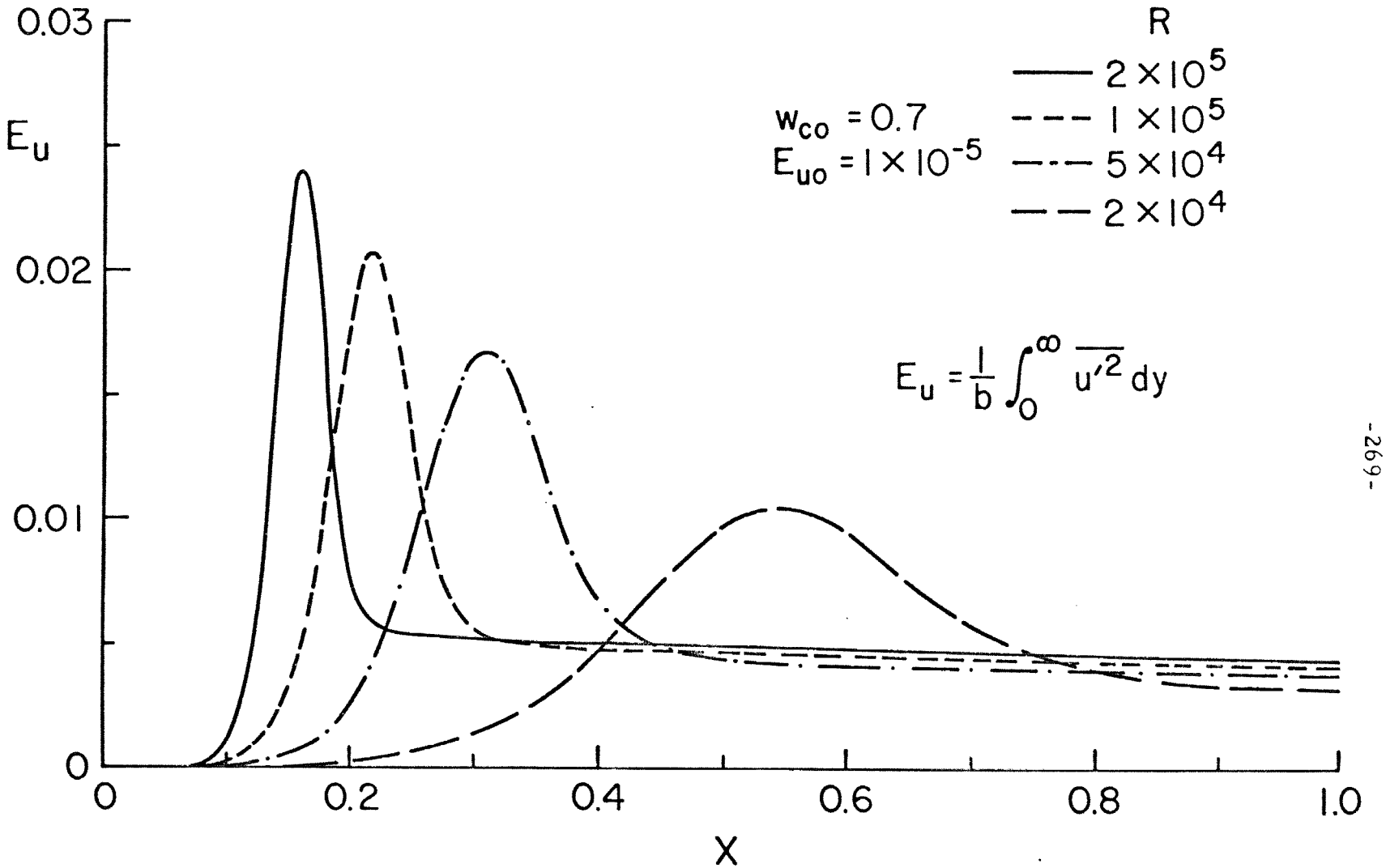

Fig. 21 Reynolds Number Effect on E_u; Case A.

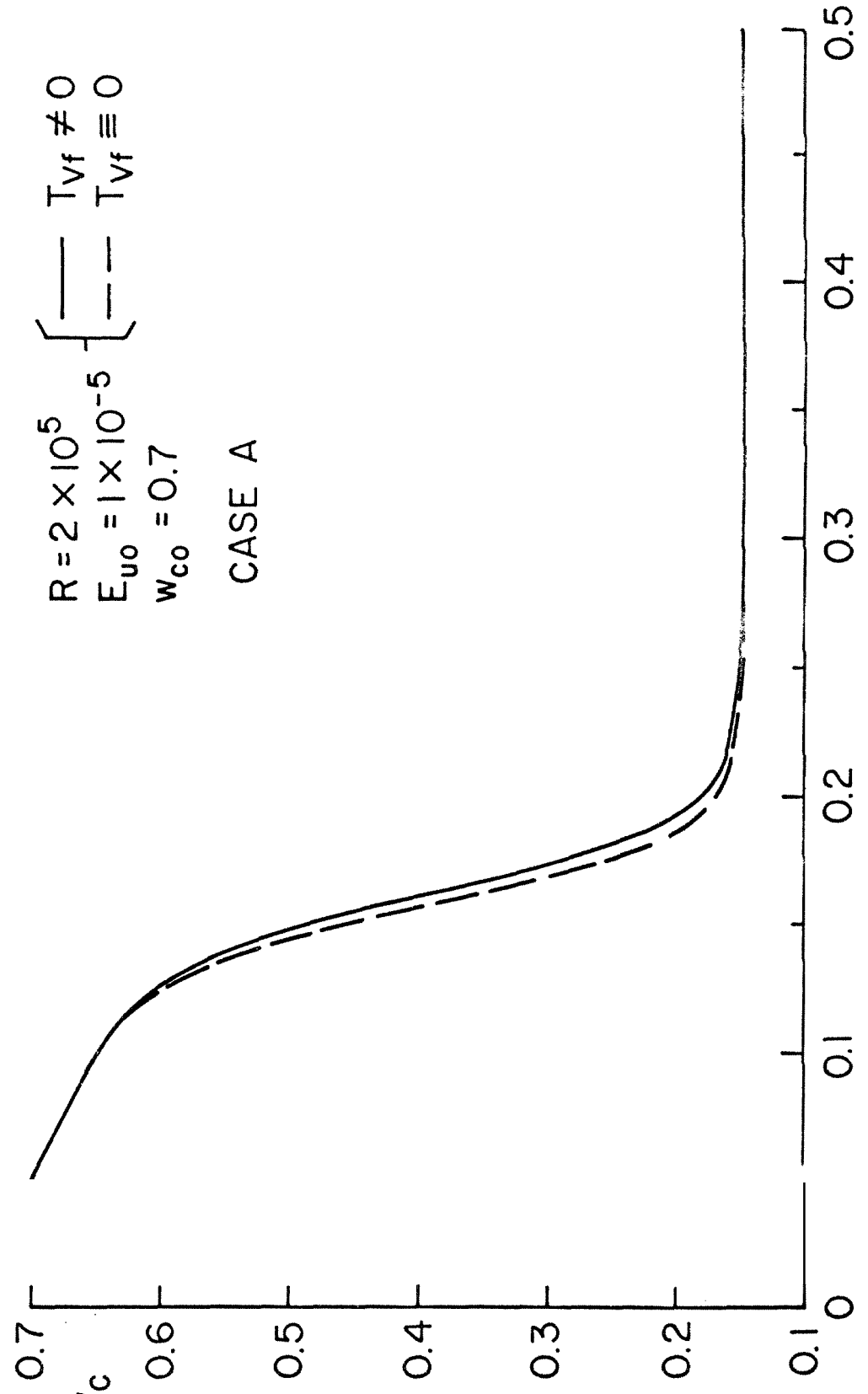

Fig. 22 Effect of the Viscous Dissipation Term T_{vf} on w_c; Case A

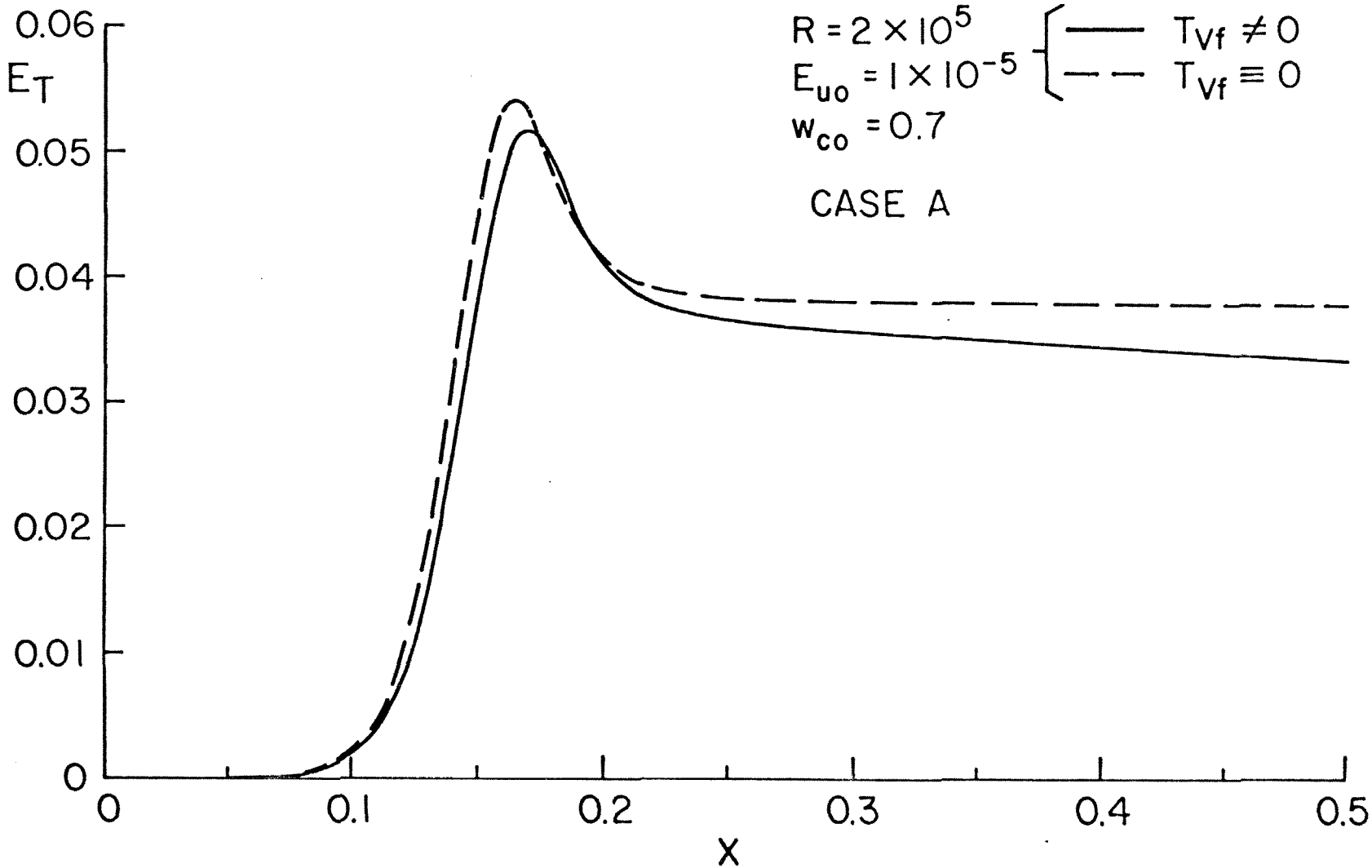

Fig. 23 Effect of the Viscous Dissipation Term T_{vf} on E_T; Case A

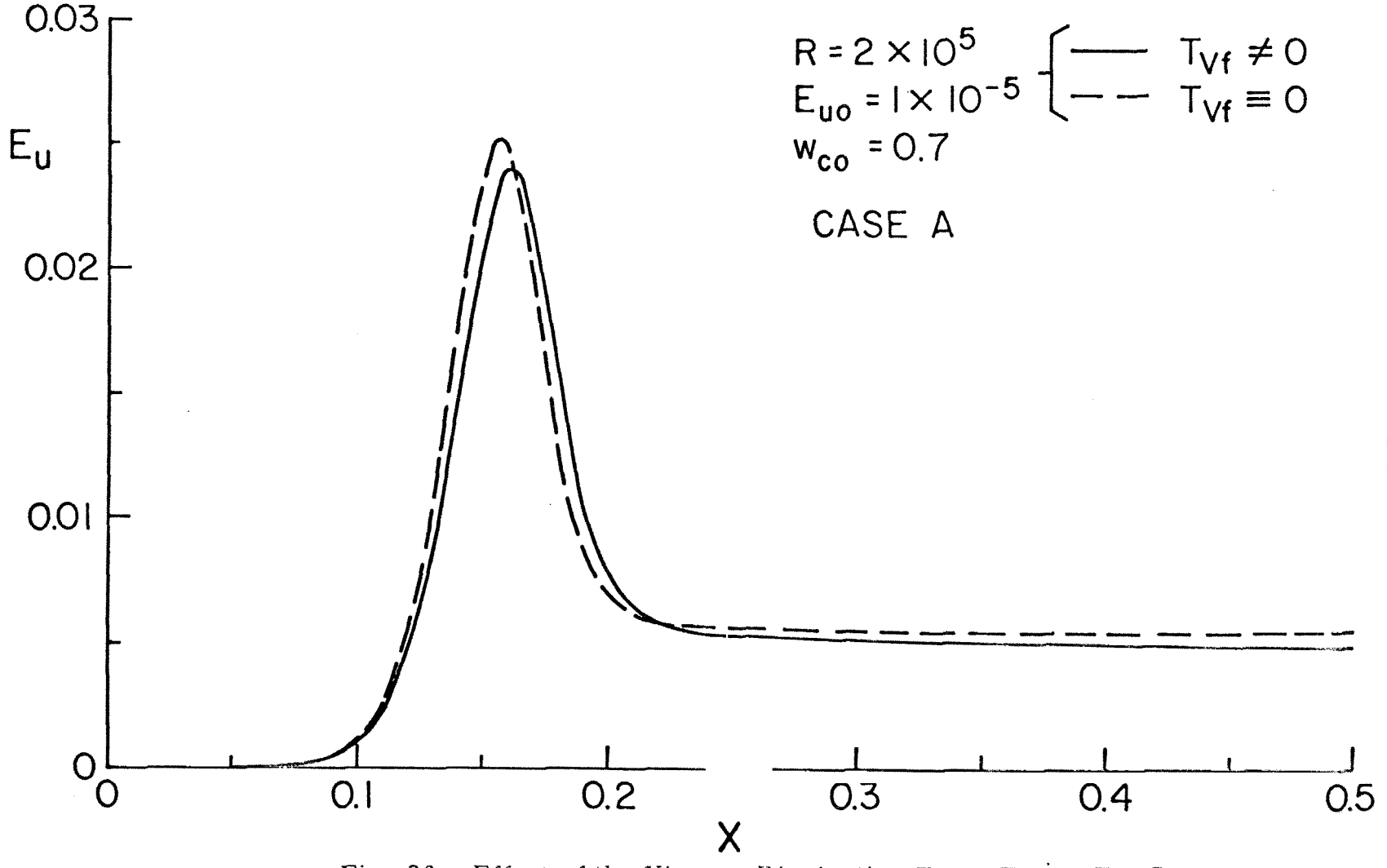

Fig. 23a Effect of the Viscous Dissipation Term T_{vf} on E_u; Case A

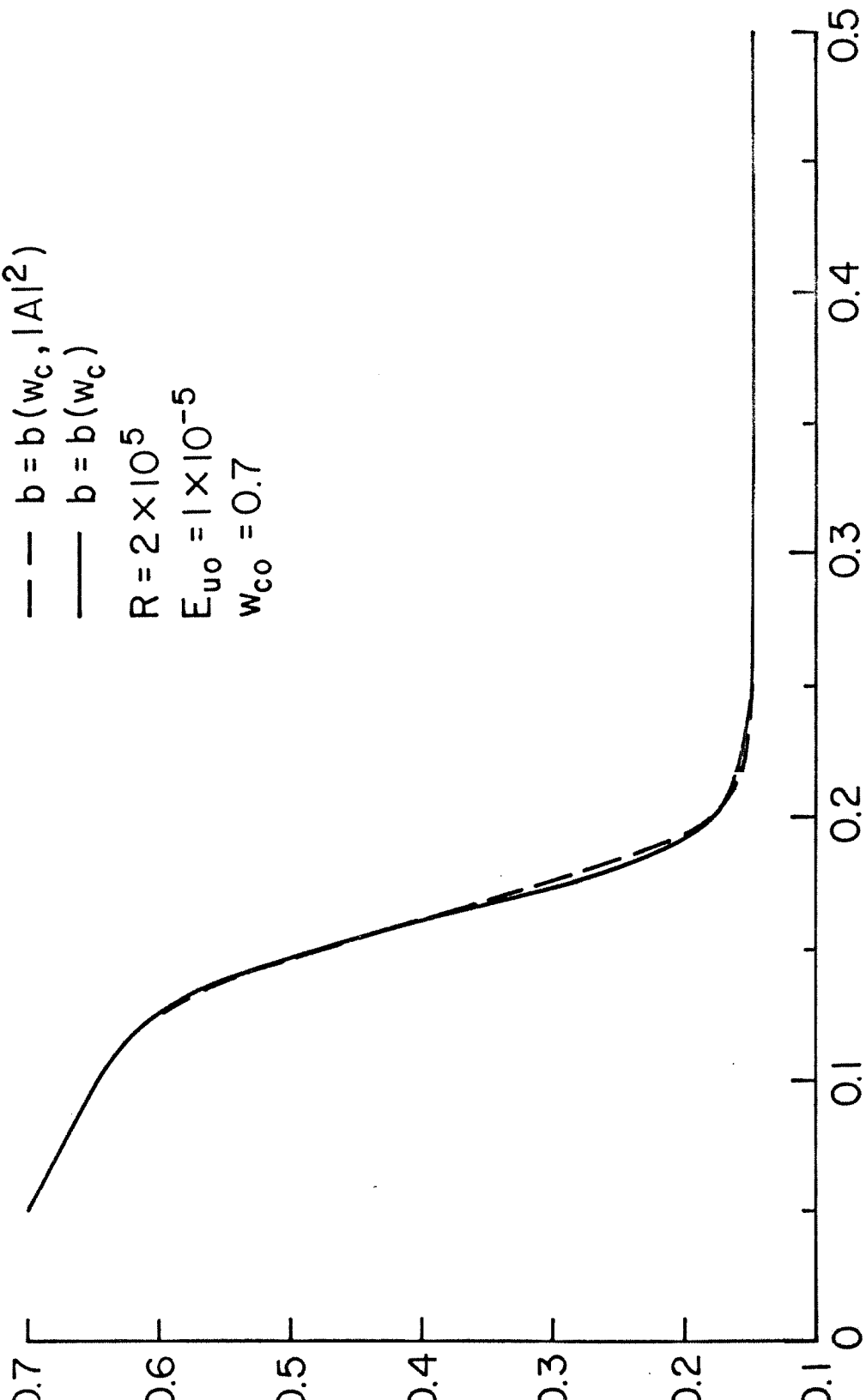

Fig. 24 Effect of Decoupling b from w_c on the Variation of w_c; Case A

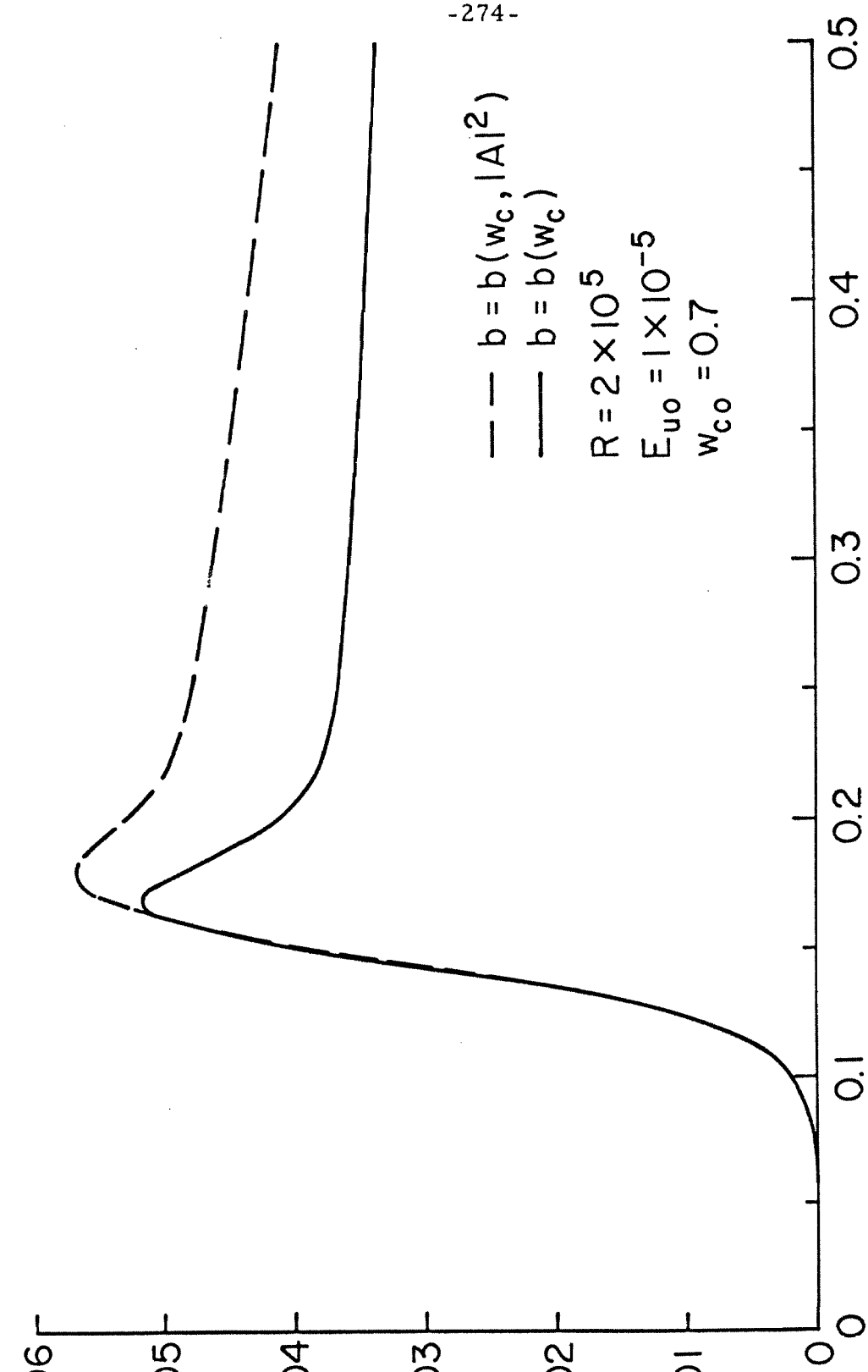

Fig. 25 Effect of Decoupling b from w_c on the Variation of E_T; Case A

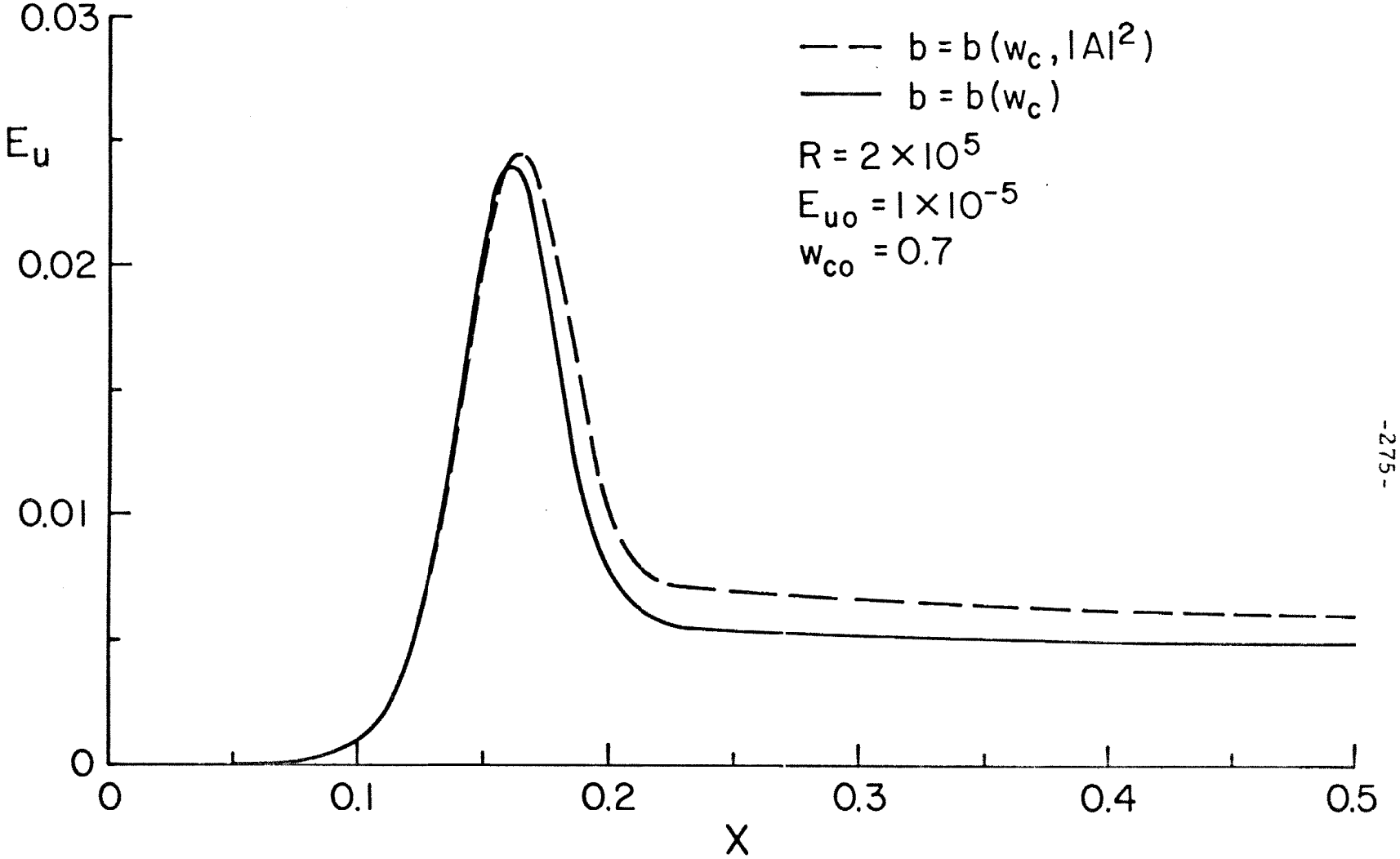

Fig. 25a Effect of Decoupling b from w_c on the Variation of E_u; Case A

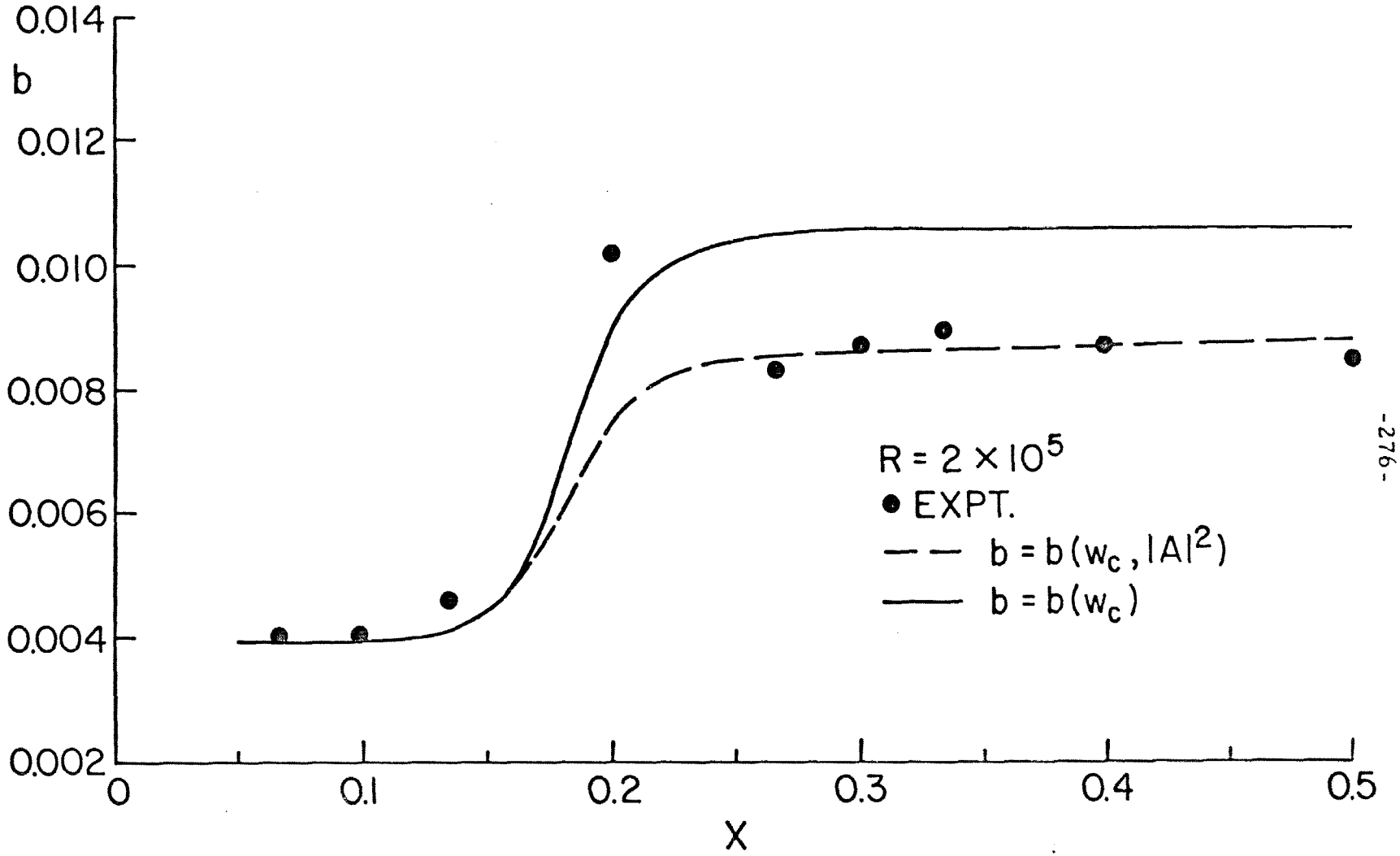

Fig. 26 Comparison of Wake Half-width for $b = b(w_c)$ and $b = b(w_c, |A|^2)$

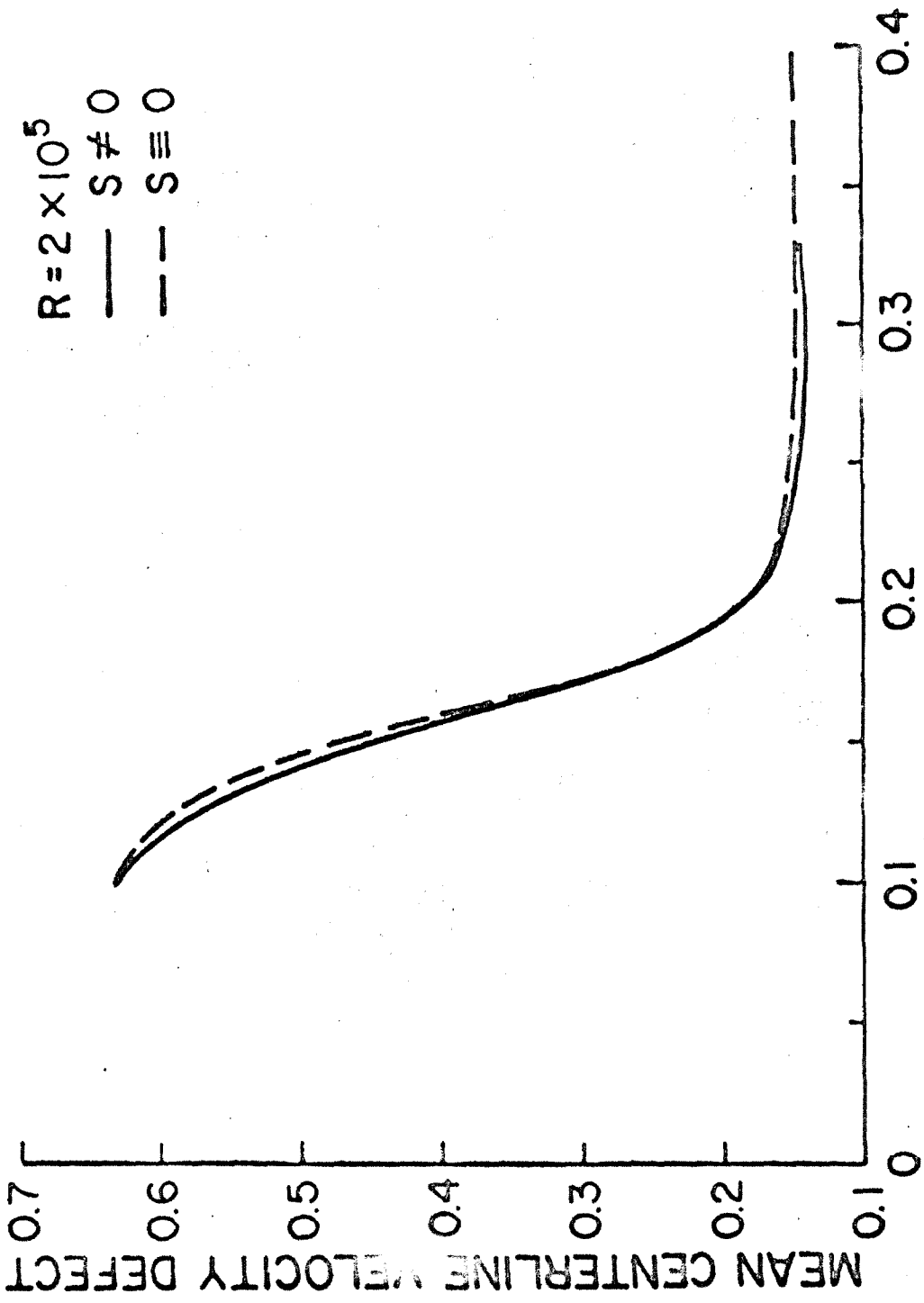

Fig. 27. Effect of the Additional Shape Parameter on the Mean Centerline Velocity Defect

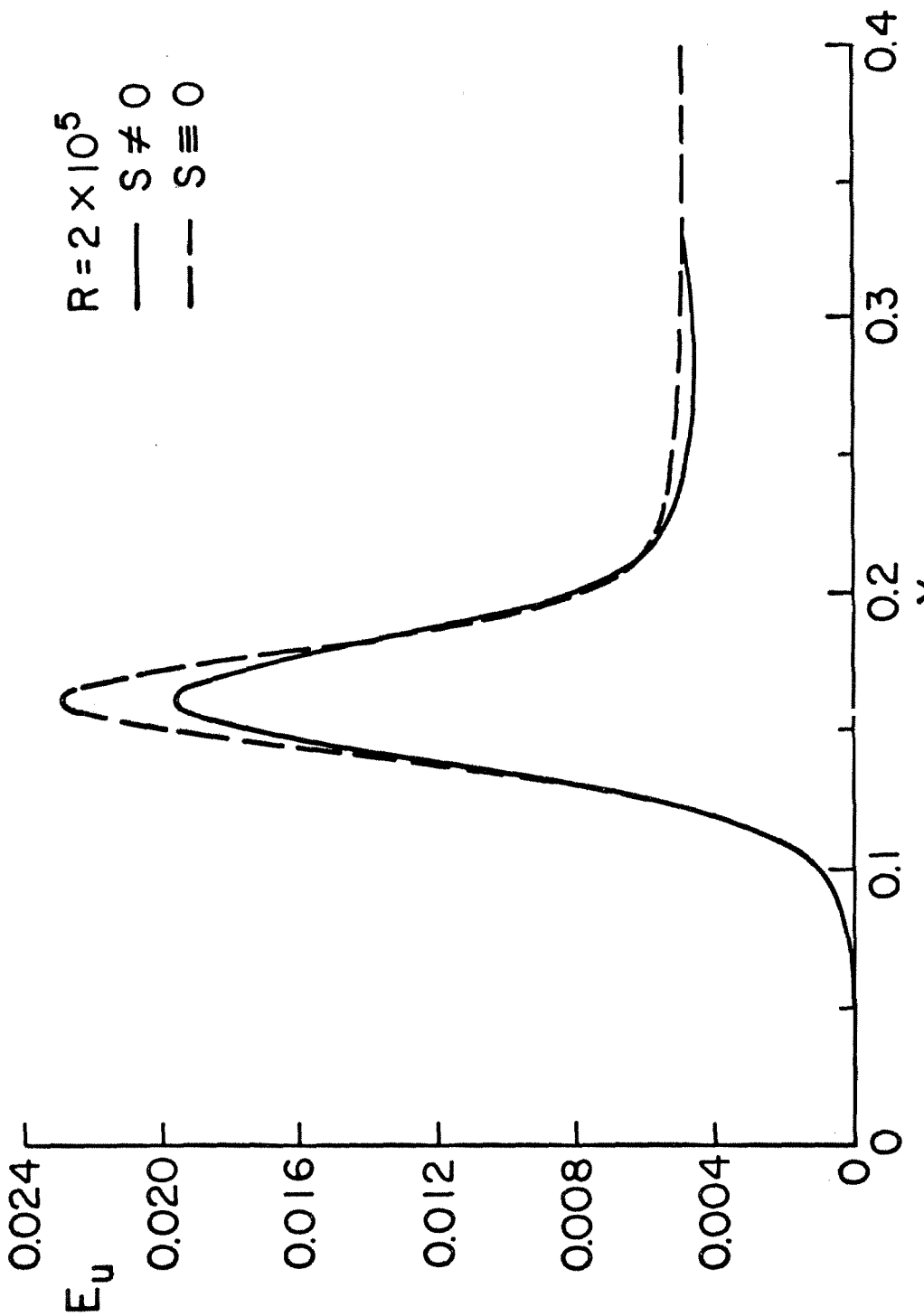

Fig. 28 Effect of the Additional Shape Parameter on E_u

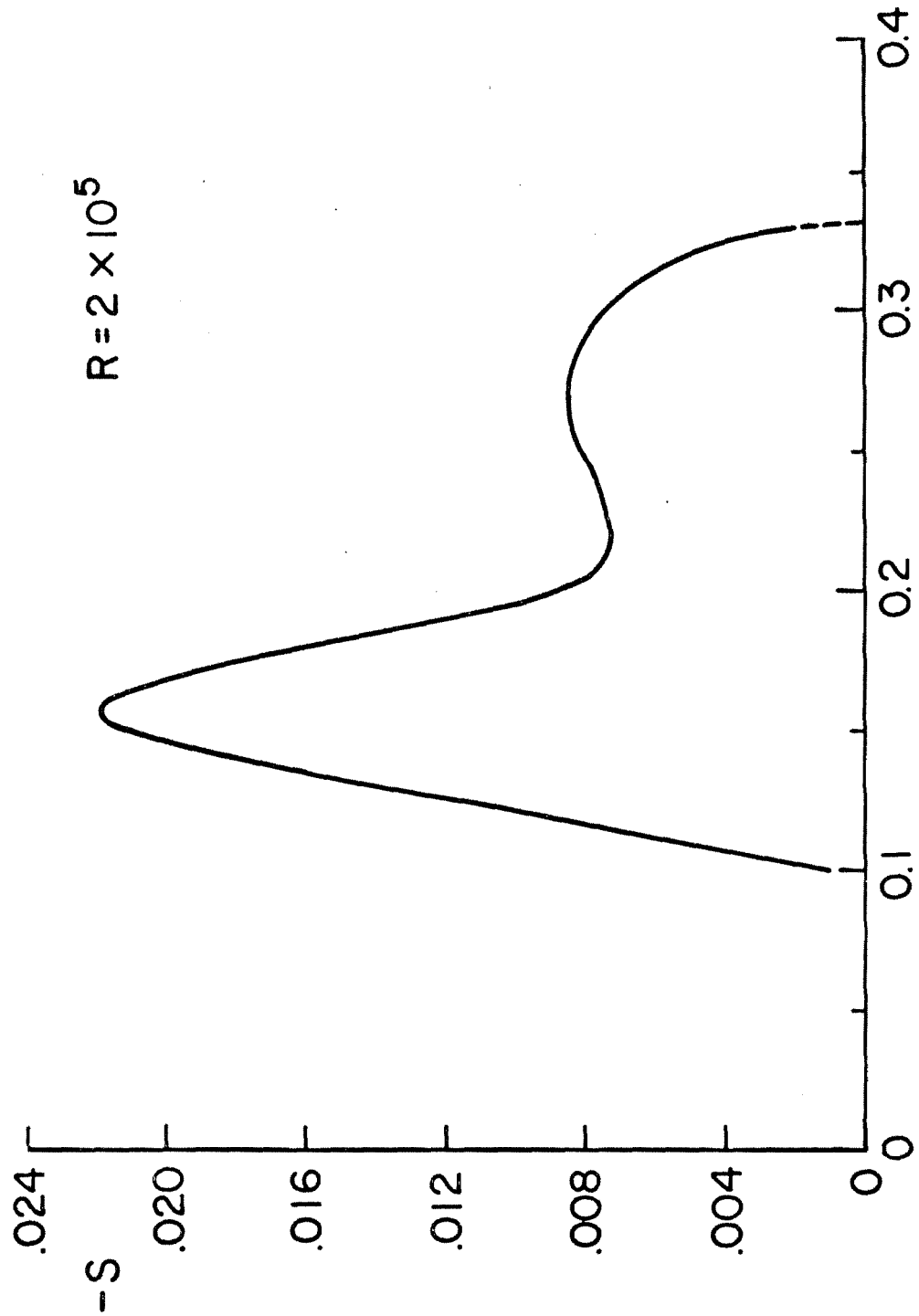

Fig. 29 Variation of the Additional Shape Parameter S(x)

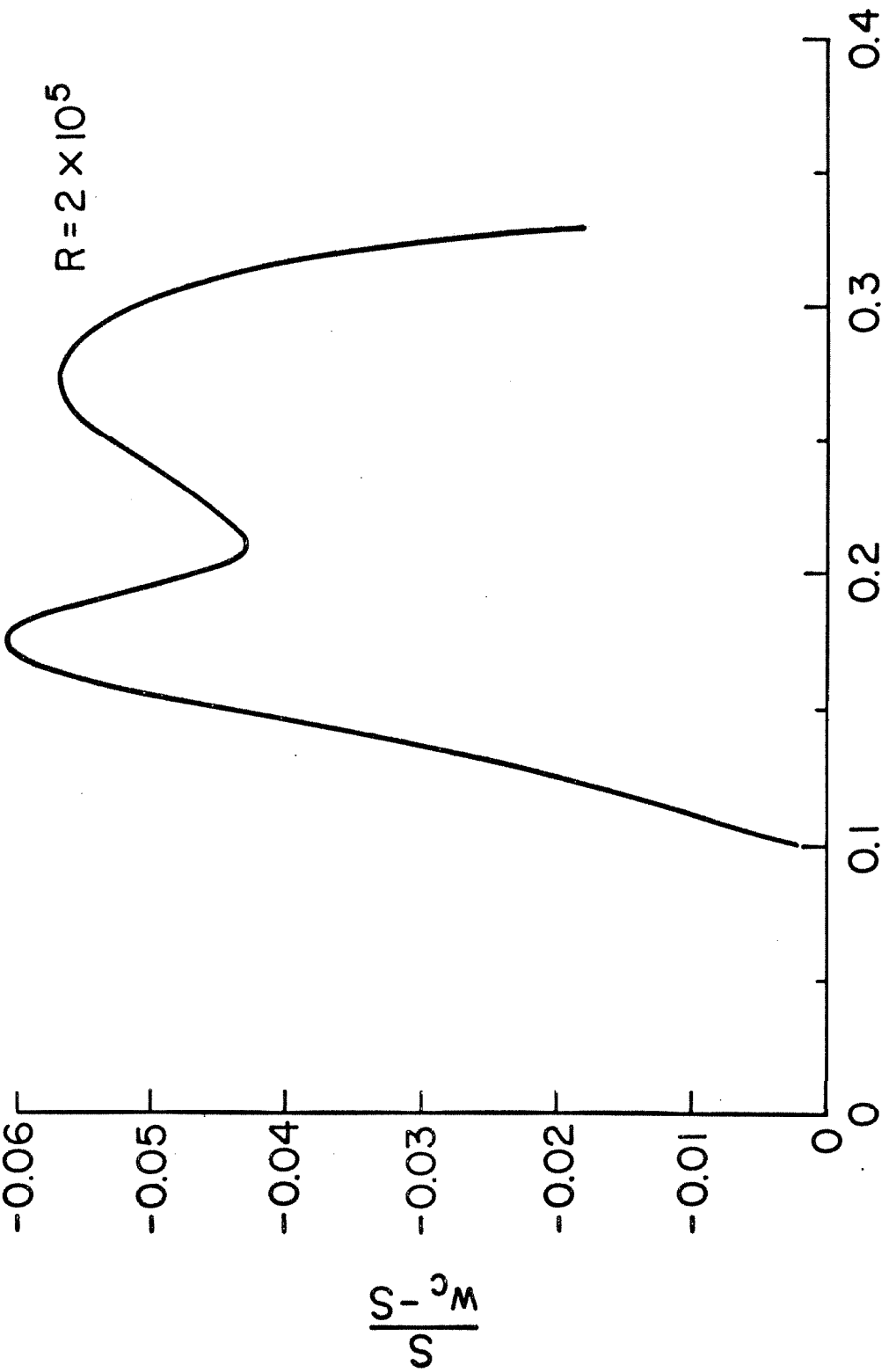

Fig. 30 Variation of $\left(\frac{S}{w_c - S}\right)$

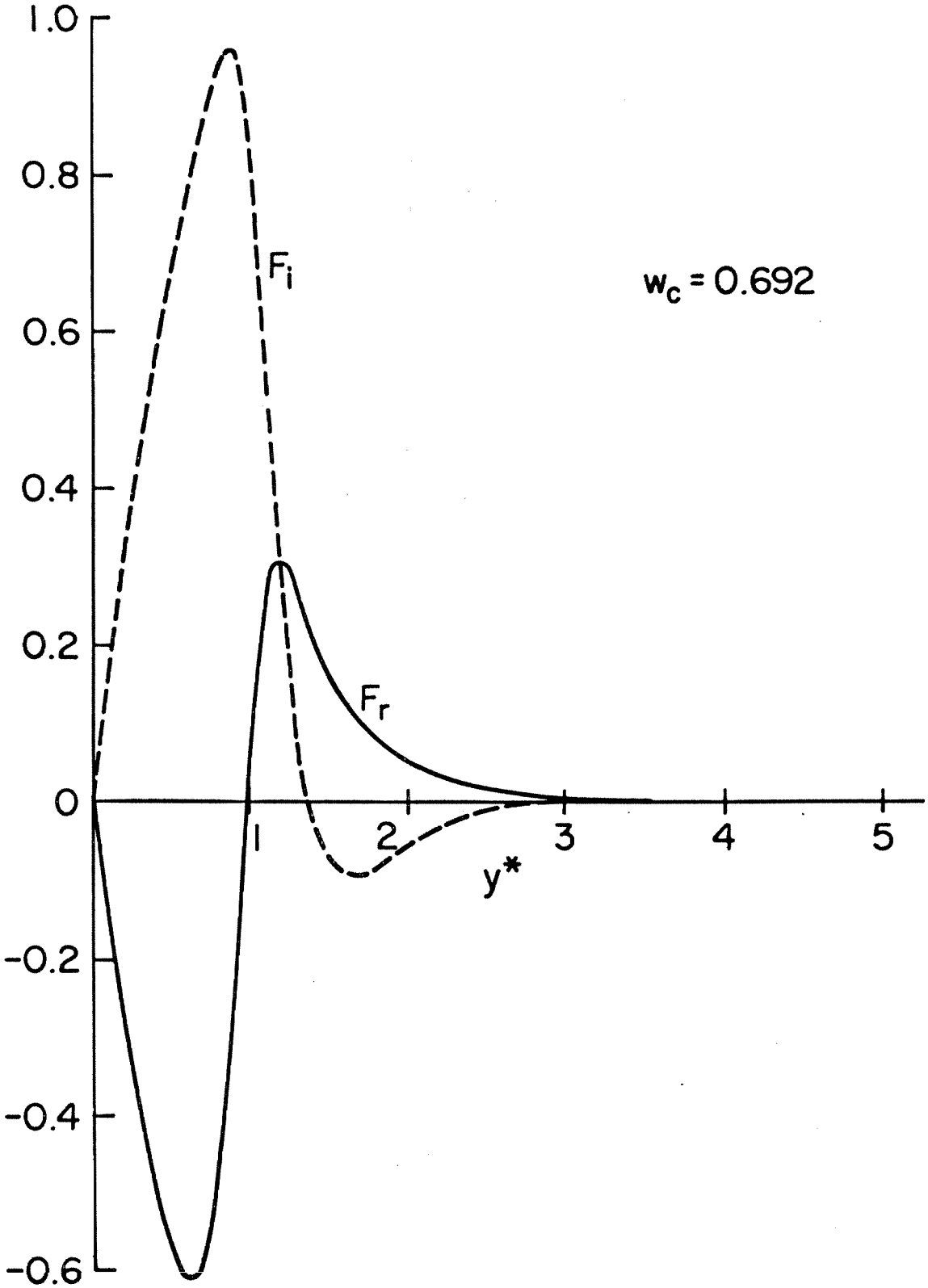

Fig. 31a Distribution of F(y*) at w_c = 0. *692*

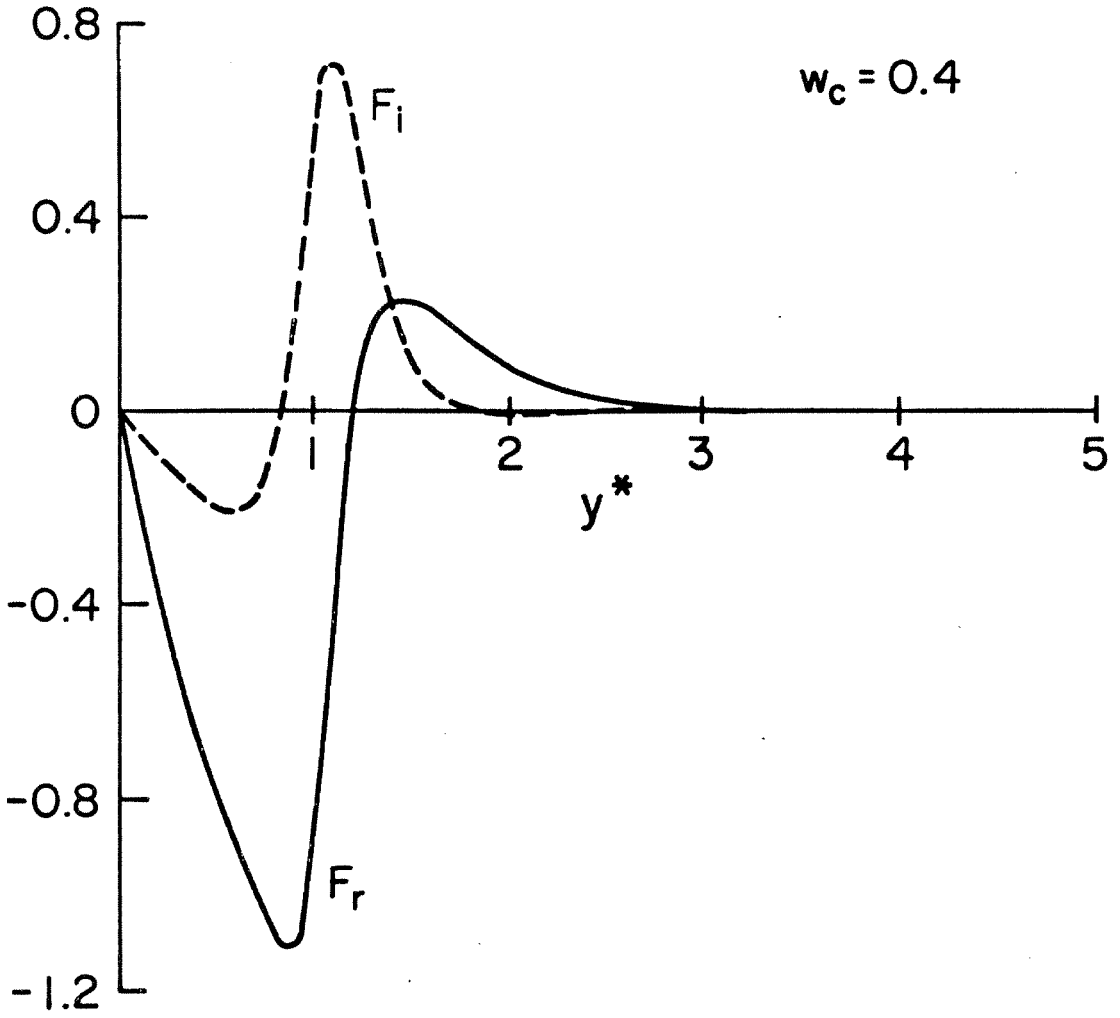

Fig. 31b Distribution of F(y*) at w_c = 0. 40

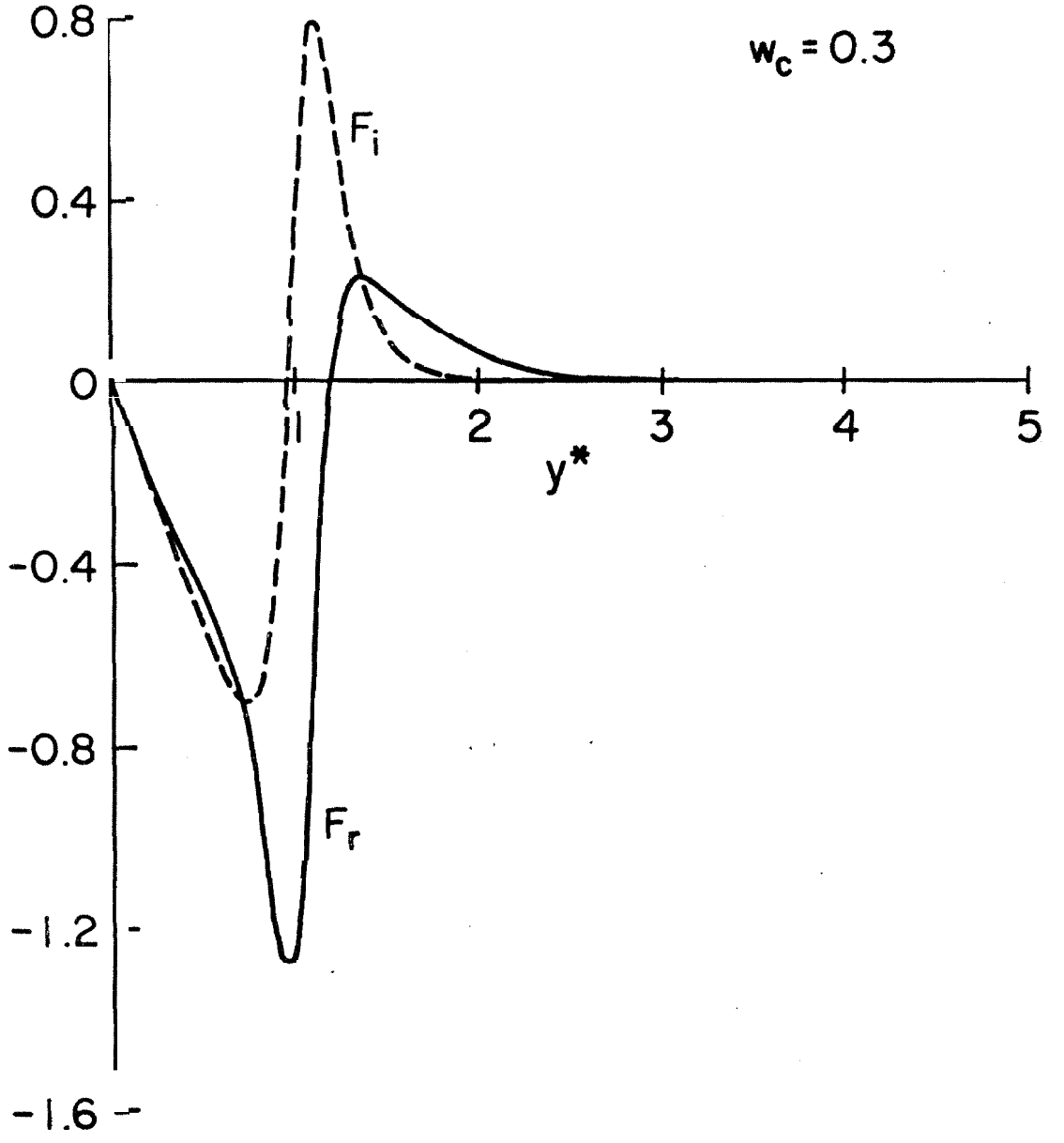

Fig. 31c Distribution of F(y*) at $w_c = 0.30$

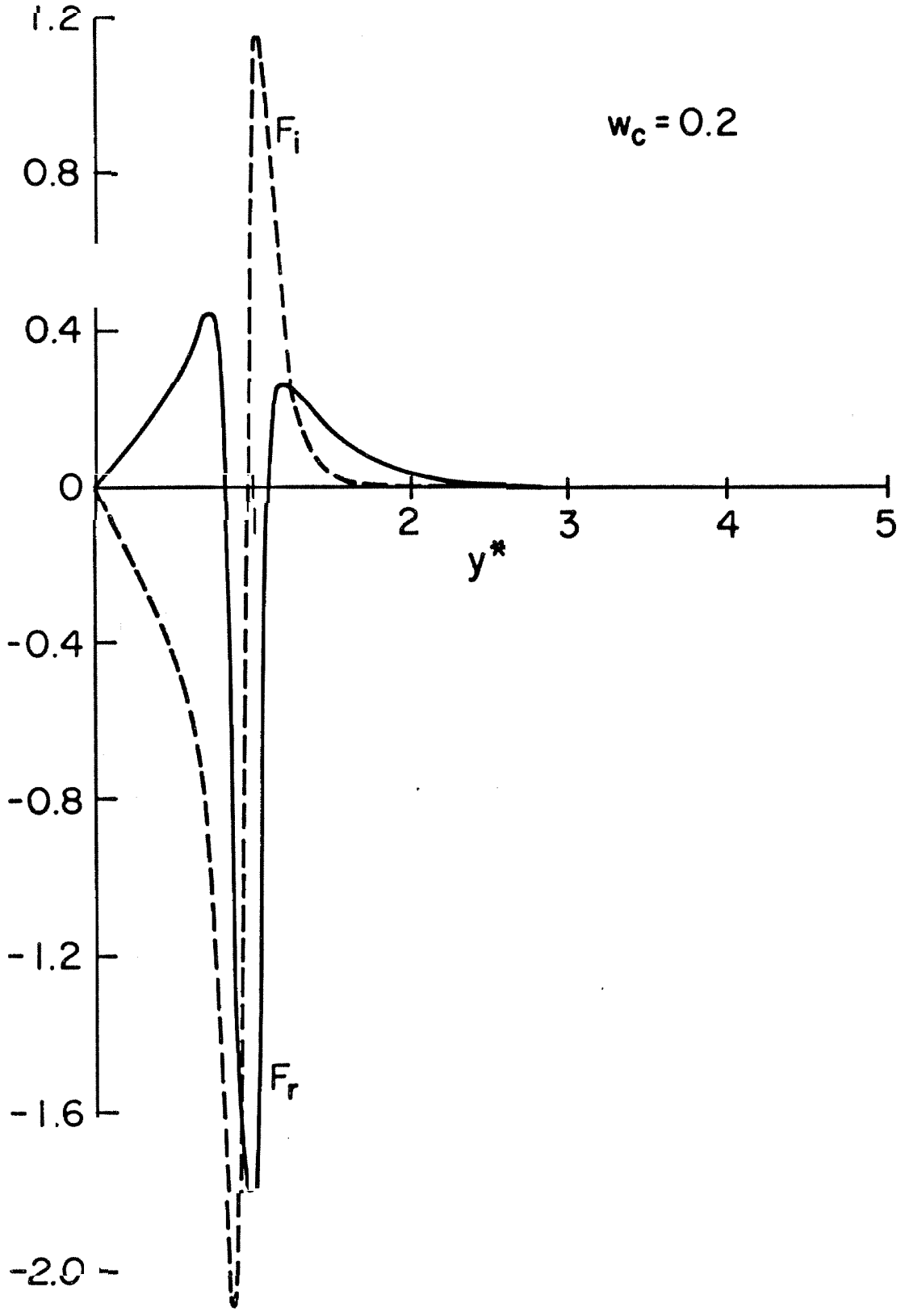

Fig. 31d Distribution of F(y*) at w_c = 0.20

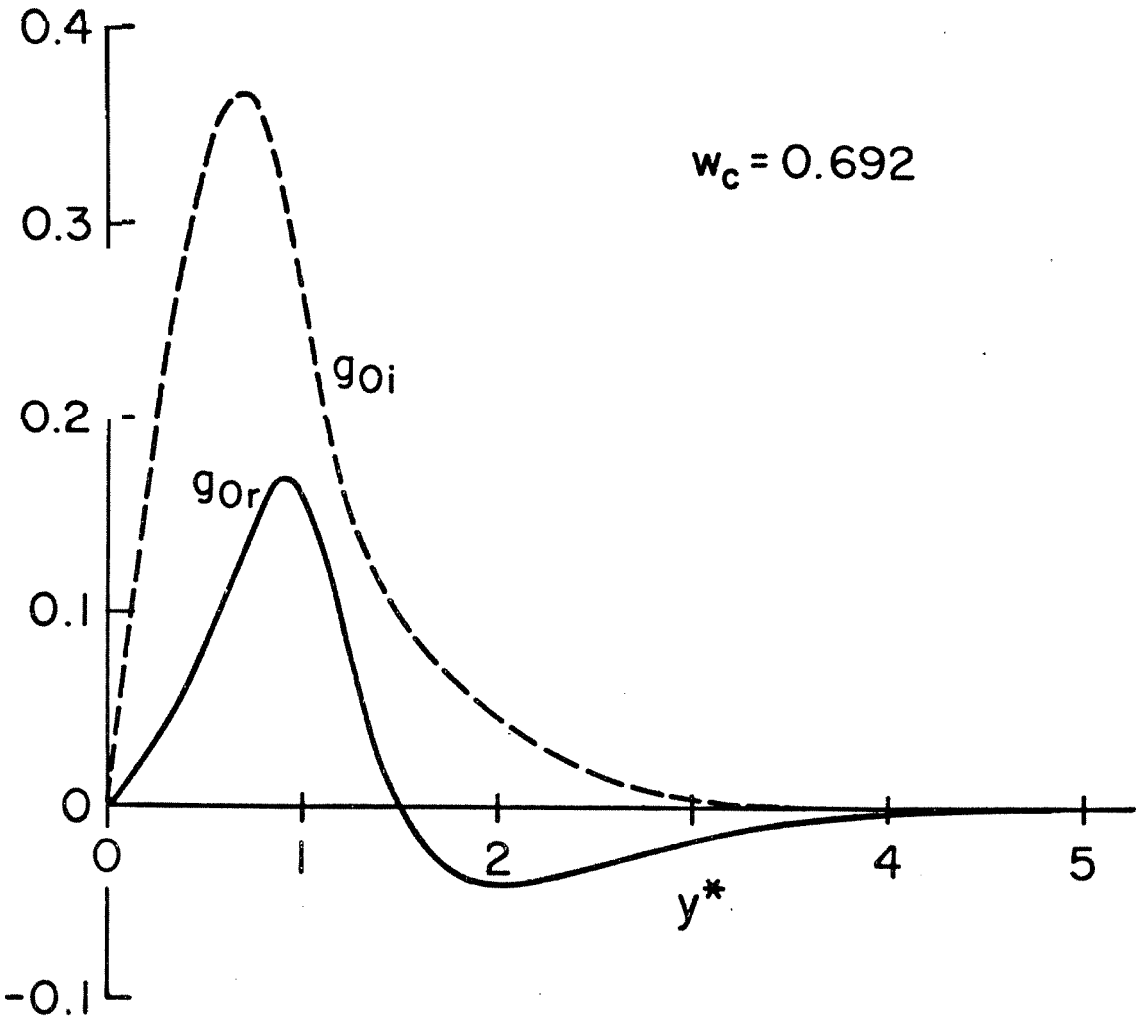

Fig. 32a Distribution of $g_0(y^*)$ at $w_c = 0.692$

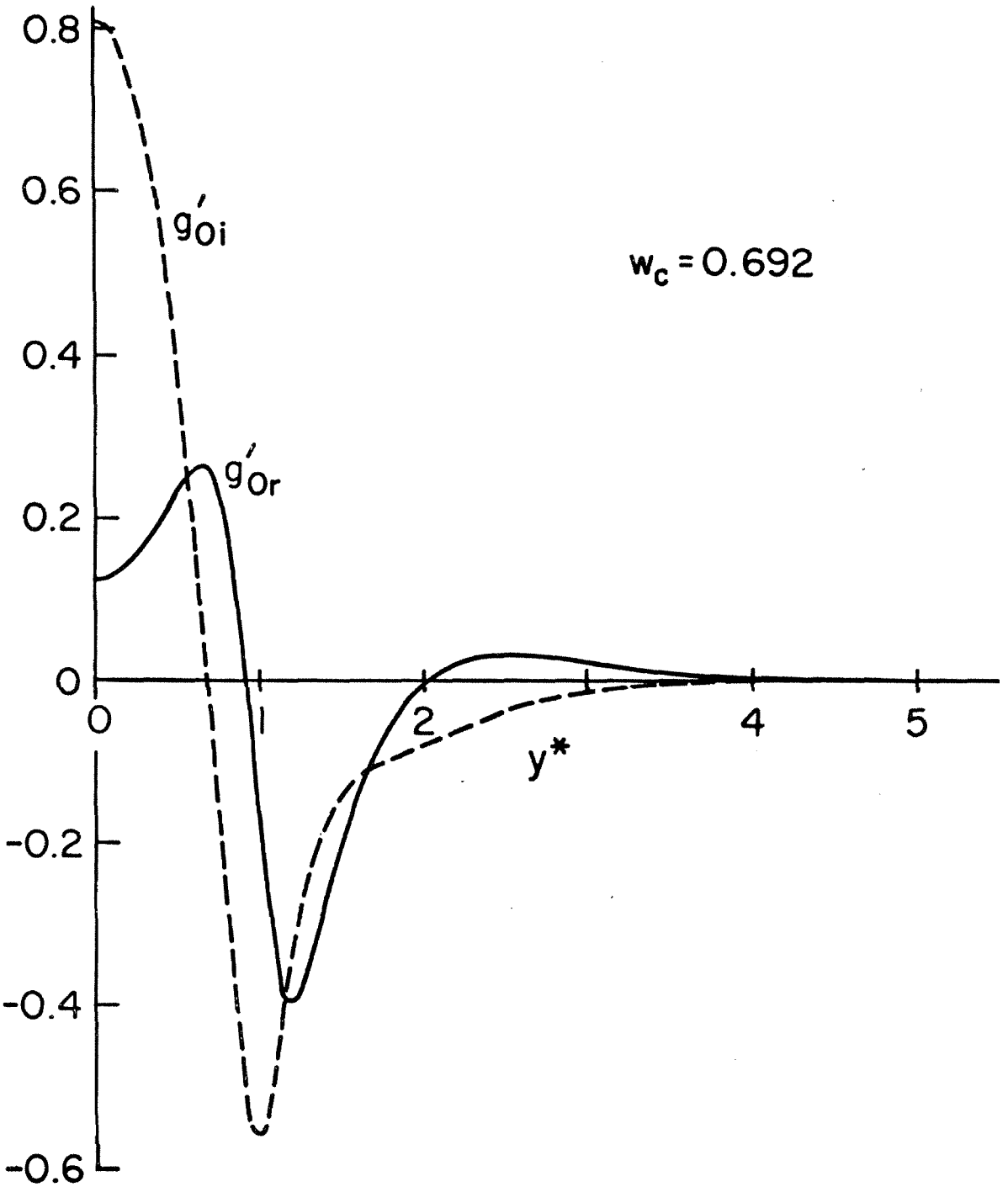

Fig. 32b Distribution of $g'_0(y^*)$ at w_c = 0. 692

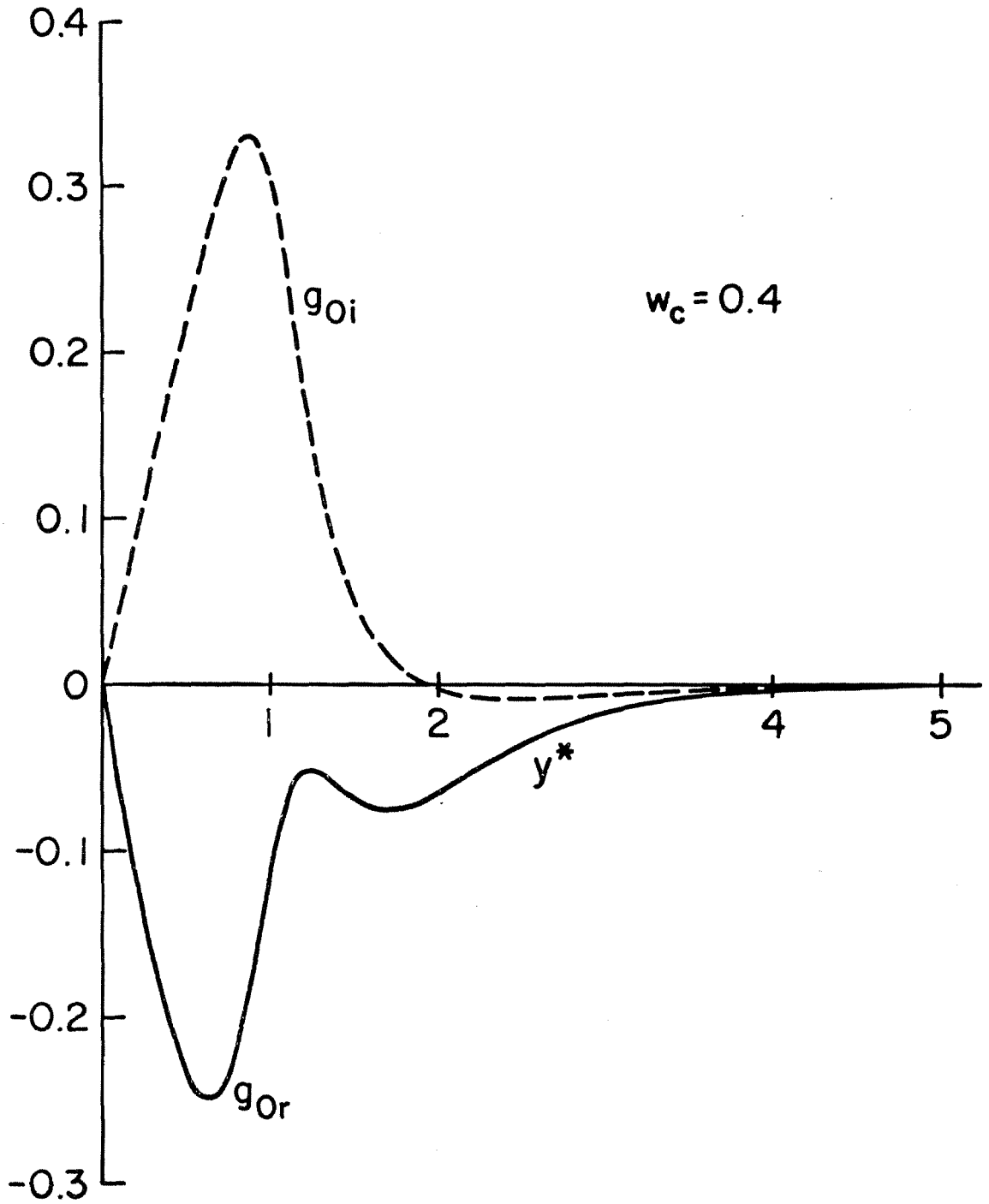

Fig. 32c Distribution of $g_0(y^*)$ at $w_c = 0.40$

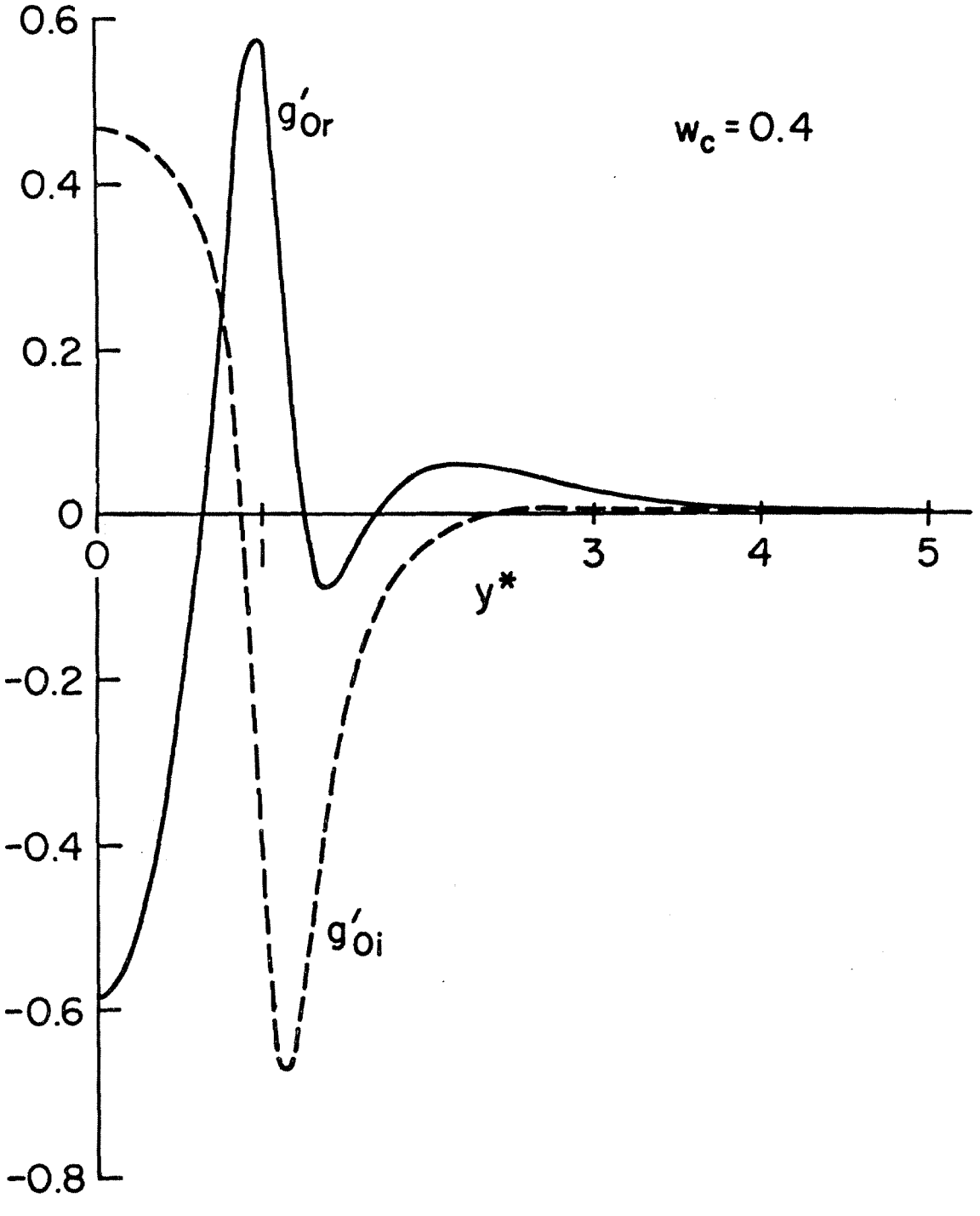

Fig. 32d Distribution of $g'_0(y^*)$ at $w_c = 0.40$

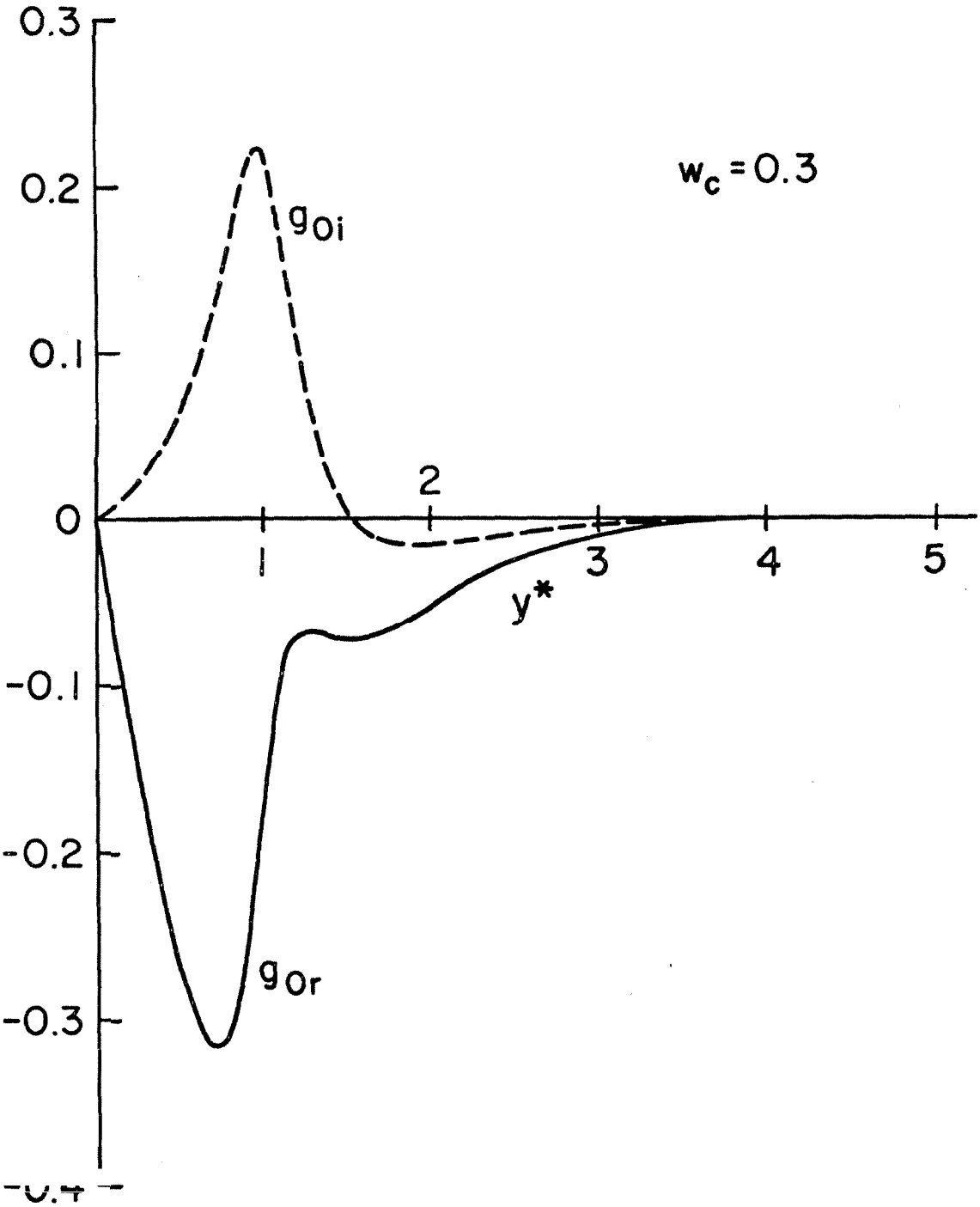

Fig. 32e Distribution of $g_0(y^*)$ at $w_c = 0.30$

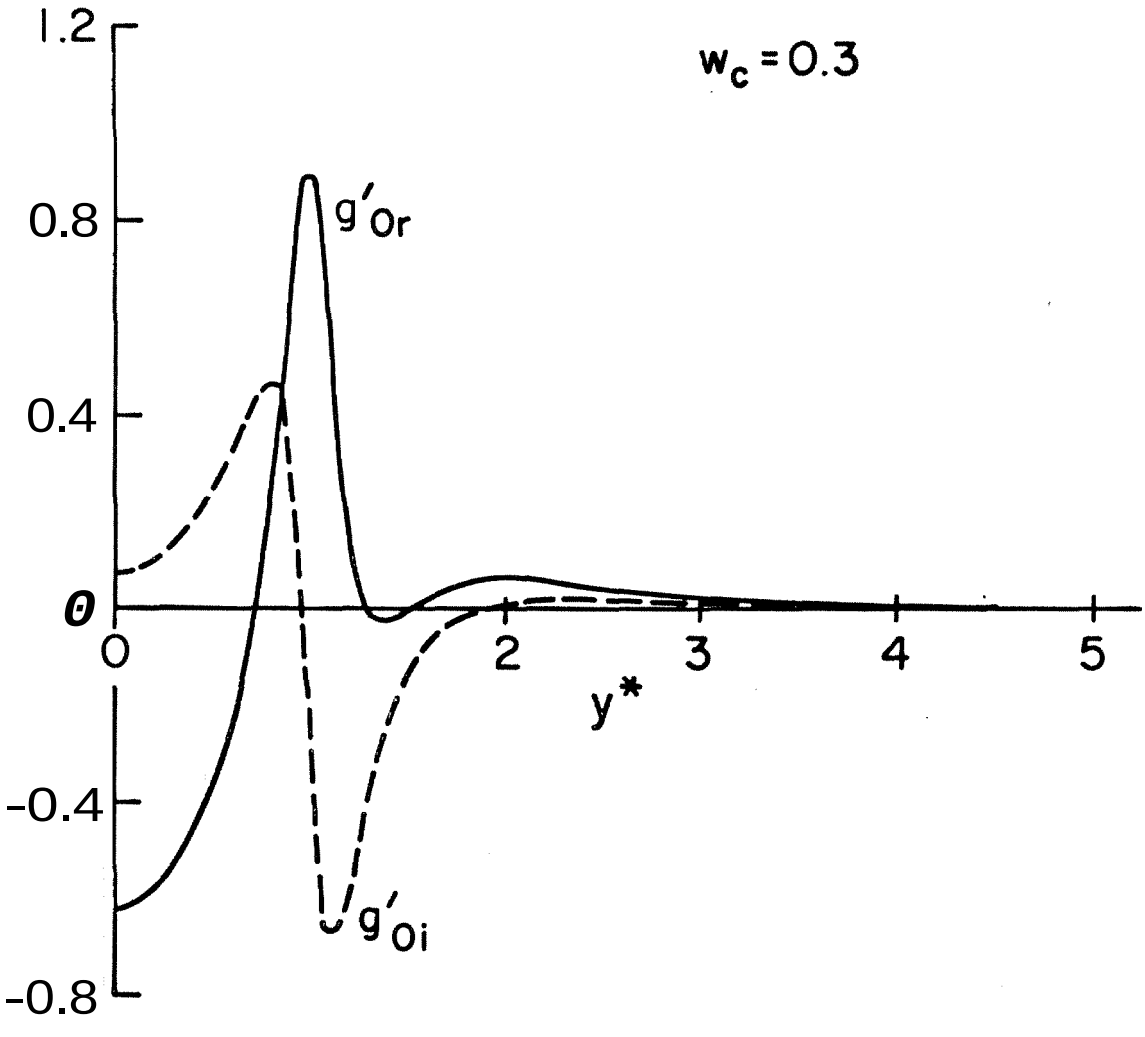

Fig. 32f Distribution of $g'_0(y^*)$ at $w_c = 0.30$

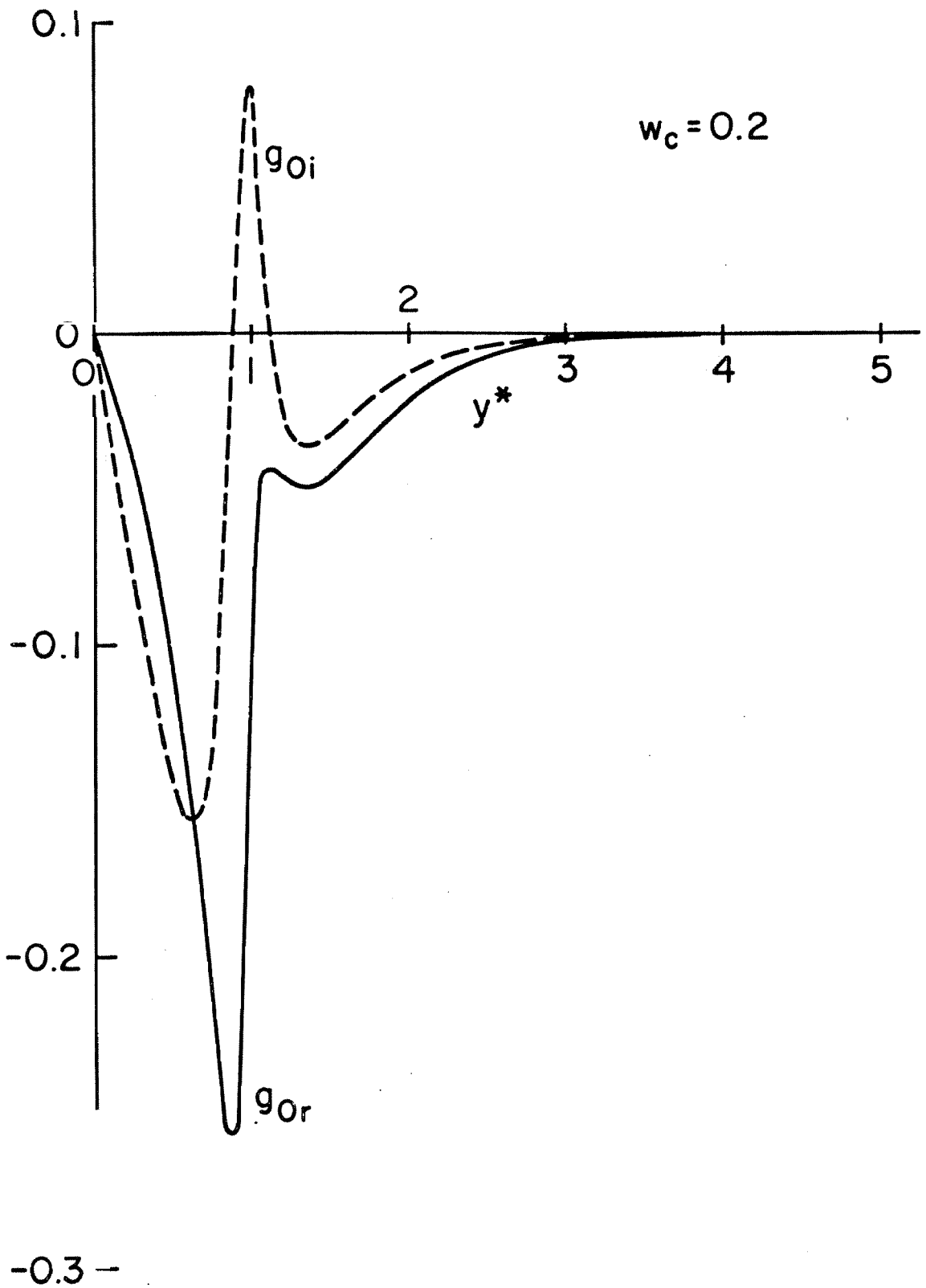

Fig. 32g Distribution of $g_0(y^*)$ at $w_c = 0.20$

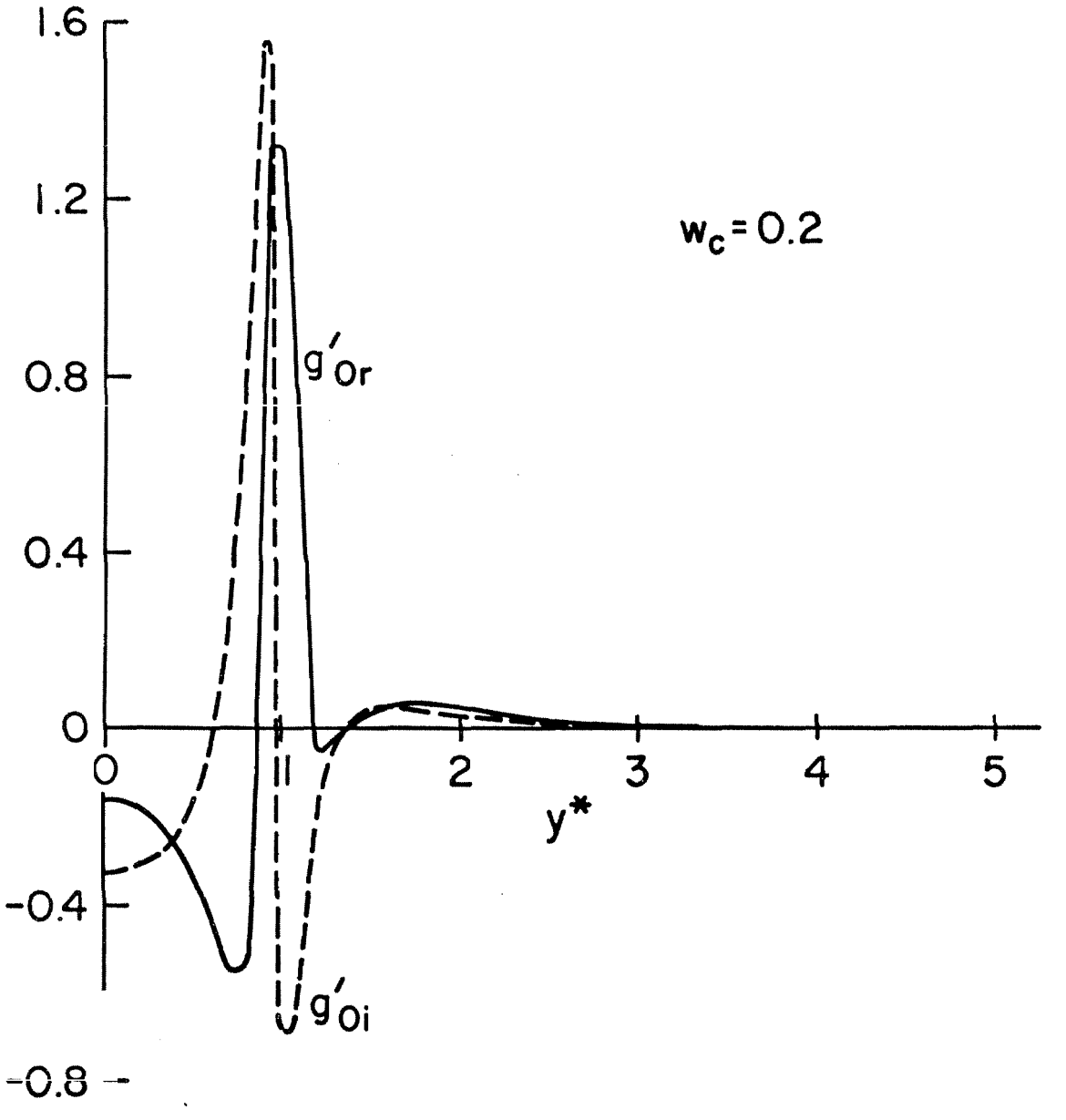

Fig. 32h Dietribution of $g'_0(y^*)$ at $w_c = 0.20$

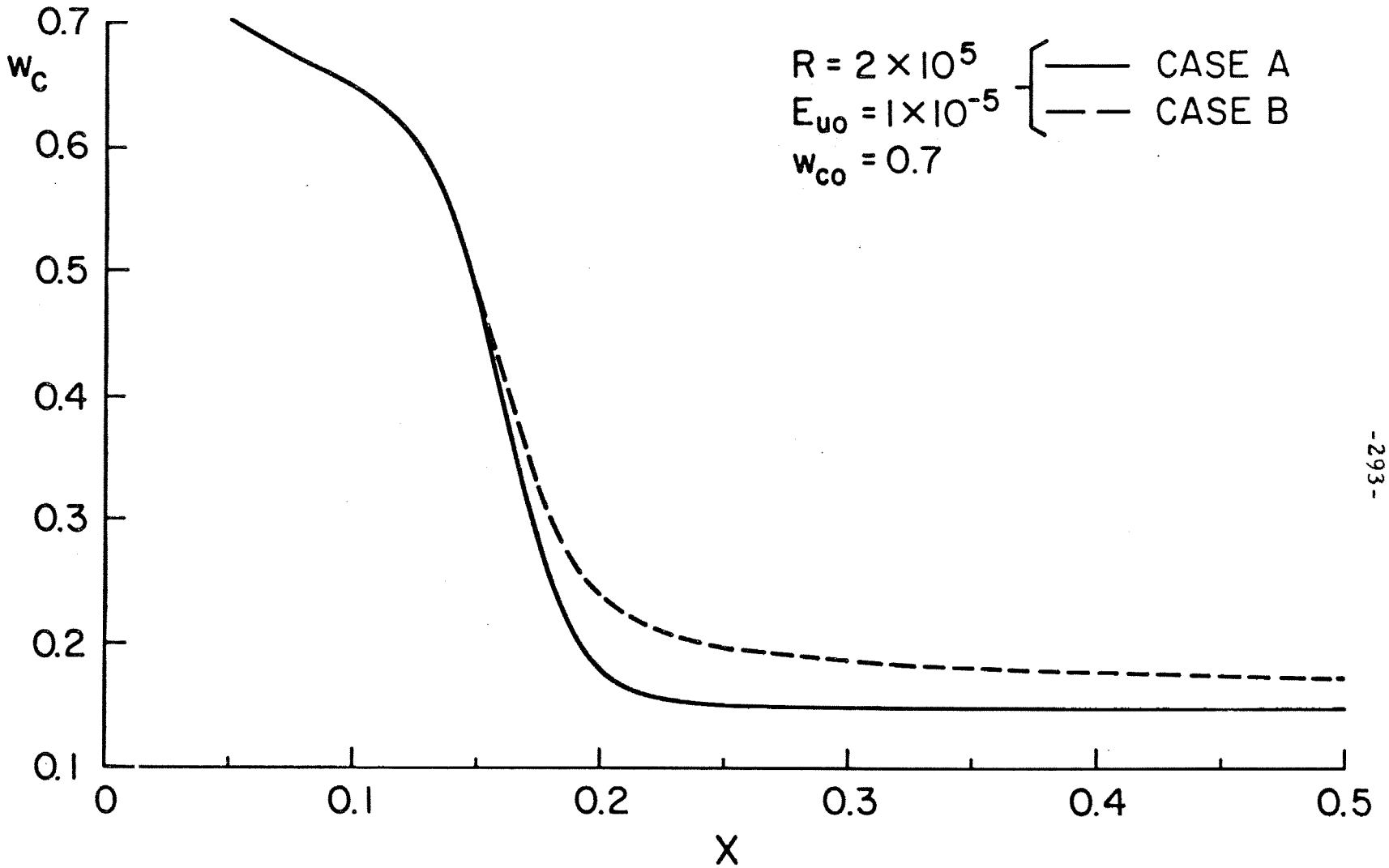

Fig. 33 Effect of the Second Harmonic on w_c

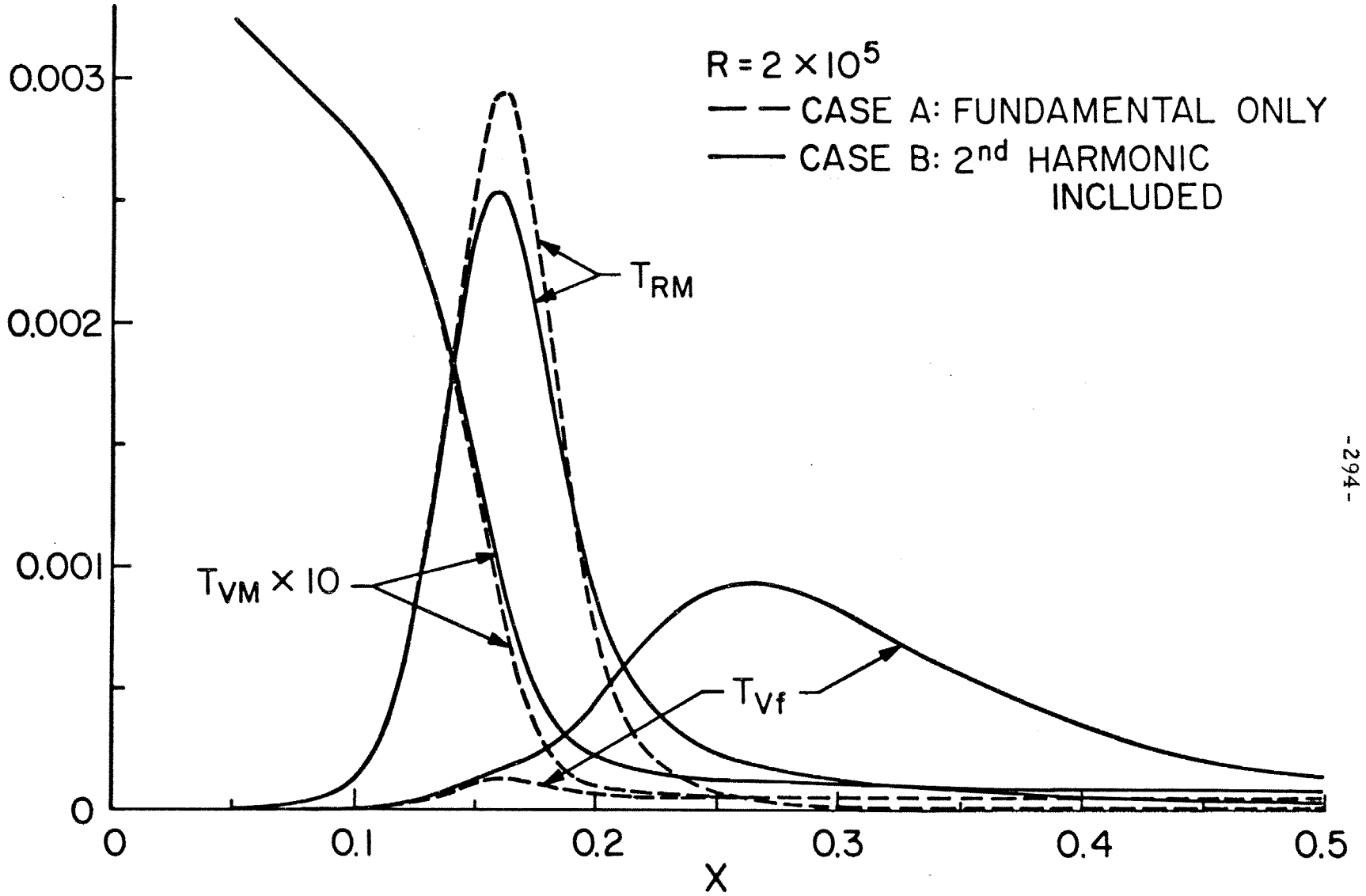

Fig. 34 Effect of the Second Harmonic on the Energy Transferring Mechanisms

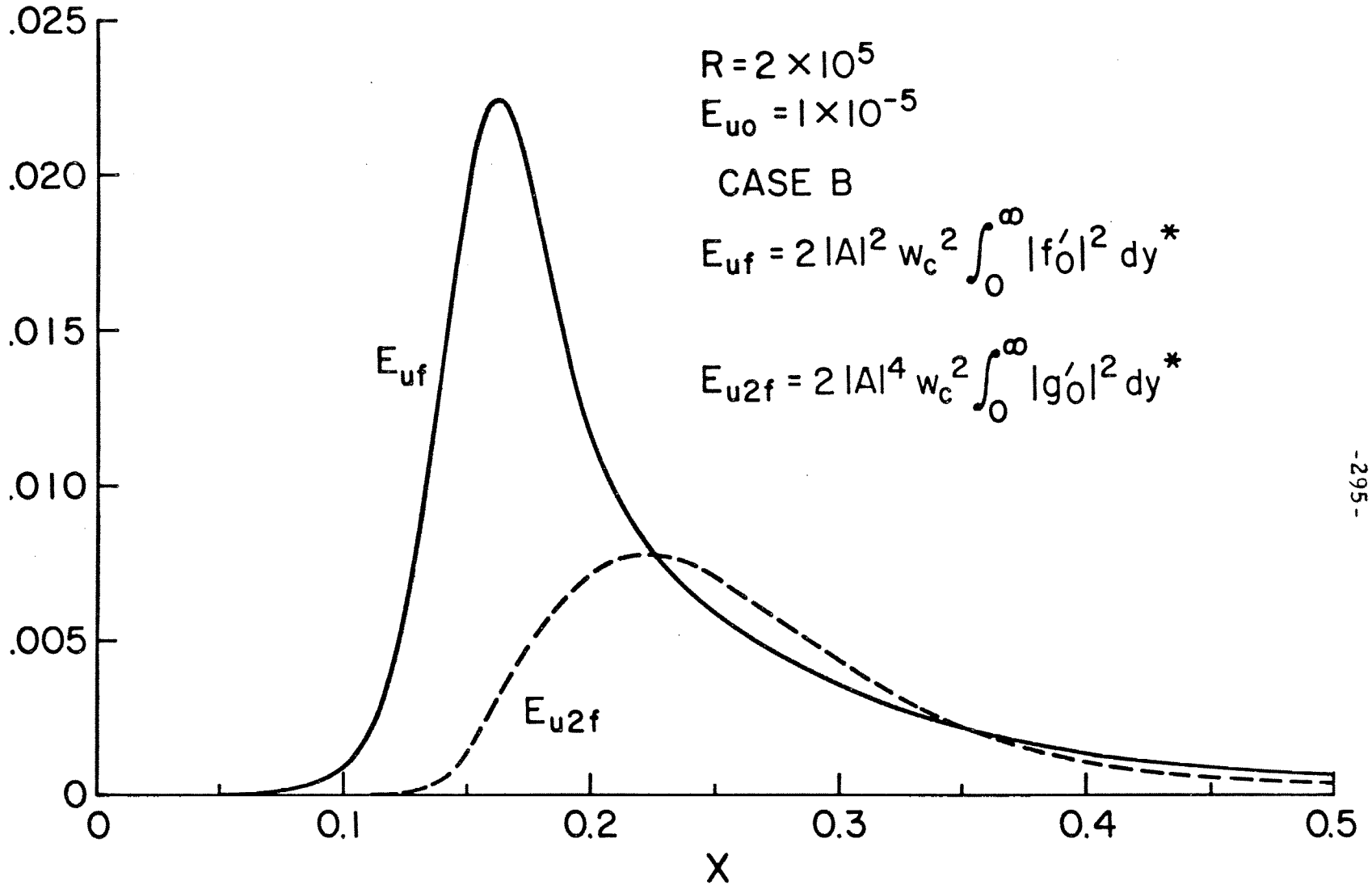

Fig. 35 Variation of the Energy Contents in the Fundamental and the Second Harmonic

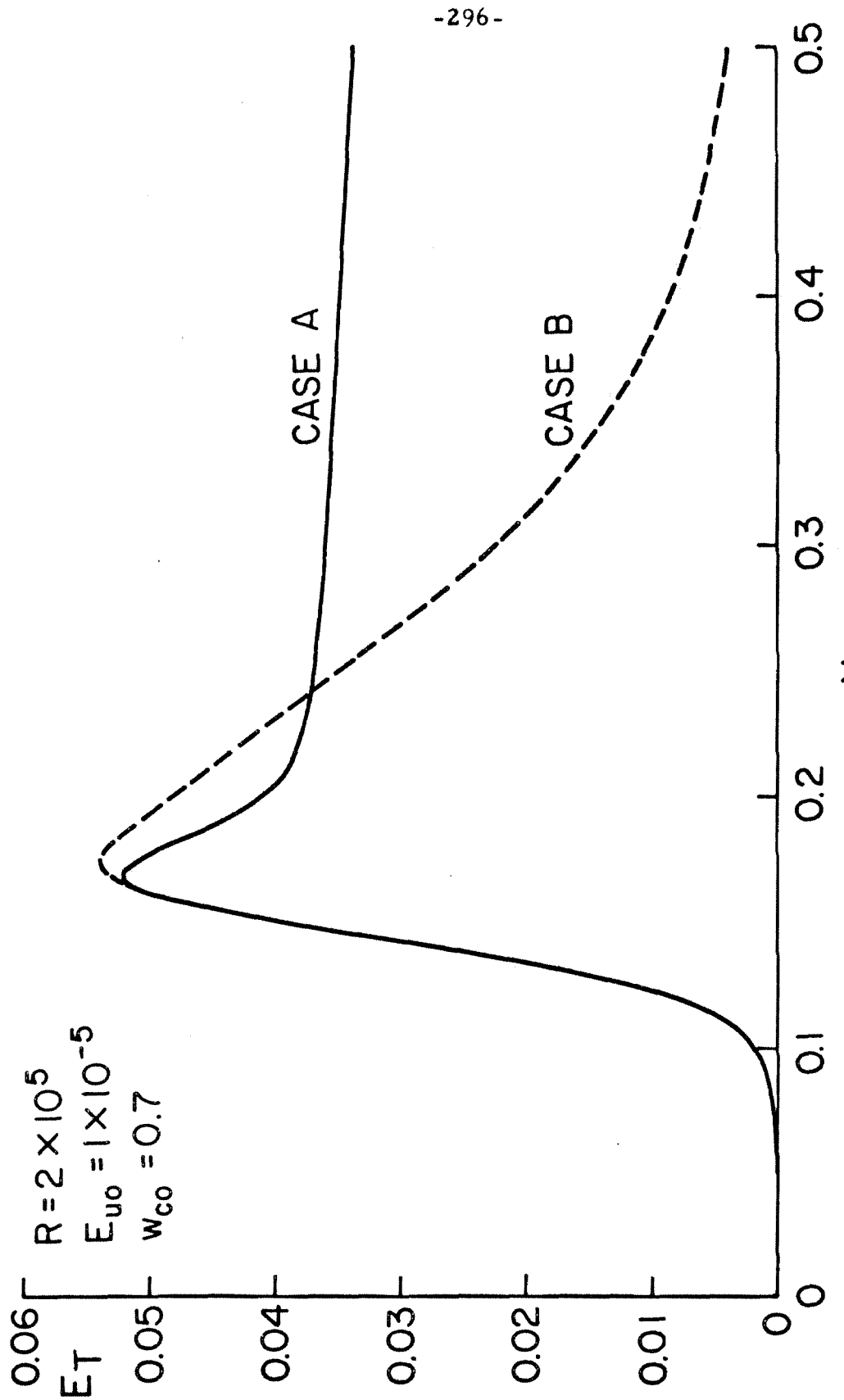

Fig. 36 Effect of the Second Harmonic on E_T

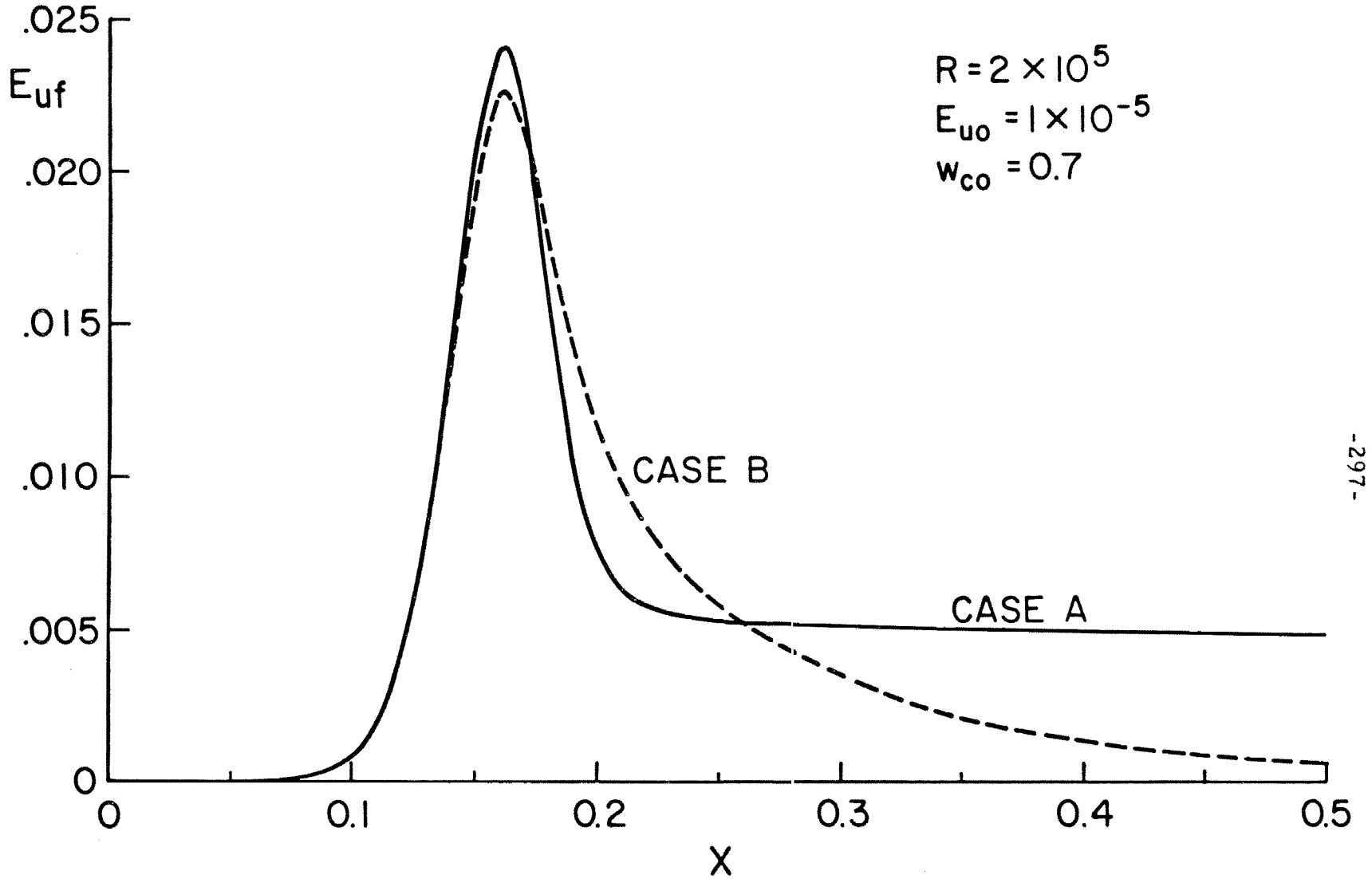

Fig. 36a Effect of the Second Harmonic on E_{uf}

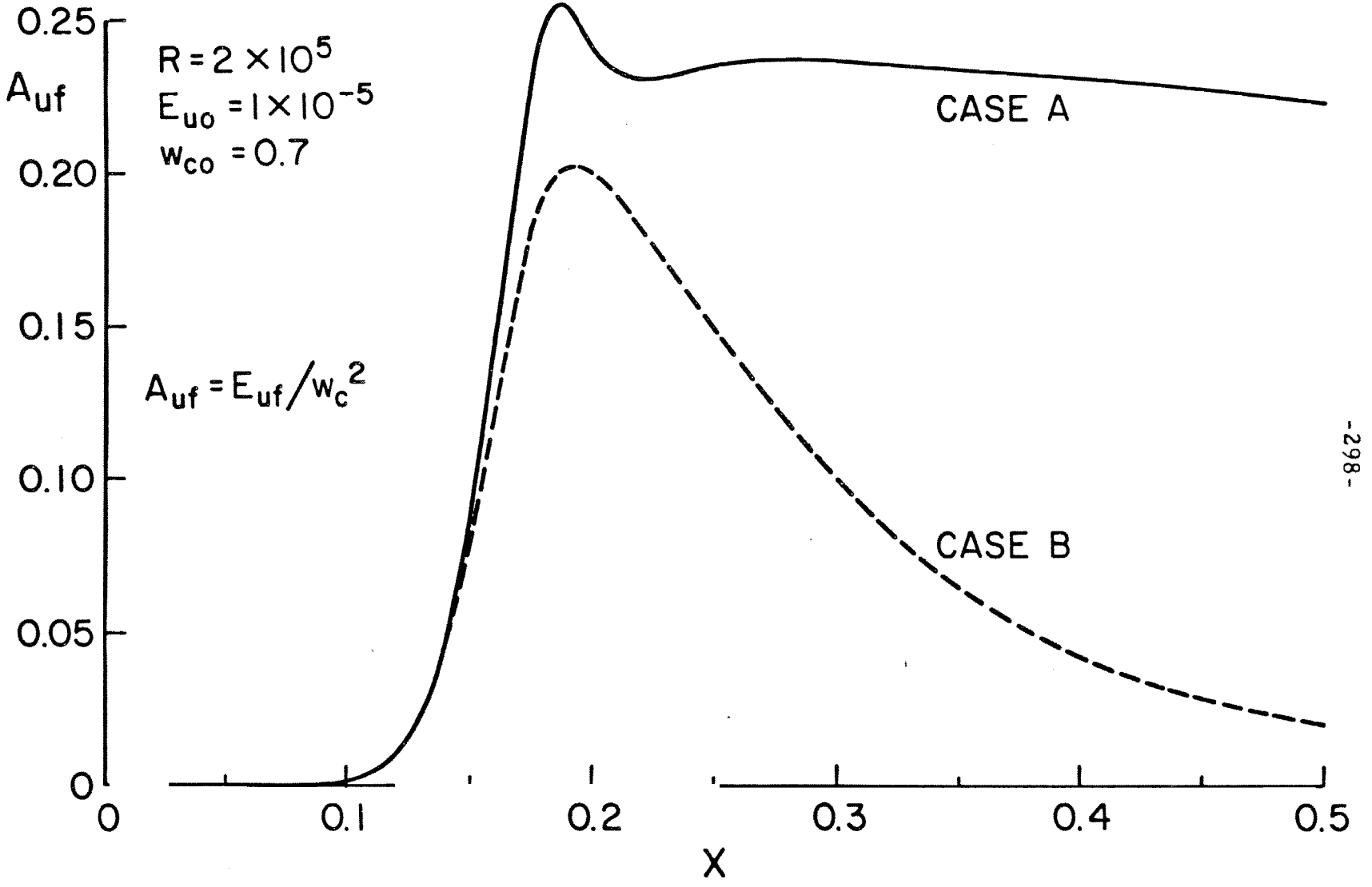

Fig. 36b Effect of the Second Harmonic on A_{uf}

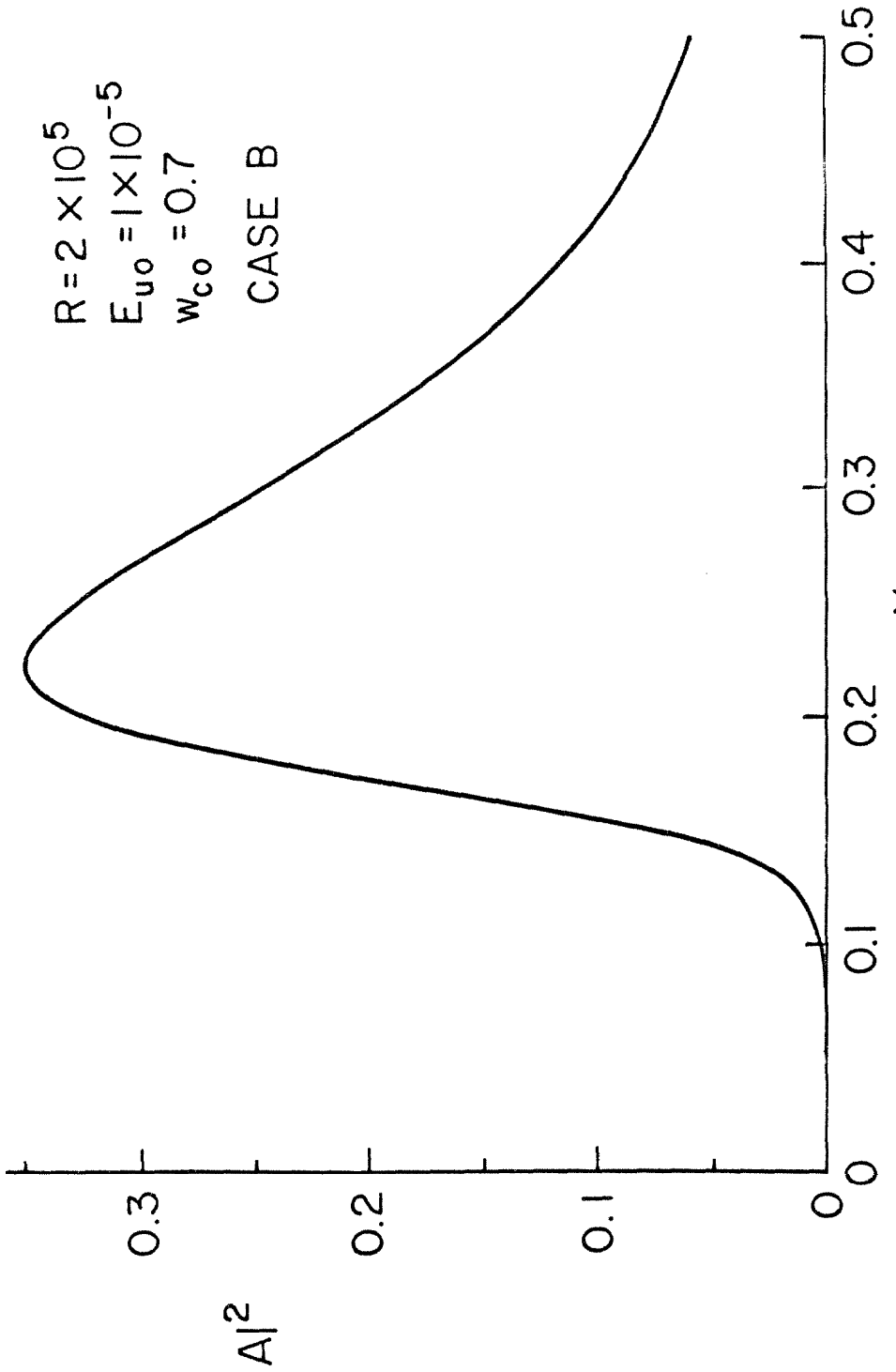

Fig. 37 Effect of the Second Harmonic on $|A|^2$

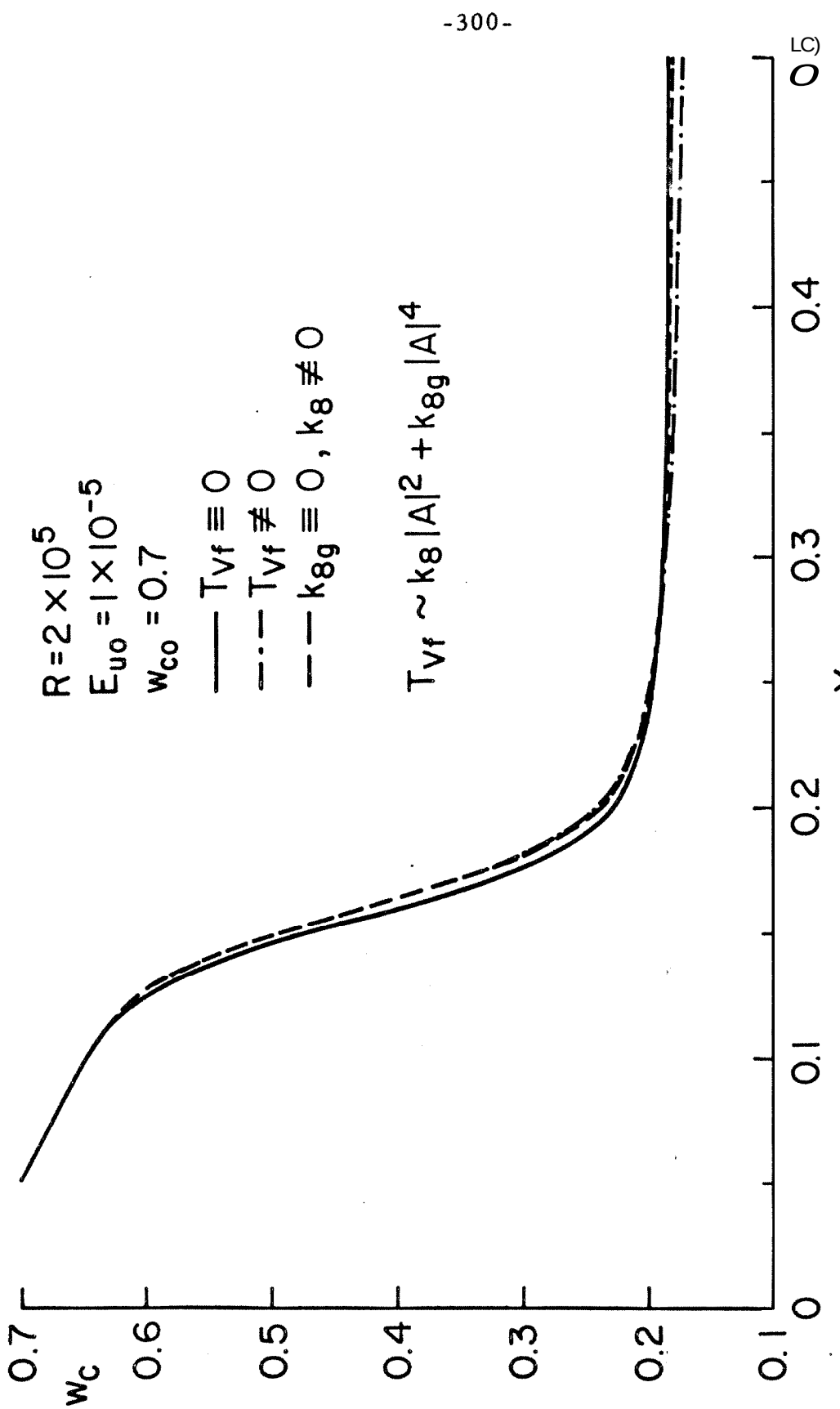

Fig. 38 Effect of the Viscous Terms on w_c; Case B

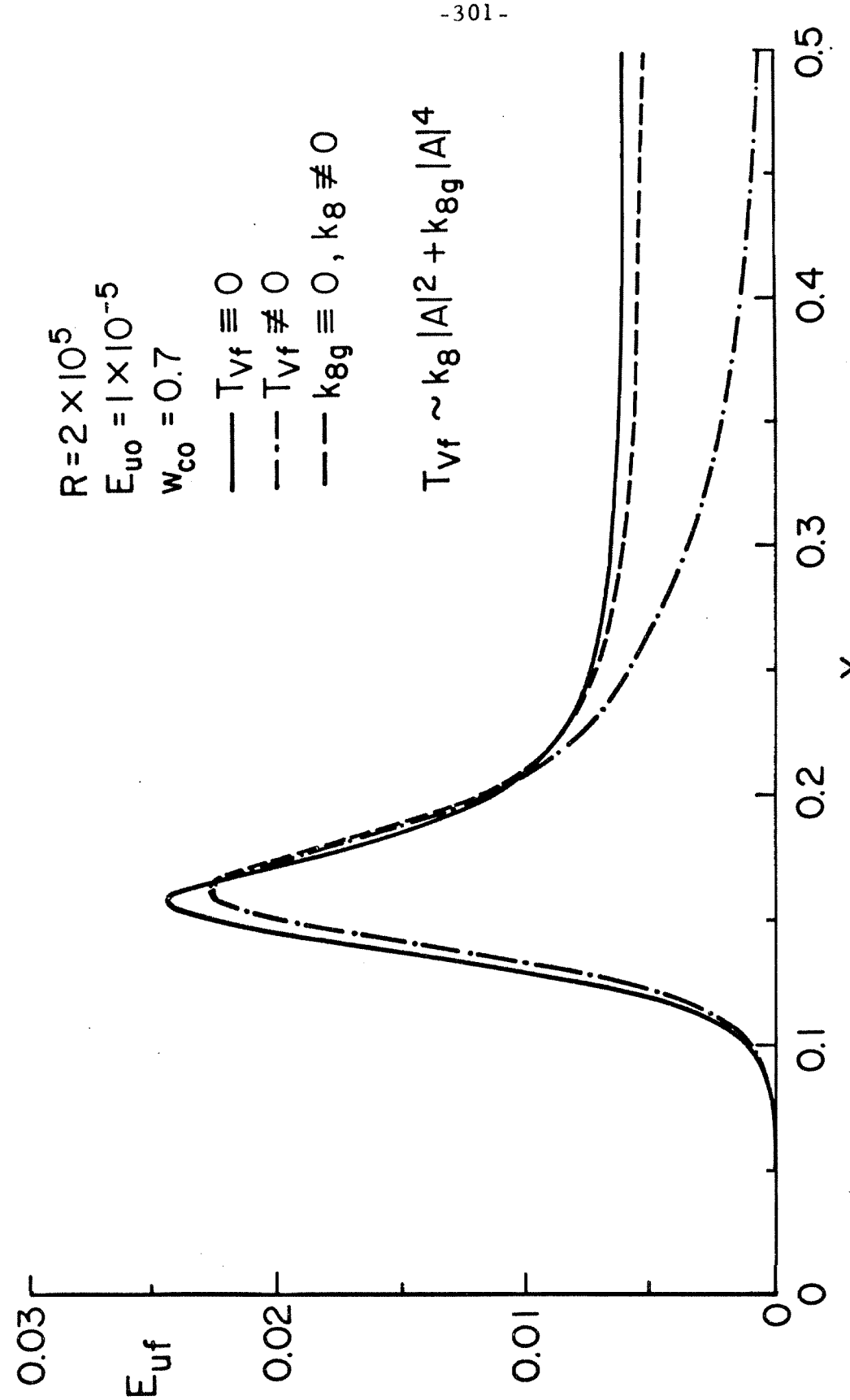

Fig. 39a Effect of the Viscous Terms on E_{uf}; Case B

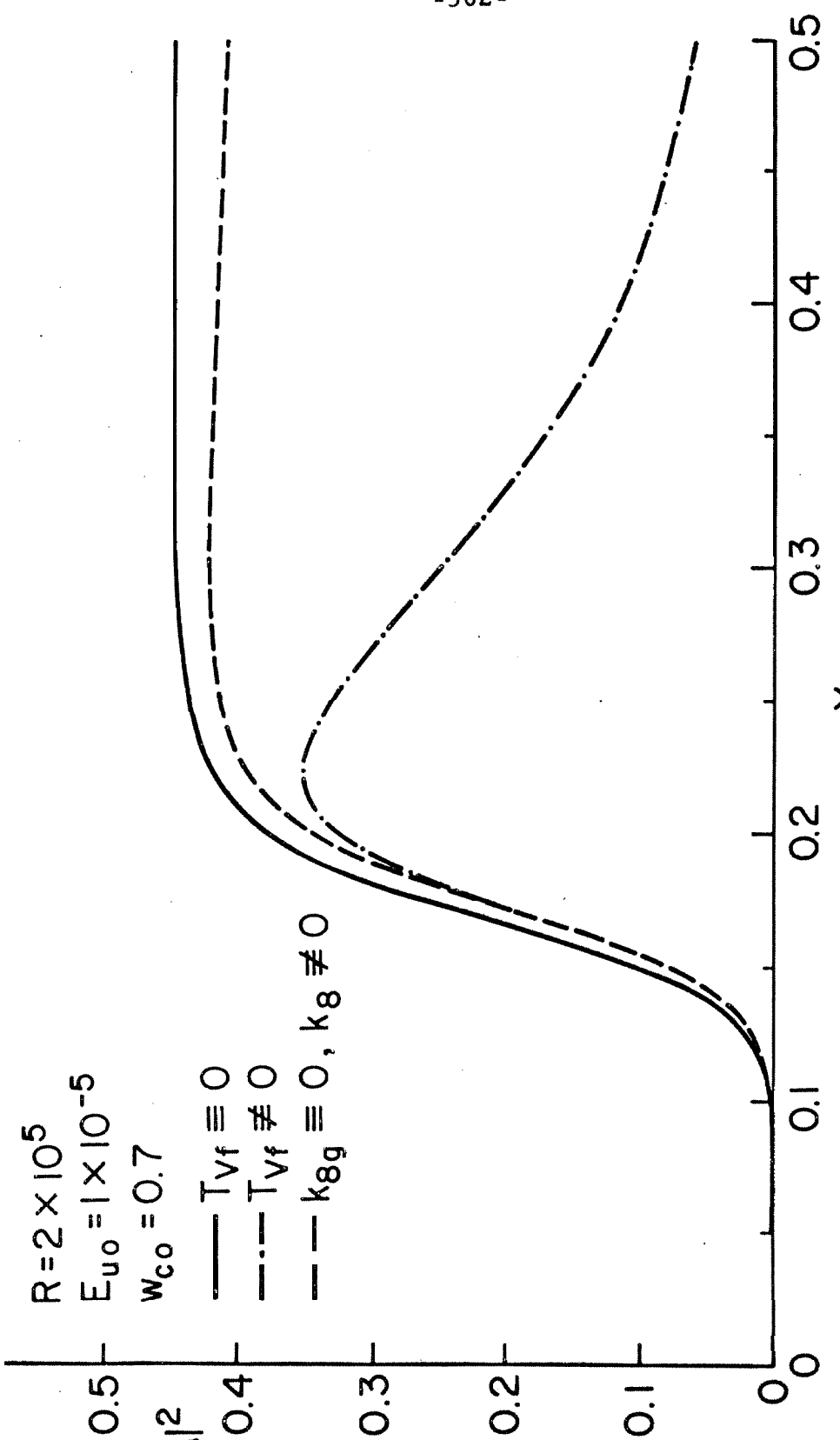

Fig. 39b Effect of the Viscous Terms on $|A|^2$; Case B

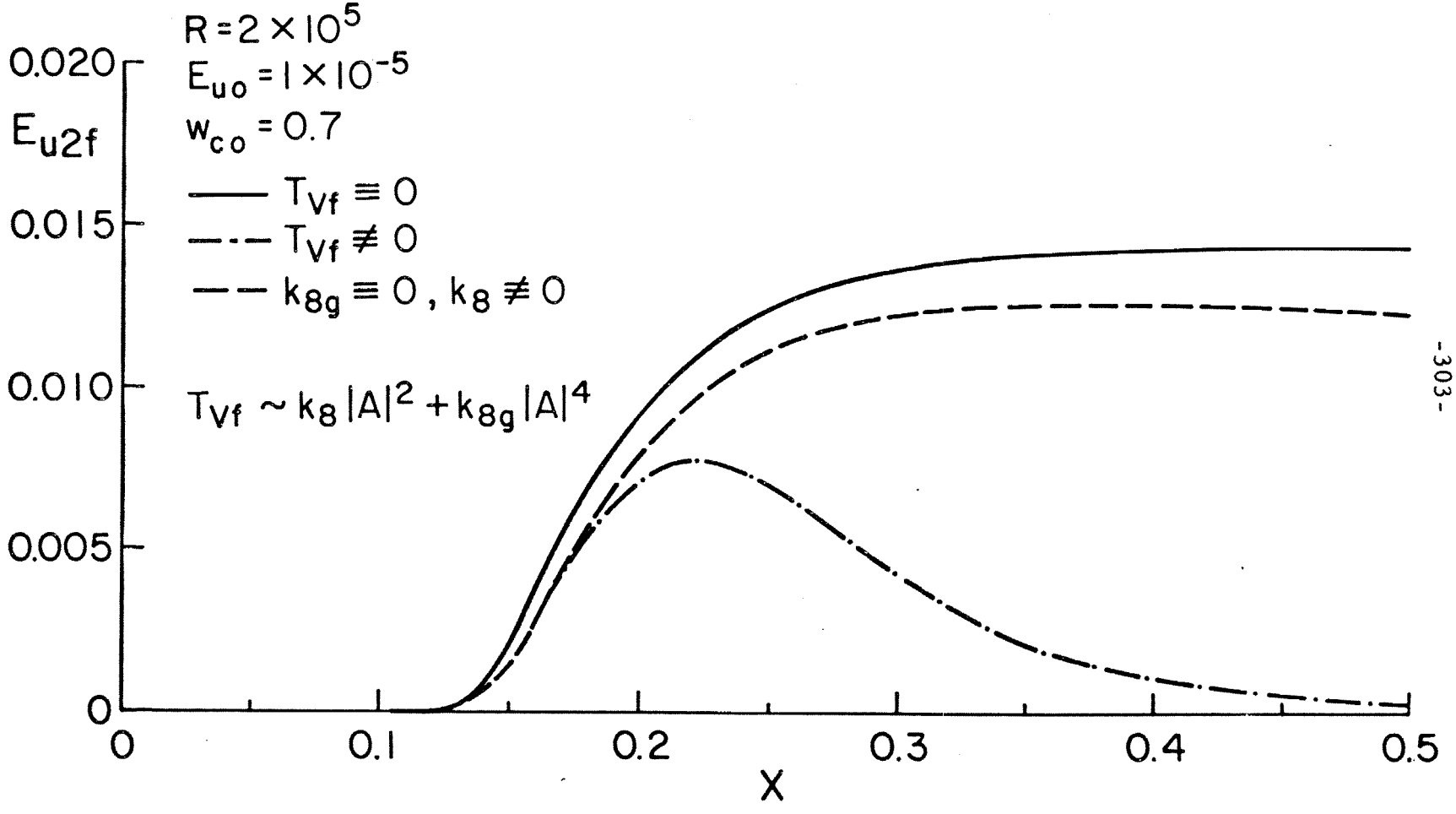

Fig. 39c Effect of the Viscous Terms on E_{u2f}; Case B

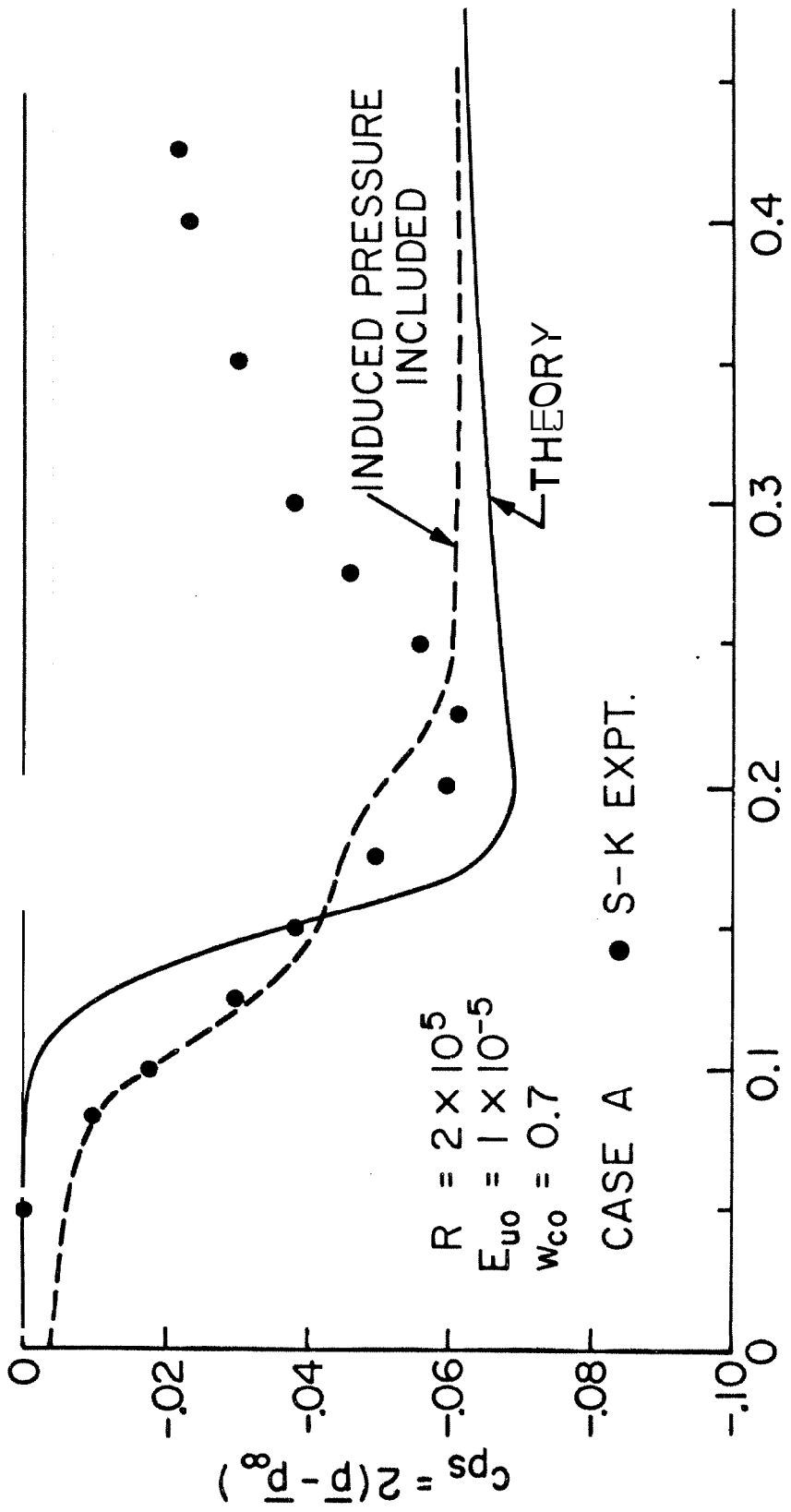

Fig. E2 Comparison of the Static Pressure Distributions along the Wake Axis

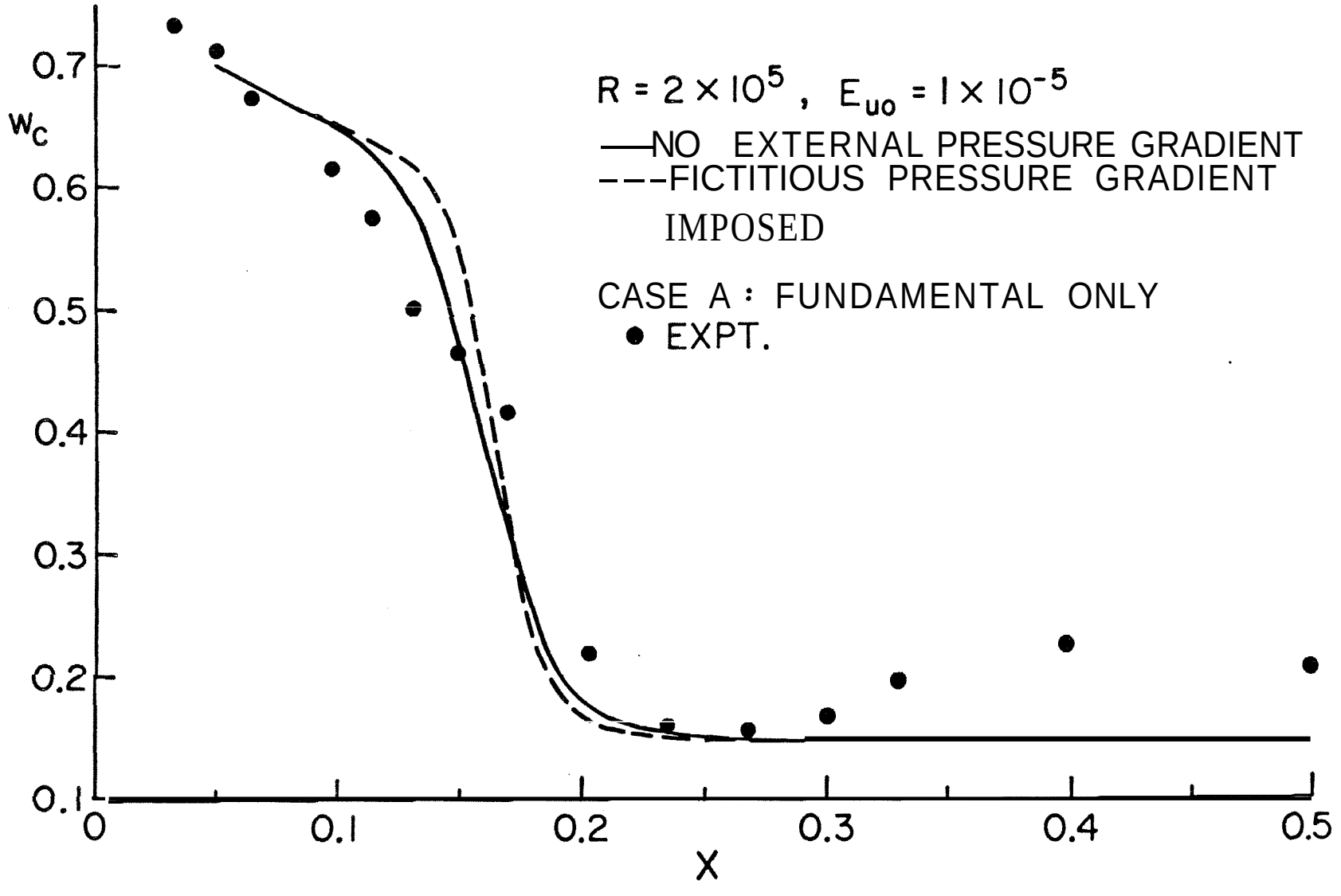

Fig. **E3** Effect of the Esternal Static Pressure Gradient on the Variation of **wc**

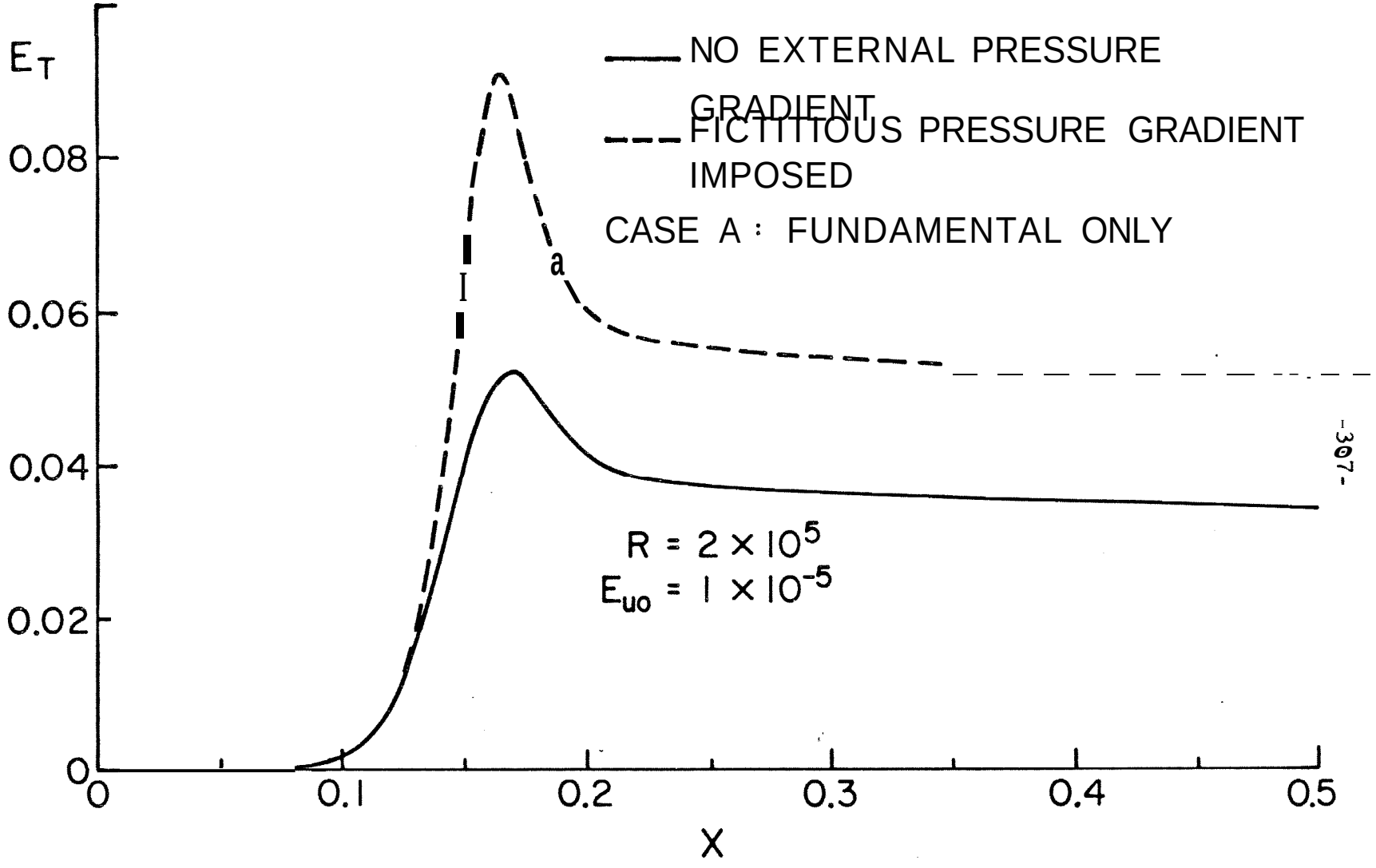

Fig. E4 Effect of the External Pressure Gradient on the Total Fluctuation Energy Density Variation

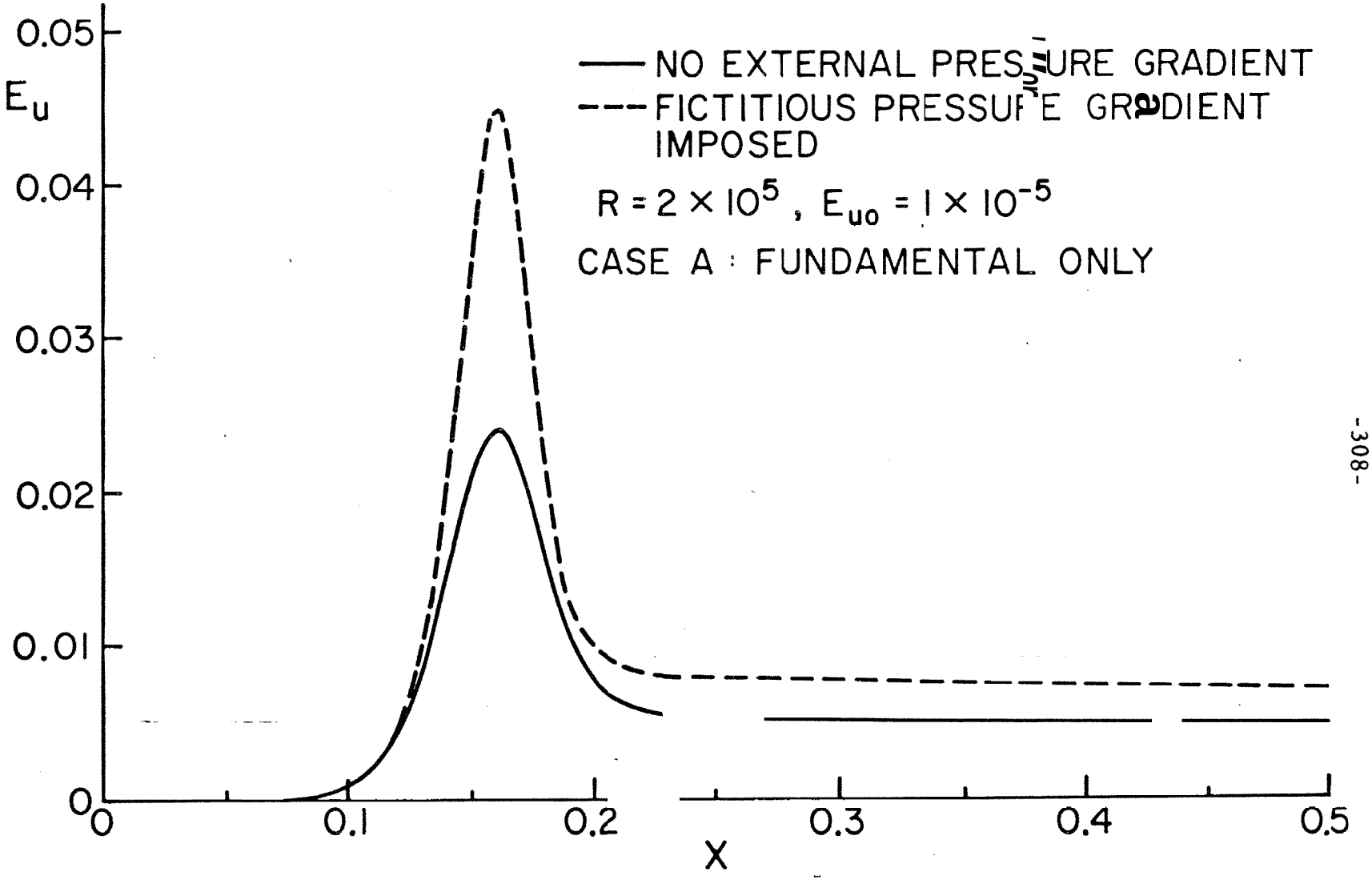

Fig. E5 Effect of the External Pressure Gradient on the Variation of E_u

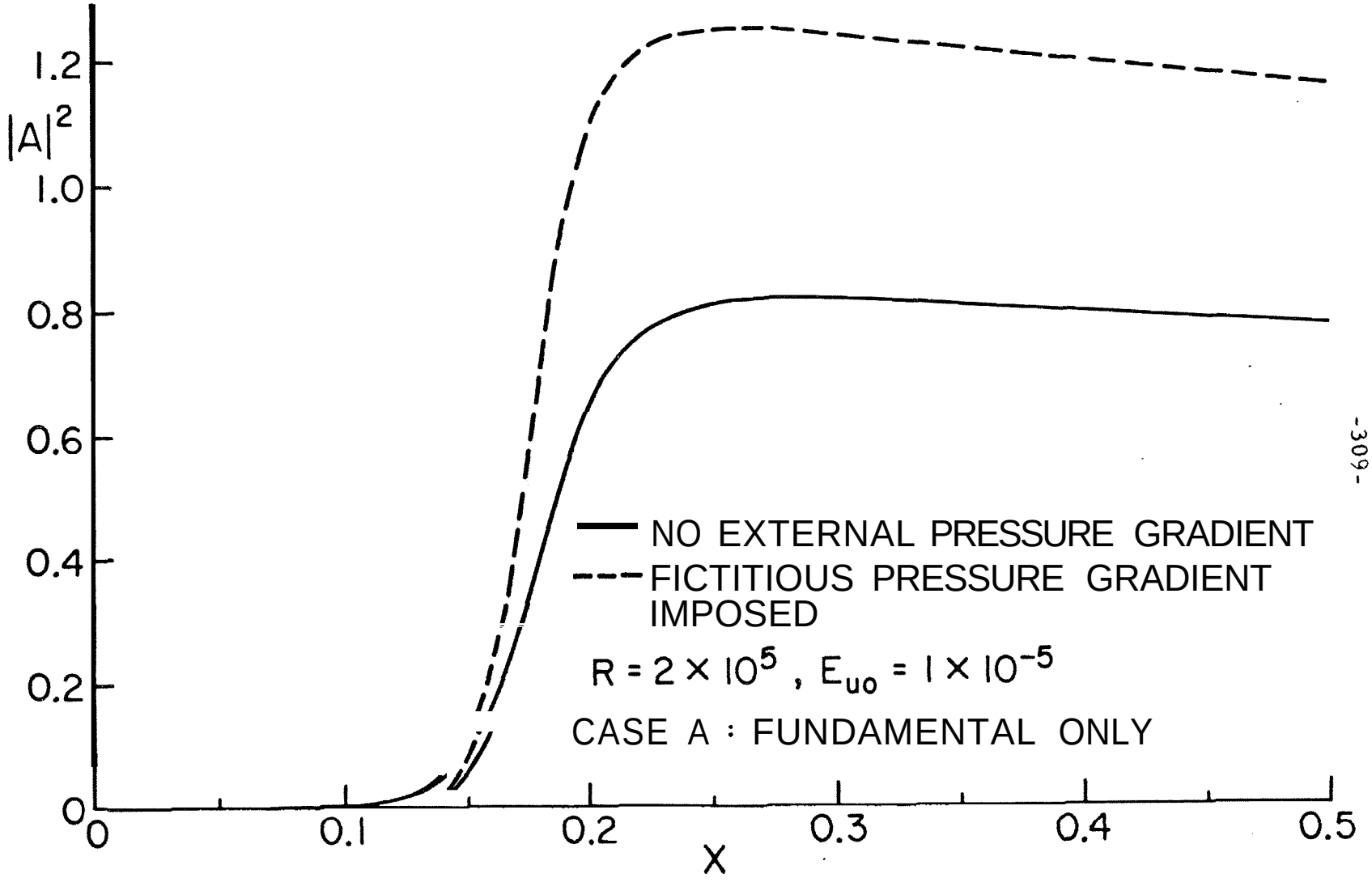

Fig. E6 Effect of the External Pressure Gradient on the Variation of $|A|^2$

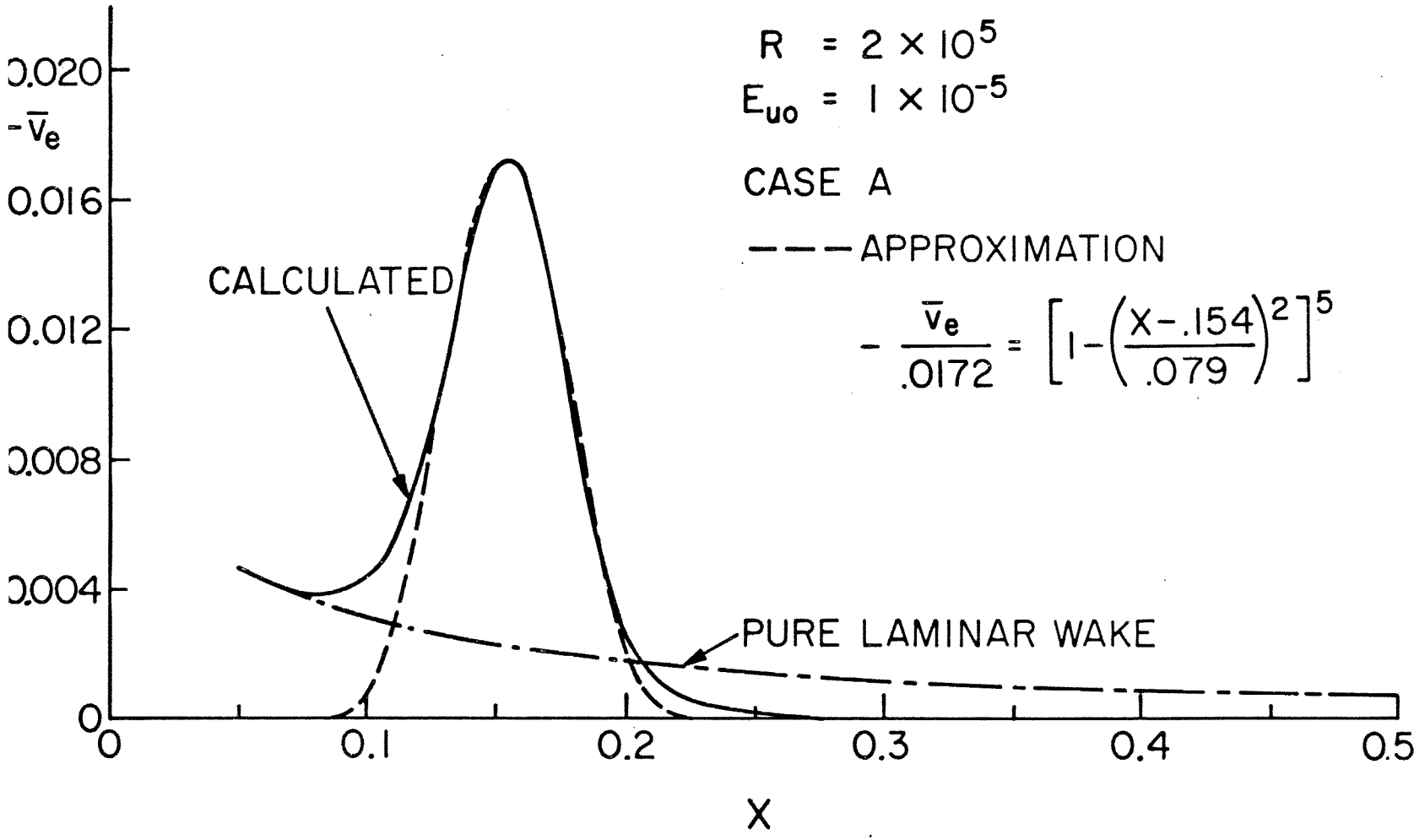

Fig. E7 Distribution of the Mean Vertical Velocity at the Edge of the Wake, $\bar{v}_e$

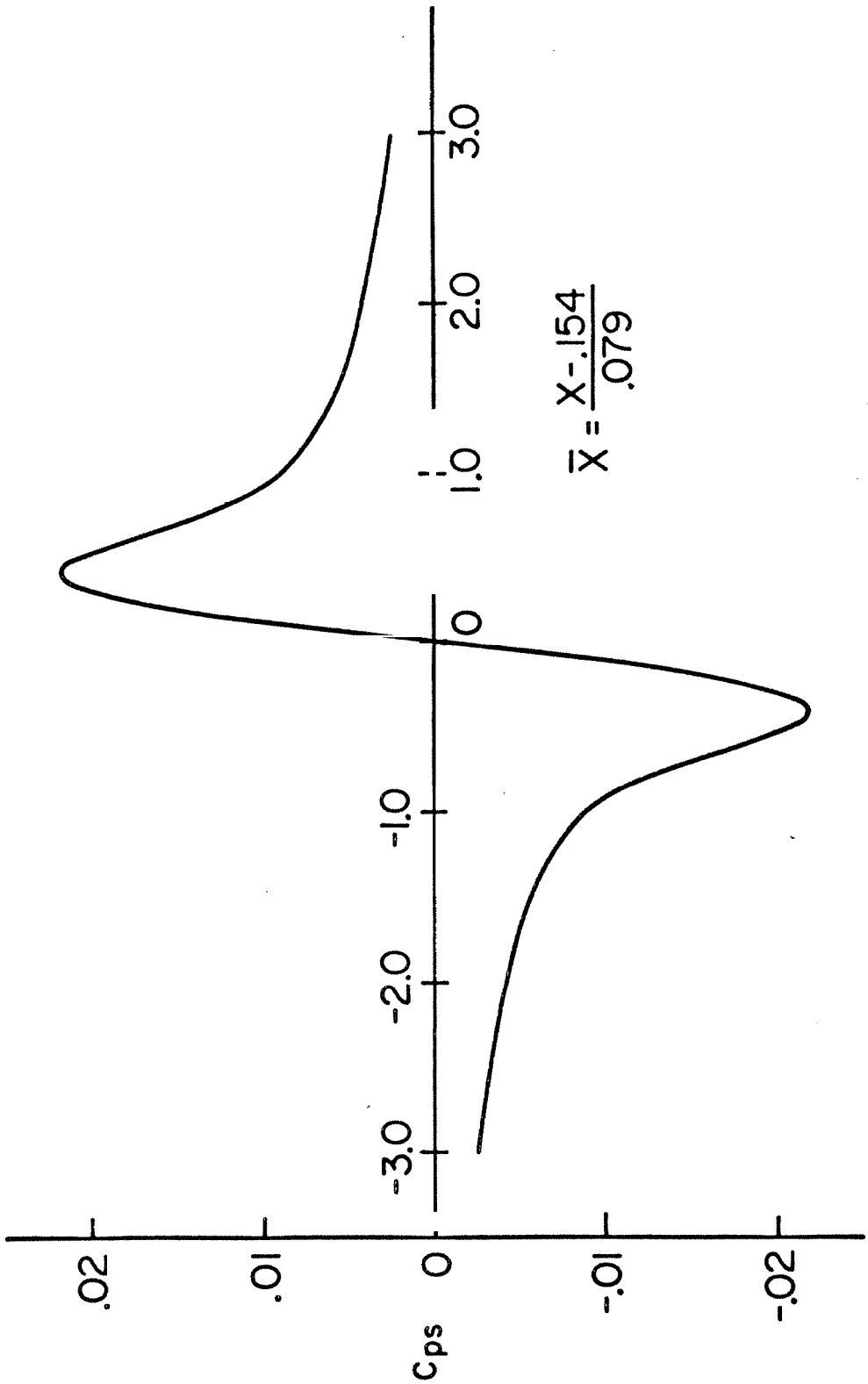

Fig. E8 Calculated Distribution of the Induced Static Pressure Coefficient

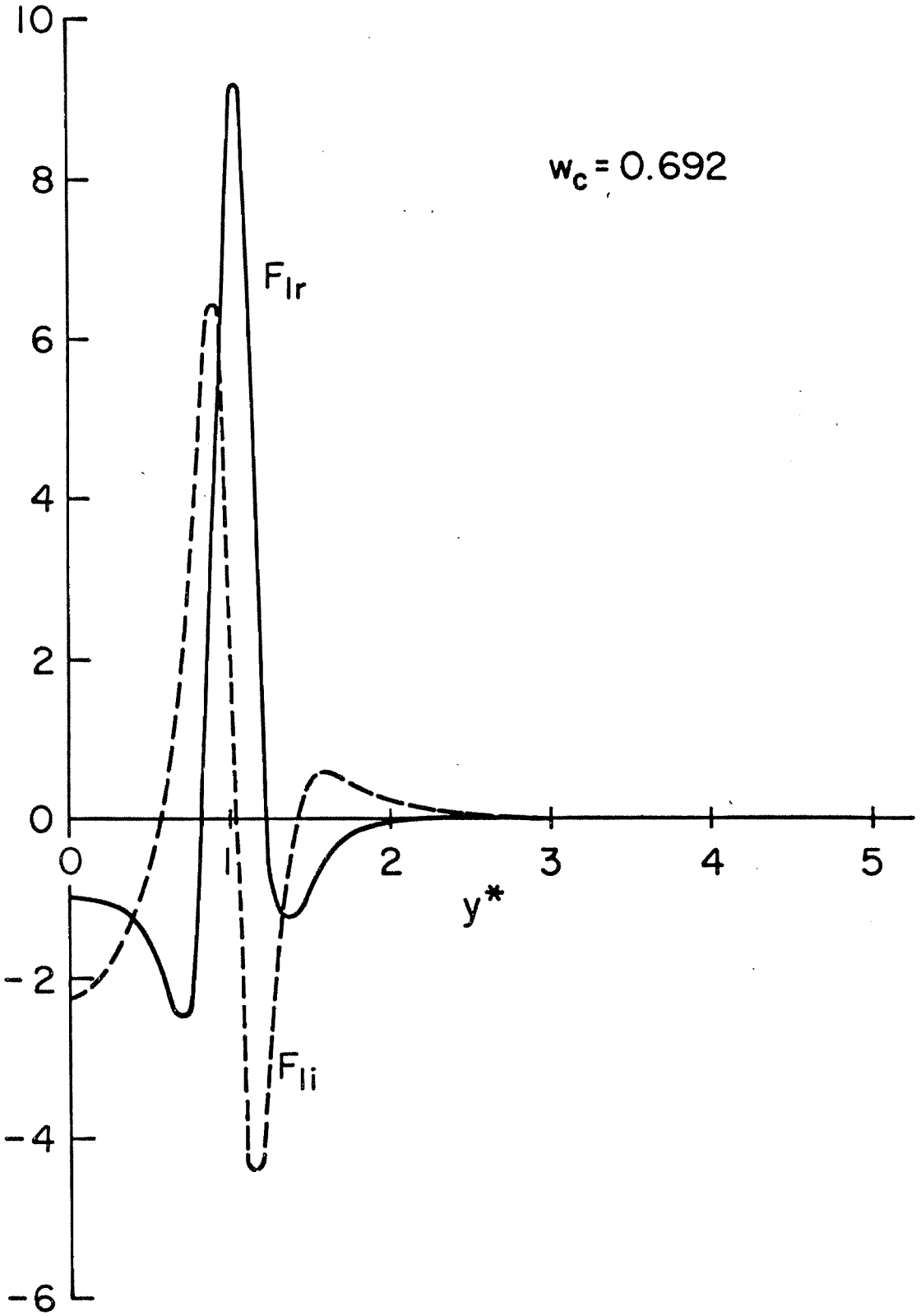

Fig. F1a Forcing Function $F_1(y^*)$ at $w_c = 0.692$

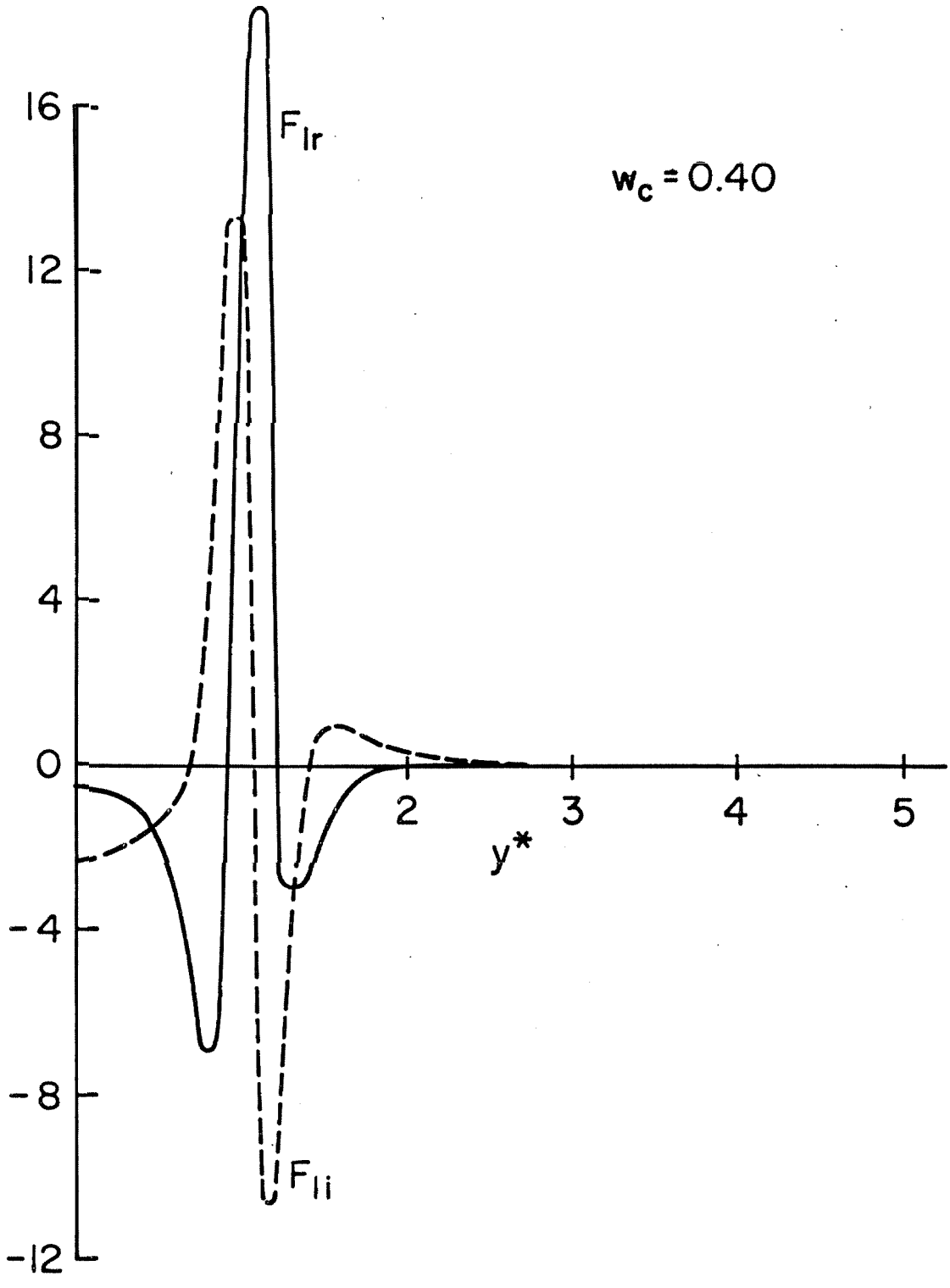

Fig. F1b Forcing Function $F_1(y^*)$ at $w_c = 0.40$

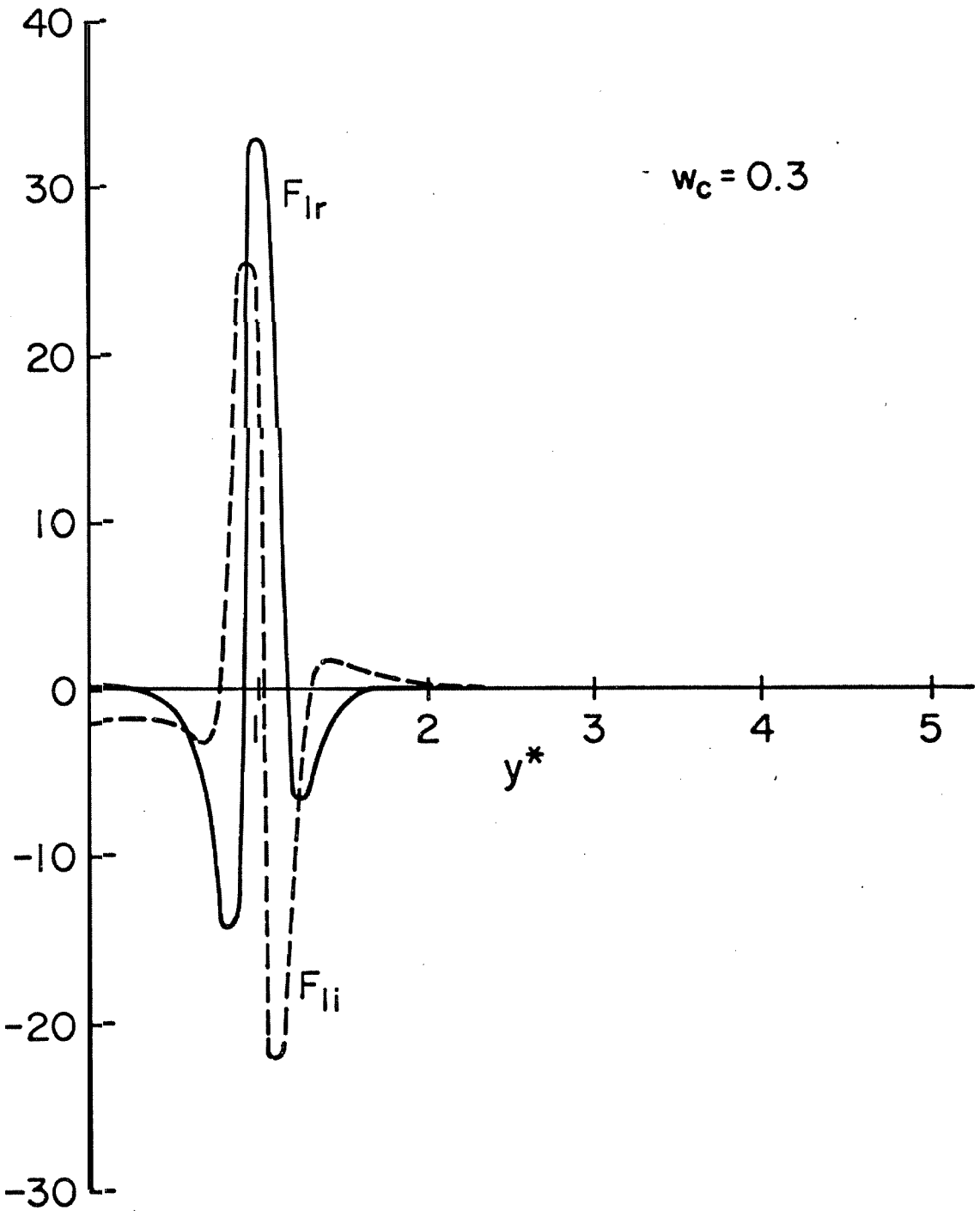

Fig. F1c Forcing Function $F_1(y^*)$ at $w_c = 0.30$

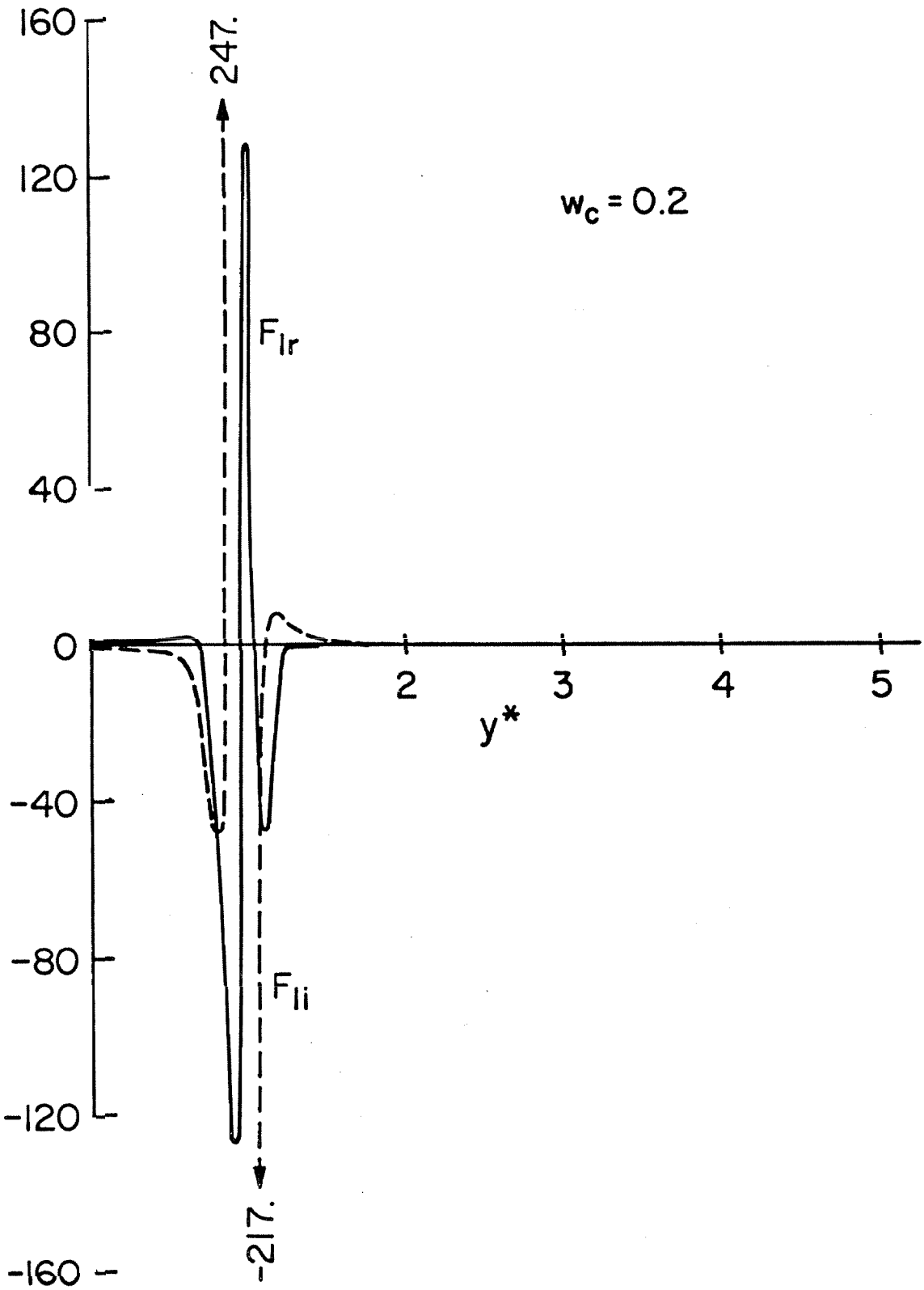

Fig. F1d Forcing Function $F_1(y^*)$ at $w_c = 0.20$

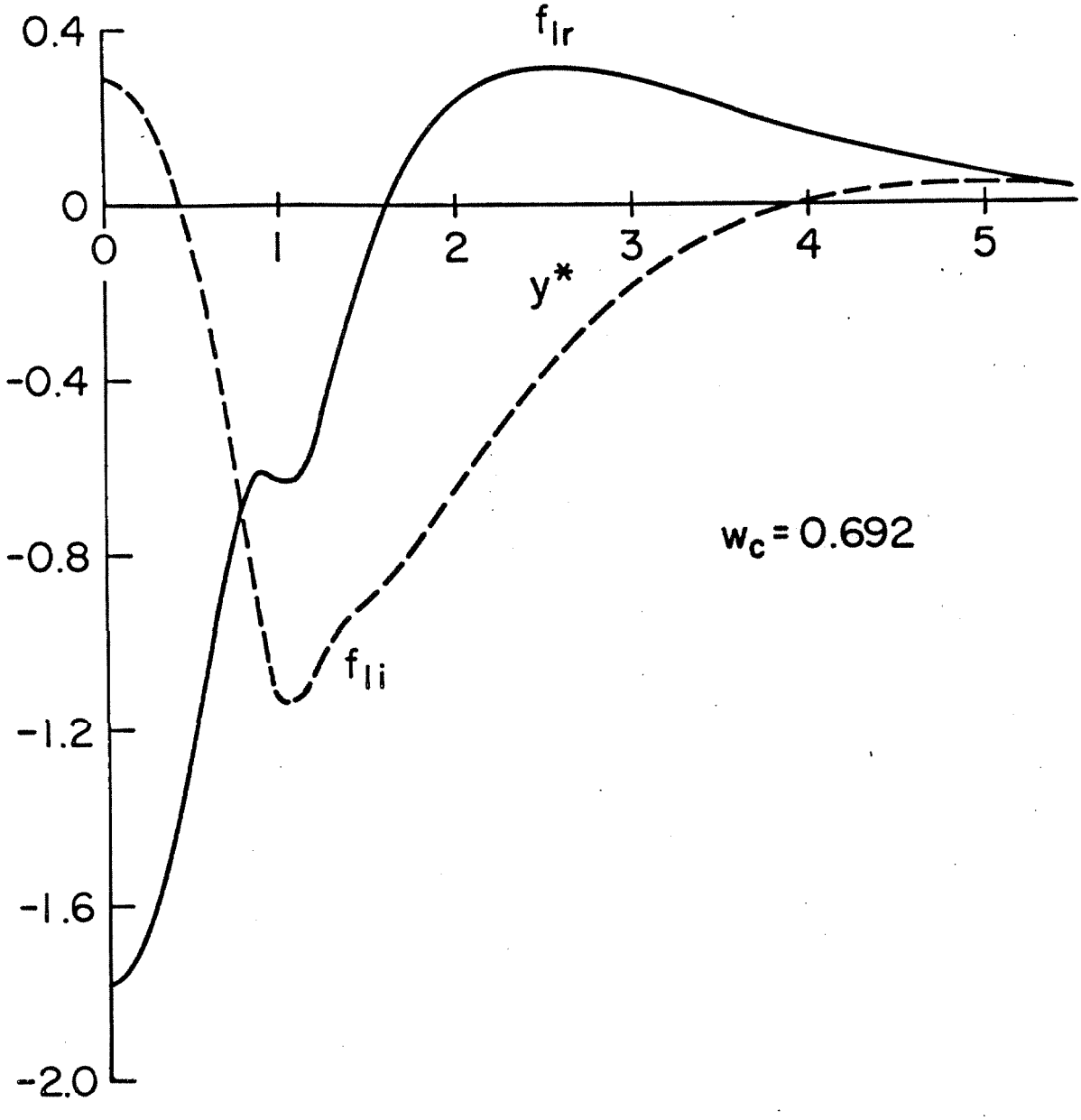

Fig. F2a Distribution of $f_1(y^*)$ at $w_c = 0.692$

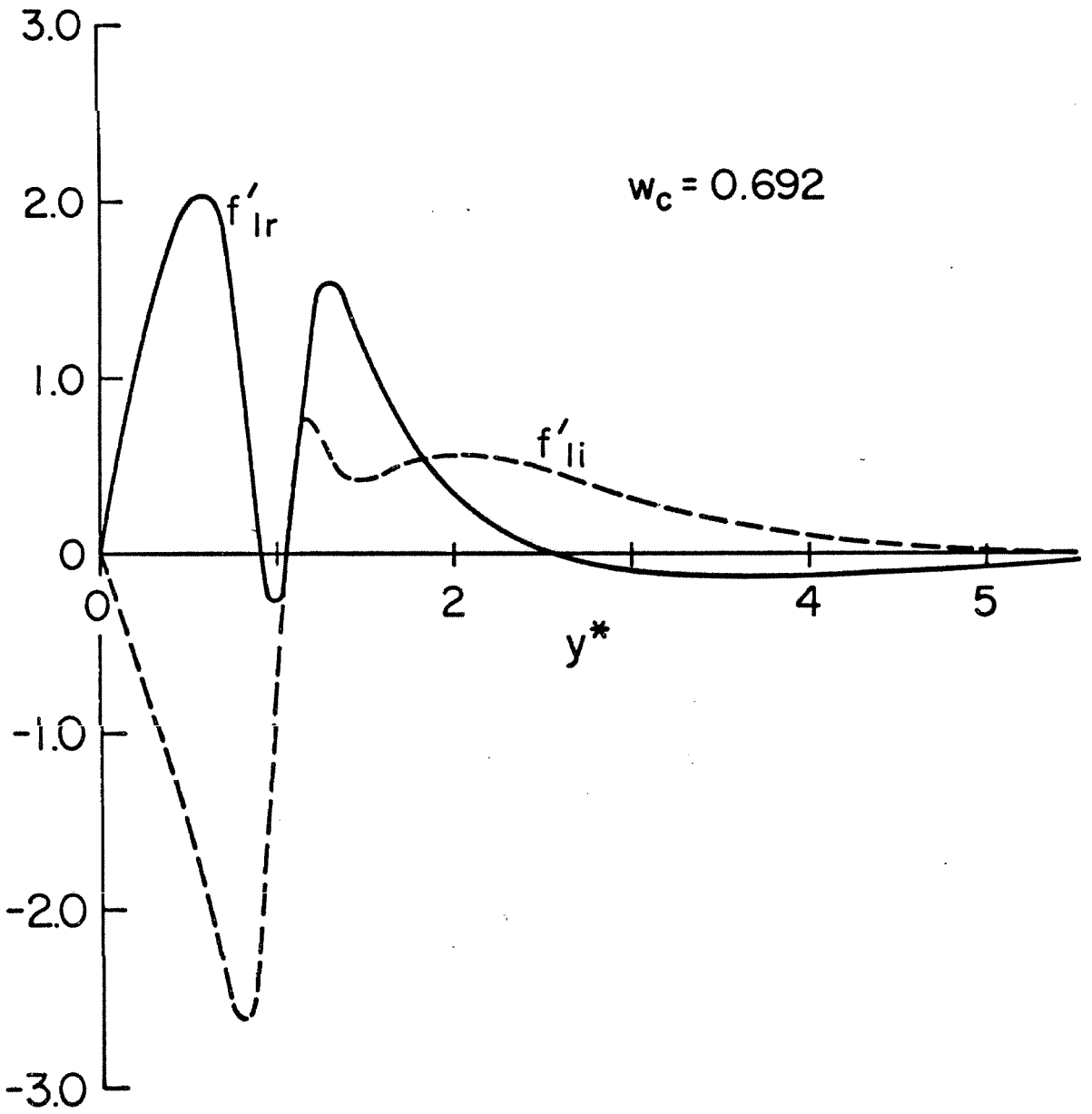

Fig. F2b **Distribution of $f'_1(y^*)$ at $w_c = 0.692$**

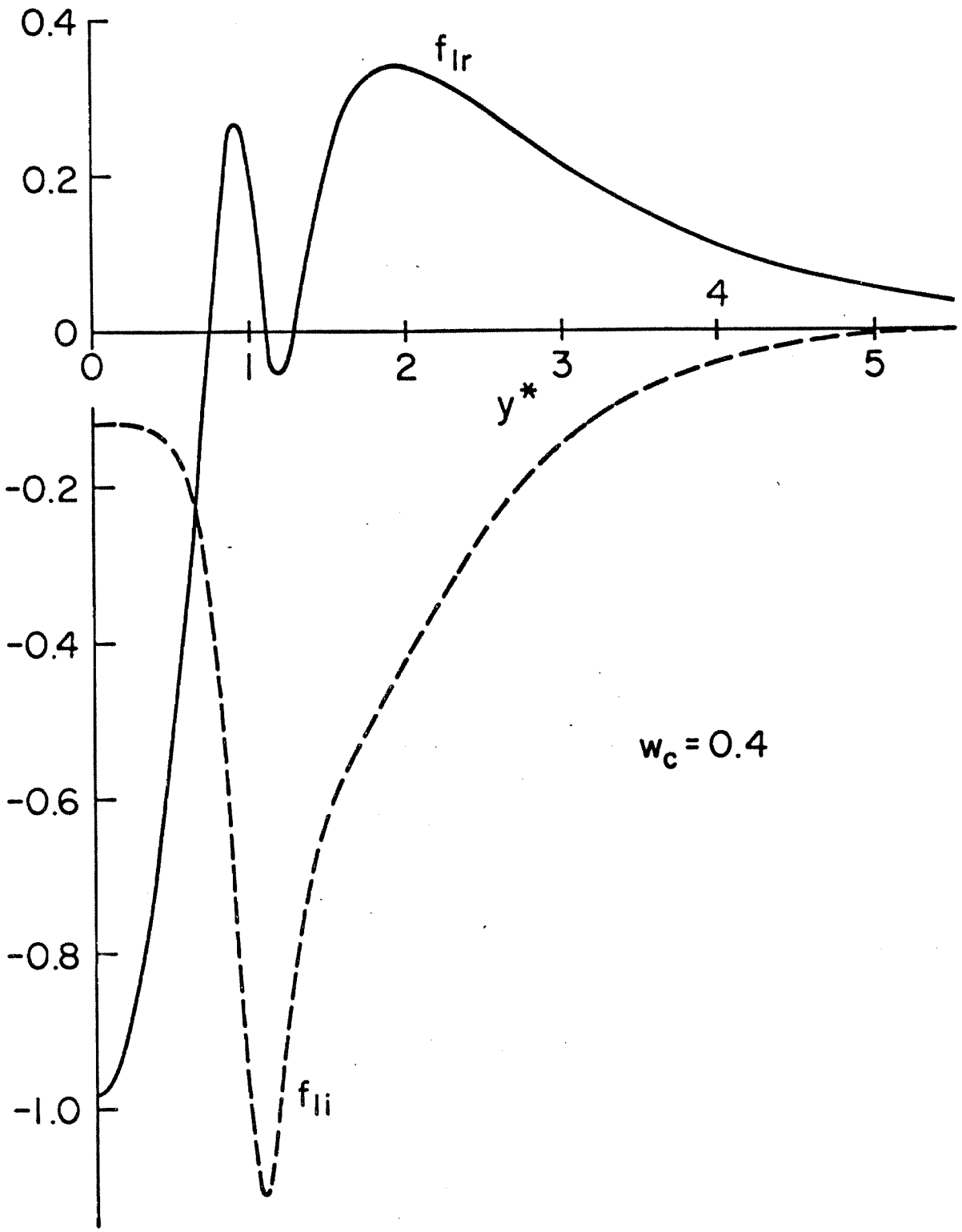

Fig. F2c Distribution of $f_1(y^*)$ at $w_c = 0.40$

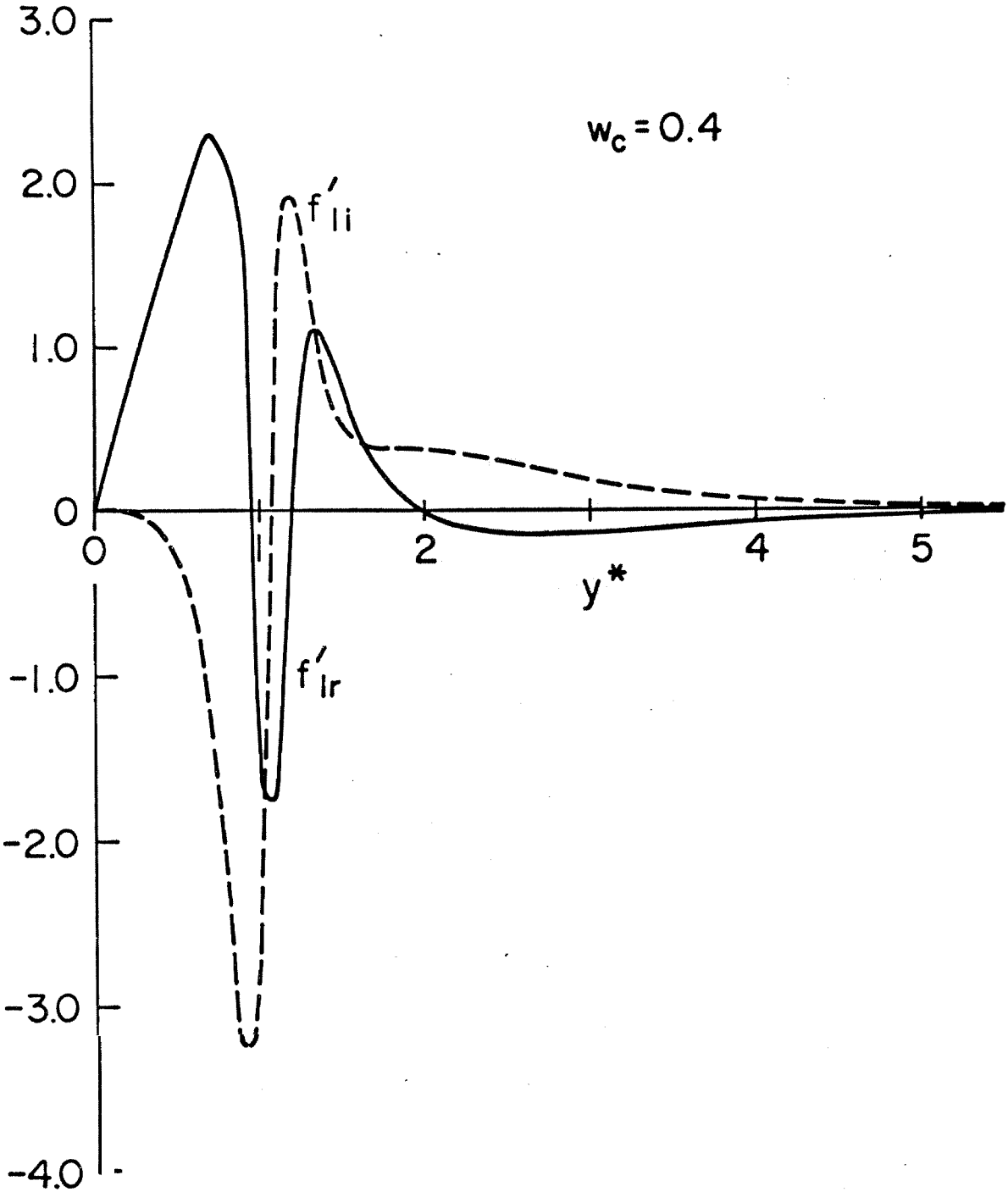

Fig. F2d Distribution of $f_1'(y^*)$ at $w_c = 0.40$

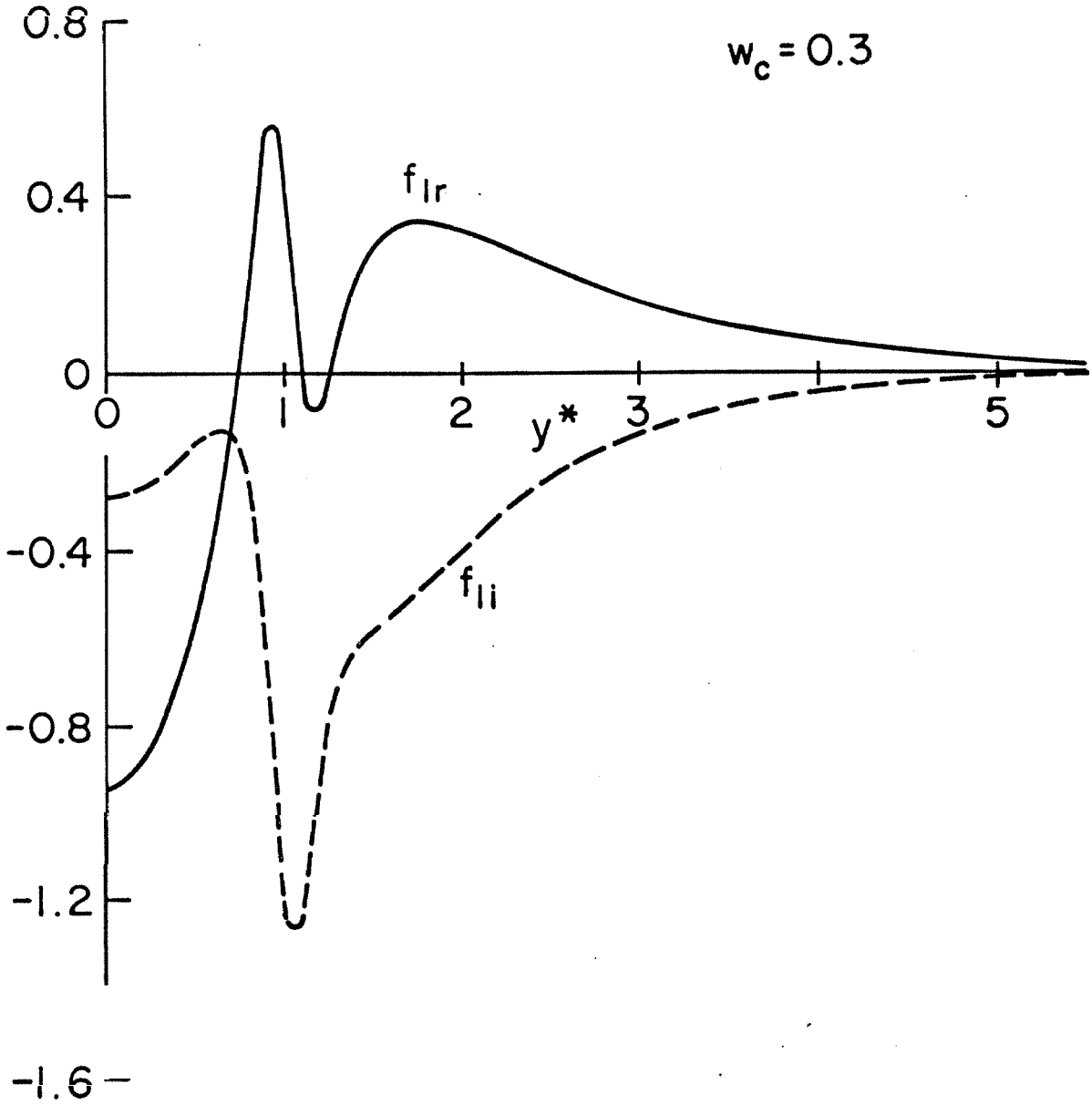

Fig. F2e Distribution of $f_1(y^*)$ at $w_c = 0.3$

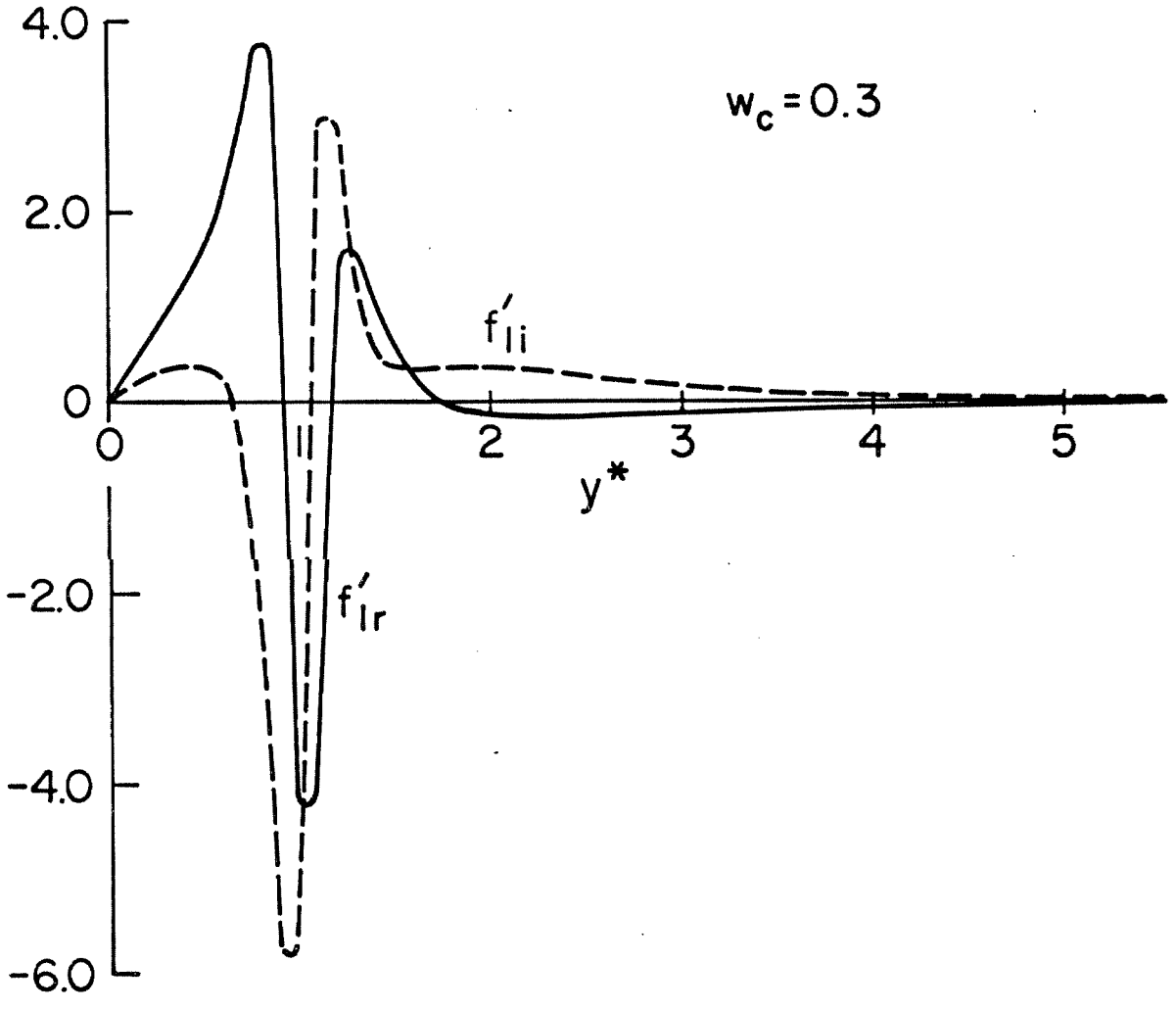

Fig. F2f **Distribution of $f'_1(y^*)$ at $w_c = 0.3$**

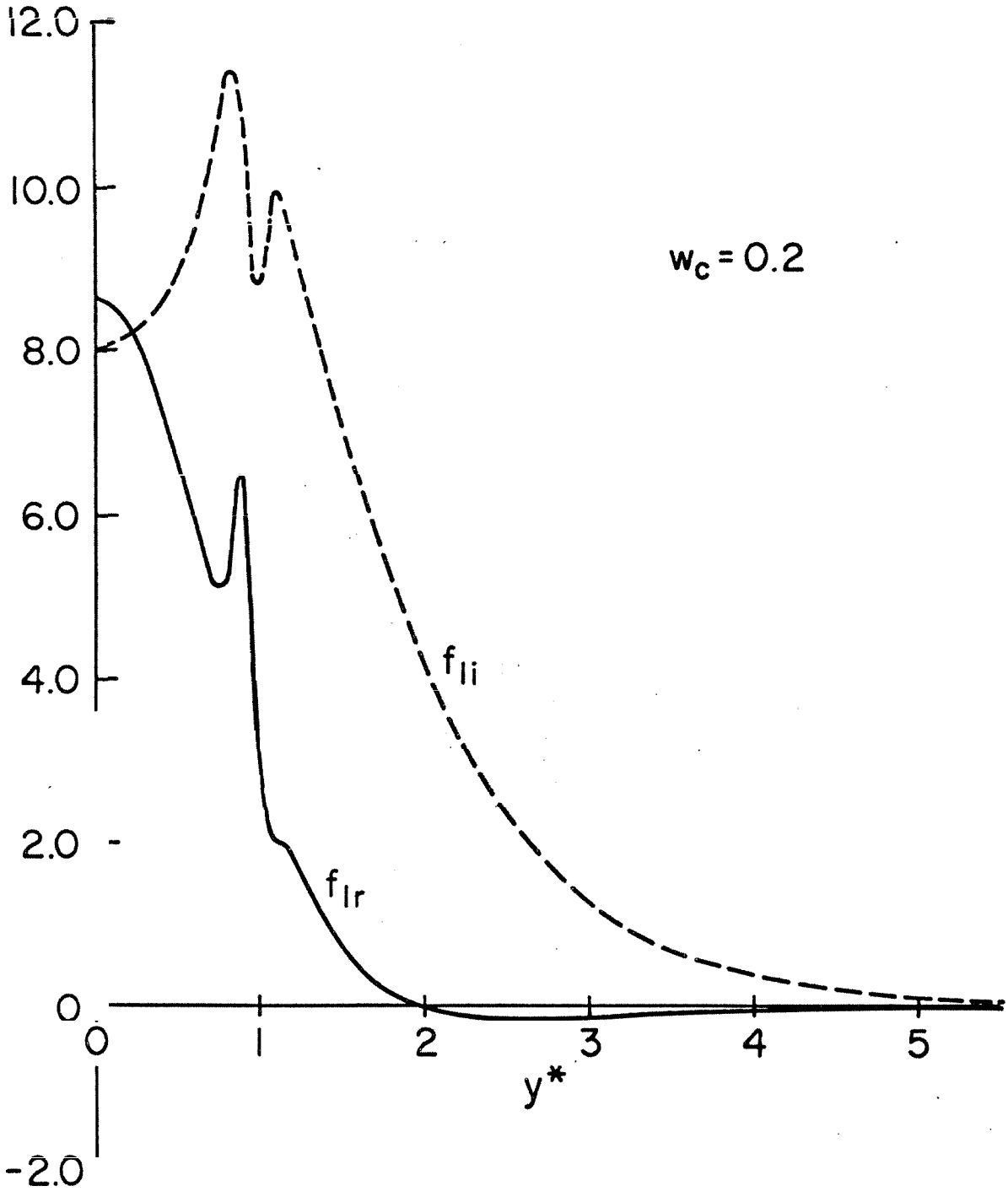

Fig. F2g **Distribution of $f_1(y^*)$ at $w_c = 0.2$**

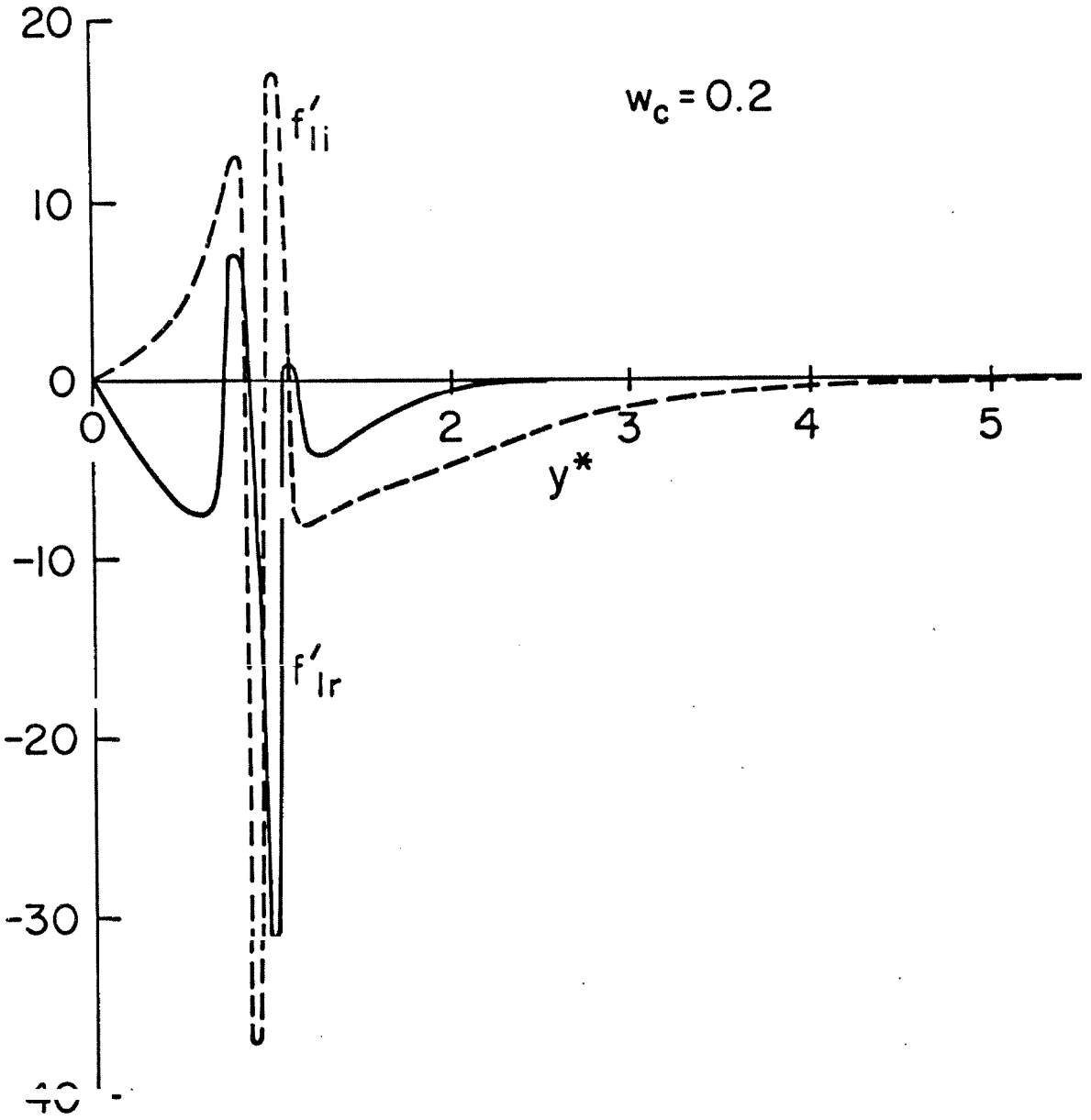

Fig. F2h Distribution of $f_1(y^*)$ at $w_c = 0.2$

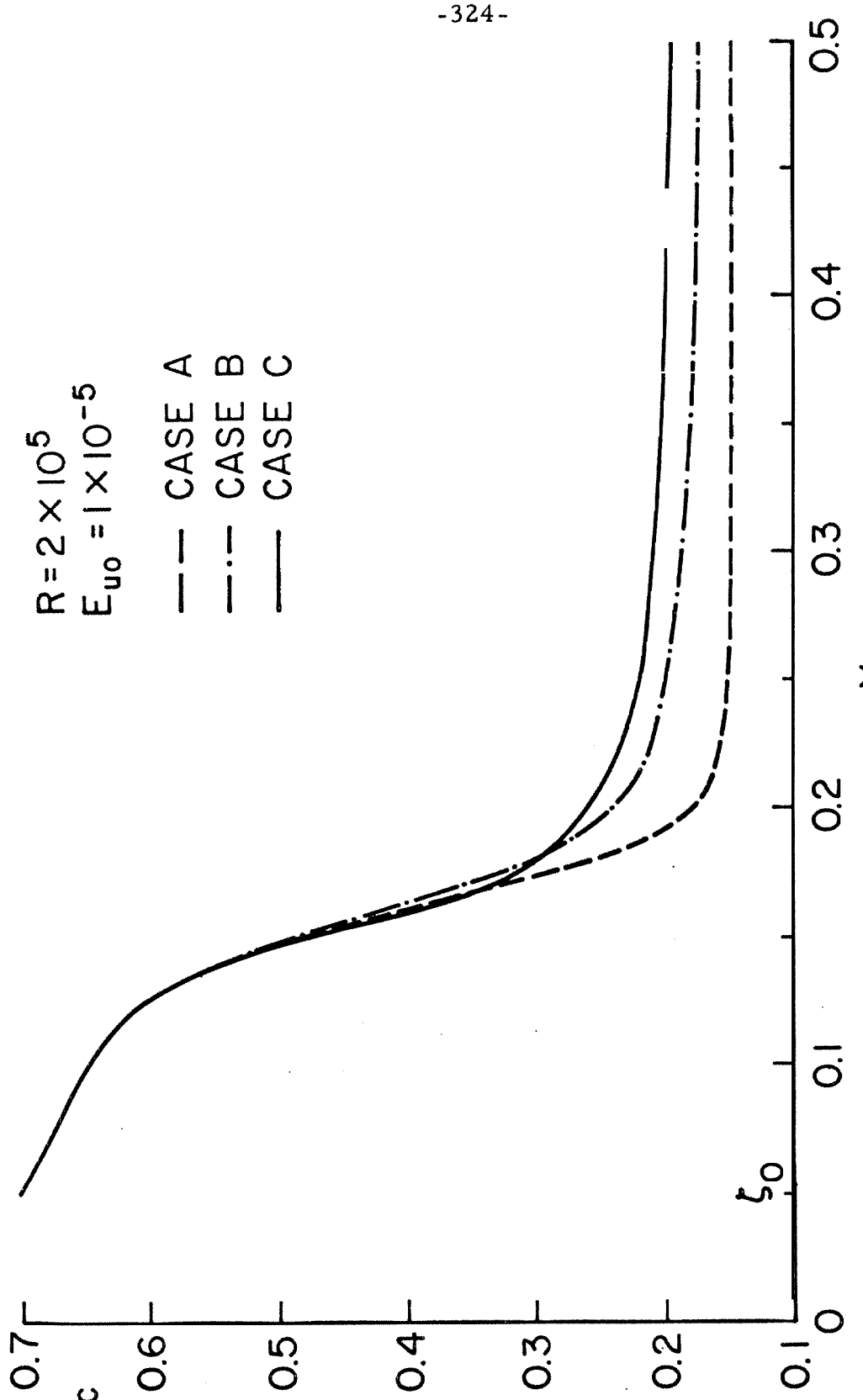

Fig. F3 Comparison of the Variation of w_c for the Three Cases

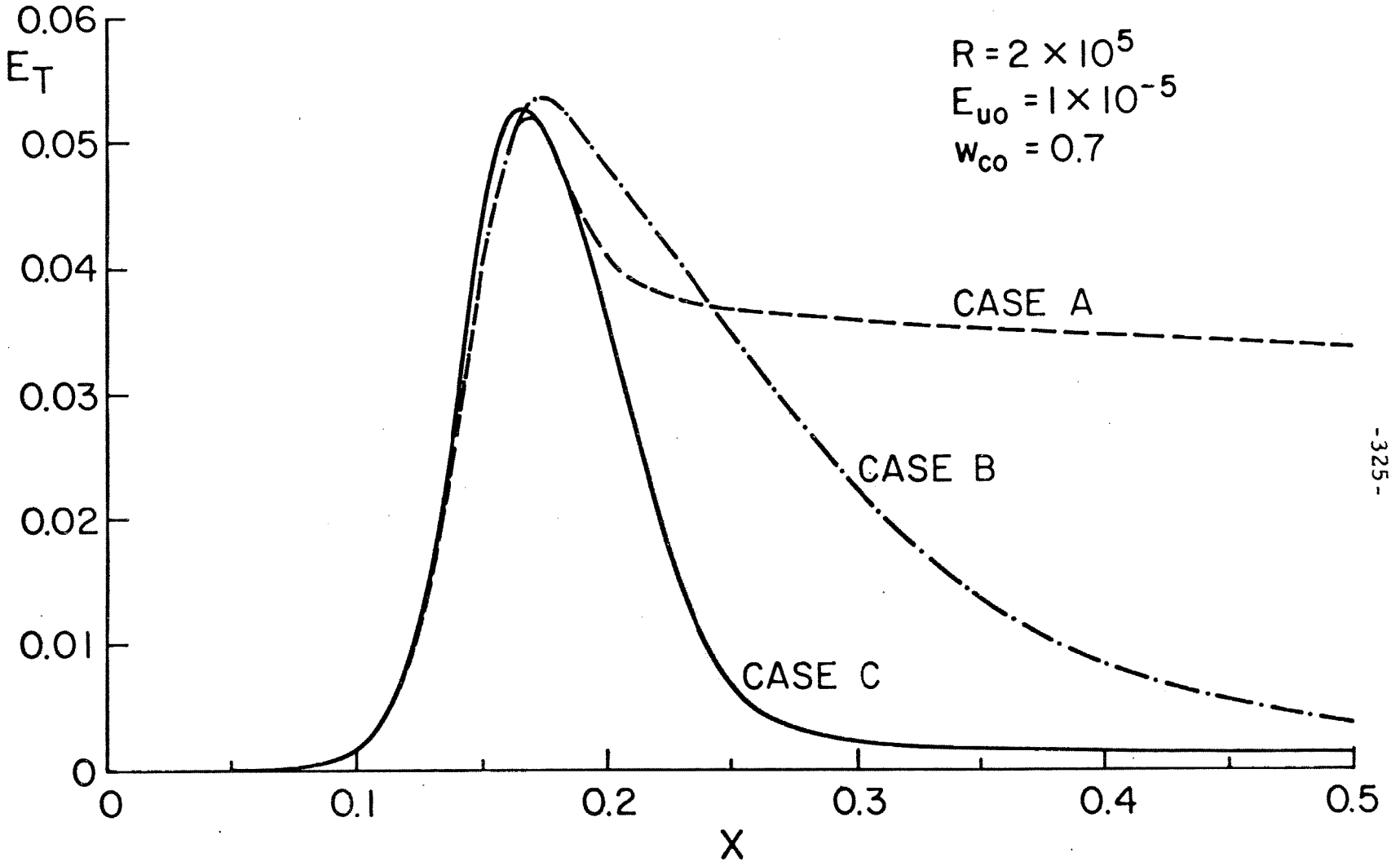

Fig. F4 Comparison of the Variation of E_T for the Three Cases

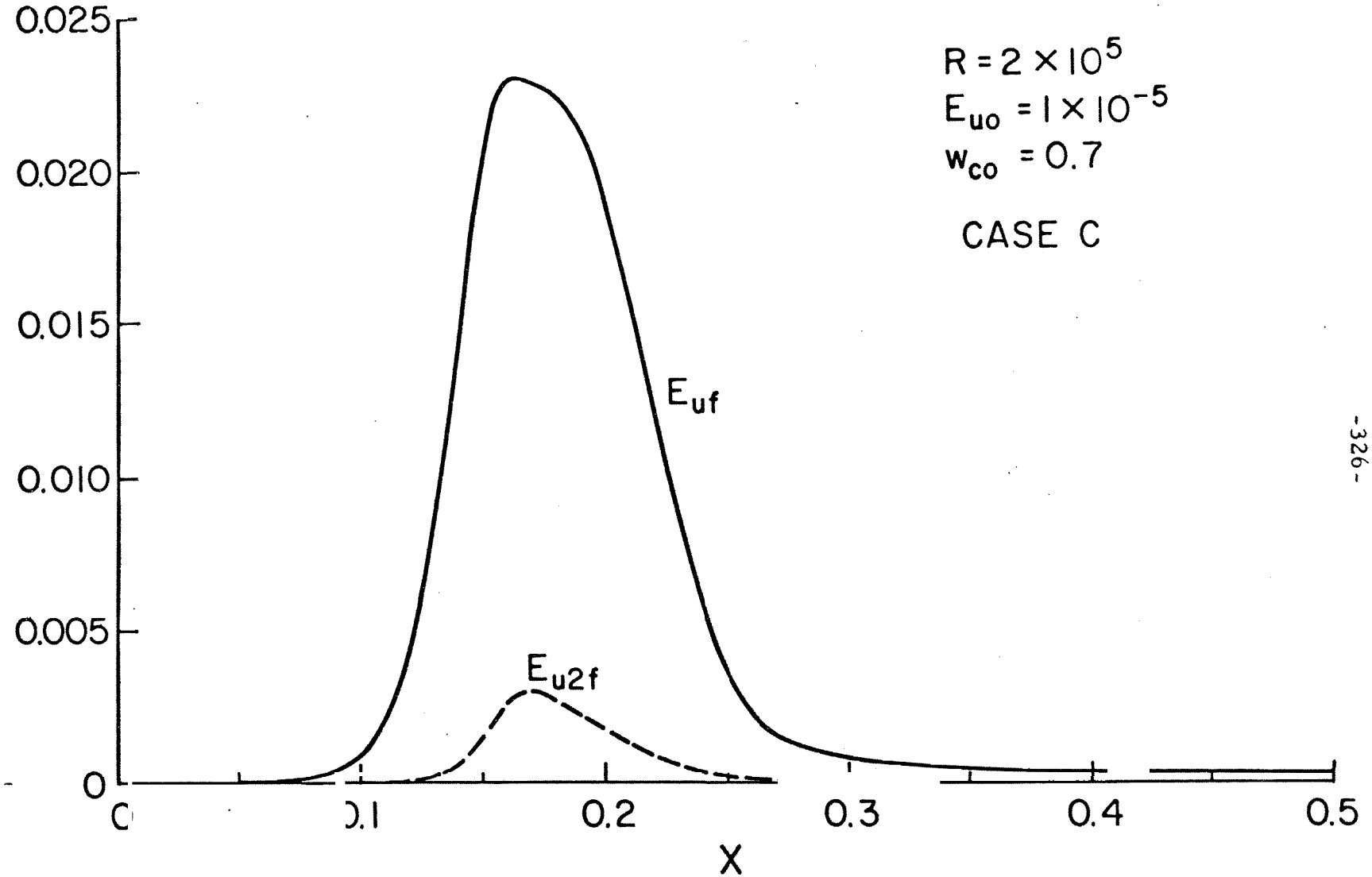

F5 Variation of E_{uf} and E_{u2f} for Case C

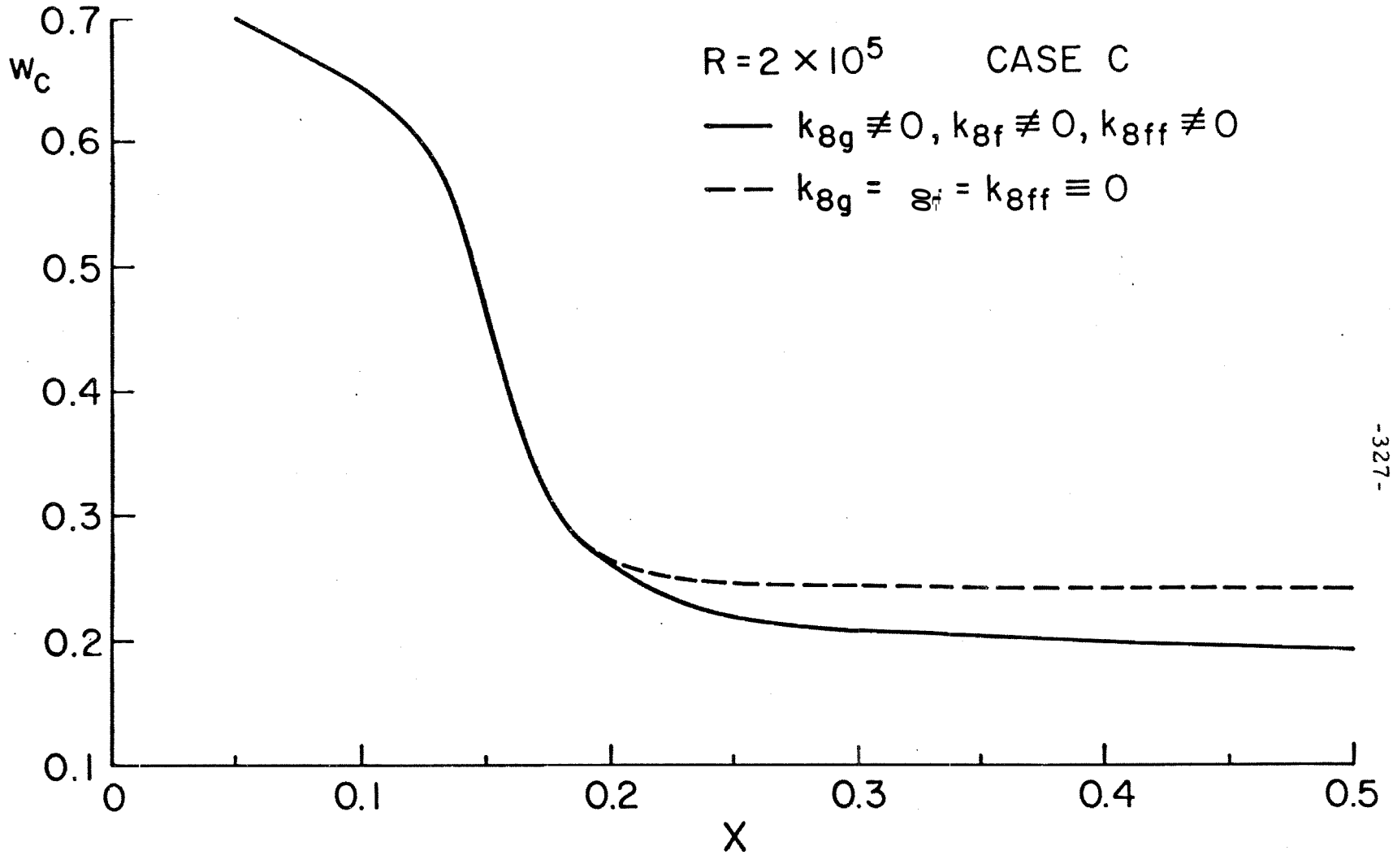

Fig. F6 Effect of the Excessive Viscous Dissipation on w_c; Case C

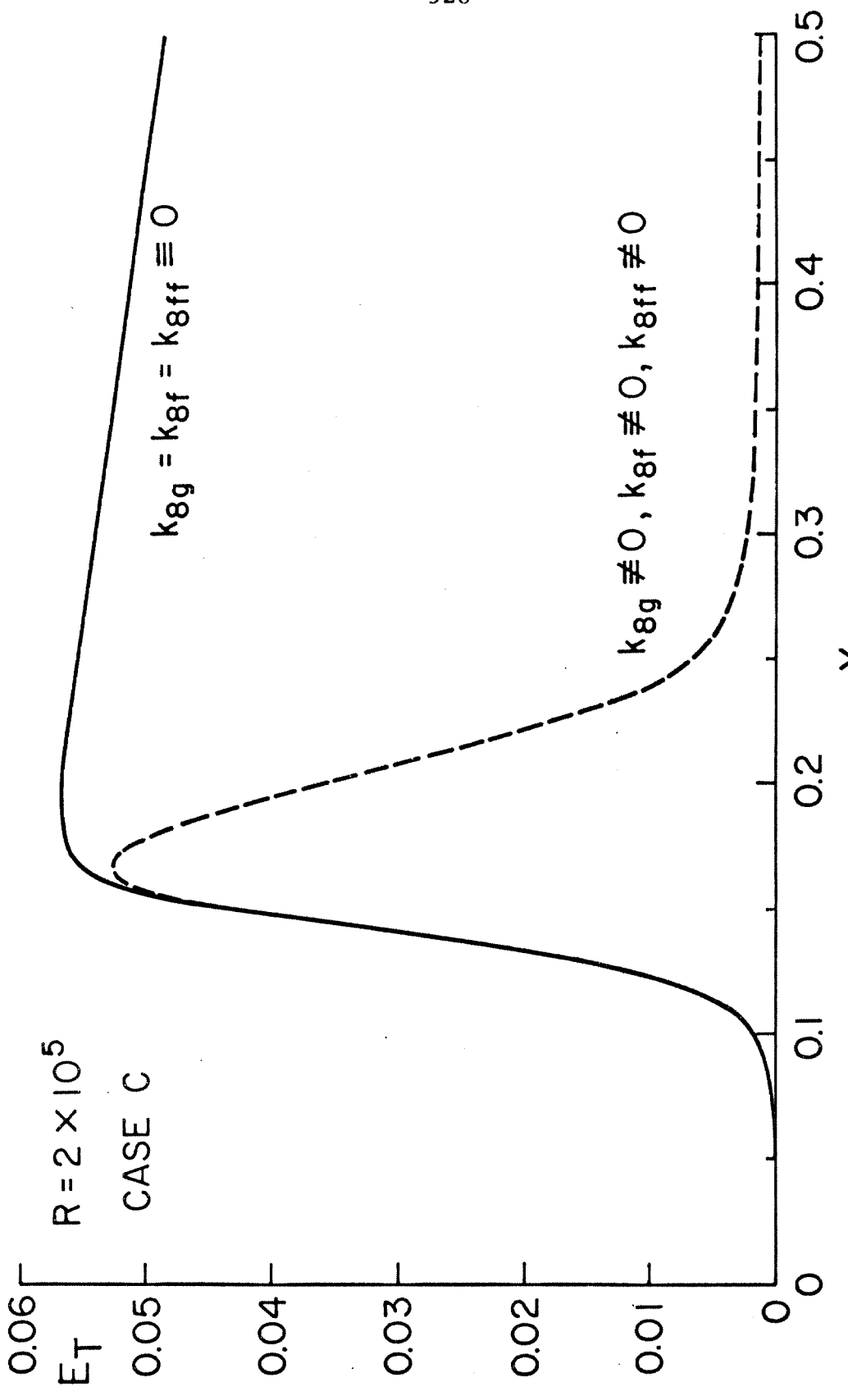

Fig. F7 Effect of the Excessive Viscous Dissipation on E_T; Case C

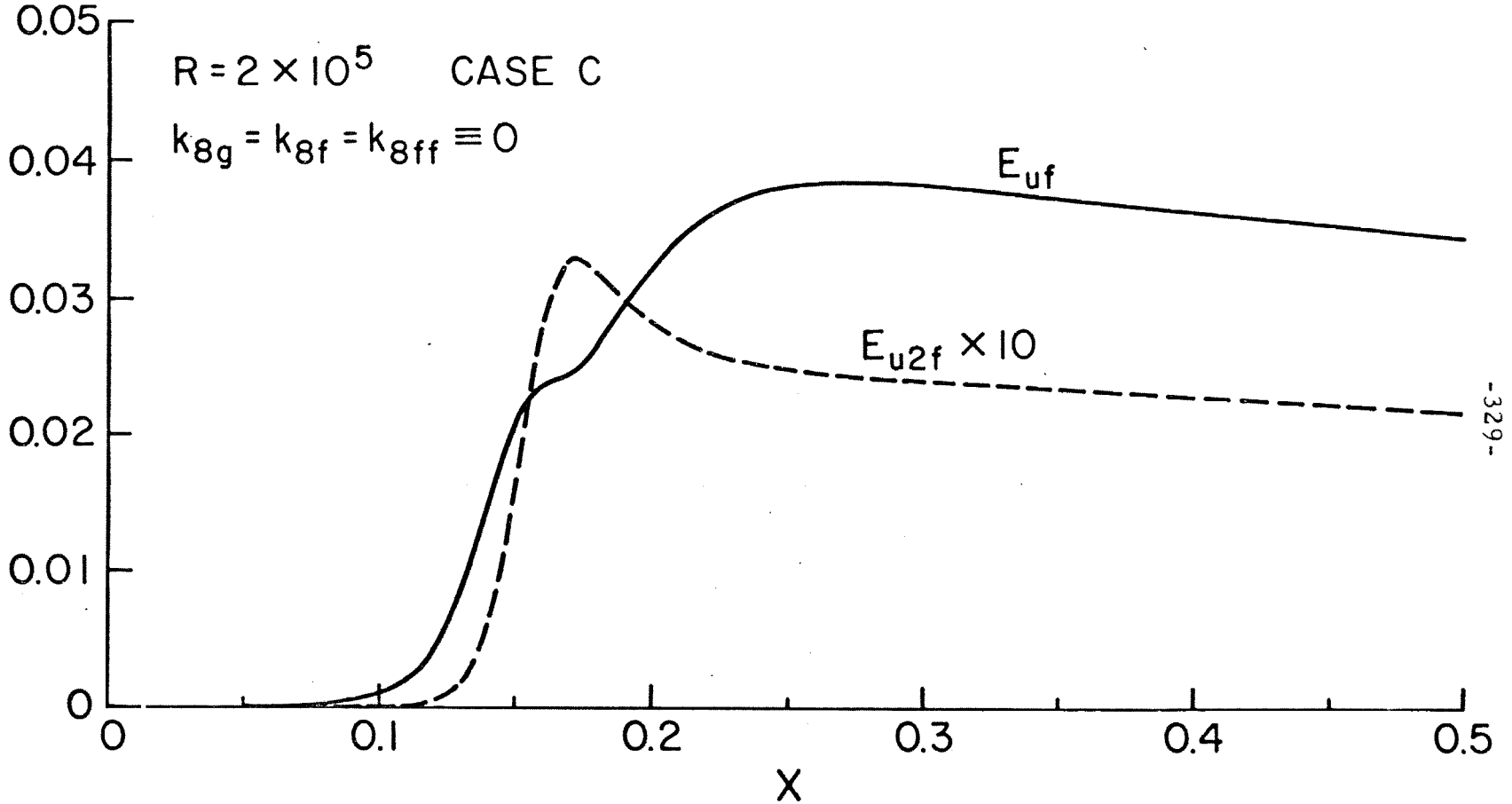

Fig. F8 Variation of E_{uf} and E_{u2f} with the Viscous Dissipation Terms Partially Ignored

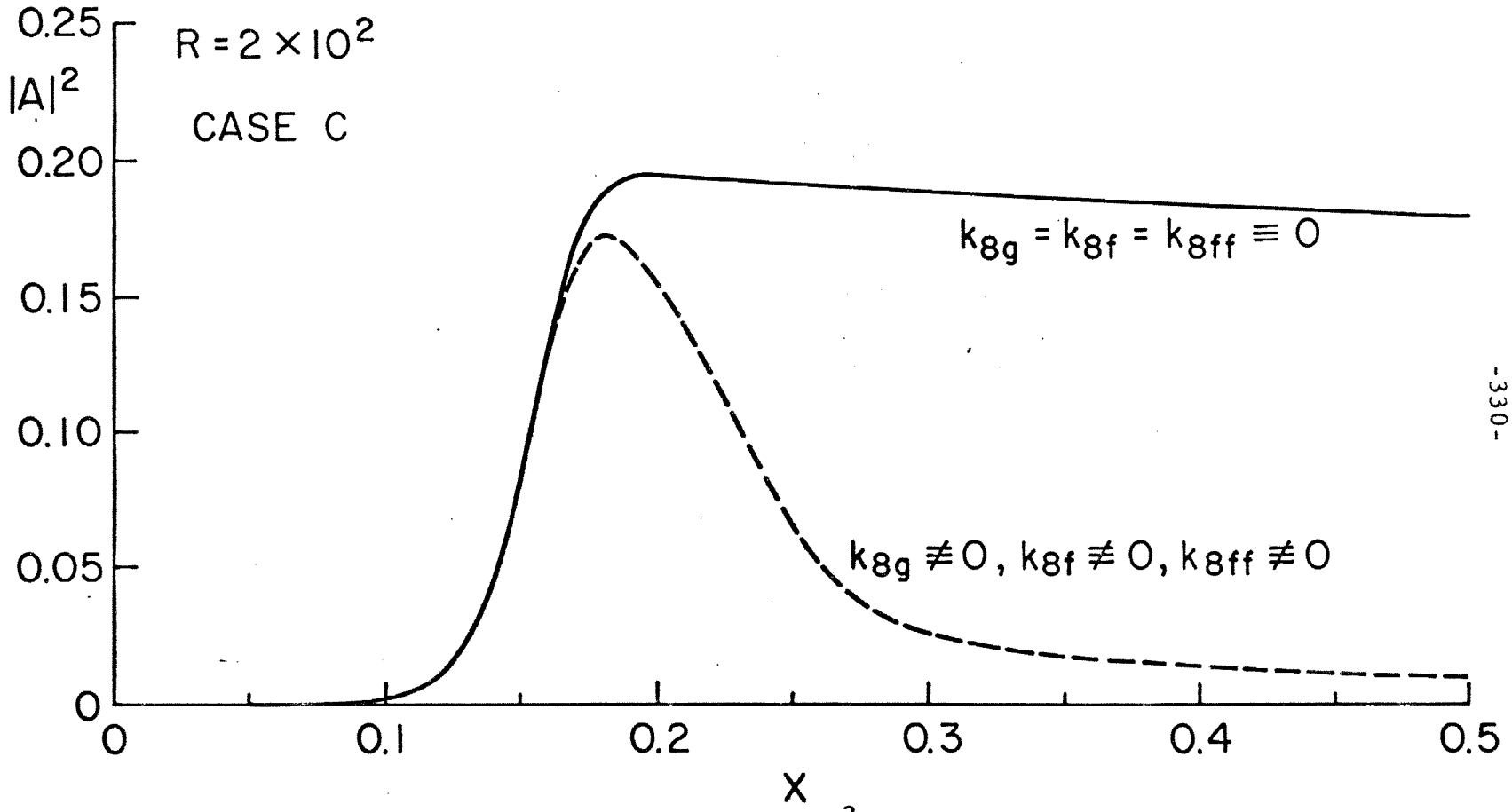

Fig. F9 Variation of $|A|^2$ for Case C